ÉCOLE CENTRALELYON

UNIVERSITÉ DE LYON

N°d'ordre NNT : **2016LYSEC31**

THESE de DOCTORAT DE L'UNIVERSITE DE LYON
opérée au sein de l'Ecole centrale de Lyon

Ecole Doctorale 34
(Ecole Doctorale Matériaux)
Soutenue publiquement le 24/10/2016, par :

ZUTTION Francesca

Effet inhibiteur des glycoclusters dans l'adhésion bactérienne de *Pseudomonas aeruginosa* caractérisé par Microscopie à Force Atomique : de la molécule à la cellule

(Glycocluster inhibition effect on bacterial adhesion of *Pseudomonas aeruginosa* characterized by Atomic Force Microscopy and Spectroscopy: from molecule to cell)

Devant le jury composé de :

MORVAN François DR/IBMM-Montpellier	Président
COHEN-BOUHACINA Touria PU/LOMA-Talence	Rapportrice
MOLINARI Michaël PU/LNR-Reims	Rapporteur
SCHILLERS Hermann DR/Institut of Physiology II-Münster	Examinateur
VERGOTEN Gérard PU/UGSF-USTL-Lille	Examinateur
CHEVOLOT Yann DR/INL-ECL	Examinateur
PHANER-GOUTORBE Magali PU/INL-ECL	Directrice de thèse

Acknowledgment

First of all, I would like to thank the members of the jury, in particular Pr. Touria Cohen-Bouhacina and Pr. Michaël Molinari for evaluating this dissertation.

Also, I thank the director and vice director of the Institut des Nanotechnologies de Lyon, Dr. Catherine Bru-Chevallier and Dr. Christian Seassal, as well as the director of the Chemistry and Nanobiotechnology group, Dr. Yann Chevolot. My acknowledgment goes also to Dr. Jean-Yves Buffière, director of École Doctorale Matériaux de Lyon.

I would to express my deepest gratitude to my supervisor, Pr. Magali Phaner-Goutorbe. Form the beginning she trusted me in making my own decisions. Nevertheless she was always there when I asked for guidance, support and encouragement. It has been a pleasure working with you from both a scientific and personal points of view.

Besides my advisor, I thank all the members of the Chemistry and Nanobiotechnology group, the permanent staff and all the doctors and future doctors that had contributed to create a great ambient in the lab. It has been wonderful to work with you guys! Also, I thank all the colleagues at the Institut des Nanotechnologies de Lyon and École Centrale de Lyon. Of course, there are some people who helped me more than others and they know who they are. I am really grateful to all my colleagues who helped me, in one way or in another, making these three years a great experience.

Moreover, all the scientific collaborators have played an important role in the work presented here. In particular, I would like to acknowledge all the members of the ANR project, especially Dr. François Morvan, Dr. Jean-Jacques Vasseur, Dr. Olivier Vidal, Pr. Gérard Vergoten and Dr. Sébastien Vidal. You always helped me in finding an answer to my questions and our discussions were always stimulating. It has been a pleasure to work with you! Then, I thank Dr. Agnès Piednoir from the ILM for having welcomed me in her lab and being always kind and helpful. Also, I would like to express my gratitude to Dr. Hermann Schillers. It was a great experience spending two weeks in your lab and working with you and Mike Wälte. I am grateful that you accepted to work with us, thank you!

Finally, there is a special group of people to whom I am thankful: my family and friends. "*Grazie per esserci sempre. Vi adoro*!". Last but not least, to Carlos to be always there: "*Somos un super equipo!*".
Thank you to all of you!

Table of Contents

List of Figures

List of Tables

Acronyms

PA	*Pseudomonas aeruginosa*
CF	Cystic Fibrosis
CRD	Carbohydrate Recognition Domain
AFM	Atomic Force Microscopy
SMFS	Single Molecule Force Spectroscopy
SCFS	Single Cell Force Spectroscopy
MD	Molecular Dynamics
ITC	Isothermal Titration Calorimetry
M1	Man(proTzEG$_3$Gal)$_4$
M2	Man(proTzAcNPhGal)$_4$
M4	Man(EG$_2$MTzAcNPhGal)$_4$
M4	Man(EG$_2$MTzAcNPhGlc)$_4$
C1	Calix[4]arene(OMTzEG$_3$Gal)$_4$
P1	Porphyrine(OMTzEG$_3$Gal)$_4$
D1	(DMCH-MTzEG$_3$Man)$_3$
Man	Mannose
Gal	Galactose
Glc	Glucose
pro	Propyl
Tz	Triazole
EG$_{2/3}$	Di/Tri ethyleneglycol
M	Methyl
OM	O-methylene
AcNPh	Acetyl-N-Phenyl
DMCH	Dimethanolcyclohexane
L1	Linker 1
L2	Linker 2
ΔG	Gibbs free energy [J/mol]
ΔH	Enthalpy [J]
ΔS	Entropy [J/mol*K]
k_{off}	Off-rate constant [s^{-1}]
k_{on}	On-rate constant [M*s^{-1}]
K_d	Dissociation constant [M]
K_a	Association constant [M^{-1}]

k_B	Boltzmann constant (1.381*10^{-23} J/K)
T	Temperature [K]
k	Spring constant [N/m]
f_{res}	Resonance Frequency [Hz]
RMS	Root Mean Square [m]
2D	2-dimensional
3D	3-dimensional
ΔE	Potential energy [cal]
F_{un}	Unbinding Force [N]
L_R	Rupture Length [m]
W_D	Detachment Work [J]
F_D	Detachment Force [N]
P_P	Peak Position [m]
DNA	Deoxyribonucleic acid
Cy3	Cyanine 3
DDI	DNA-Directed Immobilization
Lys	Lysine
PEG	Polyethylene glycol
BSA	Bovine Serum Albumin
FWHM	Full Width at Half Maximum

Introduction

The importance of single molecule approaches

Single molecule methods have become powerful tools to probe the response of biological molecules, thanks to their capabilities of disclosing molecular structures, dynamics and functions of a single molecule from the average behavior obtained in ensemble experiments. In fact, ensemble experiments are characterized by the simultaneous analysis of a large number of molecules, and their general behavior is observed. On the contrary, single molecule experiments access the information of individual properties, breaking into the knowledge of a large amount of molecular information [2].

There are different reasons that make single molecule methods powerful tools for studying biological systems. Mainly [2]:

    i)   The molecular properties are measured one molecule at the time;
    ii)   The dynamics of systems are measured at equilibrium conditions;
    iii)   Molecular forces, structural and functional responses to mechanical stimuli can be directly measured;
    iv)   The system can be studied with high sensitivity at "native" conditions.

This means that the distributions of molecular properties are easily detected as well as rare states or species. Also, single molecules methods allow studying the dynamics of systems such as molecular motors characterized by stochastic and unsynchronized behavior. Moreover, dynamic constants can be obtained between the different states that characterize the system. Finally, the high sensitivity of the techniques consents working at low concentrations, avoiding the formation of aggregates, and studying the properties of the system at the equilibrium. This also allows monitoring the behavior of species that are present only in few copies in the cell, in an environment that mimics the physiological one [2].

For this, during the last two decades, the technological advance of the field of single molecule research has been strongly promoted due to the promise of revolutionary capabilities to reveal usually hidden information. Different techniques have been developed to satisfy the demand of answering to key biological questions. Mostly, they are optical and manipulation methods and none of them are able to obtain all the characteristics that define the biological system. Therefore, most of the time, the combination of them can get inside on the complexity of the system under study. Among them, three main spectroscopic methods provide the measurement of interaction forces. Force plays a central role in biological systems since, for example, is involved in cellular motility, DNA replication and segregation, ligand-receptor interactions, etc. [1]. Single molecule force spectroscopy methods allow measuring such forces up to picoNewton resolution. The main

techniques are Atomic Force Microscopy [3], Magnetic and Optical [4] Tweezers. These methods are complementary, due to the different manipulation capabilities, both in length and force (Table I). All of them need the biochemical modification of the probe, and this allows the measurement of molecular forces as a function of distance. Maybe, the most familiar technique mentioned here is the Atomic Force Microscopy [1], also because despite of its ability of measuring forces, it is an imaging technique. In fact, it allows visualizing the equilibrium state of a biological complex with a nanometer resolution and in conditions that mimic the cellular ones.

	Atomic Force Microscopy	Magnetic Tweezers	Optical Tweezers
Spatial resolution [nm]	0.5 - 1	5 - 10	0.1 - 2
Temporal resolution [s]	10^{-3}	$10^{-1} - 10^{-2}$	10^{-4}
Stiffness [pN/nm]	$10 - 10^5$	$10^{-3} - 10^{-6}$	0.005 - 1
Force range [pN]	$10 - 10^4$	$10^{-3} - 10^2$	0.1 - 100
Displacement range [nm]	$0.5 - 10^4$	$5 - 10^4$	$0.1 - 10^5$
Probe size [µm]	100 - 250	0.5 - 5	0.25 - 5
Typical application	High force pulling Interaction assays	Tethered assay DNA topology	3D manipulation Tethered assay Interaction assay
Features	High-resolution imaging	Force clamp Bead rotation Specific interactions	Low-noise and low-drift dumbbell geometry
Limitations	Large high-stiffness probe Large minimal force Nonspecific	No manipulation	Photodamage Sample heating Nonspecific

Table I: Comparison of the three single molecule force spectroscopy techniques. Adapted from [1].

Scope of this dissertation

Atomic Force Microscopy (AFM) is an excellent tool to study the ligand-receptor and the bacteria-cell interactions at the nanoscale, to obtain a new degree of understanding of the system. Literature shows the capabilities of this technique in microbiology, pharmacology, cancer and biomedicine [5]. In particular, different studies have been performed to characterize *Pseudomonas aeruginosa* (PA) bacterium, a human opportunistic pathogen and its virulence factors at the nanoscale [6–8]. AFM imaging, Single Molecule Force Spectroscopy and Single Cell Force Spectroscopy have been

used to study the adhesion forces and relate physical properties with biological function of such virulence factors [9–11]. In addition, the behaviour of different PA bacterial strains under antibiotic treatment has been studied [6], showing the large applicability of the technique to the study of bacteria and in particular PA human pathogen.

The interest of scientific community on PA is due to the fact that this pathogen is the main cause of airways chronic infection of cystic fibrosis patients, and in general immune compromised people, leading, in the worst case, to patient death. The bacteria take advantage of an arsenal of virulence factors to infect host cells, develop biofilm and colonize epithelium. In particular, the growth of biofilm structures provides a resistance against most antibiotic treatments. Therefore, this increasing resistance to antibiotic therapies has led to the development of new therapeutic approaches against this pathogenic bacterium. The alternative to antibiotic treatments is the attenuation and inhibition of bacterial virulence such that the organism fails to successfully infect the host and it is subsequently cleared by the immune response system [12,13].

Among the virulence factors of PA bacteria, two lectins LecA and LecB are believed to be potential therapeutic targets due to their role in cell recognition, biofilm formation and cohesion [14]. In particular, LecA lectin exists as a tetramer exposing four carbohydrate recognition domains and each of them specifically interact with one galactose moiety. The binding between galactose and LecA is characterized by hydrogen bonds, hydrophobic contacts, and coordination with one calcium ion [15]. It has been shown that LecA is determinant for cytotoxicity [16] and several experiments have demonstrated its role in PA virulence. In a mouse model of PA infection, it has been shown that mutants devoid of LecA production display a lower dissemination rate within tissue as well as a higher clearance [16]. The imputative ligand, that seems to be the natural target of LecA in cells, is the antigen Gb3 (αGal1-4βGal1-4βGlc-1Cer) [17]. In fact, *in vivo* and *in vitro* studies have demonstrated the ability of LecA of targeting cells presenting this glycolipid, which is highly expressed in erythrocytes and epithelial cells of mammals, thus it is likely involved in the binding.

Therefore, a promising therapeutic approach could be based on the design and development of synthetic molecules more affine to LecA and able to compete *in vivo* with its natural ligand. Galactosylated glycoclusters were shown to be selective high affine LecA ligands [18,19] due to their high specificity of carbohydrate-protein interactions and their multivalency [20]. Different strategies to build these scaffolds were explored but most of them present a core with multiple branches terminated by a galactose residue able to interact with the lectin recognition domain. The design of the core and the spacer arms are key parameters for achieving optimal topologies allowing the so called "cluster glycoside effect" [21–23]. More recently, their inhibition of the activity of lectin-induced PA lung infection has been demonstrated in animal models, then it represents a promising therapeutic strategy against such bacterial infections [24].

Our team (Laboratory of Chemistry and Nanotechnology) is involved into an ANR project devoted to the synthesis, characterization and screening of a library of glycoclusters against LecA in order to find the best candidate for inhibit the lectin activity, and thus for the development of a new therapeutic approach. The project involves different French laboratories, such as the Institut des Biomolécules Max Mousseron (IBMM), University of Montpellier (Dr. Jean-Jacques Vasseur and

Dr. François Morvan), the Laboratoire of Glycobiologie Structurelle et Fonctionnelle of the University of Lille (Dr. Olivier Vidal and Prof. Gérard Vergoten), the Institut de Chimie et Biochimie Moléculaires et Supramoléculaires, Laboratoire de Chimie Organique 2- Glycochimie from the University of Lyon 1 (Dr. Sebastian Vidal) and finally our laboratory (Institut des Nanotechnologies de Lyon). The project has lead to the synthesis and screening of a library of more than 150 molecules [25] to find the best candidate for targeting LecA. Among this library, some glycoclusters have been selected and studied by AFM to investigate their nanoscale properties.

In this Ph.D. thesis, the lectin-glycocluster and PA-epithelial cell interactions have been studied by means of AFM technique. AFM allows the visualization of the molecular arrangement of the lectin-glycocluster complex at the nanoscale, and the characterization of the binding force of the lectin-glycocluster system. This dissertation is structured in six Chapters as described below:

- **Chapter 1** will be devoted to the state of the art of the lectin-glycocluster interaction (protein-carbohydrate interaction). The biological system such as the bacteria and its virulence factors will be presented, as well as the different types of glycoconjugates, focusing on the galactosylated glycoclusters, the synthetic molecules studied for targeting the lectin LecA.
- In **Chapter 2**, the AFM technique will be presented, highlighting the different operation modes applied on the study of biological systems and used during this Ph.D.; namely, the imaging mode *tapping* and the spectroscopy modes Single Molecule Force Spectroscopy and Single Cell Force Spectroscopy.
- **Chapter 3** will present the results obtained from AFM imaging, to study the molecular arrangement of LecA lectin created with six different glycoclusters.
- In **Chapter 4**, the interaction between the lectin and three different glycoclusters has been characterized by Single Molecule Force Spectroscopy.
- In **Chapter 5** the anti-adhesive properties of a glycocluster have been tested via Single Cell Force Spectroscopy by studying the modification of cell-bacteria interaction upon addition of the glycocluster.
- **Chapter 6** completes the manuscript with the main conclusions and outlooks.

Chapter 1.   A New Therapeutic Approach Against *Pseudomonas aeruginosa* and its Virulence Factor the Lectin LecA

La nécessité de traitements thérapeutiques alternatifs, pour aider les patients atteints de mucoviscidose à lutter contre la colonisation bactérienne de leurs voies respiratoires, est devenue un défi pour les chercheurs. En particulier, de nombreuses études ont porté sur la bactérie *Pseudomonas aeruginosa* (PA), un pathogène opportuniste chez les humains. Sa capacité à développer un biofilm, lui donne un avantage sélectif contre les antibiothérapies. Par conséquent, elle est l'une des principales causes de mortalité chez les patients atteints de mucoviscidose. Les bactéries profitent d'un arsenal de facteurs de virulence pour se fixer sur les cellules épithéliales, développer des biofilms et coloniser l'épithélium. Pour cela, elle utilise différents facteurs de virulence qui peuvent être impliqués dans les processus d'adhésion et de développement du biofilm. Par exemple, les deux lectines LecA et LecB sont considérées comme des facteurs de virulence chez PA. Elles sont capables de reconnaître et de se lier spécifiquement à certains sucres. En particulier, la lectine LecA est une molécule tétravalente qui reconnaît spécifiquement le galactose présent dans la membrane des cellules épithéliales et cette interaction aide la bactérie à adhérer sur la surface de l'hôte. Pour cela, LecA est considérée comme une cible thérapeutique potentielle en raison de son rôle dans la reconnaissance cellulaire et la formation du biofilm. Une stratégie prometteuse pour le développement d'une nouvelle approche thérapeutique contre PA est liée à la conception et au développement de molécules synthétiques ayant plus d'affinités avec LecA et capables de rivaliser *in vivo* avec son ligand naturel. Les glycoconjugates galactosylés se sont révélés être des ligands sélectifs de LecA, avec une affinité très élevée en raison de leur polyvalence. Récemment, leur utilisation thérapeutique en tant que molécules antibactériennes a été démontrée dans des modèles animaux et représente une stratégie prometteuse contre les infections bactériennes.

Ce premier Chapitre a pour objectif de présenter la problématique biologique. La bactérie et sa lectine LecA sont décrites ainsi que les motivations de cette étude. La stratégie possible d'approche thérapeutique contre la bactérie est décrite, en concentrant l'attention sur les glycomimes qui peuvent cibler spécifiquement la lectine. Le glycomime est multivalent, car il présente quatre sucres capables de se lier à la lectine. Ainsi, l'affinité du glycomime est donc plus élevée par rapport à celle du galactose monovalent.

De plus, les sept glycomimes qui ont été sélectionnés pour cette étude sont présentés. Généralement, il s'agit de molécules caractérisées par un cœur et quatre bras espaceurs terminés par un sucre, dans la plupart des cas un galactose, car il est la cible du LecA. Les bras sont formés par deux ligands (L1 et L2). Le choix du cœur et des bras influence l'architecture de la molécule et ainsi ses affinités et sa stœchiométrie. Quatre glycomimes, M1, M2, M3 et M4, présentent un cœur mannose et différents bras. M1 et M2 sont caractérisés par le même ligand rigide L1 et un ligand différent L2. M3 a le même ligand L2 que M2 mais un autre ligand

L1. M4 présente les mêmes cœur et bras que M3 mais ses bras se terminent par un glucose à la place du galactose. Cette molécule n'interagit pas avec la lectine car le glucose n'est pas reconnu par la lectine. Trois autres glycomimes ont été étudiés : C1, P1 et D1. C1 et P1 présentent les mêmes bras semi-flexibles et un cœur différent. Le cœur de C1 est un calix[4]arène et celle de P1 est une molécule de porphyrine. Le dernier glycomime D1 est un contrôle négatif car il ne présente pas de galactose, mais du mannose, donc il n'a pas d'affinité pour la lectine. C'est une molécule linéaire où l'unité principale est répétée trois fois. Les glycomime étudiés sont résumés dans le tableau ci dessous.
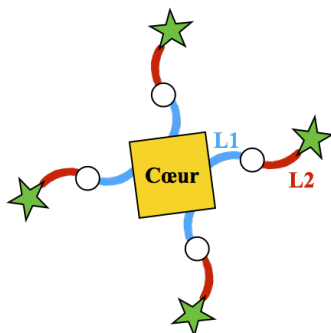
Nomenclature	Structure	K_d [nM]	n
M1	Man(proTzEG$_3$-Gal)$_4$	11000	0.28
M2	Man(proTzAcNPh-Gal)$_4$	194	0.46
M3	Man(EG$_2$MTzAcNPh-Gal)$_4$	157	0.52
M4	Man(EG$_2$MTzAcNPh-Glc)$_4$	n.a.	n.a.
P1	Porphyrine(OMTzEG$_3$Gal)$_4$	330	0.46
C1	Calix[4]arène(OMTzEG$_3$Gal)$_4$	170	0.24
D1	(DMCH-MTzEG$_3$-Man)$_3$	n.a.	n.a.

Schéma des glycomimes étudiés et leurs propriétés.

Pro = $CH_2CH_2CH_3$; Tz = $C_2H_3N_3$; EG_n= $(CH_2CH_2O)_n$; Ac = $COCH_2$; M = CH_2; Ph = phényl, DMCH = diméthanolcyclohexane; Gal = galactose; Glc = glucose ; Man = mannose.

1.1 Introduction

The necessity of alternative therapeutic treatments for helping cystic fibrosis patients, and in general immune-compromised people, to fight against bacterial colonisation of airways has become a challenge for researchers. In particular, efforts are done against *Pseudomonas aeruginosa* (PA) bacterium, a human opportunistic pathogen. The bacterium is able to colonize diverse human tissues and organs including skin, eyes, ears, intestine, urinary tract and particularly lungs of immune-compromised people. As an old human adversary, PA has developed strategy to thwart host defences. Among them, its ability to develop biofilms within the mucus layer protecting epithelium, give to the bacteria a selective advantage against antibiotic therapies leading to the bad prognosis of cystic fibrosis patients. PA takes advantage of a large arsenal of virulence factors including two soluble lectins, LecA and LecB. Based on mimetic strategy these two lectins are believed to be potential therapeutic targets due to their role in cell recognition and biofilm formation [14]. A promising strategy for developing a new therapeutic approach against PA is related to the design of synthetic molecules, highly affine to the lectins and able to compete *in vivo* with their natural ligands. Galactosylated-glycoclusters were shown to be selective high affine LecA ligands [18,19] due to their multivalency [20]. Recently, their therapeutic use as anti-bacterial molecules has been demonstrated in animal models and represents a promising strategy against such bacterial infections [24].

In this Chapter, the biological problem will be presented by a brief portrayal of *Pseudomonas aeruginosa* and how it can infect host tissues by the description of airways colonization in the case of cystic fibrosis patients. The major pathogenic weapons used by the bacteria will also be described. Then, the design, the properties and capabilities of glycoclusters as a new therapeutic approach against the bacteria are illustrated. Finally, the theory of protein-carbohydrate interaction will be detailed, focusing on the possible multivalent nature of the binding.

1.1 *Pseudomonas aeruginosa*

Pseudomonas aeruginosa (PA) is a Gram-negative bacterium with a rod shape of 1.5 μm long and 0.5-1 μm wide and a polar flagellum. Its high ability of surviving in a wide range of temperatures and its adaptability to live in aerobic and anaerobic conditions make possible to find the bacterium in different environments such as oil, water, sewage, animals, humans, plants and hospitals. Due to that, and to its constant exposition to various antimicrobials over time, PA has accumulated mutations that help to induce chronic infection and to convey antibiotic resistance [26]. In fact, PA is defined as a human opportunistic pathogen since it is able to chronically infect immuno-compromised tissues. PA is the cause of 10-30% of nosocomial infections in hospitals, it can provoke, for example, urinary and bronchial infections in healty people, serious infections on the skin if burns are present, etc. Also, it is one of the main responsible of cystic fibrosis (CF) patients death due to pulmonary insufficiency [27].

1.1.1 *Pseudomonas aeruginosa* infections: the case of cystic fibrosis

Cystic fibrosis (CF), is a life-threatening genetic disease [28] that primarily affects the digestive and lung systems, which become obstructed by a thick sticky mucus. The feature of CF and its severity vary among the affected individuals [29]. It is a recessive disease that cannot be prevented before the birth, since it is due to the probability of both parents to be unaffected carriers of the syndrome.

The syndrome is caused by the mutation of the CFTR (Cystic Fibrosis Transmembrane conductance Regulator) gene. Adults with CF experience health problems affecting the respiratory, digestive, and also reproductive systems [29]. There are more than 1500 possible mutations of this gene and the most common is the ΔF508[1]. CFTR is responsible of the codification of the cystic fibrosis transmembrane conductance regulator protein that operates as an ion channel across the membrane of cells. The channel is responsible for the transport of chloride and sodium ions inside and outside the cells. Chloride ions help to control the movement of water in tissues needed to the production of thin, freely flowing mucus. Sodium ions are necessary for the normal function of organs such as the lungs and pancreas [29]. The mutation causes the formation of a thick and sticky mucous that leads to the obstruction of the lungs and the pancreas.

Basically, mucus is a slippery substance that lubricates and protects the inner surfaces of the airways, digestive system, reproductive system, and other organs and tissues [29]. It is mainly constituted by mucins, which are highly glycosylated glycoproteins that have the ability to form gels; therefore they are the main component of gel-like secretions, such as mucus. In healthy people, the mucus entraps bacteria and is eliminated by cilia beat, ensuring the clearance of the epithelial cells, thus preventing the infection. However, for people who are affected by CF, the produced mucus is thick and sticky, thus it can obstruct the lungs and impede the cilia movement by facilitating bacterial infections. In fact, the defect in the CFTR channel leads to low hydration that is responsible of the increased viscosity of the mucus in CF patients. Therefore, the different nature of the mucus layer facilitates the formation of bacteria clusters, the accumulation of Quorum Sensing[2] molecules [30], the increasing of bacterial binding to the epithelium and the decreasing bacterial clearance via immune mechanisms [31].

Thus, CF patients are easily infected by different kind of bacteria. The bacterial infection is patient's age-dependent and most of the time it is due to PA, and/or *Staphylococcus aureus* and *Haemophilus influenza*. With time, the infections become chronicles by causing fibrosis (lung damages such as formation of scar tissue) and cysts (an abnormal cluster of cells forming a sac that grows differently from the neighbour cells and can contain air, liquid or matter) in the lungs [29]. In adults suffering CF, PA is present in up to 80% of the population and represents the principal cause of chronic infections. In fact, once the airways are colonized, the bacteria cannot be eradicated [26].

---

[1]ΔF508: Mutation (Δ) of three nucleotides that codifies the phenylalanine (F) at the position 508 on chromosome 7.
[2] *Quorum Sensing* is the mechanism that allows the regulation of the bacterial community life. It relates the bacterial density to the expression of specific genes associated to environmental essentials functions. Basically, it can be defined as a bacterial signal based on the production of small molecules (autoinducers) that are produced during bacterial growth.

The bacterial load can only be reduced mostly via inhaled antibiotics that help the improvement of patient's life quality. However, due to the fact that PA has the ability to form biofilms, it is difficult, or even impossible, to eradicate it with standard antibiotic treatments [31].

As it is a genetic disease, there is no prevention or final treatment for CF. All the possible cures are focused on increasing the life quality of patients, by making the condition easier to live with [32]. Currently, the possible remedies depend on the stage of the infection and are mainly characterized by antibiotics, physiotherapy and bronchodilators. Also, genetic and pharmacological therapies have been developed. The formers are based on the introduction of the CFTR gene to correct the chloride channel, while the latters provide the correction and bypass of abnormal CFTR genes [33].

1.1.2 Virulence Factors

PA has an arsenal of virulence factors that are responsible of the malfunctioning of the host defences and thus allow the adhesion, colonization and invasion of the host (infection process). The variety of virulence factors determines the wide range of infections in which the bacteria is involved. The virulence factors of PA can be mainly divided in extracellular (secreted) virulence and cell-associated virulence factors. Extracellular virulence factors are, for example, exotoxin A, elastases (LasB and LasA), alkaline protease, type III secretion system effector molecules, and pyocyanin; while cell-associated virulence factors include the flagellum, type IV pili, exopolysaccharide (EPS), and lipopolysaccharide [34].
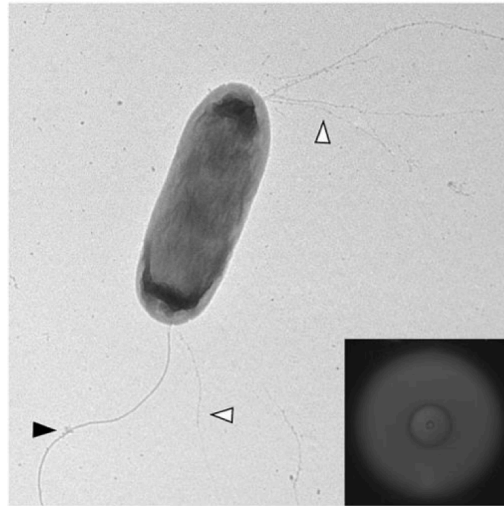
Figure 1.1: TEM image of wild-type PA bacterium. The black arrow indicates the flagella while white arrows show the position of pili type IV. Taken from [35].

The different virulence factors contribute to the different steps of the infection process, and some of them are involved in the formation of a biofilm structure. The biofilm is a complex and highly structured bacterial community surrounded by the extracellular matrix. It constitutes a protected mode of growth, which increases the bacteria defences against the immune response system of the host and allow bacterial surviving in a hostile environment [36]. Furthermore, this mode of growth gives a selective advantage to the bacteria toward many antibiotics [37]. The formation of the

biofilm occurs progressively. Firstly, the bacteria attach on the surface in a reversible way. Then, the attachment becomes irreversible and the biofilm starts to grow. In this maturation stage, the extracellular matrix is produced; the bacteria multiply and form microcolonies. Finally, some bacteria can detach from the biofilm matrix and colonize other areas of the host surface.

In the following, some of the virulence factors involved in the PA infection process will be described.

1.1.2.1 Flagella

Prokaryotes that move in liquid media produces long protein-based, flexible protrusions called flagella. PA presents a single polar flagellum (Figure 1.1, black arrow), which synthesis and function involves 50 genes. It is made by multiple proteins, in particular FliC, which is found in the filament and FliD, the flagellar cap protein.

The flagellum plays an important role, since [38]:

  i)   It is implicated in the motility allowing the bacteria to spread around the respiratory tract;
  ii)   It provides chemotaxis[3], therefore the movements is directed towards preferred substrates;
  iii)   It is involved in the acquisition of nutrients;
  iv)   It provides a ligand for clearance by phagocytic cells.

The flagellum represents a virulence factor, since it is involved in the establishment of respiratory tract infection. In fact, not only its motility function is critical for virulence, but also it acts as adhesins, probably interacting with GM1[4] glycoclipids of the host membrane, as shown by *in vitro* assays [39]. Furthermore, FliD, the cap protein of the flagellum, has been shown to link to glycosylated structure (Lewis X and sialyl-Lewis X) exposed on mucins [40]. Therefore, it is implicated in the attachment of the bacteria to the host and may act as a tether in the initial steps of the infection.

It is mainly produced by nosocomial strains. In fact, PA bacteria isolated from early colonisations of CF patients are highly motile and express the flagella, while strains isolated from chronicle CF infections are no motile and lack the expression of such organelles [41]. The lost of the capability of expressing the flagella may give a survival advantage in chronic infections as well as avoid phagocytosis [41]. Therefore, flagella play a crucial role in early stage of colonization but are not essential for bacteria survival.

1.1.2.1 Pili

Pili are protein-based hair-like appendages present on the bacteria outer membrane. Pili from PA are antigenetically diverse [38]. In general, they are necessary for attachment and motility on the surface, being therefore an important virulence factor for the bacteria.

---

[3] Chemotaxis is a movement in response to a chemical stimulus.
[4] GM1 = (monosialotetrahexosylganglioside) is a molecule composed by ceramide, oligosaccharides and one sialic acid residue linked on the sugar chain.

In particular, pili from PA are pili type IV (Figure 1.1, white arrows). They are semi-flexible rodlike fibres formed by the association of some proteins and thousands subunits called pilin, which interact weakly one to each other, giving origin to a helical structure [10]. Pili type IV are required for "twitching motility" which is a form of gliding (movement of the bacteria on a solid surface without the flagella) necessary for biofilm formation [42,43]. They are cell-associated structures that not only allow the bacteria to adhere on the host cell but also allow the bacteria to climb the biofilm formed by other bacteria and colonize the top of that, developing a mushroom structure characteristic of PA [34].

PA bacteria present also another type of pili structures called Cup that are also involved in biofilm formation. These structures consist of an outer membrane protein (usher), two periplasmic proteins (chaperones) and the fimbrial subunit [34]. It has been demonstrated that the Cup structures are implicated in the biofilm formation, since they contribute to the bacterial attachment to abiotic surfaces and their absence destabilize the biofilm development [34].

1.1.2.2 Soluble lectins: the LecA lectin

Lectins are defined as "sugar-binding proteins or glycoproteins of non-immune origin which are devoid of enzymatic activity towards sugars to which they bind and do not require free glycosidic hydroxyl groups on these sugars for their bindings" [44].

This means that lectins are proteins capable of specifically binding to some monosaccharide moieties via non-covalent interactions, without modifying the structure of the molecule. They do not have enzymatic activity and they are not synthetized as an immune response. Lectins can belong either to animal, plants, bacterial and virus kingdoms. They have numerous biological functions, depending on the species from which they belong to. For example, lectins can be involved in cell recognition, especially in virus and bacterial adhesions to the host membrane, due to the specific interaction with the carbohydrates present on the host membrane. In plants instead, lectins are probably involved in the defence and they are mainly found in seeds [45].

In the case of PA, the bacteria present two Quorum Sensing dependent soluble lectins, LecA (gene *lecA*) and LecB (gene *lecB*). The localization and properties of the two lectins make them important features of the bacteria-ambient relation [15]. LecA lectin specifically binds galactose moieties with a medium affinity (K_a = 3.4 x 10^4 M^{-1}), while LecB specifically interacts with fucose with high affinity (K_a = 1.6 x 10^6 M^{-1}) [15]. Both lectins have been identified on bacteria cytoplasm and in small amount on the cytoplasmic membrane, periplasmic space and outer membrane [46]. In particular, intracellular level of LecA has been found to be generally higher than that of LecB and the maximal activity of the two lectins has been registered during bacterial phase state [46].

The two lectins represent virulence factors. They are likely to be involved in bacterial adhesion since both are able to selectively recognize and bind the epitopes of the glycoproteins and glycolipids present on the host cell [24]. Also, they seems to be involved in biofilm formation due to their contribution to the architecture of the lipopolysaccharide-based bacterial envelope [47]. Moreover, studies made on LecA [48] and LecB [49] show the possible implication of the two

lectins in biofilm formation. Additionally, *in vitro* and *in vivo* assays show that there exists a relation between the two lectins and the pathogenicity of PA bacteria [16]. In particular, it has been demonstrated that LecA lectin is a cytotoxic factor for respiratory epithelial cells in primary culture [50] and acts as an invasin to penetrate host cells [51]. Also, they are virulence factors that in cooperation with other virulence factors can lead to cell death. For example, it has been shown that the combination of LecA and exotoxin A, which is one of the toxins produced by the bacterium, lead to a high rate of cell mortality, while the two factors alone did not have the same effect [52]. Therefore, the two lectins seem to be perfect targeting molecules for new therapeutic approaches against PA, capable of inhibiting their activity by taking advantage of their selectivity and multivalency [24]. For this, we have focused our attention on the LecA lectin as possible target molecule of a new therapeutic approach able to destabilize the activity of PA bacteria.

LecA (Figure 1.2a) is a multivalent lectin characterized by four identical subunits of 121 aminoacids (12.75 kDa) that form a tetrameric structure [17]. This means that the lectin is made by four identical monomers, each of them presenting a pocket (binding pocket) able to bind a galactose molecule. Crystallography has shown the specificity of the interaction between each monomer of LecA and a galactose sugar bridged by a calcium ion [53,54] (Figure 1.2b). In fact, crystals show the presence of both the calcium ion and the galactose in the same binding pocket [54]. The interaction with the galactose is quite weak and it involves hydrogen bonding with three different regions of the protein and hydrophobic contributions [15,54]. Different groups of the binding site of the lectin are involved in the binding of galactose, such as the Aspartate 100 (Asp100) and the Tyrosine36 (Tyr36) (Figure 1.2b) [54]. Due to its high selectivity, the interaction with other molecules is not possible. The only exception is made for N-acetyl-D-galactosamine, even tough with less affinity [54].
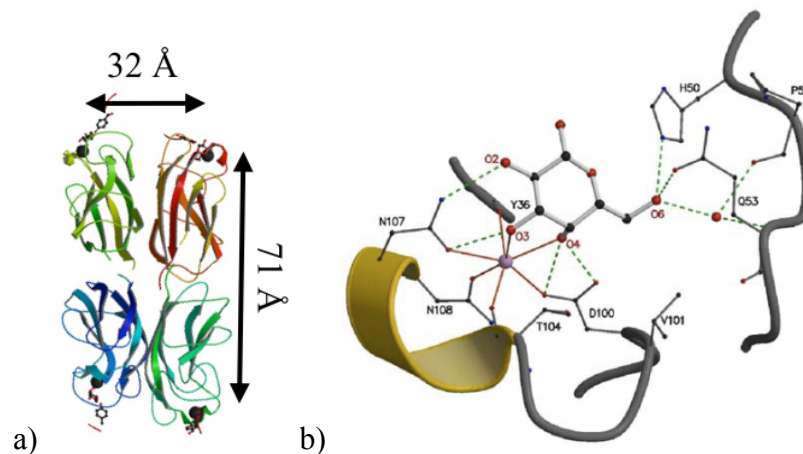
Figure 1.2: a) Crystal structure of LecA complex with GalA-QRS at 2.31 Å resolution (4LKD) [55]*; dimensions are 32 X 71 X 19 Å. b) View of the calcium and galactose binding site in the crystal structure from* [15]*.*

Blanchard et al. [17] have shown that Gb3 (αGal1-4βGal1-4βGlc-1Cer) seems to be the natural ligand of LecA. The ceramides (Cer) are molecules highly present on the cell membrane, and with the epitope αGal1-3βGal1-3Glc are highly expressed in erythrocytes and epithelial cells of mammals. Moreover, *in vivo* and *in vitro* studies have demonstrated the LecA capability of

targeting cells presenting this glycolipid, which is presumably involved in the binding. Also, the interaction of the Gb3 isomer iGb3 (αGal1-3βGal1-4βGlc-1Cer) has been studied. This last interaction is the highest affine even though the presence of the isomer in cells is not clear.

1.1.2.3 Other virulence factors

Other virulence factors related to the biofilm development are the ones that contribute to the extracellular matrix or EPS, such as the polysaccharides alginate, Psl and Pel that lead to the chronic infection [56,57], nucleic acids and proteins. The EPS is associated with the architecture of the biofilm and may contribute to its strength and material properties.

Alginate is a capsular polysaccharide that confers a selective advantage for PA in CF airways [56]. Studies have demonstrated that the presence of alginate is not mandatory for biofilm formation, but is related to resistance properties of the biofilm itself. The overproduction of alginate determines a mutation of PA bacteria from the wild-type to mucoid strains that has been only found in chronicle infections of CF airways. This switch is associated with the overproduction of alginate and, as a consequence, mortality increases [56]. Basically, this conversion provides more protection to the bacteria, increases resistances and allows the biofilm development. In fact, the mucoid phenotype is protected from dehydration, it is more resistant to antibiotics, phagocytosis and digestion [58].

Psl is a polysaccharide, rich in mannose and galactose, required for the adhesion on mucins and epithelial cells: it works as a scaffold holding cells together in the biofilm matrix [56]. Pel is a glucose-rich polysaccharide polymer necessary for the biofilm structure [56]. They are believed to participate to the first phase of biofilm development, even though their role in virulence is under examination. However, polysaccharides do not exist alone in biofilms, but they may interact with a wide range of other molecular species, including lectins, proteins, lipids, etc. [59].

Moreover lipopolysaccharide (LPS) structures are present on the outer-membrane of the bacteria. LPS consists of a hydrophobic lipid A region, a polysaccharide core and the O-specific chain. Changes in LPS molecules are thought to contribute to biofilm formation. In general, these molecules mediate interactions with the environment and are important factors for the structure of individual bacterial cells.

1.2 Glycoconjugates as a new therapeutic approach against *Pseudomonas aeruginosa*

Glycoconjugates are scaffolds characterized by carbohydrates molecules covalently linked to biomolecules, such as lipids or proteins. Natural and synthetic glycoconjugates are good candidates to interfere in bacteria, fungi and viruses infection processes. In the case of PA bacteria, they can inhibit the activity of the lectins, such as LecA, thus destabilizing the biofilm development. There are many examples of applications of glycoconjugates as inhibition systems or as vaccine; the review of Imberty and co-workers presents most of them [53].

Different multivalent architectures have been used to synthetize the glycoconjugates, depending on the application and the target [60]. In general, they are characterized by a scaffold (core), at which spacers (branches) terminated with the useful carbohydrate unit (terminal group) are bounded. Variation in the core and spacer chemistry may influence the properties of the target molecule leading to molecules with specific biological properties [60]. In fact, the nature of the core establishes the number of branches, their spatial disposition and the distance between them, while the spacer's length and rigidity are two crucial factors to obtain a potent inhibition macromolecule, maintaining its solubility [21]. Different molecules have been used as core, such as polymeric molecules, carbohydrates, protein, etc. Two reviews that explore the nature of the core and the chemistry used to attach the branches are the references [60,61]. In general, among different techniques, the most powerful and efficient ligation methodology, for covalent assembly of the glycoconjugates, is the copper(I)-catalysed azide-alkyne cycloaddition approach (CuAAc, ''click chemistry'') [61]. It is an efficient and reliable method that allows working in a wide range of reaction conditions [60,61].

A large variety of glycoconjugates have been synthetized. They are characterized by various shapes and a valence that most of the time is higher than the one of the target. In the following, an overview of the most typical structures will be presented and particular attention will be given to glycoclusters, as subject of this study.

1.2.1 Different type of glycoconjugates

In Figure 1.3 different multivalent glycoconjugates structures are represented.

Glycocluster **Glycodendrimer** **Glycopolymer**

Glyconanoparticle **Neoglycoprotein**
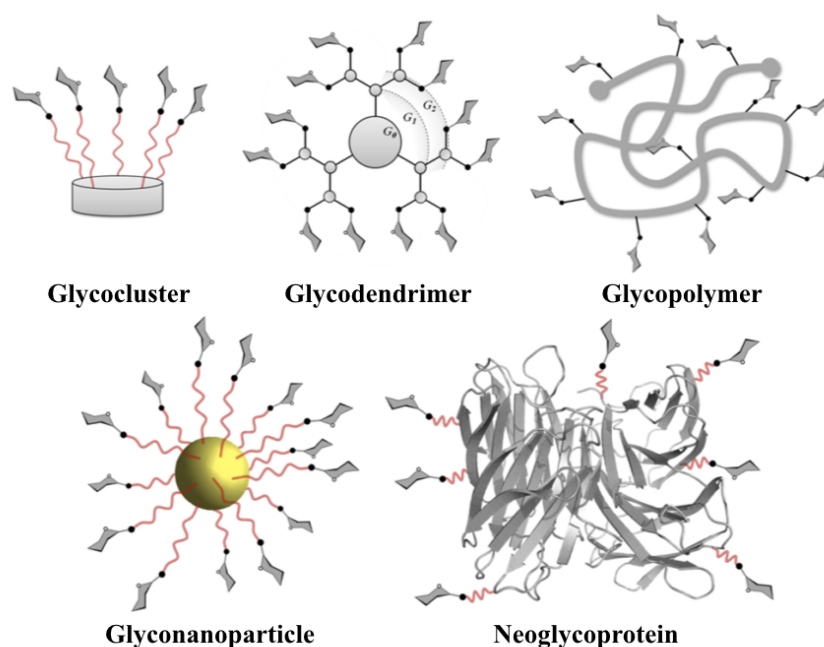
Figure 1.3: Types of glycoconjugates. Taken from [19].

Glycodendrimers are molecules with a well-defined symmetry. The centre of a dendrimer is characterized by a core to which are attached layers of "dendrimer repeating units", to form a

sphere that presents on the exterior the "terminal group" that can be recognized by the target [60]. To form the structure, one starts from the core, which is a small molecule that presents few reactive sites. The idea is to increase the number of reactive sites by adding a layer of dendrimer repeating unit to form a big sphere bearing a high number of reactive sites, where the terminal group can be bound. The resulting structure is loosely packed with a high density of binding sites. These architectures have been used to target lectins, such as LecA and LecB from PA [18,53]. Even though highly complex and symmetric dendrimers structures can be synthetized, they do not satisfy their purpose as inhibitor molecules, since they lost their biological functions [60]. In fact, the increasing valence determines an enhancement of the enthalpic contribution while the entropic one is not favoured at all, therefore there is no significant gain in free energy as well as lectin affinity [62].

Glycopolymers are long chains of repeated identical units that can be either synthetics or naturals. A wide range of molecules can serve the purpose of main unit. The size and valence of the final molecule are highly controlled [62]. Natural glycopolymers, in particular plant and polysaccharidic food additives, have been used by Zinger-Yosovich and Giloboa-Garber to study their inhibition properties against LecA and LecB lectins from PA and other two lectins (CV-IIL and RS-IIL) from two bacterial pathogens *Chromobacterium violaceum* and *Ralstonia solanacearum*, respectively [63]. In particular, they have shown that food additives such as locust-bean gum are highly effective as inhibitors of LecA lectin. In general, food additives are useful for curing external and gastrointestinal infections due to their nontoxicity and non-digestibility [63].

Glyconanoparticles technology has shown promising capabilities for anti-adhesive applications. Basically gold nanoparticles are chemically modified to present carbohydrate molecules in a globular conformation [62]. In particular, Reynolds et al. [64] have synthetized and characterized gold nanoparticles presenting galactose moieties able to target LecA. They have shown that this configuration allows increasing the binding affinity of almost 3000-fold with respect to the monovalent reference target: their glyconanoparticle has a $K_d = 50$ nM, the most effective LecA ligand up to now. Also, they underline the importance of the architecture showing that the ligand presentation influences the enhancement of the enthalpic contributions while the high density helps decreasing the entropy of the system.

Neoglycoproteins are structures characterized by a protein as multivalent scaffold [62]. Despite of their biocompatibility, it is difficult to control the number and disposition of carbohydrate binding sites on the complex, as well as the valence. The structures are quite complicated and special care has to be taken to avoid denaturation of the protein [62].

1.2.2 Glycoclusters

Glycoclusters are small clusters characterized by a small scaffold where a limited number of carbohydrate residues can be bound [19]. The final structures are generally dimers, trimers, tetramers etc. It can be more or less flexible and bring different functionalities. Different kind of glycoclusters have been synthetized and they have proved to be very efficient in relation to an enhanced cluster glycoside effect (section 1.3.2) [62]. In fact, due to the small size of the structure,

the interaction of the carbohydrate residues of the glycocluster with the binding pockets of different lectins are facilitated, rather than the interaction with different binding pockets of the same lectin. This may be associated to a situation where the linker is too short and the system pays an enthalpic penalty instead of undergoing to conformational changes [62]. Therefore, this situation leads to the formation of aggregates.

Glycoclusters have been used to target viruses and bacteria since they are able to compete and prevent the adhesion of such organisms on host cells [53]. For example, Marotte et al. [65] tested dimer and trimer glycoclusters against LecB lectin from PA. They tested various dimeric and trimeric structures with different geometries and lengths showing that dimeric structures bind LecB more efficiently than trimeric compounds, exhibiting cluster effect, strong affinity and low dissociation constant. Among the molecules they studied, the best affinity was given by a dimer glycocluster presenting a dissociation constant of $K_d = 90$ nM.

1.3 Protein-carbohydrate interactions as the cornerstone of many biological processes

Infection strategies used by pathogens involve highly specific protein-carbohydrate interactions [66]. In general, protein-carbohydrate interactions are referred as receptor-ligand interactions. The receptor is a protein with a pocket on its surface and the carbohydrate ligand is the molecular entity that fits into that pocket: the receptor is the lock and the ligand is the key [67].

These protein-carbohydrate interactions are generally weak (K_d in the micromolar range) but they can be enhanced if multiple interactions occur at the same time. Thus, both the receptor and the ligand can have a multivalent nature: the protein can present more than one Carbohydrate Recognition Domain (CRD), and/or the ligand can be synthesised with multiple carbohydrates kept together by linkers. This multivalent presentation helps increasing the strength of the binding, thanks to the so-called "cluster glycoside effect" [20].

To this class belongs the interaction of LecA lectin. In fact, the lectin has a multivalent structure since present four CRDs, while the carbohydrate can be multivalent, or if monovalent it can form clusters on the cell membrane [64]. Therefore, the development of synthetic multivalent ligands, the glycoconjugates, able to compete with the natural ligand of LecA can find applications in biomedicine. In particular, a new therapeutic approach for the inhibition of PA bacteria can be developed. In principle, the inhibition of LecA lectin can be possible by the competition between its natural ligand and these synthetized polyvalent molecules that present higher affinity for the lectin. The design of the glycoconjugates and the type of interactions that can be established with the lectin play a crucial role in the inhibition. Different examples of the power of synthetic multivalent ligands as powerful tools in cell interactions have been reviewed by Kiessling et al. [68].
In the following, the multivalency, the cluster glycoside effect and the thermodynamic of the protein-carbohydrate interaction will be detailed.

1.3.1 Multivalency

The valence of a molecule/atom is defined as the number of different identical connections that it can form with its binding partner(s) [62,67], forming a receptor-ligand interaction. For example, given a molecule with n binding sites ($n \geq 1$) and given its corresponding partner(s), the molecule is able to form n binds with the partner(s) (Figure 1.4) [62].

In biological systems, receptor-ligand interactions are mainly characterized by non-covalent bindings, such as hydrogen bonding and Van der Waals interactions. These interactions are quite weak, but they can be enhanced if multiple bindings occur. In fact, multiple interactions show increased strength compared to the corresponding monovalent binding, where affinity is most of the time weak, in the range of the micro to millimolar [60]. In the case of multiple interactions, the accumulated strength of the multiple affinities is called avidity. However, in this dissertation, no difference will be made between the two and hence the general term affinity will be used.
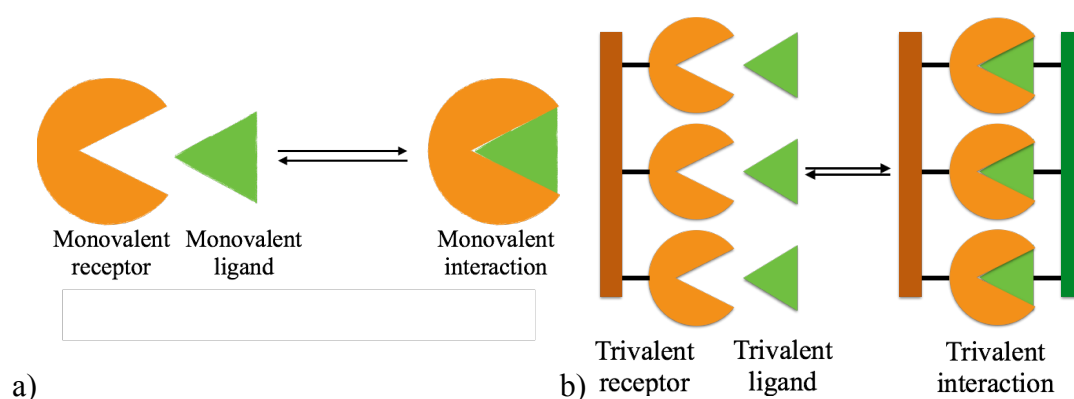
Figure 1.4: Schematic representation of the receptor (orange)-ligand (green) interaction in the case of a) monovalent receptor-ligand and b) trivalent receptor-ligand interactions [67].

The formation of the n binds can be characterised by mutually dependent or independent events. This means that, considering a receptor having $n = 2$ binding sites able to bind two monovalent ligands, if the binding of the first ligand influences the binding of the second one, by directing or impeding its formation, then the two events are dependent. The affinity of this second interaction is affected by the formation of the first one. Therefore, the affinity of the second binding can be increased or not, due to the influence of the previous interaction. In this case, the binding is considered "cooperative". However, the two events can be independent one from the other if the binding of the second ligand is not affected by the previous one. Thus, the strength of this second interaction is not influenced. Therefore, the affinity is enhanced thanks to the "multivalent" association.

Depending on the nature of the ligand and the receptor and also on the environment and/or their functions [62], different kinds of multivalent associations are possible (Figure 1.5). For example, a multiple receptor and a multiple ligand will give origin to several 2D or 3D possible interactions that are related to the competition between different binding mechanisms associated to different equilibrium states [19].
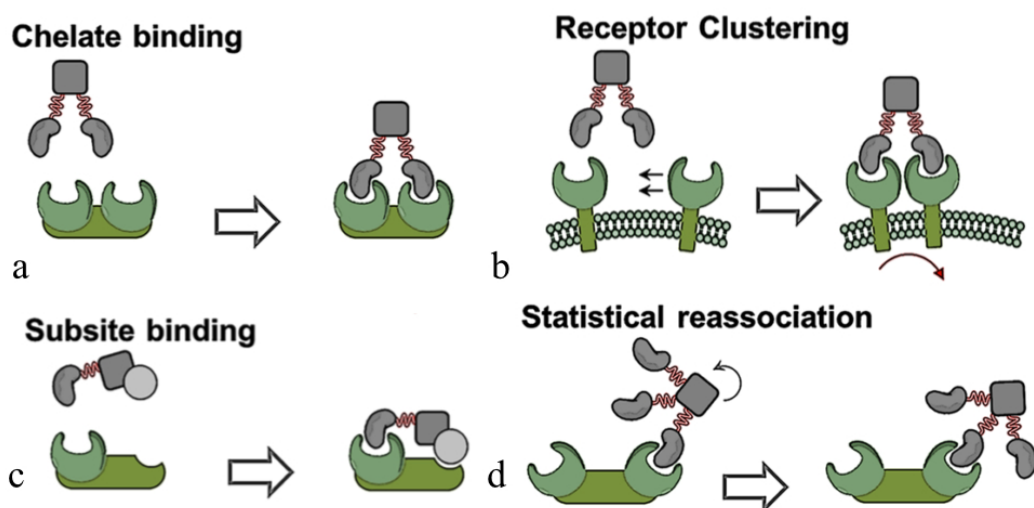
Figure 1.5: Mechanisms of non-aggregative interaction between a multivalent ligand and a multivalent receptor. Taken from [19].

In particular, the binding between a multivalent receptor and its multivalent ligand can give rise to a **chelate association** (Figure 1.5a). The chelate interaction is the most studied, since it allows increasing exponentially the affinity. It is the so-called "cluster glycoside effect". If the lectin or its ligand is monovalent and it is anchored to the cell membrane, then **receptor-clustering** (Figure 1.5b) can occur. In this case, the receptor diffuses along the membrane in order to form a cluster via multivalent interaction. Another possibility of multivalent interaction is the **substitute binding** (Figure 1.5c). For this mechanism, the receptor presents two different binding sites with different affinities. Therefore, the binding of the lower affinity site is driven by the interaction of the other one, if the correspondent receptor is in close proximity. Lastly, **statistical reassociation** (Figure 1.5d) can happen if a multivalent receptor interacts with a monovalent ligand. The improvement of the affinity can be achieved by a reassociation where the binding site is surrounded by a higher density of ligands. In this latter case, the affinity is linearly increased.

When intermolecular and intramolecular interactions take place, aggregates can be formed giving rise to 2D or 3D reticular structures (Figure 1.6). Basically, there are mainly two possible ways of interactions that lead to the aggregate formation. In **type 1 reticulation**, a linear chain is formed by the interaction of one receptor with two ligands and vice versa. In general, these complexes are soluble and due to their flexibility they have a high degree of polymorphism [69]. The **type 2 reticulation** can instead give rise to 2D or 3D aggregates where the receptor or the ligand has a valence $n > 2$. These complexes can be insoluble and precipitate.
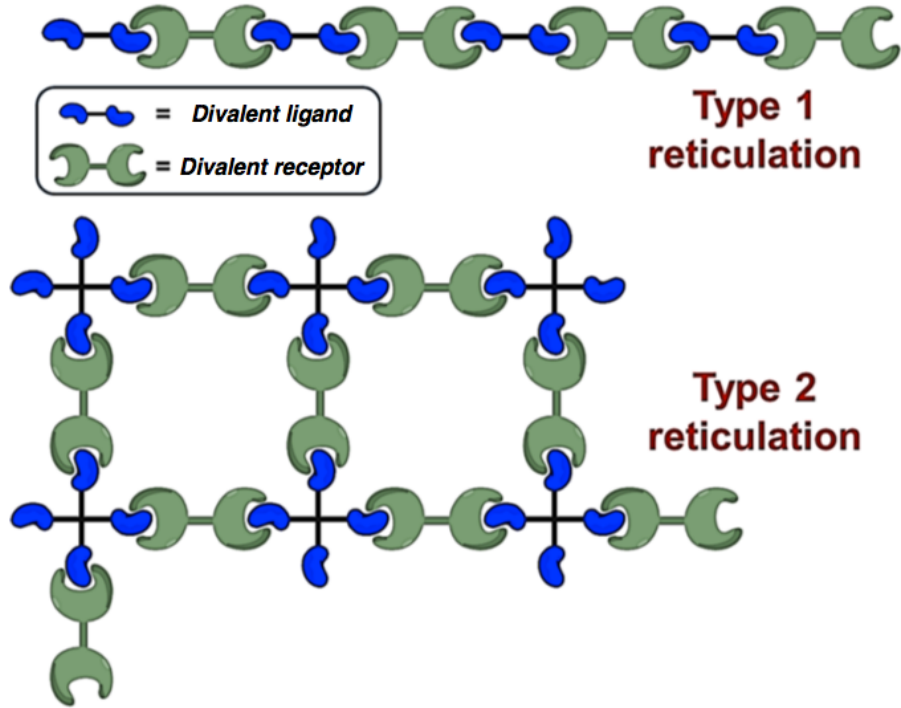
Figure 1.6: Aggregative multivalent ligand-receptor interactions. Adapted from [19].

1.3.2 The cluster glycoside effect

The concept of "cluster glycoside effect" was first presented by Lee and co-workers in 1995 and stands for the improvement in affinity of a lectin-carbohydrate complex by the multivalent presentation of the lectin and/or the carbohydrate [20]. This effect is often present in biological systems. It allows increasing exponentially the strength of the interaction of a weak bond by increasing the number of independent bonds involved in the binding. Therefore, the global interaction becomes stronger than the correspondent monovalent [62].

1.3.3 Thermodynamic and dynamic constants

Given a chemical reaction, it is possible to identify dynamic and equilibrium constants that describe the tendency of product formation or dissociation. In this case, the interaction between the receptor (*R*) and the ligand (*L*) forms the complex *RL* and it can be written as:

$$R + L \rightleftarrows RL \qquad (0.1).$$

From a microscopic point of view, the affinity of the ligand to the receptor can be associated to the rapidity of formation of the receptor-ligand complex, and on the slowness of complex dissociation. Therefore, the reaction rate can be defined as the speed of the reaction. In particular, the speed of the *RL* formation can be described with the on-rate constant k_{on}[M*s^{-1}] while the dissociation of the *RL* complex into *R* and *L* can be defined starting from the off-rate constant k_{off}[s^{-1}].

The off-rate constant k_{off} defines the speed of the backward reaction that allows forming the reactants (in the case of a receptor-ligand interaction, the reactants will be the receptor and the ligand separated) starting from the product (the receptor-ligand complex).

It is possible to relate the dynamic constants to the equilibrium state, therefore defining equilibrium constants for the reaction. In particular, once the reaction has reached the equilibrium, the tendency of the reagents (R and L) to form the complex (RL) can be expressed by the association constant (K_a); while the propensity of the LR complex to dissociate into R and L is given by the dissociation constant (K_d). K_a is expressed as the inverse of a concentration and its unit in the SI is [M^{-1}]. It is given by:

$$K_a = \frac{1}{K_d} = \frac{[RL]}{[R][L]} = \frac{k_{on}}{k_{off}} \tag{0.2}.$$

K_d is inversely proportional to the association constant and is expressed in [M]. Basically, higher the K_d is, higher is the tendency of the complex to dissociate, and thus worst is the affinity.

1.3.4 Thermodynamic aspects of protein-carbohydrate interaction

Kinetic parameters described above allow the quantification of thermodynamic quantities such as the Gibbs free energy ΔG, which is related to the spontaneity of the reaction. In general, for a receptor-ligand interaction, ΔG is associated to the affinity of the interaction (association constant, K_a) by:

$$\Delta G = -RT \ln K_a \tag{0.3}$$

where T is the temperature of the system and R is the gas constant.
If ΔG is smaller than zero ($\Delta G < 0$), than the creation of the reaction products (RL, equation (0.1)) is favoured, otherwise ($\Delta G > 0$) the tendency will be the dissociation in the corresponding reagents (R and L). In the case in which $\Delta G = 0$, the equilibrium is obtained.

The linear relation

$$\Delta G = \Delta H - T\Delta S \tag{0.4}$$

relates the change in Gibbs free energy to the changes in enthalpy (ΔH) and in entropy (ΔS).
In particular, the enthalpic contribution can be written as the sum of:

    i)   The enthalpy changes of the formation of the complex RL (ΔH_{RL});
    ii)   The variation in enthalpy due to conformational changes thanks to the binding (ΔH_{conf});
    iii)   The contribution of the solvent in the interaction (ΔH_{sol}).
Therefore, ΔH can be expressed as:

$$\Delta H = \Delta H_{RL} + \Delta H_{conf} + \Delta H_{sol} \tag{0.5}.$$

In the case of a protein-carbohydrate interaction, ΔH_{RL} would be due to the formation of hydrogen bonds, Van der Waals interactions between groups of the protein and the ones of the carbohydrate,

as well as the possible coordination bond via metal ions. The rotation of hydroxyl groups, to maximize the formation of hydrogen bonds, would contribute to ΔH_{conf}; while the formation/rupture of hydrogen bonds between the molecules of the protein and/or the carbohydrate and the solvent will influence ΔH_{sol} [62].

The entropy contribution ΔS will be given by:

$$\Delta S = \Delta S_{rot} + \Delta S_{trans} + \Delta S_{conf} + \Delta S_{sol} \qquad (0.6)$$

and represents the disorder due to complex formation. In particular, it is characterized by four terms: the rotational entropy (ΔS_{rot}), which depends on the free rotation along the main axes of the molecules; the translational entropy (ΔS_{trans}) that refers to the freedom of molecules to translate along the x, y, z-axis; the conformational entropy (ΔS_{conf}), which is related to the steric hindrance, and lastly, to the change in entropy due to the interaction with the solvent (ΔS_{sol}).

In the case of the protein-carbohydrate system, the whole structure of the protein will not change much upon the interaction with the carbohydrate. Although, some specific groups close to the CRD may be no longer free to rotate, as well as the carbohydrate will undergo conformational changes due to the steric restrictions of the protein's binding pocket [62]. Finally, the interaction between solvent molecules and the ones of the binding pocket of the protein will be replaced to the ones between the carbohydrate and the CRD of the protein.

The entropy dramatically influences the multivalent interaction. In fact, after the formation of a primary receptor-ligand bond, if the spacer is outfitted to allow establishing an intramolecular linker between second receptor-ligand couples, then the interaction will be entropically enhanced. This happens when no additional rotational, translational and conformational costs are required [67]. The water surrounding can also contribute to the entropy. Water molecules can be released from exposed faces of the biomolecules causing an increasing of the entropy, and usually this contribution is almost the same for the polyvalent and the corresponding monovalent interactions [67].

For example, considering the case of a divalent receptor and a divalent ligand, the enthalpy of the divalent interaction will be maximal with respect of the two independent monovalent ones, if both carbohydrates can fit exactly into the two CRDs. Thus, the topology of the ligand will be varied thanks to the linker. However, it is impossible to perfectly adjust the topology of the ligand to the one of the receptor. Therefore, the multivalent binding will induce a conformational change of the linker, inducing a conformational enthalpy cost, especially in the case of rigid linkers. Thus, some flexibility should be introduced within the molecule (linker). However, upon binding, an entropic cost will be paid. Consequently, an optimum compromise between enthalpic and entropic costs (in other words between rigidity and flexibility) has to be found.

In summary, both the enthalpy and the entropy of the system are influenced by the multivalent interaction, contributing to increase the Gibbs free energy. In particular, both parameters are influenced by the architecture of the ligand, since it must satisfy conformational requirements in order to enhance the energy, and so the affinity. Therefore, the linker should bring flexibility in

order to increase the fitting of the ligand in the binding pocket but, at the same time, the entropic cost should be minimized [62,67].

1.4 Glycoclusters studied in this dissertation

The different glycoclusters studied in this work have been chosen among a library of more than 150 glycoclusters [25], which have been synthetized and screened in the context of the ANR project. The aim of the project is to design, produce and characterize these glycoclusters, to find the best candidate able to target the lectin and interfere in the infection process of PA bacteria. Among all the molecules synthetized, seven of them were chosen to be studied at the nanoscale by means of Atomic Force Microscopy technique (AFM). The choice was made taking into account their affinity to the lectin and their geometry, to characterize the influence of the design on the complex formation.
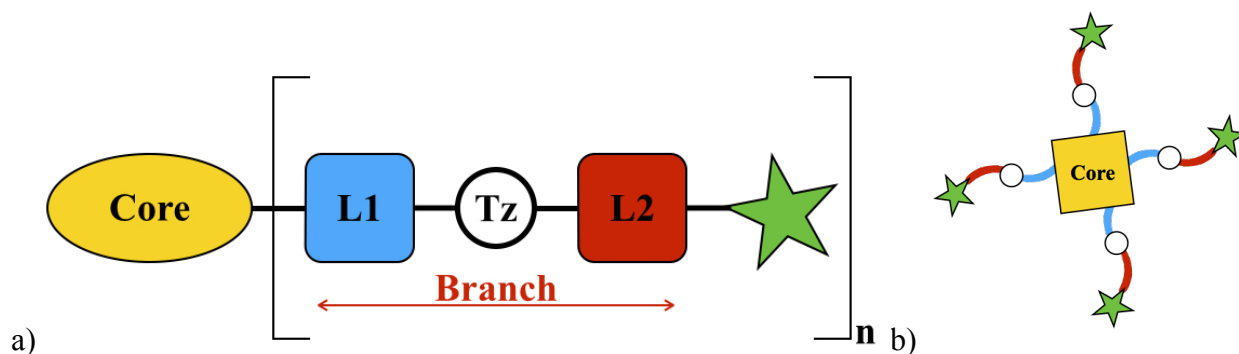
Figure 1.7: Representation of a) the general structure of the glycoclusters studied and b) its sketch.

Most of the glycoclusters (6 molecules out of 7) studied are characterized by a core and four branches ($n = 4$), as depicted in Figure 1.7a. The final shape of the structure is schematically represented in Figure 1.7b. The branch is characterized by two linkers, L1 and L2, separated by a triazole (Tz) group. The terminal group (the carbohydrate residue) is most of the time a galactose molecule (Gal), the natural ligand of LecA. The structures and their affinities are presented in Table 1.1. M1, M2 and M3 are mannose-centred glycoclusters, while P1 has a porphyrine core and C1 a calix[4]arene. Also the control glycocluster M4 present a mannose molecule as core, but the carbohydrate residue is a glucose (Glc), since it does not present a significant affinity for the lectin LecA (K_d = n.a.). A second control glycocluster (D1) has been used. Its structure is slightly different from the one of the other molecules studied (linear structure), as it has three branches ($n = 3$) and the terminal group is a mannose (Man) residue, which is not specifically recognized by the lectin.

	Structure, K_d and n	
M1	Man(proTzEG₃-Gal)₄ K_d = 11000 nM n = 0.28	
M2	Man(proTzAcNPh-Gal)₄ K_d = 194 nM n = 0.46	
M3	Man(EG₂MTzAcNPh-Gal)₄ K_d = 157 nM n = 0.52	

23
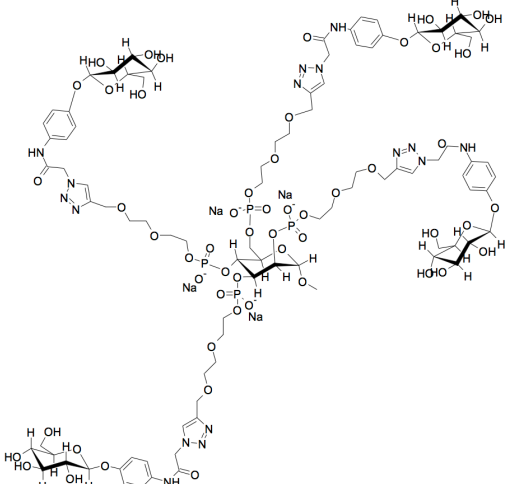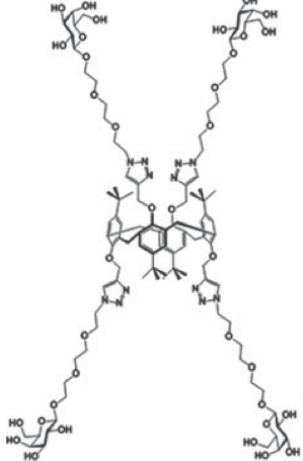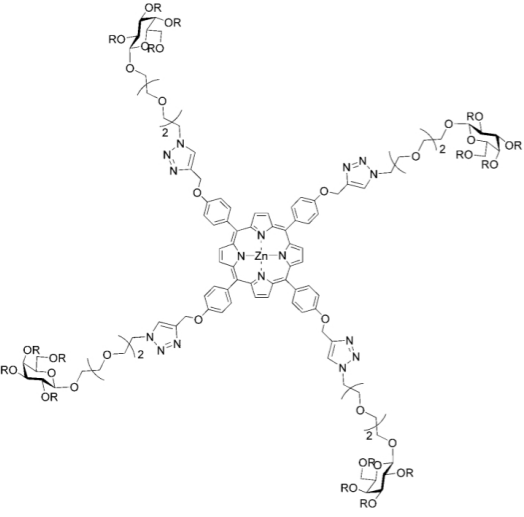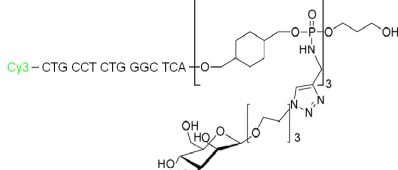
M4	Man(EG$_2$MTzAcNPh-Glc)$_4$ K_d = n.a. n = n.a.	
C1	Calix[4]arene(OMTzEG$_3$Gal)$_4$ K_d = 170 nM n = 0.24	
P1	Porphyrine(OMTzEG$_3$Gal)$_4$ K_d = 330nM n = 0.46	R = H
D1	(DMCH-MTzEG$_3$-Man)$_3$ K_d = n.a. n = n.a.	

Table 1.1: Glycoclusters studied.

1.4.1 Mannose-centred glycoclusters (M1, M2, M3 and M4)

The four mannose-centred glycoclusters (M1, M2, M3 and M4) were synthetized via "click chemistry" at the Institut des Biomolécules Max Mousseron (IBMM), University of Montpellier (France). All of them present a mostly globular form, where the branches are linked to the mannose core via a phosphate ester in positions 2 to 6. Precedent studies, aimed to find the core capable of giving the best affinity, showed that mannose is the best candidate [70].
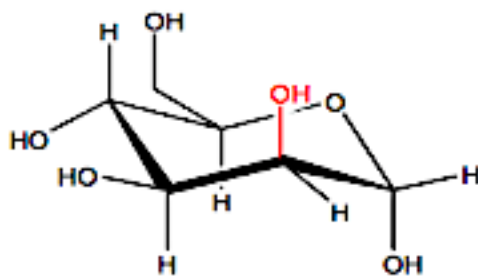
Figure 1.8: D-Mannose structure.

Therefore, the four glycoclusters differ for the linkers L1 and L2, which give more or less flexibility to the structure. In particular, M1 presents a rigid branch characterized by a propyl group (pro) as L1 and a triethyleneglycol (EG$_3$) flexible L2. This configuration gives a micromolar range affinity to the lectin, (K_d = 11000 nM) and a stoichiometry number n = 0.28, which means that each glycocluster is able to bind four lectin monomers [71]. M2 glycocluster presents a higher affinity (K_d = 194 nM) for LecA compared to M1. This is due to the presence of an aromatic group as L2 which allows the stabilization of the ligand in the binding pocket through π stacking, and also increases the rigidity of the branch [22]. The glycocluster has a stoichiometry of n = 0.46, therefore it can bind up to two lectin monomers. The affinity is slightly increased (K_d = 157 nM) for M3 glycocluster due to the presence of a more flexible L1 (EG$_2$ *vs*. pro) with respect to M2 [71]. The stoichiometry n = 0.52 allows the binding of each glycocluster with up to two lectin monomers. M2 and M3 have been used for biofilm inhibition assay, both showing an efficiency in reducing biofilm development [71].

Lastly, M4 glycocluster has the same structure than M3 but the terminal group is glucose (Glc), instead of galactose. Since there is only a paper that show the possible existence of a second binding site in the CRD of the lectin for the glucose, with an affinity that is so weak that it cannot be measured [72], we decided to use a glucose-terminated structure as a control (K_d = n.a., not available).

1.4.2 Calix[4]arene and porphyrine-centred glycoclusters (C1 and P1)

The calix[4]arene (C1) and porphyrine (P1)-centred glycoclusters [73] were synthetized via "click chemistry" by the IBMM and the ICBMS (Lyon).

Basically, a calix-arene structure is made by cylindrical oligomers formed by condensation of phenols and aldehyde groups. The complex has a 3D structure similar to a cup or a crown. The structure is hydrophobic and its dimensions depend on the number of phenol groups that form it. In the case of a calix[4]-arene, the number of phenols is 4 (indicated in square brackets) [74]. There is a great interest in these molecules since they allow forming structures with different 3D compositions. In particular, a composition 1,3-alternated has been used to form the glycocluster C1, as shown in Figure 1.9.
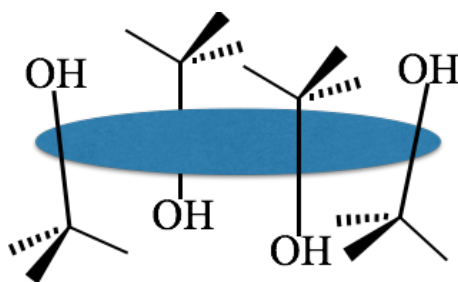
Figure 1.9: Schematic representation of the conformation of calix[4]arene 1,3 alternated structure.

The glycocluster presents galactose moieties on both faces [74]. The four branches of the glycocluster are alternated pointing upwards and downwards around the core structure. They are in perpendicular planes and the final structure is presented in Table 1.1 for C1 [75]. The branches are characterized by an O-methylene (OCH_2) linker L1 and a triethyleneglycol (L2) close to the galactose ligand. C1 glycocluster presents a high affinity for LecA (K_d = 170 nM) and a stoichiometry number of *n* = 0.24, which means that each glycocluster is able to bind four lectin monomers [73]. Due to its high affinity, C1 glycocluster has been tested on biofilm inhibition assay, cell adhesion assay and *in vivo* experiments, showing huge anti-adhesive properties [24].

Porphyrine structures are formed by the condensation of four pyrrole[5] subunits with aldehyde groups to form a planar structure [73]. To construct the P1 glycocluster, an ion of zinc (Zn) has been introduced at the centre of the porphyrine structure (Figure 1.10). The final glycocluster presents four flexible branches, the same as C1. P1 shows a good affinity for LecA (K_d = 330 nM) and a stoichiometry number on *n* = 0.46, which means that each glycocluster is able to bind two lectin monomers [73].

---

[5] Pyrrole: heterocyclic aromatic organic compound, a five-membered ring with formula C_4H_4NH.
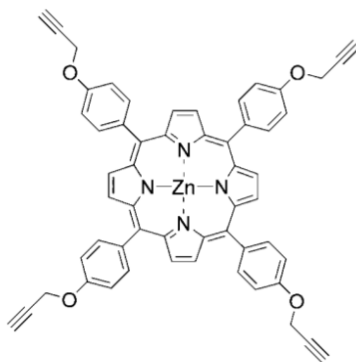
Figure 1.10: Porphyrine core. Taken from [73].

1.4.3 Control glycocluster (D1)

D1 glycocluster is characterized by a trivalent linear structure where the unit dimethanolcyclohexane (DMCH) is repeated three times and bears a flexible branch terminated with a mannose group (Table 1.1 for D1) [76]. Due to the absence of galactose residues, D1 cannot bind the lectin (K_d = n.a, not available).

1.5 Summary

In this Chapter, the biological problem has been presented. The bacterium and its lectin LecA have been described as well as the motivations behind this study. The possible therapeutic approach against PA pathogen has been described, focusing on the galactosylated-glycoclusters that can specifically target the lectin. The inhibition of LecA lectin can be possible by the competition between its natural ligand and these synthetized polyvalent molecules. This can lead to the destabilization of the infection process of PA bacteria and, in particular, perturb the biofilm formation and development.

The principles that govern the lectin-glycocluster specific interaction have been briefly detailed. The choice of glycoclusters as the agents able to target the lectin has been motivated, highlighting the fact that the design of these molecules (the core and the branches) and the type of interactions that they can establish with the lectin play a crucial role in the inhibition. Also, the glycoclusters used in this work have been presented, showing their characteristics and affinities for the lectin. The similarities and differences between these molecules can be compared by studying the spatial arrangement of the complex formed by the interaction between the lectin and each of these glycoclusters. To do that, Atomic Force Microscopy imaging technique seems to be appropriate, since it enables acquiring topological images of small object with a nanometre resolution. Also, the interaction force of the lectin-glycocluster binding can be characterized. In this case, AFM spectroscopy mode can be applied to study the interaction at the molecular level.

Chapter 2.   Atomic Force Microscopy

Le Chapitre 2 est consacré, dans une première partie, à la technique AFM. Depuis son invention en 1986 par Binnig, Quate et Gerber, l'AFM a été utilisé dans divers domaines tels que la science des matériaux, la nanotechnologie, la biologie, la médecine... En effet, il s'agit d'une technique flexible qui permet l'imagerie de la topologie d'un échantillon avec une résolution nanométrique et la mesure de forces d'interaction avec une résolution de l'ordre du picoNewton. Elle a l'avantage de ne pas nécessiter une trop grande préparation des échantillons (en comparaison des techniques de microscopie électroniques, comme le TEM et le SEM) et s'applique à tout type d'échantillons, dur ou fragile, conducteur, isolant ou semi-conducteur. Elle peut aussi fonctionner dans différents milieux: le vide, l'air, les liquides et également à des différentes températures. Le principe de fonctionnement est basé sur la mesure de l'interaction entre une pointe et l'échantillon. Depuis son développement, elle a été largement appliquée à l'étude d'échantillons biologiques tels que l'ADN, des protéines, des virus, des cellules, etc. Non seulement les aspects topologiques peuvent été révélés, mais aussi les propriétés mécaniques qui sont liées aux fonctions biologiques. Par conséquent, l'AFM est un outil puissant pour étudier les interactions moléculaires, afin de comprendre les processus biologiques fondamentaux.

Dans ce chapitre, le principe de fonctionnement, les forces mises en jeu dans l'interaction pointe-échantillon et les différents modes de fonctionnement sont présentés. Toutefois, cette présentation n'est pas exhaustive, elle est limitée à l'utilisation de cette technique aux molécules ou surfaces biologiques. Les modes d'imagerie (modes statiques et dynamiques) et les modes de spectroscopie (molécule unique et cellule unique) utilisées au cours de cette thèse sont décrits en détail, avec une présentation des paramètres caractéristiques des interactions moléculaires qui peuvent être obtenus par l'analyse des courbes de force. Enfin dans une seconde partie l'accent est porté sur la préparation des échantillons biologiques et la fonctionnalisation des pointes pour les mesures de spectroscopie, en présentant l'état de l'art sur le sujet et les protocoles choisis dans cette étude.

2.1 Introduction

Since its invention in 1986 by Binnig, Quate and Gerber [3], Atomic Force Microscopy (AFM) has been used in various fields such as material science, nanotechnology, biology, medicine, etc. In fact, it is a flexible and versatile technique that allows imaging the topology of a sample at nanometric resolution and also measures interaction forces of the order of the picoNewton. Compared to other microscopy techniques, such as the scanning tunnelling microscopy (STM), it does not require special issues from the sample (such as make it conductive) and it can work in different media: vacuum, air, liquid and also at different temperatures [77]. Basically, the working principle is based on the measurement of the interaction between a probe (a tip) and the sample. Different operation modes have been developed to satisfy all the requirements. AFM can be used to study the magnetic field (MFM) of a surface or the electric charges (kelvin probe); it can serve to fabricate nanostructures (dip-pen nanolithography, nanografting, etc.). It has been largely applied to study biological samples, thanks to the development of various operations modes such as *tapping* mode, *jumping* mode, TREC, PeakForce, etc. The description of all the possible applications of such powerful technique is quite extensive and out of the scope of this dissertation. Therefore, we deliberately chose to focus our attention on the operation modes used during this Ph.D. thesis, mainly imaging and spectroscopy modes commonly applied to study biological samples.

Thus, this Chapter is devoted to the AFM technique. In particular, the working principle, the forces that take place in the tip-sample interaction and the different operation modes are presented. In particular, imaging modes (static and dynamic modes) and spectroscopy modes (Single Molecule and Single Cell Force Spectroscopy modes) used during these three years are described in details. Additionally, the characteristic parameters of molecular interactions that can be obtained via AFM force spectroscopy are discussed as well as the preparation of biological samples.

2.2 Working Principle

AFM is a scanning probe technique based on the distance-dependence of the tip-sample interaction force that can be either repulsive or attractive. The AFM tip is attached at the end of a flexible cantilever that deflects under the interaction between the tip and the sample. A laser beam is used to monitor the movement of the cantilever. It is focused at the backside of the cantilever in correspondence with the tip position, and reflected to a four-quadrant photodiode. The photodiode delivers a voltage signal depending on the position of the reflected laser spot. The tip moves in the xy-plane and along the z-axis with respect of the sample. A piezoelectric material performs the movement with sub-nanometre precision.

A general representation of the main components of an AFM setup is given in Figure 2.1. The main components are: 1) the head and the stage, 2) the scanner, 3) the high voltage (HV) electronics, 4) the digital signal processor (DSP), 5) the computer and the software.
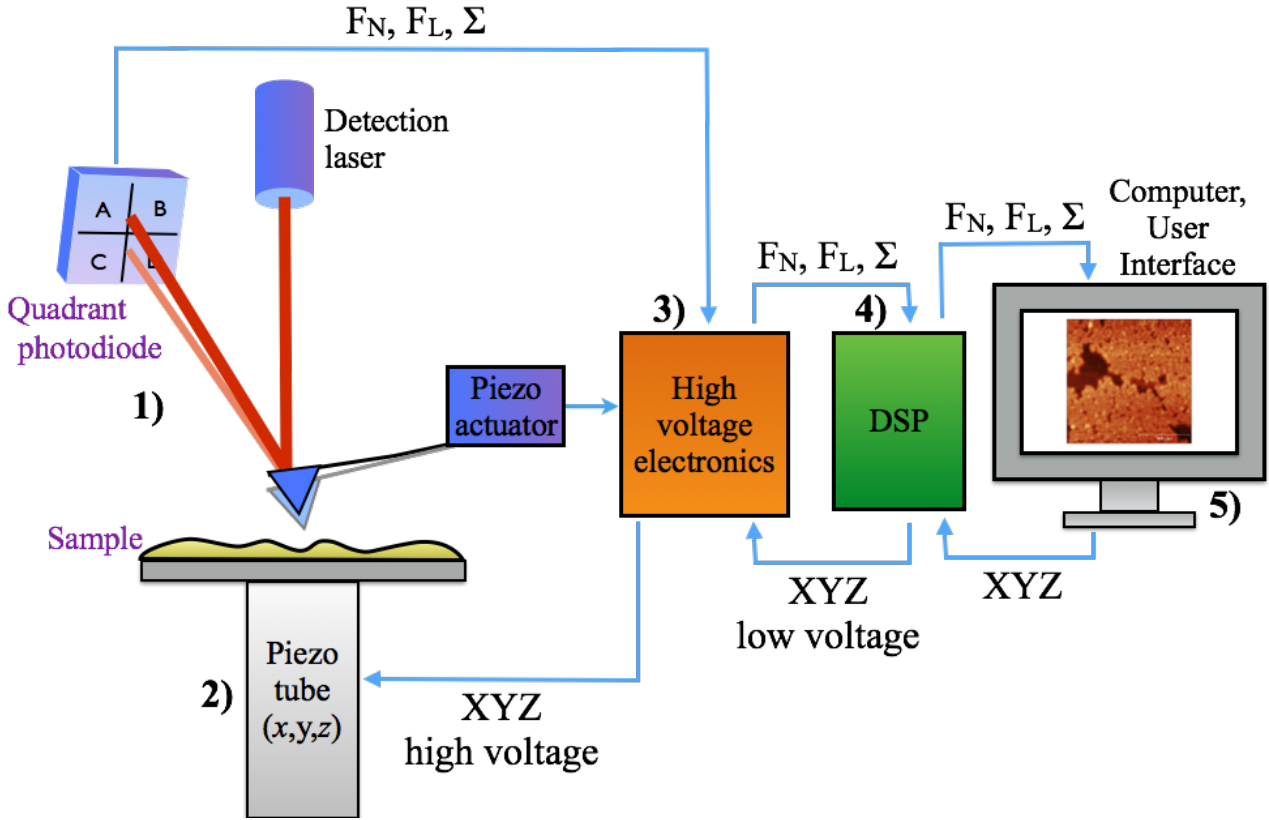
Figure 2.1: Standard setup of an AFM. Adapted from [78].

The AFM head contains the laser, the photodiode and the cantilever holder. It also contains a system for laser positioning and a small electronics able to process the laser signal of the photodiode. In particular, the intensity of the laser beam Σ, the normal F_N and the lateral F_L deflections of the laser are detected. The head is positioned over the stage where the sample is placed. In some setups, the stage is placed on the piezoelectric tube and the sample is moved close to the tip via a coarse to approach the tip to the sample with a micrometric precision, usually with step motors. The high voltage electronics allows controlling and processing the signal coming from the photodiode and sending the corresponding signal to the DSP (F_N, F_L, Σ). It also amplifies the small signal coming from the DSP into high voltage signal necessary to move the piezotube. The DSP processes all the signals coming from the high voltage electronics and performs the feedback via the PID controller (Proportional-Integral-Derivative controller). Finally, the software controls the data acquisition at real time and also sets the parameters related to the data acquisition.

To avoid noises that can reduce the resolution of AFM imaging, the AFM head, the stage and the piezotube are generally situated on an anti-vibrational table, inside a box that performs acoustic and mechanical isolations.

2.2.1 AFM cantilevers

The AFM probe (or AFM cantilevers) is one of the main parts of the microscope. It is chosen depending on the type of measurement performed, the kind of samples and the working medium. A probe is characterized by a sharp tip at the end of a cantilever, which protrudes from a macroscopic

holder (Figure 2.2). The holder has dimensions of few millimetres, to allow the user to manipulate the probe. The cantilever can have a rectangular or triangular shape and its dimensions are of the order of the micrometre (Figure 2.2a). The parameters that characterize a cantilever are the constant stiffness and the resonance frequency. The stiffness can vary from 0.01 N/m up to 100 N/m and the resonance frequency can span from 5 kHz to 1 MHz. The most common tips have a pyramidal or a conical shape with a radius that ranges from few to tens of nanometres (Figure 2.2b). Depending on the application, the shape and the material of which the tip is made can be different, as the geometry of the tip can influence the resolution while the material can affect the tip-sample interaction. The most common tips are made of silicon or silicon nitride.
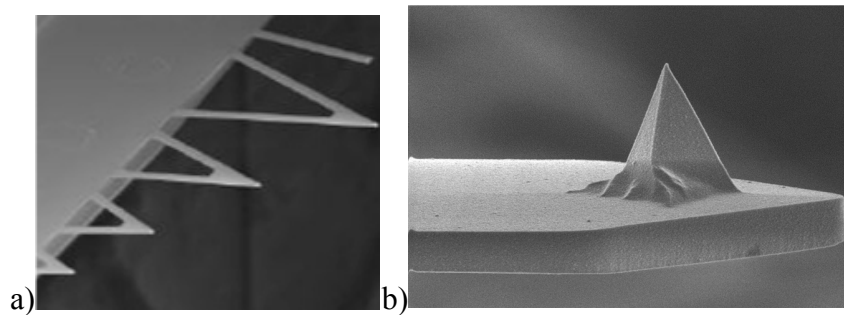
Figure 2.2: Electron microscopy images of a) AFM triangular and rectangular cantilevers and b) a pyramidal tip. Taken from www.brukerafmprobes.com.

The choice of the AFM probe and its calibration are main issues in AFM experiments. For example for imaging biological samples, in contact mode, the cantilever should have a small stiffness in order to do not damage the sample. However, in force spectroscopy experiments, probes must be as short as possible (< 50 nm), to limit thermal noise and should have small spring constant (0.01-0.1 N/m) to measure receptor-ligand interaction forces, which are of the order of the picoNewton [79]. Small rectangular cantilevers can improve both imaging speed without any loss in resolution and force sensitivity during recognition experiments [80].

2.2.1.1 Calibration of the spring constant

To convert the deflection (in nanometres) in a force value (in picoNewton), the knowledge of the cantilever stiffness is mandatory even though it is not a simple task [81]. Different methods [82] have been developed to measure the cantilever stiffness, based for example on the geometry of the tip [83,84], the addition on a known mass [85], the cantilever deflection caused by the pushing of a reference cantilever [86] or the thermal noise [87]. Few of them are presented in the following.
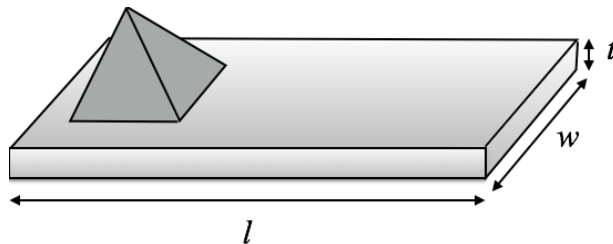
Figure 2.3: Schematic representation of an AFM cantilever.

The spring constant of a rectangular cantilever (k) with a regular cross-section is given by:

$$k = \frac{Et^3w}{4l^3}$$ (0.7)

where E is the elastic modulus, t is the thickness, w is the width and l is the length of the cantilever (Figure 2.3). The same formula can be applied at first approximation to triangular cantilever, with $w = w/2$.

Sader and White [83,84,88] developed a method to obtain the spring constant of a cantilever based on finite element analysis and the knowledge of its geometric dimensions, elastic properties, resonance frequency and quality factor. This method provides the spring constant value for both rectangular and triangular cantilevers, but the precise knowledge of tip dimensions is not easy to obtain. The expression obtained by Sader for spring constant of rectangular cantilever is:

$$k = 0.1906\rho_f w^2 LQ\Gamma_i(\text{Re})\omega_0^2$$ (0.8)

where ρ_f is the density of the surrounding fluid, w and L the width and the length of the cantilever, respectively, Q the quality factor and Γ_i the imaginary part of the hydrodynamic function. This last parameter takes into account the viscosity η of the fluid and depends on the Reynolds number (Re), which is linearly dependent on the angular resonance frequency ω_0 [81]:

$$\text{Re} = \frac{\rho_f \omega_0 w^2}{4\eta}$$ (0.9).

The "added-mass method" developed by Cleveland et al. [85] is based on the fact that the resonance frequency of a cantilever linearly changes when the mass of the cantilever changes. Therefore, by attaching different known masses to the probe, and measuring how the resonance frequency changes as the mass of the cantilever changes (Figure 2.4a), one can extrapolate the stiffness of the cantilever. In fact, when an added mass M is attached to the cantilever, the resonance frequency v is given by:

$$v = \frac{\omega}{2\pi} = \frac{1}{2\pi}\sqrt{\frac{k}{M + m^*}}$$ (0.10)

where m^* is the effective mass of the cantilever. Therefore, the added mass M can be expressed as a function of the resonance frequency ($2\pi v$):

$$M = \frac{k}{(2\pi v)^2} - m^*$$ (0.11),

and k can be extrapolated from the plot, being the slope of the line (Figure 2.4b).
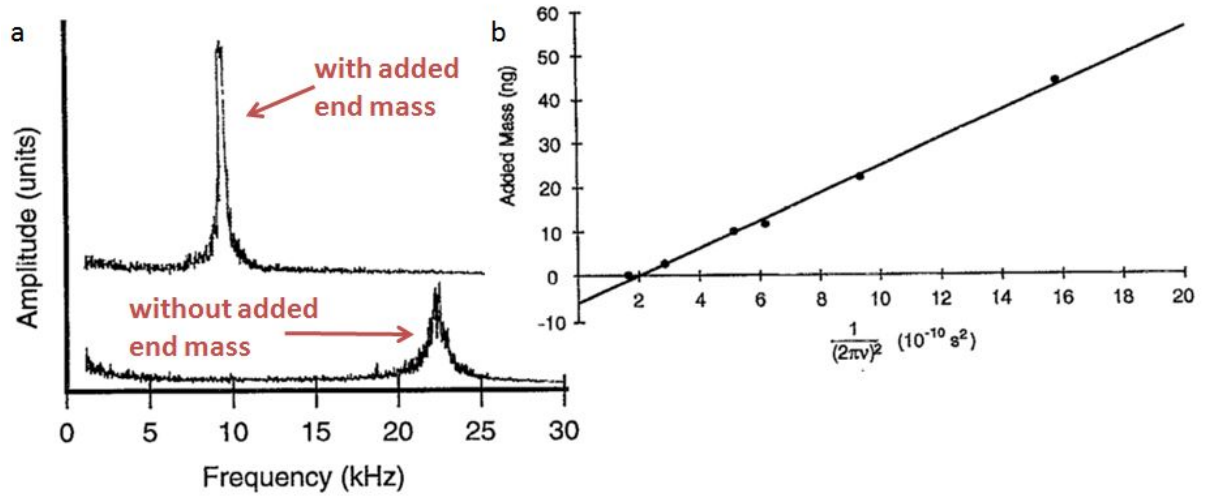
Figure 2.4: a) Resonance frequency of the cantilever with and without an added mass; b) plot of the linear dependence $M = f((2\pi v)^{-2})$. Taken from [85].

Another method used for the calibration of the cantilever spring constant is characterized by the use of a reference cantilever, which has been accurately calibrated [89]. The dimensions of the reference have been measured by scanning electron microscopy and the spring constant has been determined via equation (0.7). The uncalibrated cantilever is then mounted on the AFM and force-distance curves are recorded on the reference cantilever, as shown in Figure 2.5.
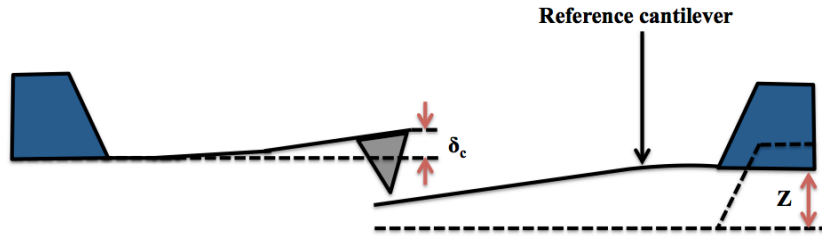
Figure 2.5: Schematic representation of the spring constant calibration method developed by Gibson et al., where δ_c is the cantilever deflection and Z the piezo vertical displacement. Adapted from [81].

The spring constant of the uncalibrated cantilever will be given by

$$k = k_{ref}\frac{Z-\delta_c}{\delta_c} = k_{ref}\frac{1-\dfrac{\delta_c}{Z}}{\dfrac{\delta_c}{Z}} \tag{0.12}$$

where δ_c/Z is the slope of the force-distance curve taken on the reference cantilever [81].

Lastly, in the method proposed by Hutter and Bechhoefer, the thermal noise intensity is measured in order to obtain the cantilever spring constant [90]. This method is called "thermal noise method". In first approximation, it does not require any knowledge on the geometry or on the material of the probe. Basically, the cantilever can be modelled as an harmonic oscillator and by applying the

34

equipartition theorem one can obtain the spring constant, knowing the mean square deflection $\left\langle \Delta \delta_c^2 \right\rangle$ due to thermal fluctuation [90]:

$$\frac{1}{2}k\left\langle \Delta \delta_c^2 \right\rangle = \frac{1}{2}k_B T \rightarrow k = \frac{k_B T}{\left\langle \delta_c^2 \right\rangle} \qquad (0.13).$$

Practically, the sensitivity of the cantilever is determined from a force-curve taken on a hard substrate (Figure 2.6a). The noise spectrum is acquired and fitted with a Lorentzian curve from which the mean square deflection is obtained as the area under the peak (Figure 2.6b). In reality, the excitation of the cantilever is shape dependent. Also, the thermal noise depends on the temperature and on the detection method (i.e. optical lever), therefore different vibration modes have to be taken into account [87]. Furthermore, the using of an optical lever as detection system implies the measurement of an inclination instead of a displacement of the lever. Lastly, the experimental limitation (bandwidth limitation) allows the accessibility of only the first vibrational modes [82]. Therefore, Butt and Jaschke have revisited the formula (0.13) to take into account these considerations, and the equation (0.13) becomes:

$$k = \beta^* \frac{k_B T}{\left\langle \delta_1^{*2}(L) \right\rangle} \qquad (0.14)$$

where δ^* is the effective deflection and β^* is the correction factor [81,91].
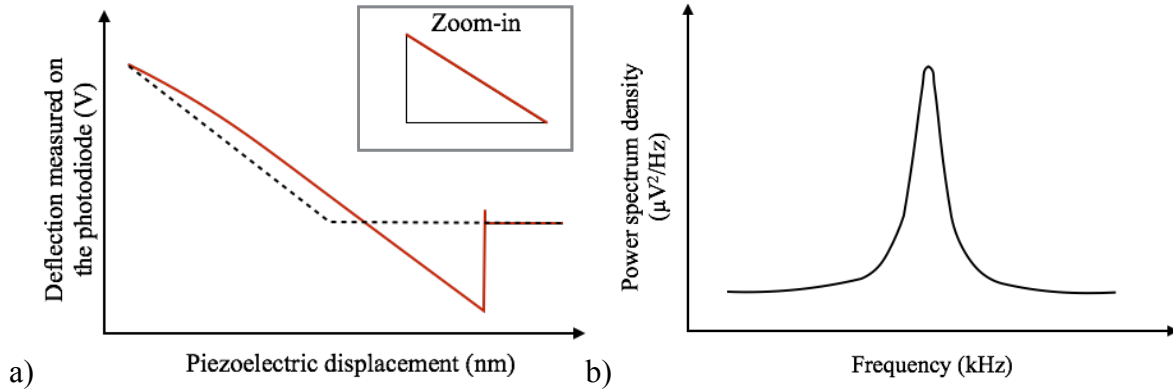
Figure 2.6: Sketches of a) force-distance curve taken on a hard material to obtain the sensitivity S[V/nm]; b) noise spectrum fitted with a Lorentzian curve. Adapted from [82].

All of these methods present some advantages and some drawbacks. For example, the "added mass" method is one of the most effective proposed approaches. It is non-destructive since the added mass is usually safely placed on the tip via adhesive forces [92]. The method developed by Sadler, implies the precise knowledge of quantities such as the mass and the density of the cantilever, which are not given by the constructor [92]. Also cantilever's dimensions are not easy to obtain. This problem can affect the calibration via a reference cantilever, since the reference must be well calibrated, thus its dimensions must be known. Moreover, the treatment of the force distance curves implies the knowledge of the tip shape and size, since the force depends on them [92]. To avoid the problem of the exact knowledge of the cantilever's characteristics, the thermal noise method can be used. It does not require the knowledge of the size and density of the cantilever since it takes

advantage of the thermal fluctuations. This method is the most widely used by many authors and it is implemented in most of commercial AFM.

2.2.2 Detection system

The optical detection is the most current detection system used in commercial AFM. Basically, the laser beam (λ = 670 nm) is focused on the backside of the cantilever and reflected on a four-quadrant photodiode. The cantilever and the laser positions are adjusted to maximize the intensity of the laser spot on the photodiode. The photodiode is constituted of four-quadrant for a better detection of the position of the spot in its lateral movement. Thanks to the four-quadrant, namely A, B, C and D, the intensity (Σ, Figure 2.7a) of the laser beam, as well as the normal (F_N, Figure 2.7b) and lateral (F_L, Figure 2.7c) deflections of the laser can be determined, as shown in equations (0.15)
.

$$\Sigma = A + B + C + D$$
$$F_N = (A + B) - (C + D) \qquad (0.15)$$
$$F_L = (A + C) - (B + D)$$
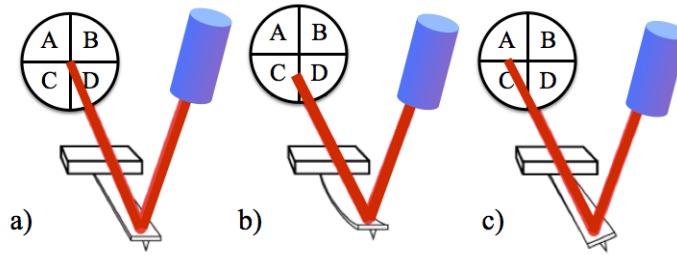
Figure 2.7: Laser beam detection of the cantilever deflection.

2.3 Interaction Forces

AFM measures tip-sample interaction and this interaction is influenced by the characteristics of the surface, the tip (material and shape) and also the working media. In general, the interaction can be described by approximating the tip and the surface as a sphere and a plane or as a cone and a plane, respectively.

The general formula that depicts the overall interaction is the one of the Lennard-Jones potential (Figure 2.8):

$$V(r) = 4\varepsilon\left[\left(\frac{\sigma}{r}\right)^{12} - \left(\frac{\sigma}{r}\right)^{6}\right] \qquad (0.16).$$

The ε and σ are empirical parameters that correspond to the depth of the potential and the atom dimensions, respectively. The first term goes as $1/r^{12}$ and describes short-range repulsive

interactions that are related to Pauli exclusion principle, so the overlap of the orbitals of the electrons. The second term represents long-range attractive interactions, such as Van der Waals forces.
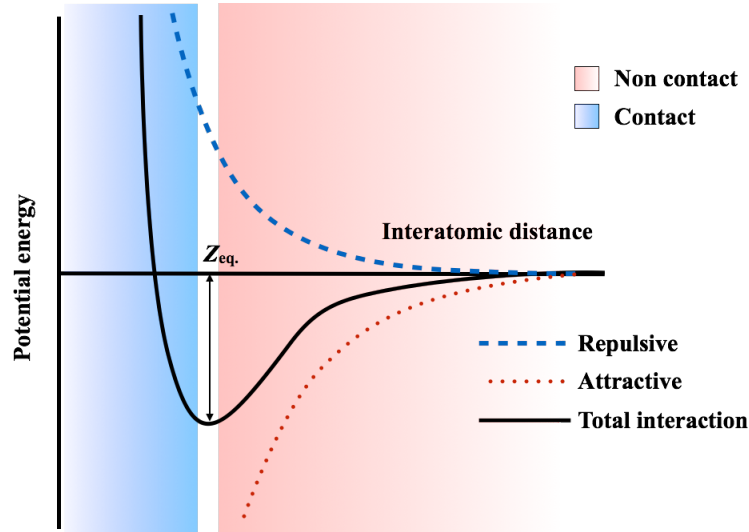
Figure 2.8: Schematic representation of the tip-sample interaction force given by the Lennard-Jones potential as a function of the distance.

At the nanoscale, interaction forces are distance-dependent. Also, they depend on the working media. In the following, we focus our attention on some of the main forces that appear in air and liquid environments and to which the tip-sample system can be subjected.

2.3.1 Contact forces

When two elastic bodies are in contact, the short-range intermolecular forces arise in the region close to the contact area [93]. Similarly, in AFM, contact forces are related to the mechanical contact between the tip and the sample, which leads to a deformation of the atoms involved in the contact.

Different models can be used to study the deformation produced by mechanical contact and to find its relationship with the applied force. In fact, it does not exist a unique model to describe mechanical deformations and the choice of the used model should depend on the particular case under study. The three most commonly used models for describing mechanical deformations are the Hertz model, the Johnson-Kendall-Roberts (JKR) and the Derjaguin-Müller-Toporov (DMT) models [92].
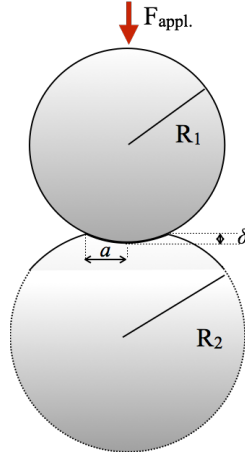
Figure 2.9: Sketch of the mechanical deformation between two spheres where the radius of the spheres R_1 and R_2, the indentation depth (δ) and the contact radius (a) are shown.

The three models describe the contact between two spheres. The Hertz model describes the elastic contact and allows calculating the force between the two spheres under the application of an external force [93]. In this model the indentation depth δ (Figure 2.9) is given by:

$$\delta = \frac{a^2}{R^*} \tag{0.17}$$

where a is the contact radius between the two spheres and R^* is the reduced radius, $\dfrac{1}{R^*} = \dfrac{1}{R_1} + \dfrac{1}{R_2}$.

The contact radius a (Figure 2.9) is expressed as:

$$a^3 = \frac{3F_L R^*}{4E^*} \tag{0.18}$$

where E^* is the Young modulus and F_L is the force needed to achieve the penetration. The Hertz theory does not take into account the surface forces and an expression of the adhesion force cannot be obtained. Therefore, starting from the Hertz model, the JKR and the DMT models have been developed. The JKR is an extension of the Hertz model where the adhesive interaction is considered only within the contact zone and outside this zone the interactions are neglected [93]. It is mainly applied in the case of soft materials, large spheres and short-range interactions. The contact radius a obtained with this model is given by:

$$a^3 = \frac{3R^*}{4E^*}\left(F_L + 3\pi w_{adh} R^* + \sqrt{6\pi w_{adh} R^* F_L + \left(3\pi w_{adh} R^*\right)^2} \right) \tag{0.19}$$

where w_{adh} is the work of adhesion. The first term is obtained from the Hertz model (equation (0.18)), while the other two are related to the adhesive interaction, which is expressed in the JKR model as:

$$F_{adh} = -\frac{3}{2}\pi w_{adh} R^* \tag{0.20}.$$

Also the DMT model is an extension of the Hertz model, where the adhesion between two elastic spheres is considered. The Hertz model is used to describe the contact and only the surface forces outside the contact area are taken into account, while the deformations due to these forces are not considered. In this case, the adhesion force has the form of:

$$F_{adh} = 2\pi w_{adh} R^*$$ (0.21).

Contrary to the JKR theory, the DMT is mainly used to describe the behaviour of hard materials, small sphere and long-range interactions. It is evident that the two theories are not perfect and both have limitations. They represent the limiting cases of a more general theory, the Maugis-Dugdale model, able to describe the transitions between the JKR and the DMT models [93].

2.3.2 Capillary forces

When working in air, capillary forces can appear due to the formation of a water layer between the tip and the sample surface [94]. Basically, the pressure difference between the liquid and the surrounding vapour phase leads to the formation of a water biofilm on both the tip and the sample [81]. Therefore, a liquid meniscus is formed when the tip is close to the sample. In general, this kind of interaction depends on the tip-sample distance and is present when $dF/dz > k$.

The capillary force is an attractive force of the order of 10 to 100 nN: it depends on the hydrophobicity/hydrophilicity of the surface, its roughness and interaction geometry [81,95]. It is responsible of the jump-into contact in the forward curve when performing spectroscopy in air, and it can be estimated by the equation:

$$F = \pi \gamma_L \kappa R^2 \sin^2 \phi_i$$ (0.22)

where γ_L is the water surface energy, Φ_i is the angle formed between the tip and the meniscus, R the tip radius and κ is the radius of the meniscus given by:

$$\kappa = -\frac{\cos\phi_i + 1}{R(1 - \cos\phi_i) + r} + \frac{1}{R}$$ (0.23)

where r is the tip-sample distance [96].

The dependency of the capillary force on relative humidity is not so clear, in fact different dependencies have been obtained for similar systems [81]. The general tendency seems to be that capillary force mostly increases with the humidity of the air, reaching its maximum at a relative humidity percentage of 60-80% [95]. This force can be reduced by working in an attractive regime, due to the fact that the attractive regime generates a torsion of the cantilever that produces elastic forces, able to counteract the capillary force [97].

2.3.3 Van der Waals forces

Van der Waals (VdW) interactions arise from electromagnetic field fluctuations. They are always present no matter of the chemical compositions of the surface and the working media [98]. VdW interactions are attractive forces due to the intermolecular interactions:

$$V(r) = -\frac{C_{VdW}}{r^6} \; ; \; F(r) = -\frac{6C_{VdW}}{r^7} \qquad (0.24),$$

where r is the separation between the two atoms and C_{VdW} is a constant that depends on the geometry and the optical properties of the two interacting atoms.

Depending on the shape of the objects, the equations (0.24) can be different. For example, in the case of the AFM tip-sample system, the atoms implicated in the interactions are the atoms of the tip close to the surface and vice versa, therefore the interaction can be modelled as the interaction between a sphere and a plane or between a cone and a plane. Thus, the VdW force can be described as:

$$F_{sphere-plane} = -\frac{AR}{6r^2} \qquad (0.25)$$

$$F_{cone-plane} = -\frac{A \tan^2 \vartheta}{6r} \qquad (0.26)$$

where R is the tip radius, ϑ is the semi-aperture of the cone, r is the tip-sample distance and A is the Hamaker constant. In general, the Hamaker constant is used to describe two interacting macroscopic bodies (1), across a media (2). The constant is given by:

$$A = \frac{3}{4} k_B T \left(\frac{\varepsilon_1 - \varepsilon_2}{\varepsilon_1 + \varepsilon_2} \right)^2 + \frac{3I}{16\sqrt{2}} \frac{\left(n_1^2 - n_2^2 \right)^2}{\left(n_1^2 + n_2^2 \right)^{3/2}} \qquad (0.27)$$

where ε_i (i = 1,2) are the dielectric constants, n the refractive index, I the ionization potential (around 2 x 10^{-18} J for most materials) and T the temperature [99]. Typical Hamaker constants are in the range of 5-10 x 10^{-20} J for the interaction of non-conducting solids in air, while in water they are around 0.5-1.5 x 10^{-20} J.

In the AFM system the VdW interaction arises at a tip-sample distance between 10-15 nm. If this distance is smaller than the intermolecular separation ($r < a_0$), then the VdW interaction can be expressed as the adhesion interaction derived from the DMT theory (section 2.3.1), which is given by [98]:

$$F = -\frac{AR}{6a_0^2} \qquad (0.28).$$

When working in liquid media, attractive forces are pH independent and the VdW should overcome the sum of the applied force and the repulsive interaction in order to be measured (a jump-in in the tip-sample approach curve) [100].

2.3.4 Electrostatic double-layer forces

In addition to the VdW forces, the other main long-range interaction force is the electric "double layer" (DL) that takes place at the interface of two similarly charged macromolecules or surfaces immersed in a ionic solution [81,99].

The electrostatic interaction between two similarly charged surfaces is most of the time repulsive and decays exponentially with the distance between them [99]:

$$V(r) = +C_{ES} e^{-\lambda_D r} \tag{0.29}$$

where C_{ES} is a constant characteristic of the interaction that depends on the properties of the two surfaces, such as their geometry, charge density and on the solution conditions. λ_D is the characteristic decay length, called Debye length, which is given by:

$$\lambda_D = \frac{\varepsilon\varepsilon_0 k_B T}{\sqrt{2ce^2}} = \frac{3.04}{\sqrt{c}} \text{ Å} \quad \text{(for water at 25ºC)} \tag{0.30}$$

The Debye length depends only on the solution conditions (monovalent, divalent ions), the concentration of the electrolyte (c) and the temperature (T). It decreases as the ion strength and the valence of the ions increase. For example, given the concentrations of ions in solution such as [NaCl] and [CaCl$_2$], expressed in mol/L, the Debye length is given by:

$$\lambda_D = 0.30 [NaCl]^{1/2} nm \tag{0.31}$$

for 1:1 electrolytes such as NaCl, and

$$\lambda_D = 0.18 [CaCl_2]^{1/2} nm \tag{0.32}$$

for 1:2 or 2:1 electrolytes such as CaCl$_2$ [99]. Therefore, increasing the salt conditions leads to a fast decreasing of the repulsion.

2.3.5 DLVO theory

Most of the time, both VdW and DL forces are present in aqueous solutions. The combination of these two forces gives the DLVO theory, named after Derjaguin & Landau and Verwey & Overbeek. The theory describes particle aggregation in aqueous dispersions. Basically, it plots the VdW and DL forces together, in order to describe the net interaction (the DLVO force, F_{DLVO}) between two surfaces (Figure 2.10). The general formula used to describe the resulting F_{DLVO}, for a tip-sample system, is:

$$
\begin{aligned}
F_{DLVO}(r) &= F_{DL}(r) + F_{VdW}(r) \\
&= \frac{4\pi\sigma_{sample}\sigma_{tip}R\lambda_D}{\varepsilon_e\varepsilon_0} e^{-r/\lambda_D} - \frac{AR}{6r^2}
\end{aligned}
\tag{0.33}.
$$

The first term is the electrostatic double layer contribution, where σ_{sample} and σ_{tip} are the surface charge densities of the sample and the tip, respectively; ε_e is the dielectric constant and ε_0 the permittivity of the free space. The second term represents the VdW contribution for a sphere-plane system [101].
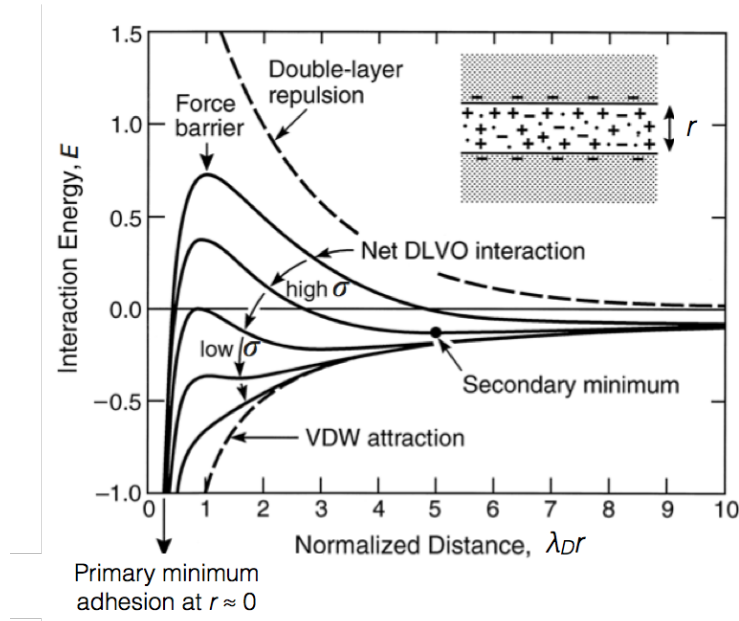
Figure 2.10: Plot of the VdW and the DL forces that make-up the net interaction of the DLVO theory. Adapted from [99].

In general, the net DLVO interaction is expected to be attractive, both at small and large separation distances between the surfaces [99]. The strength of VdW and DL interactions can determine if the net interaction will be attractive at all separation distances, or weakly attractive at finite separation (Figure 2.10). This is due to the nature of these two forces and their dependency on the distance: VdW decays as a power of law as a function of the distance, while the DL interaction decays exponentially. Also, they behave differently when the ion concentration or the charge of the two interacting surfaces change. In fact, the VdW is little affected by such modifications, while these changes have a huge effect on the DL interaction, which under certain conditions can become attractive [99].

The influence of these forces has been investigated by AFM. It has been shown that, when working in liquid media, the ion concentration (therefore the electrostatic interactions) can misfit the height of the sample under study [101]. Müller and Engel showed the necessity of screening the repulsive electrostatic interactions by adjusting the pH and the ion concentration to obtain a reliable height value [101]. Also, Medalsy et al. [102] studied the influence of the electrostatic interaction on the stiffness of purple membranes. They demonstrate that the mechanical properties of purple membranes depend on the pulling parameters used during the experiments (i.e. pulling speed and loading rate). Also, by lowering the salt concentration, they obtained stiffness values twice smaller than at high salt conditions. This is due to the fact that the electrostatic repulsion increases when the salt amount decreases, creating an electrostatic layer that requires the application of high forces to be overcome. Basically, the electrostatic repulsion increases the total stiffness of the system by following this formula:

42

$$k = \frac{k_{El.} k_{sample}}{k_{El.} + k_{sample}} \tag{0.34},$$

where $k_{El.}$ is the contribution of the electrostatic repulsion to the measured stiffness (k) and k_{sample} is the real stiffness of the sample under study. Thus, the electrostatic repulsion is a long-range interaction (several nm) that can be reduced by increasing the salt concentration of the working solution (> 50-100 mM). The interaction is distributed over a large area of the biological object and the AFM tip, thus it hardly contributes to the deformation of the sample, but it increases the force necessary for approaching the tip to the membrane. This is a factor that has to be taken into account, since the force values that one can obtain can be smaller than expected due to the presence of electrostatic repulsion.

2.3.6 Other forces: Hydration repulsion and hydrophobic forces

In liquid, the strength of forces is reduced by a factor of 10-100 compared to the forces in air (ex. capillary forces). In most of the cases these forces can be explained by the DLVO theory, but in some cases one should also take into account other forces, related to the chemical nature of the liquid, the tip and the sample. Thus, solvation forces hydration repulsion, hydrated forces, etc. must be considered. In the following, hydration repulsion and hydrophobic forces will be described since they are important in biology.

2.3.6.1 Hydration repulsion

Hydration force is quite important in surface science and biology but its origin is still not clear. It is a short-range repulsive interaction since at salt concentration smaller than 0.1 M can be distinguished from VdW and electrostatic double layer interactions [81]. It probably depends on the interaction between hydrophilic surfaces and it is related to the energy needed to dehydrate ions, since they tend to become stronger with increasing hydration number ($Mg^{2+} > Ca^{2+} > Li^{2+} \cong Na^+ > K^+ > Cs^+$) [81,92]. This force acts at a very small range. In general, it is very weak and decays exponentially with distance:

$$U_A = Ae^{-x/\lambda_H} \tag{0.35}$$

where λ_H is the characteristic decay length that ranges from 0.2 to 1.4 nm [81]. These forces are quite difficult to be determined by AFM studies, especially when biological systems are under study, since it is difficult to register accurate force curves due to the deformability and elasticity of the material [81].

2.3.6.2 Hydrophobic forces

Hydrophobic surfaces attract each other in water originating strongly attractive hydrophobic forces. These long-ranged distance-dependent interactions can be so far stronger than VdW interactions and depend on the degree of hydrophobicity of the surfaces. In fact, surfaces with contact angles (θ) between 75º and 90º and interfacial energy $\gamma_i = 6\text{-}30$ mJ/m^2 are classified as partially hydrophobic, while surfaces with contact angle $\theta = 100º\text{-}115º$ and $\gamma_i = 40\text{-}55$ mJ/m^2 are considered strongly hydrophobic [99]. Hydrophobic interactions are affected by different factors, such as temperature,

pressure and additives present in the solution [103]. The interaction between two hydrophobic surfaces decays exponentially and becomes weak sensitive to changes in ion concentration for distances larger than 10 nm. The origin of this interaction is not clear. Different theories have been proposed and, for example, one of them proposes a non-electrostatic origin of the interaction [99]. Nevertheless, these forces are quite relevant for both non-biological and biological systems, since they drive self-assembly processes, protein folding, molecular recognition, membrane formation, etc. [103].

2.4 Operation Modes

Depending on the information that one wants to obtain, the sample and the working conditions, different operation modes have been developed. In fact, AFM is not only a topographic technique; it also gives mechanical information about the sample under study. AFM is capable of measuring the elasticity of membranes [102] and polymers [104], quantifying the receptor-ligand interaction at the nanoscale [105], or the mechanical properties of viruses [106]. One can follow real-time process such as the walking of the myosin on an actin filament, via high-speed AFM [107]. As already said, the description presented here is not exhaustive since few of the most common operation modes used to study biological samples are detailed in the following.

2.5 Imaging

AFM is an imaging technique that allows acquiring three-dimensional high-resolution topographic images of the sample. For this, the AFM tip scans a given area of the sample surface by performing a line-by-line scanning. Depending on the operation mode, a characteristic parameter (i.e. force, amplitude or frequency) is maintained constant. Also the tip-sample distance can vary as a function of the operation mode, therefore the tip can be, during the scanning, always in contact (Contact mode), or in intermittent contact (Amplitude Modulation mode) with the sample, or the tip-sample contact can be prevented (Frequency Modulation, Noncontact mode).
A feedback loop is used to control the variations of the given parameter with respect of the value chosen by the operator (setpoint value). Once a change in the settled parameter is detected, the control system applies a given voltage to the piezoelectric tube to deform it and displace the sample in the vertical direction. The setpoint value of the monitored parameter is then re-stabilized (Figure 2.1).

2.5.1 Contact Mode

From an historical point of view, the contact mode is the first mode invented [3]. Basically, in contact mode the tip scans the surface by maintaining a continuous contact with the substrate and nanometre resolution images can be acquired on a huge range of samples.

Essentially, when working in contact mode, the cantilever deflects once the tip makes contact with the sample and the deflection is proportional to the applied force (Figure 2.11). For small displacements, the Hooke's law:

$$F = kz_C \tag{0.36}$$

can describe the relation between the deflection and the applied normal force, where k is the cantilever stiffness and z_c is the cantilever deflection. With this technique, the torsion of the cantilever can be also measured, leading to a direct information on the lateral force, which is related to the friction between the tip and the sample [108].
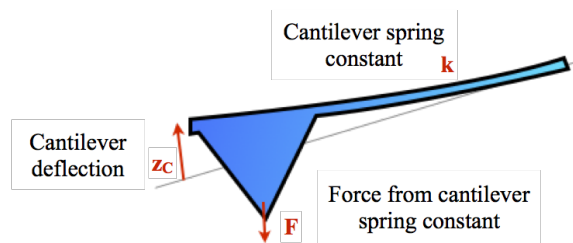
Figure 2.11: Relation between the tip-sample interaction force F and the cantilever deflection z_c and the spring constant k.

There exists two ways of working: at constant force or at constant height. At constant force, the feedback tries to maintain the force constant during all the scanning. To ensure this, the piezoscanner acts on the relative position of the tip with respect of the sample, maintaining the deflection (and so the applied force) constant. On the height constant mode, the tip-sample distance is kept constant. This method is particularly suitable for extremely flat surfaces; otherwise the tip breaks easily.

The contact mode is mostly used for imaging hard materials in air, as for a biological sample it can damage or displace it. The damage on soft substrates, such as biological ones, is reduced when working in liquid environment. In fact, the applied forces due to the contact are in general of the order of nN when working in air, while in liquid environment the strength of forces can be reduced by a factor of 10-100.

2.5.2 Dynamic Modes

Even though contact mode has been successfully applied, in the case of soft samples the resolution has been found to be limited due to the tip-sample lateral forces [108,109]. To avoid this effect, dynamic modes have been developed.

In dynamic modes, the tip oscillates above the sample during the scan. The tip-sample contact is intermittent, at constant amplitude (Amplitude Modulation, AM) or at constant frequency (Frequency Modulation, FM). During scanning, the cantilever is oscillating at a frequency close to its resonance frequency, thanks to a piezoelectric modulator. Its sinusoidal oscillation is characterized by amplitude, oscillation frequency and phase shift. This last parameter refers to the difference between the mechanical excitation and the one obtained from the cantilever due to the

interaction with the sample [110]. Since all these parameters can be recorded, as well as the cantilever deflection, different properties can be simultaneously studied even though the information on the applied normal force is not directly accessible [111].

By considering the tip-sample system as a point mass spring, the cantilever motion can be described by the equation of motion of a damped harmonic oscillator:

$$m\frac{dz^2}{d^2t} + \frac{m\omega_0}{Q}\frac{dz}{dt} + kz = F_{ts} + F_0\cos(\omega t) \tag{0.37}$$

where m is the effective mass of the cantilever defined as $m = k/\omega_0^2$, k the spring constant of the cantilever and ω_0 its angular resonance frequency. Q is the quality factor given by $Q = m\omega/b$ where ω is the cantilever angular frequency ($\omega = 2\pi f$) and b the attenuation factor. Finally, $F_0\cos(\omega t)$ is the driving force and F_{ts} is the tip-sample interaction force, which is characterized by repulsive (i.e. Pauli repulsion, DL forces) and attractive contributions (i.e. VdW and capillary forces), and depends also on the working environment [96,112].

2.5.2.1 Amplitude Modulation

In amplitude modulation (AM-AFM), the cantilever is kept oscillating at constant amplitude over the sample thanks to a feedback loop system, which adjusts the cantilever position and maintains the parameter constant. For this, the feedback compensates the amplitude change by increasing or decreasing the voltage applied to the piezoscanner, leading to a correspondent displacement of the sample in the vertical direction (Figure 2.1). AM-AFM can be applied both in liquid and air, leading to high-resolution topographic images of the samples under study. During scanning, also the phase signal can be registered. It is related to the dissipation energy of the tip-sample interaction and gives information on the chemical properties of the substrate.

Depending on the tip-sample distance and on the range of the amplitude, the interaction can be always attractive or can range from an attractive to a repulsive regime. Generally, at small amplitude oscillations (< 10 nm), the interaction regime is always attractive. For large amplitude oscillations (20-100 nm), the interaction force shifts from an attractive to a repulsive regime, due to the modulation of the tip-sample distance during each cycle [113]. Once the tip undergoes to repulsive interactions, it contacts the sample surface leading to a reduction of the initial amplitude of 60-75%, thus to an intermittent contact. This operation mode is called *tapping* mode. This mode is highly suitable for imaging biological samples, since applied normal forces are weak and the lateral contribution is negligible [114].

When working in *tapping* mode, the transition between the attractive and the repulsive regimes can be smooth or abrupt, depending on the sample properties and on the free amplitude [96]. The existence of a smooth transition is related to the presence of only one oscillation state, while abrupt step-like discontinuities are due to the existence of two stable oscillation states [96]. These two stable oscillation states can be observed in the amplitude *vs*. distance curve: they will appear as "jumps" in the approach and retraction curves (Figure 2.12) [108]. These "jumps" happen at

different tip-sample distances in the two curves, causing hysteresis (bistable regime). The hysteresis splits the tip-sample interaction into two regimes: before the hysteresis (lower branch in Figure 2.12), where attractive forces dominate the tip-sample interaction; while after the hysteresis (higher branch in Figure 2.12) the tip-sample interaction is also sensitive to repulsive forces [108].
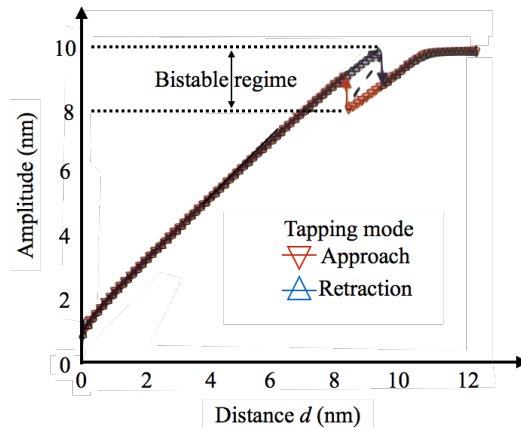
Figure 2.12: Amplitude vs. distance curve for tapping mode. Adapted from [108].

2.5.2.2 Frequency Modulation (FM)

To obtain high-resolution images, working in vacuum is widely preferred to maintain samples clean and avoid contaminations. At low-pressure conditions, silicon cantilevers present a Q-factor of the order of $Q \sim 10^4$, which can limit the acquisition time if working in AM mode [108]. To avoid this problem of long response time in vacuum, while achieving atomic resolution images, Frequency Modulation mode (FM-AFM) has been introduced by Albrecht et al. [115].

FM-AFM is based on the detection of small changes in frequency with respect of the resonance frequency of the cantilever. Basically, during scanning, the oscillation amplitude or the excitation amplitude is maintained constant (*constant-amplitude mode* or *constant excitation mode*, respectively) and the cantilever is let self-oscillate at its resonance frequency. Since the frequency depends on the tip-sample interaction, the change in the tip-sample distance causes a change in frequency; so a feedback is used to control and re-establish the resonance frequency setpoint. Once the system detects a modification of the offset, an increasing or decreasing voltage is applied to the piezoelectric scanner leading to a displacement of the sample in the vertical direction, and the frequency setpoint is re-established.

FM-AFM is considered as a noncontact technique (NC-AFM), since this operation mode is assumed to avoid destructive repulsive tip-sample interactions [108]. Therefore, VdW attractive forces are the dominant ones. FM-AFM is considered as the mode which gives the best resolution in AFM, as demonstrated by the images of pentacene molecules, where the molecular orbitals can be observed [116]. Since several years, some groups are using this operation mode for studying biological systems in liquid [117]. A significant example is the high resolution images of the DNA double helix [118].

2.5.3 High-speed AFM

The main drawback of the imaging modes is the low image speed: acquiring an image takes more than 30 s, in general several minutes. To avoid this inconvenient, high speed AFM (HS-AFM) has been developed by Ando in 2001, allowing decreasing time acquisition imaging to 100 millisecond or less, despite a loss in resolution [119]. This low-invasive imaging mode pioneered in the study of dynamical processes and got insight on protein functioning [107]. To achieve such a high speed, some requirements must be satisfied, such as the time delay of the feedback loop must be reduced, the feedback control must be able to eliminate *parachuting effect* and the damping of mechanical vibrations due to fast scanner displacement must be removed [107]. Images are performed in *tapping* mode with cantilevers that must be short and with high resonance frequency to reduce noise.

This technique has allowed, for example, visualizing the walk of double-headed myosin V along actin filament via walking steps of ~ 36 nm [107].
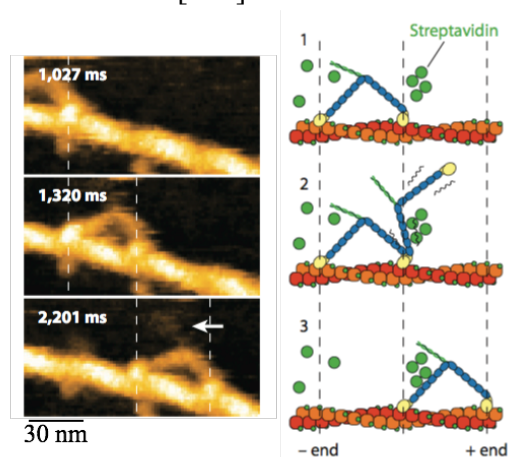
Figure 2.13: AFM images and schematic representation of myosin V walk. Adapted from [107].

2.5.4 Image artifacts

Images artefacts can arise from tip dimensions and/or the choice of feedback parameters. From an ideal point of view, the apex of the AFM tip should be a single atom, but this is rarely the case. The finite dimensions of the tip apex induce objects to appear larger on the image than their real size. This phenomenon is known as tip dilatation. The final AFM image is given by a convolution of the finite tip dimensions and the dimensions of the object under study (Figure 2.14a). In particular, this *convolution effect* is more pronounced when the size of the object is smaller than the one of the tip. For example, Moreno-Herrero et al. show that, due to the tip convolution effect, DNA molecules appear to have a Full Width at Half Maximum (FWHM) of around 10 nm while the real dimension is 2 nm [120].
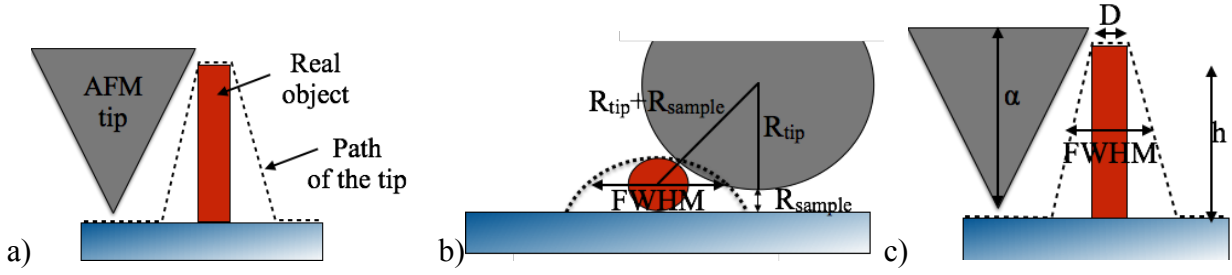
Figure 2.14: Tip dilatation effect. In a) the dimensions of the object appear larger in the tip path (image) than the reality. Two models b) and c) can be used to estimate the FWHM. Adapted from [78].

Depending on the shapes of the imaged object and the tip, different geometrical models can be used to determine the FWHM of the object. In particular, for a spherical tip of radius R_{tip} and a cylindrical object of radius R_{sample} on the surface (Figure 2.14b) FWHM is given by:

$$FWHM = 2\sqrt{2R_{tip} + R_{sample} + R_{sample}^2} \qquad (0.38).$$

While, considering a conical tip of angle tip apex 2α and a rectangular object of dimensions $h \times D$ (Figure 2.14c), FWHM is given by:

$$FWHM = D + h\tan\alpha \qquad (0.39).$$

Also, tip can cause *double tip* artefacts. This is due to the fact that tips can have more than one apex that scans the surface. Therefore, the recorded topography is characterized by two or more copies of the image of the object separated by a given distance equal to the separation between the two apexes (Figure 2.15).
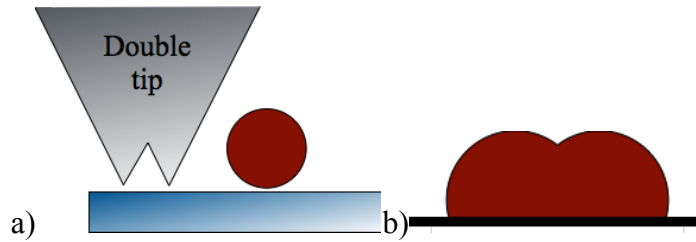
Figure 2.15: Double tip effect. Sketches of a) the configuration and b) the recorded image. Adapted from [78].

Other common sources of artefacts are the setpoint and the feedback. Their choice depends on different factors, such as the sample, the cantilever and the vibrations of the building [78]. The setpoint is the value chosen by the user for the parameter that has to be maintained constant by the feedback during the scanning (force, amplitude, etc.). The choice of this parameter influences the voltage applied to the piezoscanner by the feedback, thus the tip-sample distance will change as a function of the setpoint. For example, in the case of AM-AFM, the choice of the amplitude setpoint is related to the working regime. Thus, the quality of the image is highly influenced by this choice and can lead to noisy images. Also, the adjustment of the feedback will influence how fast is the response of the system. If the feedback is too low, then the image will be elongated and asymmetric

(called *parachuting* effect [107]), otherwise the image will be noisy and the system unstable, if the feedback is too high.

2.5.5 Resolution Limits

2.5.5.1 Lateral and Vertical Resolution Limit

A crucial concept that concerns all kind of microscopes is the resolution. AFM images are a 3-dimensional representation of the sample, therefore a distinction between lateral and vertical resolution has to be made.

The lateral resolution l has been defined by Bustamante and Keller as the minimum separation for which the indentation depth, arising from the intersection of individual images of two samples features, is larger than the noise [110]. This definition stands under the assumption that the tip and the surface are non-deformable objects. This means that the lateral resolution of a tip of radius R can be described as [121]:

$$l = \sqrt{2R}\left(\sqrt{\delta z} + \sqrt{\delta z + \Delta h}\right) \tag{0.40}$$

where δz is the vertical resolution and Δh is the height difference between the two features (Figure 2.16).
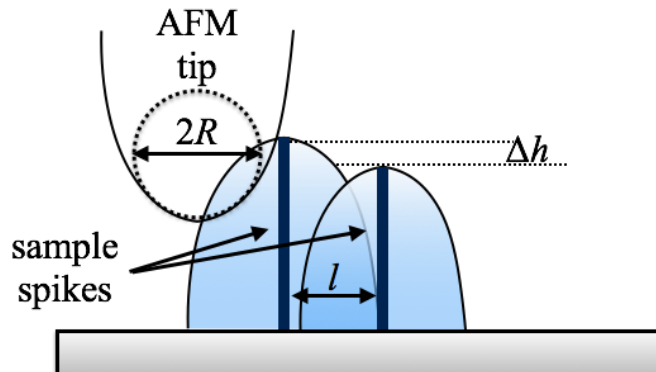
Figure 2.16: Sketch of the resolution limit of AFM. Adapted from [110].

From an experimental point of view, the final image is determined by the convolution of the tip and the sample, the tip geometry and the actual separation between the two points, leading to a dilatation effect of the object. Algorithms of deconvolution [122] exists. They can be used to treat AFM images, but the problem is that the geometry of the tip and its radius are not well known. Also, the tip radius may change during the experiments due to contaminations, giving rise to artefacts.

Vertical resolution depends on the thermal cantilever vibrations and the detection noise of the system. For AFM designs where the detection system is characterized by a photodiode, the thermal noise contribution is usually higher than the one of the detection system and defines the resolution limit. Its contribution can be obtained by applying the equipartition theorem [123]:

$$\delta z_{thermal} = \sqrt{\frac{4k_B T}{3k}} = \frac{0.074}{\sqrt{k}} nm \qquad (0.41)$$

The thermal noise is related to the cantilever geometry and the environment. By choosing a cantilever with high resonance frequency and large force constant, the thermal noise can be reduced [110]. The applied force can also affect the vertical resolution, if a soft material is studied. In fact, the application of a high force can lead to the compression of the sample faking the real height of the object, as well as electrostatic forces when working in liquid ambient [101].

2.5.5.2 Intrinsic Resolution Limit

One of the intrinsic limits of AFM is the determination of the height of an isolated nano-object adsorbed on a flat substrate. The problem is that even when the feedback parameters are well adjusted, the apparent height of the structure does not correspond to the real one, obtained for example via X-ray crystallography. Different reports have attributed this deformation to salt deposition, dehydration, compression [124], etc. Santos et al [112] have shown that the finite size of the object and the tip radius are responsible for the loss of true height in all AFM measurements, in any mode. Basically, they demonstrated that the height depends on the effective area of interaction between the tip and the sample. The particular geometry of the interaction causes the lateral spread-out and the consequent loss of vertical information.
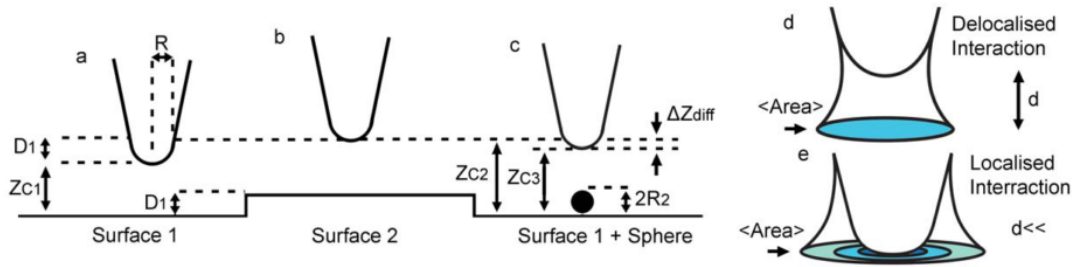
Figure 2.17: Scheme of the interaction between the tip, a finite sample object and an infinite substrate. Taken from [112].

The type of interaction (repulsive or attractive) between the tip, the sample and the surface support influences the height value: the tip-surface interaction force differs to the interaction force between the tip and a finite nano-object, from a geometrical point of view. In particular, for biomolecules, the convolution effects are intrinsically defined by the VdW interactions between an effective region given by the tip and the background supporting surface [112,124]. Under tip-sample repulsive interactions, the height value is greater than the one obtained when the interaction is attractive. One has also to take into account that the shape of the tip may change from one scan to another, thus the interaction may change too. The deviations from the real height can be up to 90%, which means that in general the real height of the sample is almost never obtained [112]. In addition, the spreading out does not only affect the height value but also the lateral size, hence its volume. This effect is added to a significant tip-sample convolution enlargement due to the fact that the nano-object size is small compared to the tip size.

Different methods have been developed to characterize the real dimension of a nano-object visualized by AFM, in particular in the case of proteins. Basically, they are geometric and direct methods capable of determine the volume of a protein when imaging in AM-AFM mode in liquid environment. Recently, a new volumetric method has been published by Fuentes-Perez et al. [124]. In this method, they use a DNA filament as a fiducial marker to minimize AFM artifacts and determine protein volumes with an error of 6-10%.

2.6 Force Spectroscopy Mode

Since its invention [3], AFM has been largely used as a force detector by means of force-distance curves. Especially, it has found many applications in the fields of biology and pharmacology. In fact, AFM is a "multifunctional molecular toolkit" [125] able to quantify surface forces, surface charge and hydrophobicity; and to study inter and intra-molecular interactions such as receptor-ligand interactions [126,127], protein unfolding [128], polymers elasticity [104,129] but also cell adhesion and mechanics [125,130].

In this working mode, information on the tip-sample interaction can be obtained, such as the adhesion force, and mechanical information on the sample (i.e. the Young modulus), such as the viscosity and elasticity. Also, molecular interaction can be monitored, since the AFM tip can be converted, by chemical modification, in a specific biosensor to study receptor-ligand binding. The force resolution is up to pN in liquid environments, since capillary forces are no longer the dominant ones and VdW forces can be monitored [92]. The high force resolution arises from small spring constant (0.5-0.01 N/m), but the stiffness of the cantilever and the laser power limits the force sensitivity [131].

To obtain a force-distance curve, the tip is displaced in the Z direction towards the sample until the tip interacts with the sample and then backward, until there is no more interaction between the tip and the sample (Figure 2.18a). There are two different working modes for force spectroscopy: the static and the dynamic modes. In the static mode, the deflection of the cantilever is collected as a function of the tip-sample distance while the tip gets close to the sample, is pressed against it and then retracted. In the dynamic mode, the tip is vibrating while it is moved close and far from the surface. The amplitude or the resonance frequency of the oscillation is detected as a function of the tip-sample distance [92,131]. The output of these kinds of measurement is a force-distance curve, a plot where the interaction force between the tip and the sample is represented as a function of the tip-sample distance [92] (Figure 2.18b). The tip and the sample are respectively moved one close to the other and then far away. During this, the deflection of the cantilever (δ_C) is detected as a function of the piezo displacement (Z) (Figure 2.18). The force is obtained via the Hooke's law:

$$F = -k\delta_c \qquad (0.42),$$

where k is the cantilever stiffness and the actual tip-sample distance (D) is given by:

$$D = Z - \left(\delta_c + \delta_s\right) \qquad (0.43).$$

Therefore, one should distinguish between the plot where the force is represented as a function of the piezo displacement (force-displacement curve, solid line in Figure 2.18b) and the one where the force is a function of the tip-sample distance (force-distance curve, dashed line in Figure 2.18b).
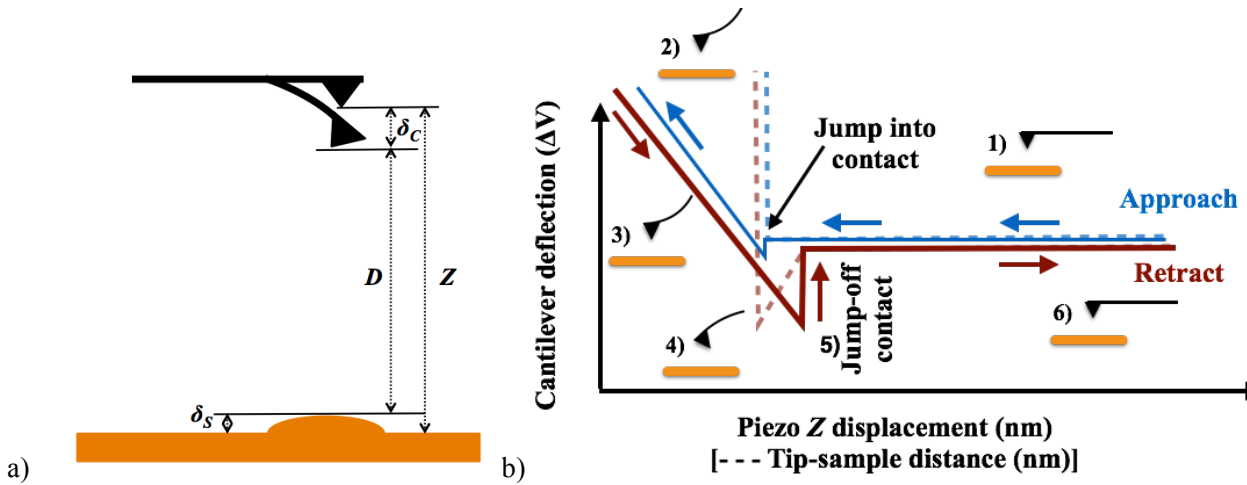
Figure 2.18: Schematic representation of a) the tip-sample system adapted from [92], where Z is the piezo displacement, D the actual tip-sample distance, δ_C the cantilever deflection and δ_S the sample deformation; b) force-distance curve, adapted from [131].

In Figure 2.18b, a typical force-distance cycle is depicted: the blue curve is the forward pattern (the tip approaches the sample) and the red one is the backward pattern (the tip is retracted from the sample). Three different regions can be detected: the zero line, the contact line and the non-contact region [92]. The zero line is given far from the surface (points 1 and 6 in the Figure) where the interaction between the tip and the surface is zero. The contact line (points 2 and 3) is obtained when the tip is in contact with the sample: the tip-sample distance is zero but the tip is pushed into the sample and therefore the deflection is different from zero ($\delta_C = Z$). The non-contact region is characterized by the jump-into-contact in the approach curve (the tip is snapped to the sample from a great distance due to attractive interactions) and by the jump-off-contact in the withdrawal curve (the point where the force given by the effective elastic constant of the cantilever becomes larger than the adhesive force between the probe and the sample) [131]. The non-contact region in the approach curve can give information about the attractive or repulsive forces before the contact. After this point, the force experienced by the tip and the sample is repulsive due to the overlapping of the orbitals, and both can undergo to reversible and/or irreversible deformations [131]. The withdrawal pattern gives information on the adhesion forces that can be used to study interaction strengths. Depending on the type of interaction between the tip and the sample, the shape of both curves changes, as shown in Table 2.1.
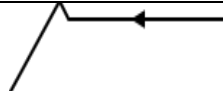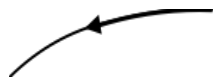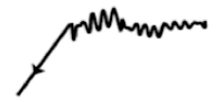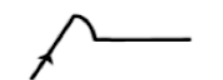
Force	Description	Shape of Curve
	FROM APPROACH CURVE	
Attractive Van der Waals force	Creates jump-to-contact peak: depends on force between tip and sample and the system geometry; Meniscus forces must be eliminated by working in a low humidity environment or liquid.	
Repulsive double-layer repulsive force	Due to charging both tip and sample surfaces with like charges (adsorption of ions from solution and dissociation of functional groups on surface).	
Repulsive hydration force	Comes from repellent interactions between hydrated ions bound to tip and sample surfaces; apparent at high salt concentration.	
Solvation force	When tip and sample are within a few molecular diameters from each other, oscillation between attraction and repulsion may be observed; caused by ordering of non-polar liquid molecules between the two liquid-solid interfaces; force follows density of solvent.	
	FROM RETRACTION CURVE	
Adhesion	Due to Van der Waals forces and indentation of sample by tip (which increases contact area); Meniscus force must be eliminated.	
Hydrophobic force	Appear on imaging hydrophobic samples in water; Results in gradually pull-off instead of a jump-off-contact.	

Table 2.1: Types of tip-sample interactions. Adapted from [131].

In the following, two spectroscopy modes largely used to study biological interactions are detailed.

2.6.1 Single Molecule Force Spectroscopy

Single Molecule Force Spectroscopy (SMFS) experiments have been largely applied in the study of biological interactions at the nanoscale, since they allow studying non-covalent interactions involved in all biological systems. Different information can be obtained from SMFS experiments, depending on which kind of study one wants to perform and which system is under investigation. One can obtain information about unbinding force, rupture length (receptor-ligand interaction) [126,132], energy landscape [133,134], and fit the force-distance curve with worm-like chain (WLC) and free joined chain model (FJC) to obtain information about elasticity and conformational transition (stretching of polymers, as polysaccharides and DNA molecules) (Annex I) [104,135].

2.6.1.1 Analysis of a curve

When performing SMFS experiments, a functionalized probe is approached to and then retracted from the sample surface, at a given speed (pulling speed). The probe bears the receptor and the corresponding ligand is immobilized on a solid substrate. Therefore, specific receptor-ligand interactions can be detected and in most of the cases they have a characteristic shape of polymer stretching events (Figure 2.19). In the backward curve, stretching events can be detected: they present a characteristic pattern that is attributed to a particular interaction, and information such as the unbinding force and the rupture length can be extracted. The **unbinding force** ($F_{un.}$) is described as the maximal force of the characteristic adhesion peak of the interaction, calculated from the zero line. The **rupture length** (L_R) is defined as the distance of the peak position to the contact point. Another important parameter is the **adhesion rate**, the percentage of curves that presents an unbinding event.
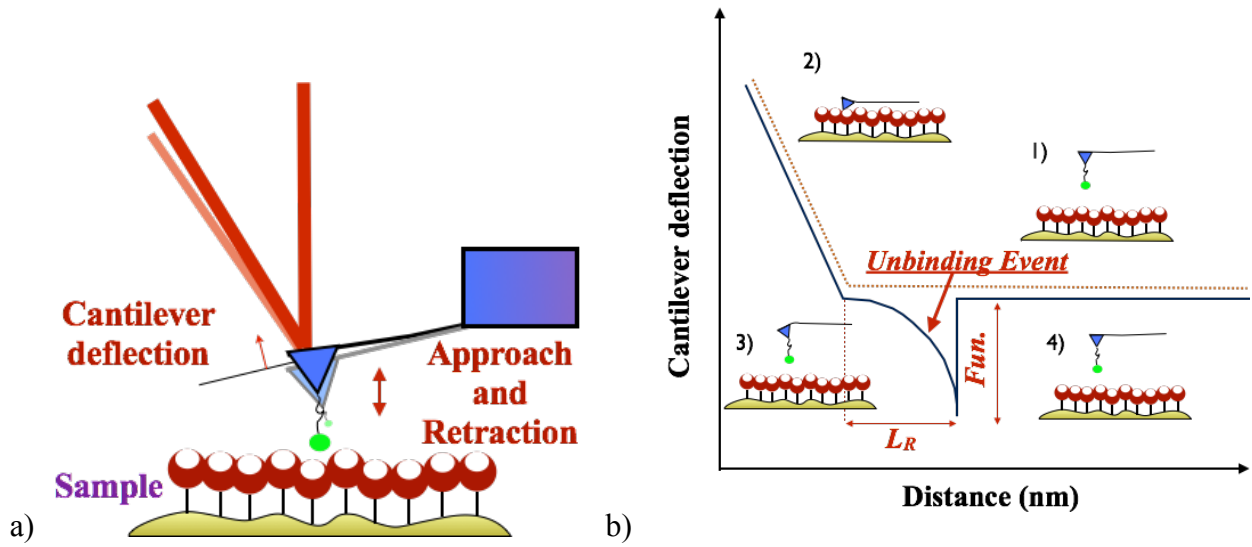
Figure 2.19: Sketch of a typical a) receptor-ligand interaction of a SMFS experiment and b) force-distance curve where the characteristic stretching event is detected.

In general, the unbinding force depends on the dynamic of the process (the applied force and the kind of instrument used). For AFM measurements, the applied force helps to decrease the activation barrier of dissociation and to increase the off-rate of the complex [136]. The unbinding is a probabilistic event well described by a Gaussian distribution; therefore a lot of statistics is needed (around 1000 curves). Another reason of collecting a large amount of data is related to the static and dynamic disorder of the system. This means that the behaviour of each molecule of an ensemble population is not exactly the same, and can be different under the same stimulus [137]. Also, biological systems can show heterogeneous properties which are related to biological functions [102]. For these reasons, one should perform a statistical study of the behaviour of the receptor-ligand pair and express the data via histograms, showing the distribution of at least 1000 events.

2.6.1.2 Determination of the dissociation constant

SMFS experiments provide a method for measuring the dissociation constant (k_{off}, section 1.3.3) of the receptor-ligand interaction. The off-rate of a reaction is related to the strength of the bond, thus to the thermal energy and the activation energy barrier of the dissociation process (Figure 2.20a) [138]. The activation energy for the dissociation is given by the difference in energy between the initial state and the transition state at highest energy, which must be overcome to get the dissociation.

If the dissociation process is analysed upon the Kramer's theory [139] for activated processes, considering a null applied force, then the off-rate for the dissociation can be written as:

$$k_{off}(F_{appl.} = 0) = we^{-\Delta E/k_B T} \qquad (0.44),$$

where w is a frequency prefactor and ΔE is the activation energy.

When performing SMFS experiments, one applies a force to the system that obviously influences the dynamic of the receptor-ligand interaction. Due to the differences of various orders of

55

magnitude in the timescale of the thermal motion and the timescale of the variation of the force, the applied force can be considered as constant [138]. The bond lifetime is reduced under the applied force due to thermal activation as well as the mechanical properties and the unbinding force [127]. In fact, the mechanical properties and the unbinding force depend on the applied force and the pulling speed: increasing the applied force means increasing the bond strength of the non-covalent interaction. Therefore, the rising of the applied force influences the energy barrier of the interaction by lowering it and, consequently, amplifies the dissociation kinetic in an exponential way (Figure 2.20a) [140]. In particular, the energy barrier is modified by a factor Fx:

$$\Delta E(F_{appl.} = F) = \Delta E - Fx \tag{0.45}$$

assuming F and x parallel. Therefore, the off-rate constant will depend on the applied force by a Boltzman distribution:

$$k_{off}(F_{appl.} = F) = k_{off}(F = 0)e^{-Fx/k_B T} \tag{0.46}.$$

From an experimental point of view, the shift of the unbinding force to higher force values is linearly related to the natural logarithm of the loading rate r. The loading rate can be defined as the force applied during a time interval, and can be expressed through the product of the stiffness of the system (k) and the pulling speed (v) during retraction:

$$r = -\frac{dF_{appl.}}{dt} = kv \tag{0.47}.$$

By studying the unbinding force as a function of the applied loading rate, one can estimate the off-rate constant of the unbinding process at zero force ($k_{off}(F_{appl.} = 0)$). In fact, due to the linear relation between the maxima unbinding forces (F^*), obtained at different loading rates, and the natural logarithm of the loading rate, one can plot the maxima force values F^* as a function of the logarithm of the loading rate (Figure 2.20b). The linear regime is related to the energy barrier of the dissociation process and it can be expressed by the equation:

$$F^* = f_\beta \ln\left(\frac{r}{f_\beta k_{off}(F_{appl.} = F)}\right) \tag{0.48},$$

where f_β is the slope of the curve [127]. Then, from the plot of Figure 2.20b one can extrapolate the value of the $k_{off}(F_{appl.} = 0)$ as:

$$k_{off}(F_{appl.} = 0) = \frac{r(F^* = 0)}{f_\beta} \tag{0.49}.$$
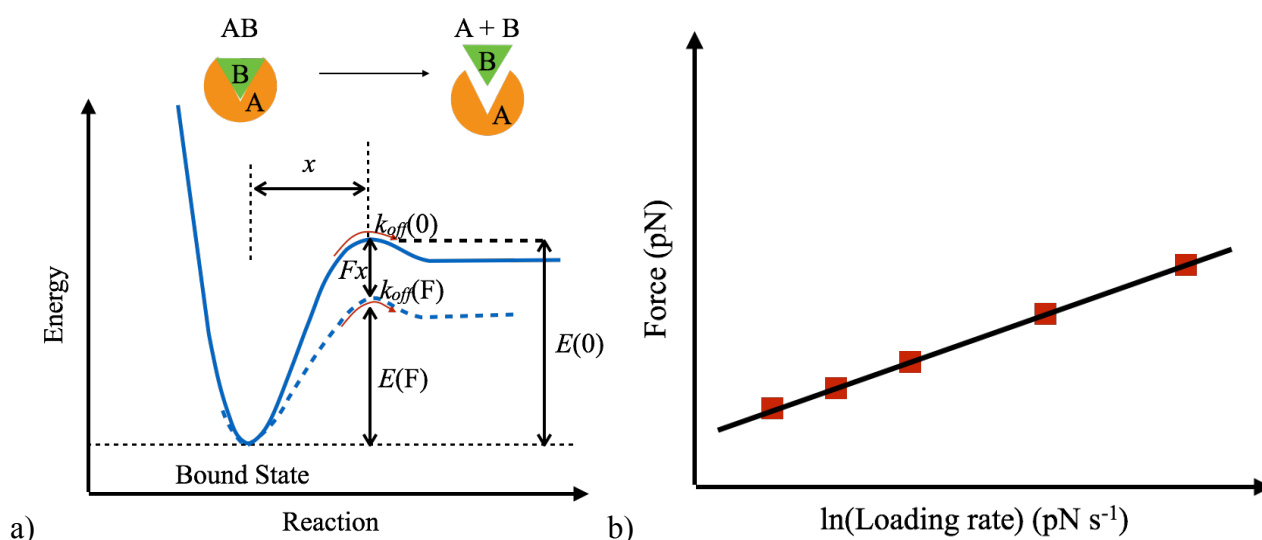
Figure 2.20: a) Schematic diagram of the energy landscape, where the dissociation without an external force (solid line) and with an applied force (dashed line) are represented, characterized by the dynamic parameters $k_{off}(0)$ and $k_{off}(F)$, respectively. The exponential increase of the barrier is located at a distance x, projected along the direction of the applied force, corresponding to the transition state. b) Schematic force spectra. Adapted from [138].

2.6.1.3 Tip functionalization

To study receptor-ligand interactions, AFM tip has to be transformed in a specific biosensor in order to study intermolecular interactions [11,141]. Different strategies have been developed in order to attach biomolecules to AFM tips. They are based on chemical modifications of the tip and the using of a spacer molecule to link the biomolecule of interest to the tip. The choice of the spacer depends on the type of molecule that has to be attached to the tip, while the length of the spacer can be affected by the kind of measurements performed. Also, the spacer allows distinguishing specific and non-specific interactions, and due to its flexibility, it allows the free orientation of the receptor with respect to the ligand at the surface (Figure 2.21).

The main requirements for tip functionalization protocols are that:

i)   The biomolecules must be covalently bound (1-2 nN) to the tip to allow a binding stronger than the intramolecular forces under study (10 times stronger) [127,142];

ii)   A low density of the attached biomolecules is requested (1-3 molecules) to allow single molecule studies and a good access (mobility and orientation) of the ligand molecule grafted on the surface [126,127,142];

iii)   The detection of specific adhesion forces should be enhanced by inhibiting the unspecific unbinding.

Various laboratories have developed different tip functionalization techniques to satisfy these requirements [143–145].

57
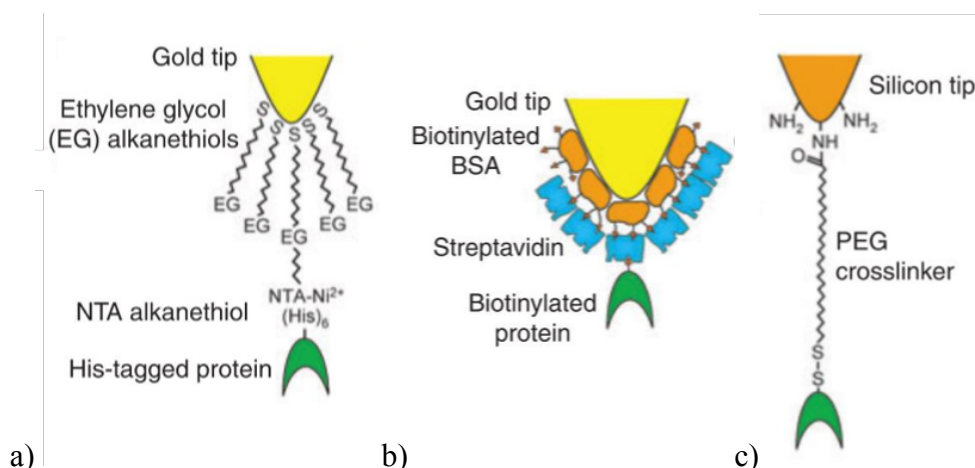
Figure 2.21: Strategies used for tip functionalization: a) chemisorption of alkanethiols, b) physisorption of proteins and c) covalent binding of silanes. Adapted from [127].

Generally, self-assembled monolayers (SAMs) characterized by specific terminal groups are used to chemically modify the tip [127,143] (Figure 2.21). Depending on the tip material, ethylene glycol (EG) alkanethiols or silane molecules are used to create the SAM.

If the tip is made of gold or silicon nitride tip coated with gold, EG alkanethiols are used due to the strong covalent bond formed between Au and S molecules [127]. The protein can subsequently be linked to the tip via an NTA-Ni-hystidine system. With this linking method, the system is site oriented with a disadvantage of a low binding strength (150-200 pN), of the same order of the receptor-ligand forces under study (Figure 2.21a). Another functionalization approach that involves gold-coated tip is characterized by the use of biotinylated BSA that can bind to streptavidin molecules used to immobilize the biotinylated protein under study (Figure 2.21b). With this strategy, the interaction between complementary oligonucleotides has been studied [127].

To functionalize a silicon nitride AFM tip, the group of Hinterdorfer have used standardized 3-step procedures to evaluate the effects of amino-functionalization by studying three amino-modifications of the tip [136,143,145] (Figure 2.21c). They studied the interaction of the model system biotin-streptavidin by adsorbing the streptavidin on a mica surface, while the AFM beard the biotin. The results obtained, by functionalizing the AFM cantilevers and performing molecular recognition experiments, were compared with results obtained via functionalization of silicon nitride wafers (5 x 5 mm), used to perform enzyme assay measurements. Three different methods were used to generate NH_2 groups, as depicted in Figure 2.22 [143]:

i)   Ethanolamine coating,
ii)   (3-Aminopropyl)triethoxysilane (APTES) silanization or
iii)   AphS functionalization.
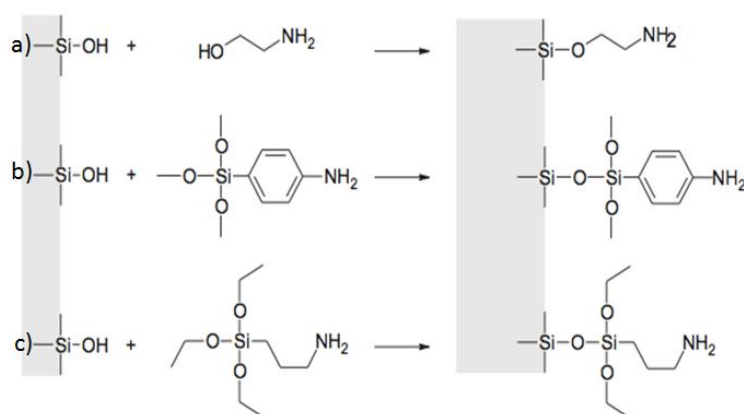
Figure 2.22: Amino-functionalization of Si₃N₄ tips. The SiOH groups present on the tip surface react respectively with a) ethanolamine, b) APhS and c) APTES molecules. Taken from [143].

They studied the final density of the immobilized receptor on the surface to have an idea of the density on the tip surface. They found that all the three procedures gave ~2000 surface-bound antibody molecules/μm^2 (after the binding of Extravidin®-peroxidase to immobilized biotin-IgG), which should be correlated to one active receptor per AFM tip [136]. By judging the SMFS curves one can say that the functionalization procedure gives from 0 to sometimes 3 tip-bound probe molecules [136]. Fluorescence tests can also be done to check the density of the receptor on the tip [126]. Furthermore, they performed single molecule experiments to test the three silanization methods. For each tip, they recorded 1000 consecutive force-distance curves, showing that the percentage of unbinding events were 23% with APhS tips, 19% with ethanolamine tips and 16% with APTES tips; while the rate of unspecific binding events after the tip was blocked (with streptavidin) were 3%, 2%, 4% respectively, providing a specificity of the interaction of 20%, 18% and 12%, respectively. Also, they showed that the unbinding length is almost the same while unspecific unbinding events can happen at various distances.

Therefore, the grafting of amino-silane molecules does not influence the spectroscopy measurements: the density of surface-bound antibody molecules is more or less the same, and the results are similar, in terms of unbinding forces and rupture lengths: only the unspecific binding changes [143]. Of course, the difficulties are related to the functionalization protocols: ethanolamine coating is the simplest procedure but needs an overnight reaction. For APTES silanization the freshness of the silane molecule and exclusion of air are mandatory. Also, it requires a curing of 2 days. Lastly, APhS has the advantage of a short overall time even if the storage and the dosage are critical [143].

After the amino-functionalization, heterobifunctional spacers, usually poly(ethylene)glycol (PEG), are bound to the NH_2 groups with one end, while the other one reacts with the receptor molecule, resulting in a covalent binding of the receptor to the tip [143]. These last two steps are typically done under conditions that ensure high turnover, while the amino-functionalization is performed under conditions that develop a low surface density of attachment sites (one to two receptors per tip apex) [143]. Depending on the kind of molecule studied, different PEG can be used to covalently

tethering the molecule to the tip. The aim of the spacer is always to give motional freedom to the receptor, which is able to freely orient itself with respect to the molecules immobilized on the surface [127]. For example, acetal-PEG-NHS and aldehyde-PEG-NHS linkers can be used to bind proteins such as LecA lectin [135], thanks to the lysine groups of the protein.

In using a flexible molecule as spacer, it has to be taken in mind that also the PEG linker (not only the receptor) is stretched during the retraction. The use of a soft polymer as a linker can affect the loading rate and alter the expected unbinding force [146]. The unbinding force of a receptor-ligand couple depends on the loading rate but also on the linker used to attach the receptor to the tip. In fact, longer and more flexible the linker is, lower the unbinding force will be. Also, the flexibility of the linker can modify the applied loading rate. The presence of the linker can determine a non linear relationship between the increasing of the loading rate and the increasing of the unbinding force, thus the applied loading rate is not the effective one, since the binding undergoes to a non-uniform accumulation of force [146]. Therefore, the choice of the polymer length and stiffness, as well as the loading rate, is of great importance in molecular recognition experiments.

2.6.2 Single Cell Force Spectroscopy

A crucial question in biology is how cells work. Basically, cell bindings and cell mechanics are the cornerstone to understand cell-cell interaction, cell adhesion, embryonic, tissue and cancer development, cellular communication, etc. To this end, single cell techniques are largely applied to answer these questions. Single Cell Force Spectroscopy (SCFS) has become a field of great interest for AFM community, since it consents studying the interaction between two cells as well as their mechanical properties in an environment that mimics physiological conditions [147]. Also, AFM-SCFS is the only technique that allows sensing and localizing specific interactions between cell surfaces with high resolution over a wide range of forces (from 5 pN to 100 nN) [130,148].

2.6.2.1 Analysis of a curve

A typical setup of SCFS is depicted in Figure 2.23a, where the cell-cell interaction is represented as example. In this case, one single cell is attached to the cantilever, while a second cell is immobilized on the substrate. The cell-tip is approached to the sample and the contact between the two cells is formed. After a certain contact time, that allows the interaction between the two cells, the probe is retracted leading to the rupture of the formed bonds until the two cells are completely separated.
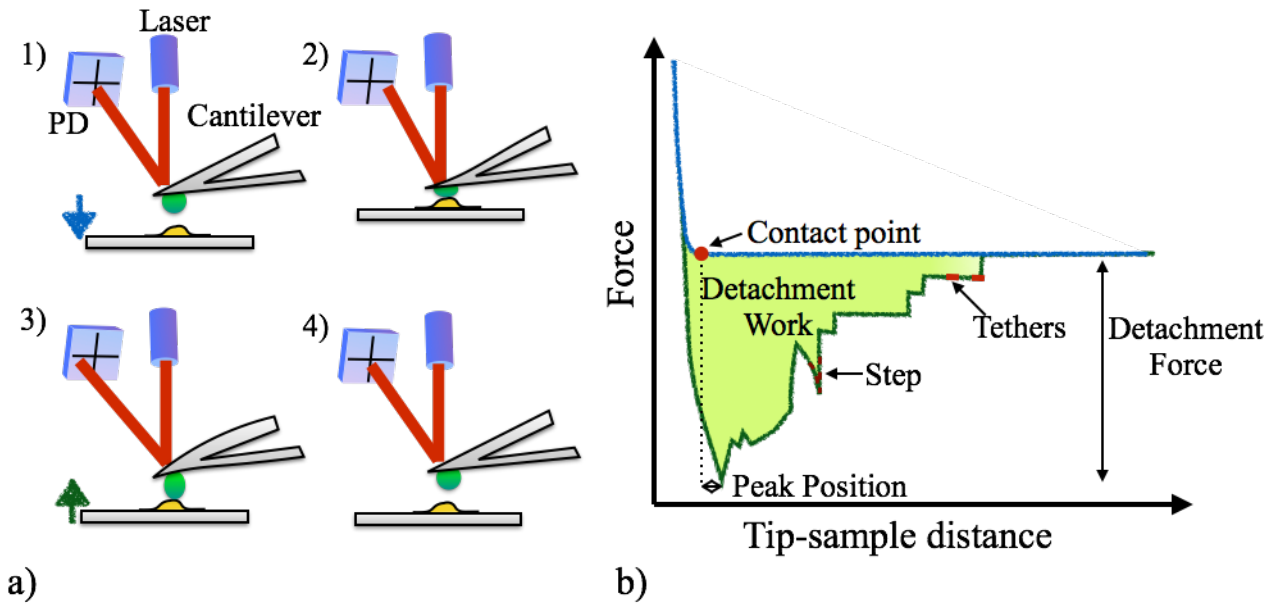
Figure 2.23: SCFS force-distance curve. a) The four steps that characterize the approach and retract patterns are represented and b) the corresponding approach and retract curves, adapted from [130]. *1) The probe is far from the sample and the zero force interaction is detected; 2) the contact between the probe and the sample is formed. The probe is pushed on the sample and then retracted. 3) The probe is moved forward and the cell-cell bond is broken until 4) the zero force is reached.*

The retract curve contains a lot of information (Figure 2.23b). The detachment depends on the number, position and binding strength of the receptors that are involved in the binding. Also, it depends on possible non-specific interactions and on cell properties, such as cell elasticity, membrane composition, cytoskeletal dynamics and glycoalyx. They can affect the interaction, leading for example to the deformation of the cell cortex [130,149]. Once the cell is detached, discrete events such as step events, due to the detachment of the receptors from the cell cortex, and tethers events, due to the detachment of membrane tethers (plateau in the retraction pattern), can be monitored. The important parameters that can be collected from a series of SCFS experiments are shown in Figure 2.23b.

The **detachment work** (W_D) is defined as the integral of the area between the baseline and the retraction curve. It describes the dissipated energy of the cell-cell detachment process. It is associated with the whole cell-cell interaction, given by the sum of all involved types of bindings. The **detachment force** (F_D) is the maximal force obtained as the distance between the baseline and the point where the maximum detachment force is detected. F_D characterizes the maximum adhesion between the cells. It depends on the binding strength, the number, and the placement etc. of the different receptors that are involved in the interaction. If the cooperativity of the different receptors is strong enough, the cell cortex can be mechanically deformed [130]. The **peak position** (P_P) is defined as the distance between the contact point and the position of F_D. A change of peak position can be explained by [150]:

i)   Extremely compliant cells;

ii) Membrane tethers, which are pulled out of the cell membrane by the external force;

iii) Filopodia or other micro-extensions, which are actively formed by the cells.

Also discrete events can be analysed, in particular **steps** (Figure 2.24a) and **tethers** (Figure 2.24b) events. Steps are defined by a slope before rupture, while tethers present a force plateau prior to rupture. The former are related to receptor-ligand interactions and can give information on the affinity of cell adhesion receptors [149], while tethers events are related to the formation of viscous membrane tethers, which facilitate intracellular attachment and communication [148,150,151]. Membrane tethers formation happens when the probe anchor the membrane and pulls it, forming a viscous membrane tube that is characterized by a constant plateau force. The parameters that can be analysed for such events are: the **step height** (the distance in force between the baseline and the individual event), the **frequency** (the percentage of curves that show at least a step event), the **step position** (the distance between the step event and the contact point) and the **average number of step per curve** [150]. Tethers events display a characteristic constant force plateau that can be characterized by the **tethers height** (difference in force before and after the event), the **frequency** (the percentage of curves that show at least a nanotube event) and the **average number of tethers per curve** [151].
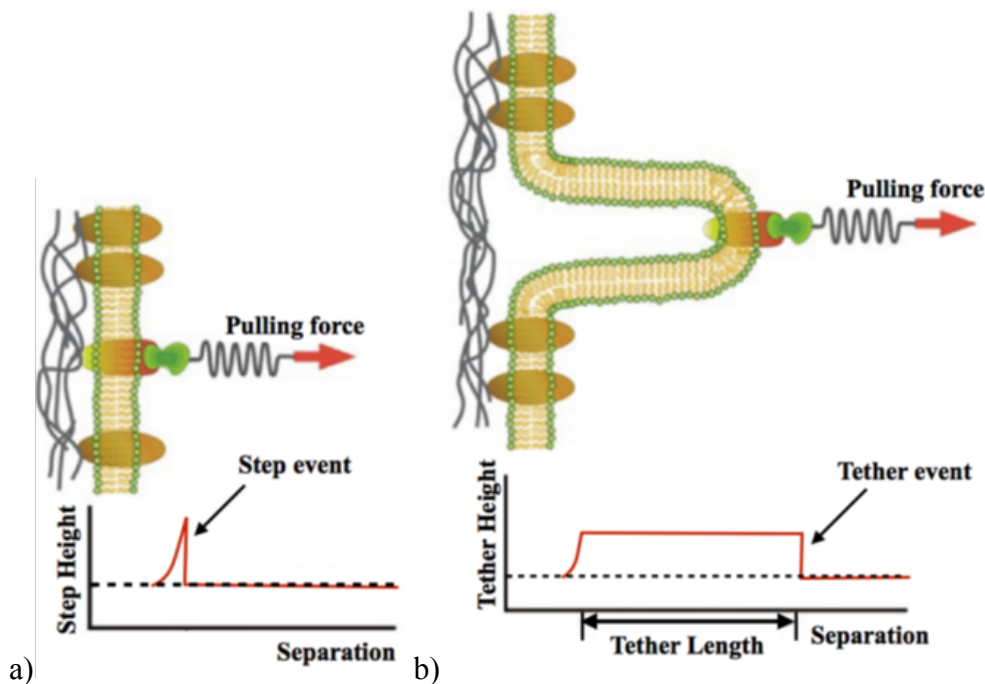
Figure 2.24: Sketch of discrete events (steps on the left and tethers on the right). Adapted from [148].

Steps events are related to receptor-ligand interactions. In fact, SCFS experiments are platforms to study single binding-receptor interactions for short contact-time conditions. In contrast to SMFS experiments, receptor-ligand interactions are studied in their natural cellular environment, allowing the use of native proteins (and not purified ones such as in SMFS) in an ambient that mimics the physiological conditions [130,152]. Of course, the complexity of SCFS experiments is higher than SMFS as all the interactions are together and their signatures can overlap. The complexity is also due to the fact that cells can deform under the application of a mechanical stress, and other

phenomena can appear due to the mechanical contact between the two membranes. Using mutants (cells that express only certain receptors) and playing with contact time can help in discriminating the interaction under study. Dynamic studies of the receptor-ligand interactions can be performed, and information on the energy landscape of the interaction can be acquired, such as dissociation constant, free energy and transition state [140].

Membrane tethers appear when the probe anchors the membrane of the immobilized cell and it is mechanically pulled originating tubes with a diameter of few nanometres. These structures appear in the retracted curve as long plateau [149]. Membrane tethers give information on the adhesive state of the cell. The detachment force (F_m) of the tether is associated to the mechanical properties of the cell, since the force is related to the membrane tension (T_m) and stiffness (S_m) by the relation [149]:

$$F_m = 2\pi\sqrt{T_m S_m}$$
(0.50).

Studies show that tethers may be implicated in cell-cell adhesion, in intra- intercellular signalling and also tethers force should depend on the disruption of the cytoskeleton [153]. The adhesion force and the unbinding events are contact-time dependent: increasing the contact time between the probe and the substrate leads to an increase of adhesion force, consequently cell properties can be explored by modifying the contact time [130].

Unfortunately, limitations of the system do not allow long-contact-time experiments (more than 20 minutes) due to the strong cell-cell adhesion after longer-contact-time (1 hour) which defeats the capabilities of the technique [130]. Many force-distance curves have to be acquired and the experiment has to be repeated with different probes and substrates to have a statistical interpretation and consistent results. Also, control experiments must be performed to ensure the specificity of the interaction. SCFS are time-consuming experiments because one has to take care of the reproducibility of the setup in order to have reliable results. For example, cell should be in the same state in all the experiments to show similar adhesive properties [149]. Also, the complexity of the system studied makes difficult the comprehension and interpretation of the results [130]. Therefore, researchers are always trying to improve the capabilities of the technique and to develop methods for data analysis and mathematical models to describe the system.

2.6.2.2 Tip functionalization

Due to the flexibility of the setup, two experimental configurations are possible and different information can be obtained. The cell can be attached to a tipless cantilever (Figure 2.25a and b), making the cell the AFM sensor, and the adhesion with another cell or a substrate can be studied. Otherwise, the cell can be immobilized on a solid surface and the interaction with either a functionalized tip (Figure 2.25c) or a bead (Figure 2.25d) can be studied to obtain adhesive information [149]. Both configurations present some advantages and disadvantages. In particular, a cell probe allows using the same probe with different samples and in different parts of the sample, diminishing the risk of contamination due to residuals left behind. The sample substrate can be another cell to study cell-cell interactions. The main disadvantage of this configuration is the immobilization step where the cell is anchored on the cantilever, since it can affect the cell state

[149]. If the cell is immobilized on the substrate, and a functionalized probe is used for SCFS experiments, then the same probe can be used to study different cells. In this case, contaminations of the probe can occur due to the cellular contact, therefore short contact times are preferred. Also, the shape of the probe can influence the measurement (tip or colloidal cantilevers) since the contact area changes and thus the adhesion [149].
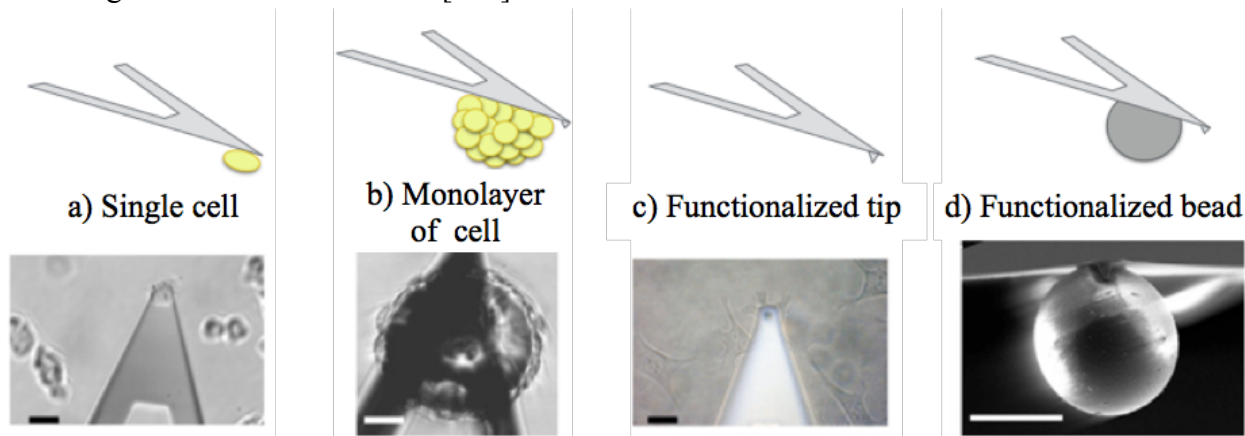
Figure 2.25: Sketches and microscopy images of the different functionalization techniques used in SCFS studies. Adapted from [149].

Both tip and tipless cantilevers can be functionalized for cell attachment (Figure 2.25). For tipless cantilever, the cell suspension is deposited on a substrate ready for the attachment. The cantilever is than pushed onto a single living cell, and maintained in contact for a certain amount of time in order to fix the cell on the cantilever [130].
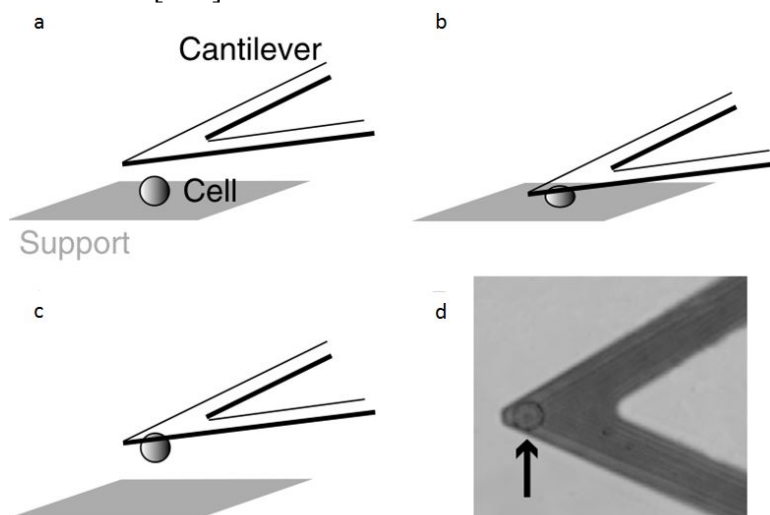
Figure 2.26: Modification of an AFM cantilever with a cell. a) The functionalized cantilever is brought into proximity of a single cell lying on the substrate; b) the cantilever is gently pressed onto the cell and c) the cell is finally converted in a probe for AFM-SCFS experiments; d) optical image of the cell attached to the cantilever. Taken from [130].

Otherwise, the entire tip is covered with cells (Figure 2.27). In both cases, the silicon nitride probe must be chemically functionalized to ensure cell attachment. Different chemical modification can be used, such as lectins (i.e. wheat germ agglutinin) [152], PEI [154], poly-L-lysine [155], Cell-

Tak™[6] or polyadopamine [156] coatings. Depending on the kind of cell used (animal or bacterial) the functionalization result can lead or not to reliable single-cell measurements [156]. In fact, for animal cell-probes, there exist well established protocols that allow the attachment of a single cell on the cantilever [152]. On the contrary, for bacterial cells, denaturation or death of the bacteria, weak bonding and multiple cell attached on the cantilever determine unreliable single-cell measurements [156]. Vadillo-Rodriguez et al. [157] compared the interaction forces between bacteria and silicon nitride tips for three common immobilization methods (mechanical trapping, physical adsorption and coating). They demonstrated that the immobilization method not only influences the characteristic shape of the interaction force between bacteria and silicon nitride, but also the fixation of the bacteria on the tip, which gives incomplete coverage and not well reproducible results (see Figure 2.27).
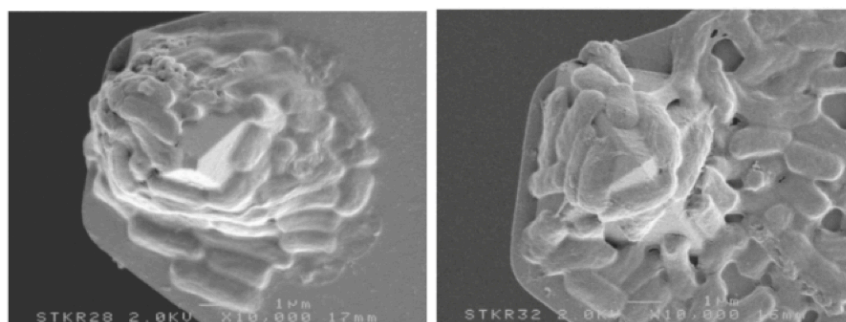
Figure 2.27: Electron microscopy images of bacterial functionalized AFM tip from Ref. [157].

Furthermore, colloidal probes (Figure 2.25d) are also widely used to study cells due to the increasing of the measured force that induces an increasing in the sensitivity [158]. In particular, the so called "colloidal probe technique" is quietly used to study the adhesion forces [159] between a sphere and a surface, the hydrophobic forces and also the cell mechanics. The technique was introduced in 1991 by Ducker [160] and Butt [100]. Recently, Beaussart et al. [161] have developed a protocol, which involves the use of a colloidal probes to attach a single bacterium on it. The protocol allows a better control of the position of the bacterium on the cantilever, an increasing of bacterial lifetime during experiments up to 1 h and it avoids problems of non reproducibility of tip functionalization [157].

2.7 Preparation of biological samples

A big issue when performing biological AFM (both imaging and force spectroscopy measurements) is the sample preparation. The biological molecules should be well attached to a flat biocompatible substrate. Commonly used substrates are mica, glass, silica and ultra-flat gold [162]. The biomolecules can be immobilized on the surface by covalent binding or physical adsorption, depending on the type of molecules and the type of study performed [127].

---

[6] Cell-Tak™ is a formulation of "polyphenolic proteins" obtained by extraction from the marine mussel *Mytilus edulis* that it is used to anchor to solid structures [149].

Mica is the most widely used substrate to adsorb positively and negatively charged molecules. It is a layered mineral, which can be cleaved with adhesive tape to obtain an atomically flat surface [163]. Since at neutral pH mica is negatively charged, the physical adsorption of positively charged molecules is possible. Therefore, positively charged molecules, such as avidin molecules [164], lysozomes and even membranes, can be easily adsorbed on this mineral. Also, DNA molecules, which are negatively charged, can be imaged on mica substrate in presence of divalent cations such as Ni^{2+}, Co^{2+}, Zn^{2+} or Mn^{2+} [165].

When covalent binding is required for the immobilization of biomolecules, glass, silica and flat gold surfaces can be used. In particular, flat gold is obtained by thermal evaporation of gold on a flat mica substrate. It is subsequently glued onto a silica substrate, and lastly it is peeled by removing the mica: an ultra flat gold with a roughness of the order of 2 Å per 2.25 μm^2 is obtained [166]. The substrates are then functionalized in the same way as AFM tips can be functionalized, via silanization or alkanethiol substrate modifications. Depending on the technique used to modify the surface, the final density of the grafted molecules can change. In fact, silanes lead to a lower surface density (>1000 molecules/μm^2) while the adsorption of streptavidin on mica is ~60000 molecules/μm^2 and that of a phospholipid monolayer may go beyond 10^6 molecules/μm^2 [127].

The immobilization of cells has to be done in a way in which the cellular integrity and viability are conserved [162]. For animal cells, a simple preparation method is to exploit their abilities to spread and adhere to solid surfaces [127,162]. Otherwise, the immobilization can be enhanced by coating of the substrate with Cell-Tak™, gelatin, collagen, poly-L-lysine or chemical fixation can be obtained using crosslinking agents such as glutaraldehyde, which is more suitable for imaging than force spectroscopy [127,162]. Bacteria cannot be spread on a solid support, therefore simple adsorption of microbial cells is not possible [127,167]. In this case, immobilization can be achieved by treating the substrate with polycations or lectins or by mechanically trap the cells in a polymer membrane with a pore size comparable to the dimensions of the cell [127]. Meyer et al. [167] tested different immobilisation techniques to block Gram-positive bacteria *Staphylococcus* on a substrate and image them in different liquid media. They compared (Figure 2.28) physical confinement, physicochemical interaction, covalent bonding and adhesive polyphenolic proteins; showing that some methods do not allow successful immobilisation and the best results were obtained with polyphenolic proteins Cell-Tack™ and adopamine modified surfaces even though the tip can be contaminated by these proteins.
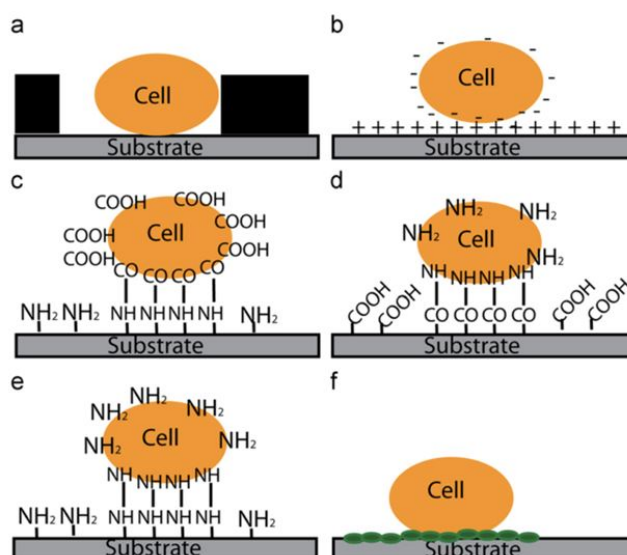
Figure 2.28: Schematic representation of the different methods used to immobilize bacteria on the surface: a) physical confinement, b) attractive electrostatic interactions, c) covalent binding to amino-functionalized surfaces by EDC-NHS[7], d) covalent binding to carboxyl-functionalized surfaces, e) covalent binding to amino-functionalized surfaces by glutaraldehyde, and f) attachment to Cell-Tak™. Taken from [167].

2.8 AFM on PA bacteria

In this Chapter, the AFM technique has been presented. In particular, the working principles, the interaction forces and the different operation modes used during this Ph.D. thesis have been shown. Particular attention has been paid on the capabilities of the technique to study biological systems: AFM is a nano-toolbox for biology [107]. Since its development it has been largely applied to study biological samples such as DNA [165], proteins [168], viruses [106], cells [169], etc. With AFM, not only the topological aspects can been revealed, but also the mechanical properties that are related to biological functions. Therefore, this technique is a powerful tool to investigate molecular interactions, forces and motions, providing additional opportunities to understand fundamental biological processes [1].

In particular, AFM has been largely used in the field of bacteriology, to study mechanical properties of bacteria and relate them to biological functions. Also, it has been applied to study the effects of antibiotics on bacteria via AFM imaging, Single Molecule Force Spectroscopy and Single Cell Force Spectroscopy [5]. In fact, various groups have shown interest on PA bacterium and its virulence factors. For example the group of Terri A. Camesano have largely applied AFM technique to study Lipopolyssaccharide (LPS) and Extracellular Polymeric Structures (EPS) virulence factors (section 1.1.2.3) [9,170]. LPS and EPS are present on the outer-membrane of the bacteria and play a role in bacterial adhesion. The density, distribution and the thickness of the LPS coverage are not the same all along the outer membrane as well as for EPS. This heterogeneity is a

---

[7] EDC = 1-ethyl-3-(3-dimethylaminopropyl) carbodiimide hydrochloride; NHS = N-hydroxysuccinimide.

key point in understanding and predicting bacterial adhesion [171]. In fact, both LPS and EPS are involved in adhesion and in particular they influence the properties of the outer-membrane, the electrostatic interactions and the steric repulsion [170]. Moreover, the group have performed nano-indentation single-molecule studies to understand the relation between LPS and the virulence of PA. By analysing approach curves, they looked for connections between the length of the O-antigen chains and the virulence, by analysing the steric repulsion of the bacteria against a silicone nitride tip. Unfortunately, no clear evidence were found [9]. Nevertheless, they showed the existence of a correspondence between the increasing of adhesion force and virulence, since wild-type bacteria presented higher adhesion forces than mutants.

Great interest has been provoked by pili structures of PA. In particular, various studies have been carried out on pili type IV. Pili type IV are semi-flexible rodlike fibers that serves to the bacteria to adhere to host cells and are involved in biofilm formation (section 1.1.2.1) [10]. They are formed by the association of some proteins and thousands subunits called pilin, which interact weakly one to each other, giving origin to a helical structure. Touhami et al. [10] have characterized the morphology and the adhesion force of pili on mica surface, finding that pili are mostly attached on the polar part of the bacteria and often aggregate to form clusters. They have a diameter between 4-6 nm and a length that varies from 0.5 to 7 μm. The group measured adhesion forces of pili structures of ~ 95 pN with rupture length up to ~ 600 nm. They tried to fit the single stretching events with either WLC or FJC model to find the persistence length of the molecule and get information on the stiffness. Unfortunately, it wasn't possible since the persistence length was not reliable. Also, they analysed the slope of the events, which did not depend on the length of the stretched molecule, therefore it could not be related to the elastic properties of the pili. More recently, the group of Dûfrene has studied the interaction of pili type IV with hydrophilic and hydrophobic surfaces (and vice versa) [7]. To do that, they have developed a new protocol of tip functionalization, by means of attaching a single bacterium on a colloidal probe [161]. What they found is that the pili are responsible for long-range interactions and that the other LPSs and proteins present on the surface membrane of the bacterium are probably responsible of the short-range interactions. Also, they showed that pili interactions with abiotic and biotic surfaces come mainly with plateau tethers, and this mechanical response enables the adhesion of the bacteria to the host cell.

Studied have also been conducted on PA biofilm structures. For example, Kannan et al. [172] have studied the adhesion force of PA biofilms as a function of the roughness of the silicon substrate. As expected, they found out that the adhesion force increases as the roughness increases due to the increased production and accumulation of extracellular polymeric material.

Antibacterial experiments have also been performed on PA bacteria, by taking advantage of AFM imaging and single-molecule force spectroscopy. Formosa et al. [6,169] used the electrostatic interaction to immobilise PA on positively charged surfaces and studied the PA bacterial resistance against three different antibiotics. They analysed the changes in bacterial surface membrane roughness before and after the treatment with antibiotics. They also analysed the changes in adhesion properties by means of a functionalized tip. Furthermore, they performed force volume measurements and indentation measurements to check the adhesion force and the stiffness of the

membrane, respectively. They showed that the surface membrane changes when PA is incubated with Cx1 antibiotic: the roughness and the Young modulus drastically diminished after antibiotic incubation, and also the force-curves showed an increasing interaction between the bacteria and ConA (ConcanavalinA lectin) functionalized tips. This is due to the fact that the Cx1 causes a disorganization of the cell membrane at the molecular level [6,169].

Finally, the specific interaction of LecA with galactose residues has been investigated via Single Molecule Force Spectroscopy. Francius et al. [135,173] studied the localization, the adhesion and the extension of polysaccharide molecules on live *Lactobacillus rhamnosus* strain GG (LGG) bacteria. In particular, they were interested in mannose and galactose molecules and to study them, they performed spectroscopy experiments by taking advantage of the specific affinity of ConA and LecA lectins to the two polysaccharides. They found out that both polysaccharides are homogeneously distributed on the bacteria surface. The LecA-galactose interaction presented a longer rupture distance (100-1000 nm) with respect to ConA-mannose interaction (20-400 nm). Both interactions presented a specific adhesion force and the LecA-galactose pair was characterized by multiple peaks adhesion force due to multiple interactions. The distribution of the adhesion force presented a maximum at 51 ± 24 pN for the LecA-galactose interaction. These values are the ones obtained for the measurements performed with wild-type LLG cell, which differs from the data obtained with a LLG mutant cell. In particular, in the experiments performed with the mutant, they found out that the density distribution of the polysaccharides on the mutant surface is lower to the one of the wild-type and also the rupture length and the adhesion force present different values. The shape of the adhesion curve was well fitted with the FJC model, yielding Kuhn length and segment elasticity in the range of those reported for polysaccharides [104,135].

In our study, imaging and spectroscopy techniques have been used to study the interaction between LecA lectin from PA bacteria and different glycoclusters. Topographic images have been acquired in *tapping* mode, using an amplitude ratio ($A_{free}/A_{setpoint}$) between 60 and 80%, taking care of not damaging the sample. The lectin-glycocluster complex has been formed *in vitro* and then deposited on a flat mica substrate, taking advantage of the attractive interaction between the negatively charged substrate and the polar groups of the protein [174]. With this setup, the complexes formed by the lectin and five different glycoclusters (M1, M2, M3, M4, P1 and C1) have been compared in order to understand the influence of the topology of the glycocluster, such as the core and the branches, as well as the stoichiometry on the complex formation (Chapter 3).

Later, the spectroscopy mode has been used to study the lectin-glycocluster interaction by means of SMFS (Chapter 4) and also the anti-adhesive effect of the glycocluster on the cell-bacteria system via SCFS (Chapter 5). To perform SMFS experiments, the silicon nitride AFM tip has been chemically functionalized. Taking advantage of the amino-functionalization process developed by the group of P. Hinterdorfer [143,145], the LecA lectin has been attached to the probe and used to perform SMFS experiments against the glycoclusters grafted on a solid silica support. The unbinding force of the interaction between the lectin and three glycoclusters (M1, M2 and M3) has been studied to investigate the possible differences in the unbinding force parameter as a function of the affinity of the glycoclusters to the lectin.

Finally, the anti-adhesive properties of the best candidate to inhibit LecA activity (M3) has been tested via single-cell spectroscopy (Chapter 5), in particular the modifications of cell-bacteria interaction upon addition of the glycocluster has been studied. SCFS experiments have been performed between a tipless cantilever, where a single epithelium human cell has been fixed via CellTak™, and bacteria adsorbed on a glass support. Measurements have been performed in liquid (HEPES buffer) and the glycocluster has been directly introduced on the working media to test its anti-adhesive effect.

Chapter 3.   Topographic Imaging of the LecA lectin-glycocluster arrangements

Le Chapitre 3 traite des résultats expérimentaux obtenus par imagerie AFM, en mode *tapping*, des arrangements lectine-glycomime. L'AFM a permis d'observer directement les structures créées à l'échelle nanométrique et de démontrer l'influence du glycomime sur l'organisation. En effet, les structures créées sont différentes les unes des autres en fonction de plusieurs facteurs, tels que la géométrie et la nature du cœur et des branches, la stœchiométrie et l'affinité du glycomime pour la lectine. En combinant l'AFM avec des calculs de dynamique moléculaire, il a été possible d'étudier le rôle des bras et du cœur sur la géométrie des structures créées.

En comparant les structures créées à partir des molécules M1, M2, M3 et M4 (même cœur, bras différent), il a été montré que la rigidité de la branche induit la formation de structures petites, compactes et denses, parfois 3D plutôt que des arrangements 2D étendus. L'augmentation de la flexibilité de la branche implique une augmentation du degré de liberté alors que l'affinité diminue. L'interaction entre lectines conduit à la formation de structures 2D en monocouches étendues, similaires à celles obtenues avec un glycomime qui ne réagit pas spécifiquement avec la lectine (contrôle négatif). Ces résultats nous permettent de supposer que la formation des arrangements est principalement due à la compétition entre les interactions lectine-lectine et lectine-glycomime. La présence du glycomime améliore l'agrégation tandis que l'interaction entre lectines entraîne l'étalement de la structure.

De plus, le rôle joué par le cœur a été étudié en comparant les complexes formés avec des glycomimes présentant des cœurs différents mais des branches similaires (C1, P1 et M1). Les images AFM montrent que la nature du cœur influe sur l'arrangement spatial et l'orientation de la liaison ainsi que sur la distance entre les branches. Pour une même branche flexible, l'affinité est ainsi augmentée en présence d'un cœur rigide capable d'orienter fortement les branches. De petites structures linéaires caractéristique d'une forte affinité entre la lectine et le glycomime se forment, plutôt que des structures étendues latéralement comme dans le cas d'une affinité d'intensité intermédiaire ou faible.

En conclusion, pour des glycomimes à quatre branches comme ceux utilisés dans cette thèse, la nature du cœur et du ligand L2 en bout de branche influence fortement la géométrie des complexes créées et dépend de l'affinité du glycomime pour la lectine. Toutefois, il semble que l'arrangement final de la structure ne soit pas uniquement déterminé par l'interaction lectine-glycomime mais que l'interaction lectine-lectine joue aussi un rôle important.

3.1 Introduction

To better understand how the architecture of the glycocluster can influence the binding and the shape of the created complexes, the molecular arrangements of six different glycoclusters with LecA lectin were studied. AFM appears as an appropriate tool to study LecA lectin-glycocluster interaction at the nanoscale [175,176]. In particular, AFM imaging can be applied to directly observe the arrangements of the glycocluster-mediated self-assembly of the lectins. The combination of this imaging technique with Molecular Dynamic (MD) simulations and Isothermal Titration Calorimetry (ITC) measurements can also reveal the interaction from a molecular point of view. Mainly, the combination of these methods provide the tools to investigate the influence of the chemical groups that form the molecule, the architecture and the rigidity properties of the glycocluster on the LecA lectin-glycocluster complex formation [177].

3.2 Experimental Setup

3.2.1 The setup

The lectin-glycocluster complexes formed with six different glycoclusters were separately studied. For each experiment, the lectin and the glycocluster were incubated *in vitro* before being immobilized on a freshly cleaved mica support. To be consistent, we took care of performing the incubation always in the same conditions as well as the imaging settings were maintained constant. High-resolution AFM images were performed in *tapping* mode to avoid damaging of the sample. Also, MD simulations were carried out to relate the topological images of the arrangements to the more energetically favourable conformations. The choice of the glycoclusters studied was based on their high affinity but also on the nature of their core and branches, to quantify the contribution of each part. The complexes formed with three mannose-centred glycoclusters characterized by different branches were compared, such as the complexes created by three glycoclusters having similar branches but different cores (Chapter 1).

3.2.2 Sample Preparation

3.2.3 Glycoclusters
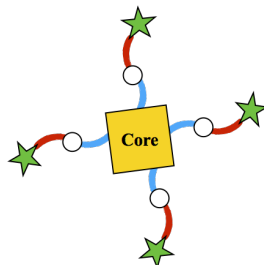
Figure 3.1: Sketch of the glycocluster.

The glycoclusters under study are tetravalent molecules characterized by a core and four branches (Figure 3.1), as previously described in section 1.4. Briefly, each branch is formed by two linkers, L1 (blue) and L2 (red), separated by a triazole (Tz) group (white). L2 linker is bound to the carbohydrate residue (green star) that should interact with the CRD of the lectin. In most cases, it is a galactose molecule since it is the natural ligand of the lectin.

Name	Core	Branch				K_d [nM]	n
		L1		**L2**	**Termination**		
M1	Mannose	pro	Tz	EG_3	Gal	11000	0.28
M2		pro	Tz	AcNPh	Gal	194	0.46
M3		EG_2M	Tz	AcNPh	Gal	157	0.52
M4		EG_2M	Tz	AcNPh	Glc	n.a.	n.a.
P1	Porphyrine	OM	Tz	EG_3	Gal	330	0.46
C1	Calix[4]arene	OM	Tz	EG_3	Gal	170	0.24

Table 3.1: Glycoclusters under study. Pro = $CH_2CH_2CH_3$; Tz = $C_2H_3N_3$; EG_n= $(CH_2CH_2O)_n$; Ac = $COCH_2$; M = CH_2; Ph = phenyl; Gal = galactose; Glc = glucose.

Table 3.1 presents the six different glycoclusters under study. Four of them have a mannose core. Among them, three display galactose terminations (M1, M2, M3) and one a glucose residue (M4). Different branches characterize M1, M2 and M3 glycoclusters, allowing the study of the influence of the linkers in the arrangement. In particular, M1 and M2 are characterized by the same rigid linker L1 and a different linker L2 (Table 3.1). M1 presents a flexible triethyleneglycol (EG_3) group, whereas M2 has a more rigid aromatic group (phenylacetamide, AcNPh). It was demonstrated that aromatic molecules can increase the affinity to the lectin by forming an hydrogen bond with the histidine (His50) situated close to the CRD of the lectin [22,178]. The same interaction is possible when LecA interacts with M3 glycocluster, but in this case the L1 of the branch is composed of a more flexible group that facilitates the entry of the galactose in the CRD of the lectin. M4 glycocluster should act as a control molecule since only an evidence of a very weak interaction between glucose moieties and LecA have been reported. A. Imberty et al. [72] have

shown the possible existence of a second binding site for glucose, but due to the weakness of the interaction they weren't able to measure its strength.

These four mannose-centred glycoclusters present different affinities: very low (not available, n.a.) for M4, low for M1 and close and high for M2 and M3, described by their K_d values (Table 3.1). The discussion around the interpretation of the different arrangements observed by AFM will take into account these different K_d and the stoichiometry values n.

The other two glycoclusters (P1 and C1) are characterized by the same flexible branch (O-methylene-triazole-triethylene glycol) and different cores: P1 is phorphyrine-centred and C1 has a calix[4]arene as a core. By comparing C1, P1 and M1, one can characterize the influence of the core on the lectin-glycocluster arrangement.

3.2.3.1 Complex immobilization for AFM analysis

The lectin-glycocluster complex was prepared *in vitro* by mixing 20 µL of $CaCl_2$ (final concentration 0.3 µM), 10 µL of LecA (final concentration 25 pM) and 10 µL of glycocluster (final concentration 25 pM). Then, the solution was incubated for 1 hour at room temperature, as previously described [75,179] (Figure 3.2). Finally, 20 µL of the solution were deposited on a freshly cleaved mica surface, and dried overnight in a desiccator at room temperature and ambient pressure. These conditions were used for the preparation of all the samples studied. They provide a lectin-glycocluster ratio of 1:1, thus the concentration should be low enough to avoid the formation of huge aggregates and promote the formation of isolated monolayer structures [179,180].
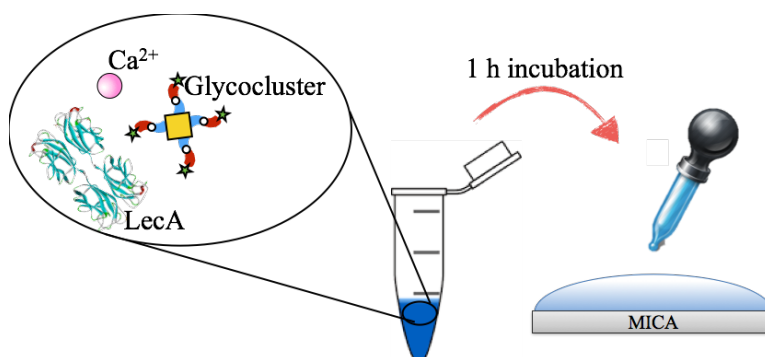
Figure 3.2: Sketch of the sample preparation protocol.

3.2.1 AFM measurements and image treatment

Topographic AFM images of the lectin-glycocluster arrangements were acquired with a commercial apparatus P7 "stand-alone" SMENA B (NT-MDT, www.ntmdt.com) (Figure 3.3). In a stand-alone setup, the tip is scanned over the sample; therefore a unique piezoelectric scanner is situated on the head of the microscope. It ensures the vertical and horizontal displacements, with maximal amplitude of 50 x 50 x 2.5 (± 10%) µm. The best resolution given by the constructor is of the order of 0.012 nm in the *x-y* plane and 0.006 nm along the *z*-axis.

Figure 3.3: Experimental apparatus SMENA B AFM. Taken from www.ntmdt.com.

Lectin-glycocluster complexes were imaged in air at room temperature. Due to the soft nature of the sample, *tapping* mode was applied by using an amplitude ratio ($A_{\text{free}}/A_{\text{setpoint}}$) between 60 and 80% (section 2.5.2.1) [181]. Cantilevers with relatively low resonance frequency were used: NSC21 ($f_{\text{res.}}$ = 21 kHz), CSC tip B ($f_{\text{res.}}$ = 21 kHz) from Mikromasch and NSCTR ($f_{\text{res.}}$ = 160 kHz) from NanoWorld (NanoWorld, Neuchâtel, Swizerland).

3.2.2 Isothermal titration calorimetry

To evaluate the affinity and stoichiometry of the binding, Isothermal Titration Calorimetry (ITC) measurements were performed. ITC assays were performed by our collaborators Dr. Jean-Jacques Vasseur and Dr. François Morvan at the Institut des Biomolécules Max Mousseron (IBMM), University of Montpellier (France).

ITC evaluates the lectin–glycoconjugate interaction by the determination of thermodynamic parameters, such as the dissociation constant (K_d) and the stoichiometry number (n). This method allows a direct measurement of the thermodynamic binding energies: the Gibbs free energy (ΔG), the enthalpy (ΔH) and the entropy (ΔS) [20,182] (section 1.3.4). Basically, the technique is based on the determination of the heat exchange generated by the lectin-glycoconjugate interaction [183]. The system is composed of two cells at thermal equilibrium. One cell, named the sample cell, contains the lectin while the other one acts as reference and is maintained at constant temperature (Figure 3.4). The glycoconjugate is injected in the sample cell at constant time intervals. Due to the glycoconjugate addition, the temperature of the sample cell decreases with respect to the one of the reference cell. Therefore, the condition of thermal equilibrium is no longer satisfied and the sample cell has to be heated up to recover the equilibrium. By measuring the voltage applied to preserve the thermal equilibrium as a function of time, one can obtain information on the binding enthalpy and extrapolate all the thermodynamic parameters. This technique is appropriate to study receptor-ligand interactions. The only disadvantage is the necessity of a great amount of material (in the order of milligrams) [20]. However, it appears complementary to structural or topological techniques such as AFM.
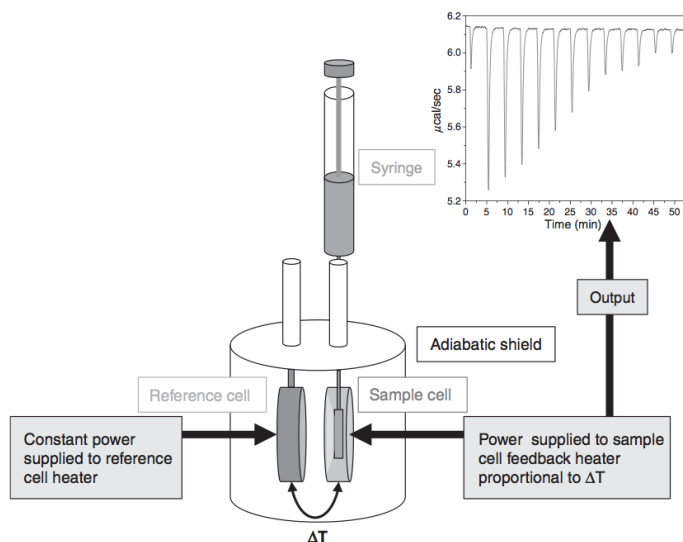
Figure 3.4: Schematic representation of the ITC system. Adapted from [184].

3.2.3 Molecular Dynamics Simulations

To understand the molecular arrangements of the LecA lectin-glycocluster systems, nanosecond molecular dynamics (MD) simulations were performed. MD simulations can predict the most energetically favourable interactions between the different molecules that form the complex. In this way, the influence of the glycocluster architecture, thus its affinity and stoichiometry can be studied. In particular, MD simulations can be combined to AFM images to explain the spatial arrangements of the complexes, providing the tools to get inside on the interactions involved. MD simulations were realized by Prof. Gérard Vergoten from the "*Laboratoire of Glycobiologie Structurale et Fonctionelle*" of the University of Lille (France), and were carried out by combining Monte Carlo method [185] with Spectroscopic Potential Algorithm for Simulating Biomolecular conformational Adaptability (SPASIBA) force field [186].

Monte Carlo is a statistical method to study differential equations [185]. Basically, given an ensemble of algorithms that rely on repeated random sampling, a statistical numerical result can be obtained. This means that the result is given with a confidence interval that describes the range in which the solution will most likely lie. This statistical method finds application in various fields such as biology, economics, physics, etc. In our simulations, the method is used to find the most probable arrangement of the lectin(s)-glycoconjugate(s) complex in order to subsequently apply the SPASIBA force field to perform molecular docking. Molecular docking predicts the most energetically favourable orientation of one molecule when it binds a second one, to form a stable complex. SPASIBA force field is characterized by the combination of AMBER Van der Waals, electrostatic interactions and Urey-Bradley-Shimanouchi (USB) terms for bond stretching, valence angle bending and torsional parameters [186,187].

To simulate the complex obtained from the lectin(s)-glycocluster(s) interaction, the stoichiometry number *n* (Table 3.1) was used to establish the number of possible bonds formed by each glycocluster. In fact, depending on the stoichiometry, a glycocluster is able to bind *N* recognition

domains of one or more lectins. For example, for a stoichiometry of $n = 0.25$ the molecule is able to target $N = 4$ lectin monomers, while for $n = 0.5$ the glycocluster will be able to interact with $N = 2$ lectin monomers.

Firstly, Monte Carlo simulations were run to minimize the energy and find the most probable conformations. To this aim, boundary conditions were applied to the lectin structure as it was considered as a rigid object. The LecA lectin structure (PDB code 4LJH), retrieved from the RCSB Protein Data Bank website (http://www.rcsb.org/pdb/home/home.do), was used since it presents already the galactose moieties on the recognition domains of the protein. Next, one or more branches of the glycocluster structures, lacking of the galactose termination, were then connected to the galactose on the lectins. Then, Monte Carlo simulations were performed for these structures and the most probable ones were selected and minimized in energy by means of molecular docking with SPASIBA force field.

For this, all the previous constrains on the protein structure were released and the minimum energy was found. The potential energies (ΔE) of the most probable arrangements were calculated by the difference between the energy of the whole complex ($E_{complex}$) and the energies of both the protein(s) ($E_{protein(s)}$) and the ligand (E_{ligand}) independently, as shown in the equation:

$$\Delta E = \Delta E_{complex} - (\Delta E_{protein} + \Delta E_{ligand}) \qquad (0.51)$$

If the aggregate is characterised by the binding of n proteins and m ligands, then the potential energy (ΔE) for each ligand f will be calculated as:

$$\Delta E = \Delta E_{complex} - (\Delta E_{n+(m-f)} + \Delta E_f) \qquad (0.52).$$

ΔE should be negative and smaller than the energy of the protein to ensure the formation of a stable complex. Finally, the simulated structures were visualised with Discovery Studio Visualizer 4.0 Software (Accelrys, San Diego, CA, USA).

3.3 Results and Discussion

The experiments were performed with a tiny amount of material (25 pM) to avoid formation of huge aggregates. In fact, the complex tends to aggregate [179] and stacked structures are energetically favoured as previously shown [180] and confirmed by MD simulations. Figure 3.5a presents an example of MD simulations for the M1 glycocluster. Considering the lectin as a parallelepiped, we refer to its sides as "large", "middle" and "small" faces, as depicted in Figure 3.5b. In the complexes formed (Figure 3.5aI), the two lectins (in blue) interact with each other and with the glycocluster, forming a 2D structure of potential energy $\Delta E = -98$ kcal/mol. In this configuration, the lectins are close one to the other along their "middle" faces. Otherwise, a 3D structure of potential energy $\Delta E = -229$ kcal/mol can be formed, where lectins are piled one on the other along their "large face", as in Figure 3.5aII.
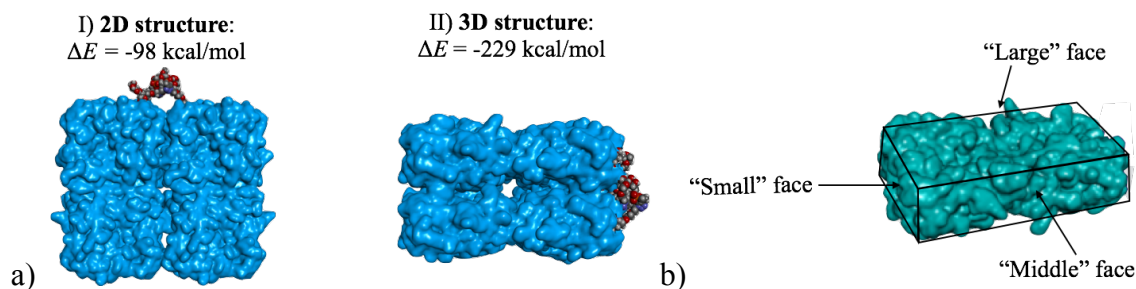
Figure 3.5: a) Example of MD simulations of 2D and 3D structures obtained for 2 lectin + 1 M1 glycoclusters and b) lectin structure where its faces are indicated.

If we then consider the lectins alone, they can interact with each other forming long isolated 2D objects of an average height of 1.5 ± 0.4 nm (Figure 3.6). The interaction seems to be mainly longitudinal at low lectin concentration (50 nM), as observed in solid state by X-ray crystallography and evidenced by AFM [179]. 3D aggregations are less probable, as shown by AFM images. Therefore, the complex formation seems mostly characterized by lectin-lectin interactions along "middle" and "small" faces, as lectin-lectin interaction along "large" faces could be related to the formation of piled structures, characterized by a height bigger than 1.5 nm.
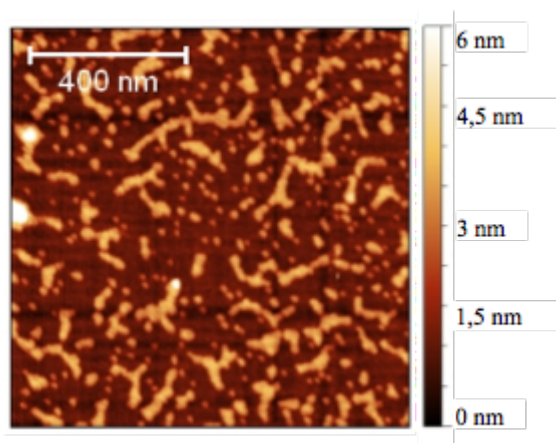
Figure 3.6: AFM topography image of lectins adsorbed on mica surface, size 1 x 1 μm². Adapted from [179].

To support these hypotheses, we investigated the privileged lectin-lectin interaction by MD simulations. The simulated structures show that the most energetically favourable lectin-lectin interaction happens between the "middle" faces of two lectins (Figure 3.7a), showing a potential energy of ΔE= -98 kcal/mol. This type of interaction is 29 kcal/mol smaller than the one along "large" faces (Figure 3.7b) and almost 99 kcal/mol smaller than the one between "small" faces (Figure 3.7c). This means that the most probable lectin-lectin interaction happens mostly between "middle" faces. "Large" faces interaction is not negligible, whereas "small" faces interaction is almost impossible. Therefore, AFM images of the low concentrated lectin complex can be mostly explained by a "middle" face lectin-lectin interaction that originates elongated 2D structures. The formation of stacked aggregates is less probable due to the low concentration [179] and the interaction along "small" faces is unlikely.

Figure 3.7: MD simulation of lectin/lectin interaction along a) lectin's "middle" faces, with a potential energy of ΔE = -98 kcal/mol; b) lectin's "large" faces, with a potential energy of ΔE = -69 kcal/mol; c) lectin's "small" faces, with a potential energy of ΔE = +0.68 kcal/mol, not an energetically favorable interaction.

Consequently, as the ΔE values are not negligible, the lectin-lectin interaction should be taken into account to explain the complex formation in presence of the glycocluster: the interplay between lectin-lectin interaction and lectin-glycocluster interaction will drive the formation of the structures. In fact, as it has been shown by D. Sicard et al. [179], even in presence of a tiny amount of a high affine glycocluster, compared to the concentration of the lectin (i.e. glycocluster/lectin ratio of 1/20 000), the formation of the complex is driven by the glycocluster, which stabilizes the binding and favours the stacking.

3.3.1 Influence of branches on the complex arrangement

To investigate the influence of branches in the formation of LecA-glycocluster complex, three mannose-centred glycoclusters were studied, M1 M2 and M3 (Table 3.1). Since the core is the same for the three molecules, it will be not a crucial parameter for the understanding of the complex formation.

3.3.1.1 M1 glycocluster

M1 glycocluster allows the formation of 2D monolayer structures characterized by rounded and well-defined borders. The aggregates are dense, homogeneous, well organized and some holes can be found on the structure. The shape and the extension of the assemblies can be attributed to the flexibility of the branches that provides several degrees of freedom. The monolayers have an average height of 1.4 ± 0.2 nm (Figure 3.8), which is slightly below the theoretical height estimated for the dried protein (1.9 nm), but compatible with what reported in literature [179]. In fact, the adsorption on the mica surface is due to an attractive interaction between the negatively charged substrate and the polar group of the protein, leading to an interaction that probably deform the protein by flattening it [174]. The high-resolution image (Figure 3.8c) shows some small grains that could be attributed to lectin molecules. The average size of the grain is 30.8 x 6.8 nm, larger than the size expected for one molecule due to tip effect (section 2.5.4) and the flattening.

Figure 3.8: AFM topographic images of the LecA-M1 complex of size: a) 5 x 5 μm² (detail of an aggregate), b) 2 x 2 μm², c) 0.2 x 0.2 μm² (detail of an aggregate) and d) the profile of the structure shown in c).

MD simulations can help to interpret the structures. Due to the stoichiometry of ($n = 0.28$, $0.25 < n < 0.33$), M1 can bind up to four lectin monomers. MD simulations obtained for 2 lectins *vs.* 1 glycocluster confirm that the most favourable structures are characterized by the interaction of all residues of M1 with 4 lectin CRDs (Figure 3.9). In particular, comparing 2D and 3D structures, 2D arrangements seem to be more energetically favoured than 3D stacked assemblies. In fact, the smallest energy is obtained for "V dimer" structures where one glycocluster binds four CRDs belonging to two different lectins (ΔE = -309 kcal/mol, Figure 3.9aI). Also, the interaction with four CRDs associated to three ("distorted Y trimer", ΔE = -267 kcal/mol, Figure 3.9aII) and four ("X tetramer", ΔE = -260 kcal/mol, Figure 3.9aIII) lectin monomers are more energetically advantageous than a piled disposition where the lectin-glycocluster binding coordinates the lectin-lectin interaction ("2 LecA + 1 M1", ΔE = -229 kcal/mol, Figure 3.9b). This 3D organisation was never observed on AFM images.

a) **2D structures**

I) V dimer   II) Distorted Y trimer   III) X tetramer

ΔE = -309 kcal/mol

ΔE = -267 kcal/mol

ΔE = -260 kcal/mol
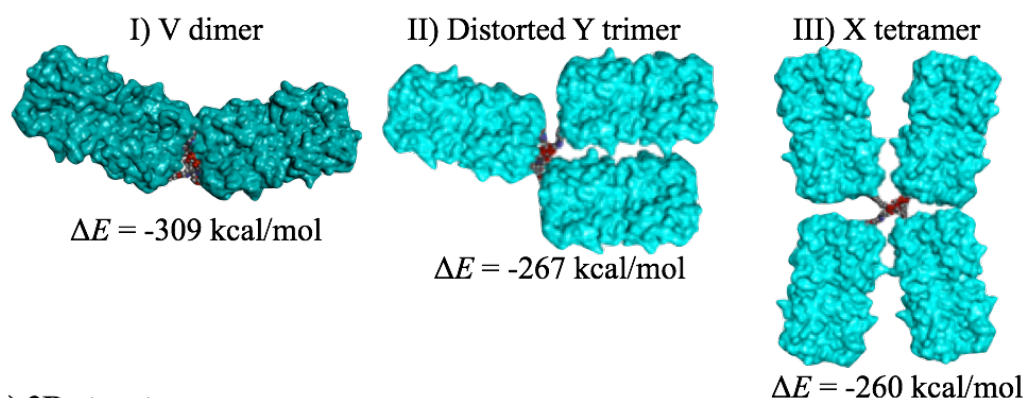
b) **3D structures**

2 LecA + 1 M1

ΔE = -229 kcal/mol
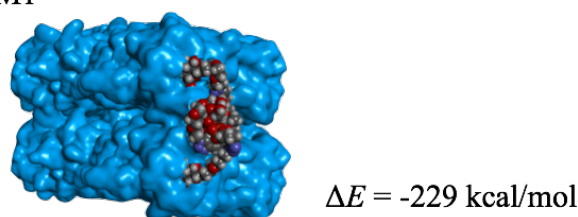
Figure 3.9: MD simulations of a) 2D and b) 3D arrangement of the most energetically favorable interactions between M1 glycocluster(s) and LecA lectin(s) monomers.

The AFM images and the organisations obtained by MD simulations seem to show that the complex is mainly formed by 2D architectures where the arrangement of the lectins is coordinated by the presence of the glycoclusters. Since the glycocluster prefers to bind four CRDs of two lectins rather than occupying the four CDRs of a single protein, the chance of creating expanded structures is enhanced, leading to the formation of extended aggregates. Also, the blobs that forms the small aggregate presented in Figure 3.8c suggest a disposition given by the combination of the 2D modelled structures, even though we are not able to make the correspondence between each blob and a single lectin, due to the fact that no isolated lectins were found. Therefore, it is not possible to convolute the image of a single lectin to find its dimensions.

What is more surprising is the possibility to create 3D structures with a ΔE = -229 kcal/mol (Figure 3.9b), only 80 kcal/mol higher than the more likely structure (Figure 3.9aI), but not so far (only 31 kcal/mol) from the "X tetramer" conformation (Figure 3.9aIII). Therefore we should have observed some 3D arrangements at some places in the AFM images, but we just obtained some brighter spot on the 2D structures (Figure 3.8a). Therefore, due to the low affinity of M1 glycocluster and the competition between the lectin-lectin and the lectin-glycocluster interactions, the equilibrium is achieved by forming extended 2D structures where the complex takes advantage of the "middle" faces lectin-lectin interaction (Figure 3.7a).

3.3.1.2 M2 glycocluster

M2 glycocluster differs from M1 only for the linker L2 that determines a completely different arrangement of the complex formed. M2 glycocluster leads to the formation of small compact and

elongated structures (Figure 3.10). For example, Figure 3.10a presents an arrangement of dimensions 1.3 μm x 373 nm, with an average height of 1.32 ± 0.12 nm (Figure 3.10b). The central part of the structure is characterized by an incremented height of 0.16 nm that does not seem to be due to the substrate roughness, but rather than to a particular disposition of the lectins [180]. The assemblies are quite dense and it is not possible to distinguish any motif inside the structure that could indicate the spatial arrangement of the lectins. However, some aggregates present edges with kinks that could be attributed to the edges of the lectins (Figure 3.10c).
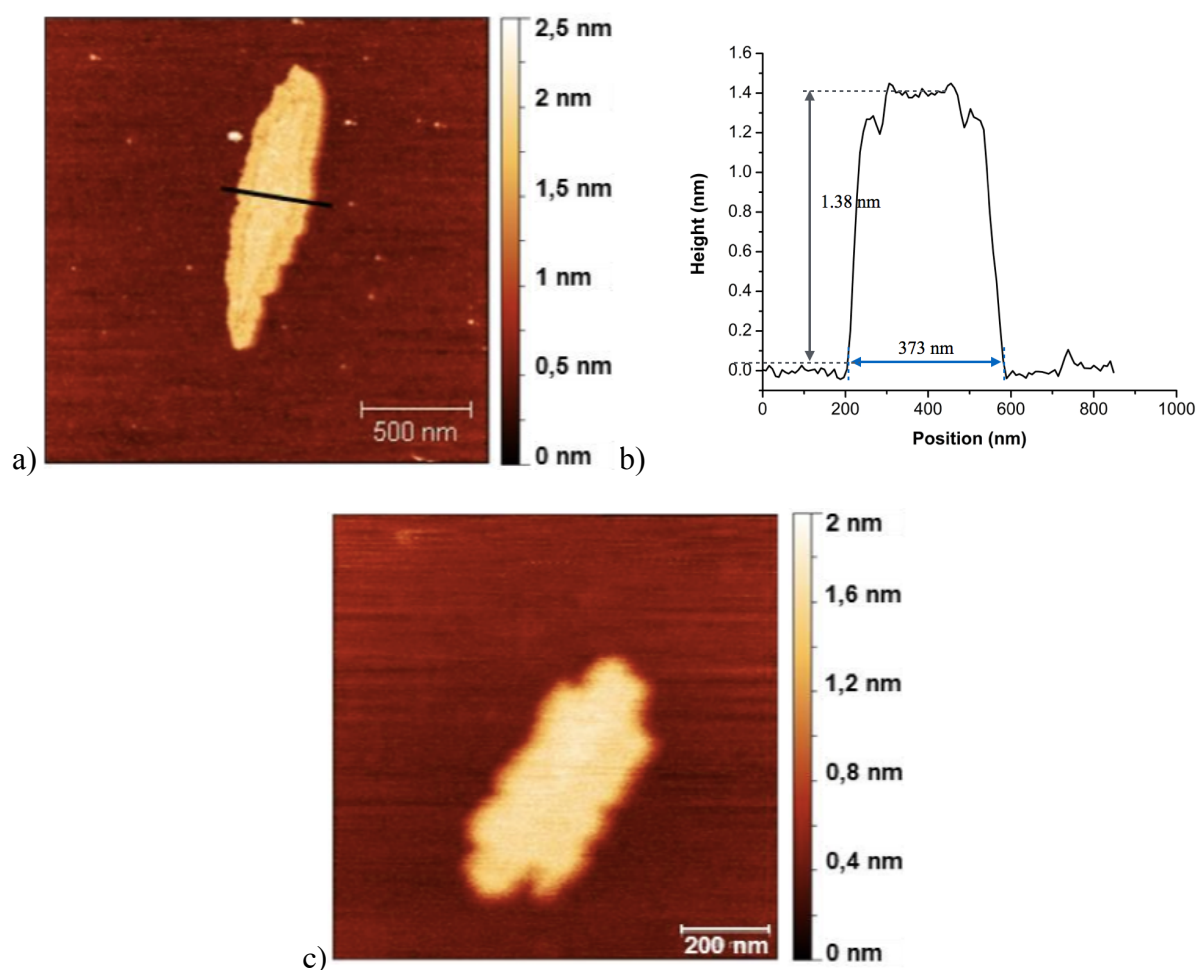
Figure 3.10: AFM topographic images of the LecA-M2 complex of size a) 2 x 2 μm², b) profile of the structure shown in a) and c) 1 x 1 μm². Adapted from [180].

For M2 glycocluster, the linker L2 is more rigid than the L2 linker of M1. This rigidity implies a less degree of freedom for the complex. Once the complex is deposited on the mica surface and let adsorbed, it maintains a packed disposition rather than expanding on the mica surface. This can be due to the fact that the glycocluster seems to interact mostly with two monomers of the same lectin (ΔE = -240 kcal/mol, Figure 3.11aI), leading to a "monomer" arrangement. This architecture can block the growth of the structure in the *x-y* plane, forcing a development along the *z*-coordinate. Stacked architectures are in general favoured (Figure 3.5), but experimental conditions were chosen to avoid the formation of 3D structures [180]. Nevertheless, LecA lectin-M2 glycocluster interaction mainly originates compact arrangements (Figure 3.10; Figure 3.11b) due to the rigid

nature of the branch that favours the compactness of the structure. The complexes found are small compared to the assemblies obtained in presence of M1 glycocluster. This can be explained by the conformations found by MD simulations where the glycocluster mainly interacts with two lectin monomers originating "monomer" or "dimer" ("Monomer", ΔE = -240 kcal/mol, Figure 3.11aI; "V dimer", ΔE = -193 kcal/mol, Figure 3.11aII; "V perpendicular dimer", ΔE = -181 kcal/mol, Figure 3.11aIII) assemblies.

a) **2D structures**

     I) Monomer   II) V dimer   III) V perpendicular dimer

     ΔE = -240 kcal/mol

                ΔE = -193 kcal/mol ΔE = -181 kcal/mol
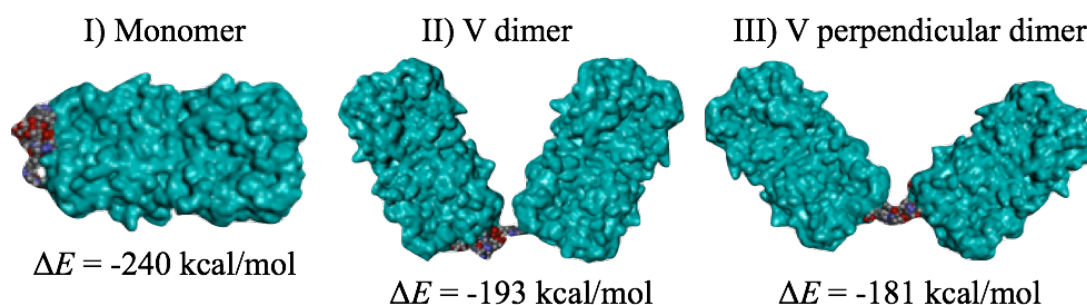
b) **3D structures**

     I) 2 LecA + 1 M2

                ΔE = -143 kcal/mol
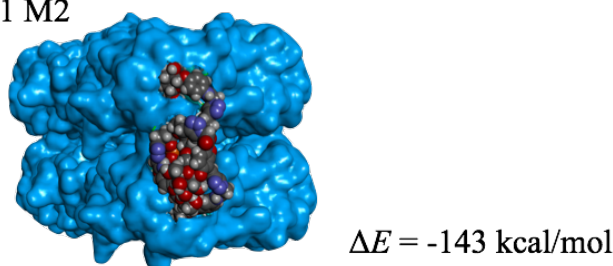
Figure 3.11: MD simulations of a) 2D and b) 3D arrangement of the most energetically favorable interactions between M2 glycocluster(s) and LecA lectin(s) monomers.

3.3.1.3 M3 glycocluster

M3 glycocluster differs from M2 glycocluster only by the linker L1. As in the case of M2 glycocluster, M3 forms small, compact isolated assemblies when interacts with the lectin (Figure 3.12). The aggregates are characterized by variable height, bigger than the dimensions of a single lectin (Figure 3.12a and b). The structures are no longer monolayer architectures but clearly 3D structures. The width of the objects is mostly of 43 ± 9 nm and the height varies between 1.2 nm and 25 nm, clearly showing a stacking disposition of the lectins (Figure 3.12c and d). The clusters tend to be close one to the other, probably due to the deposition, and in general no large aggregates were found.
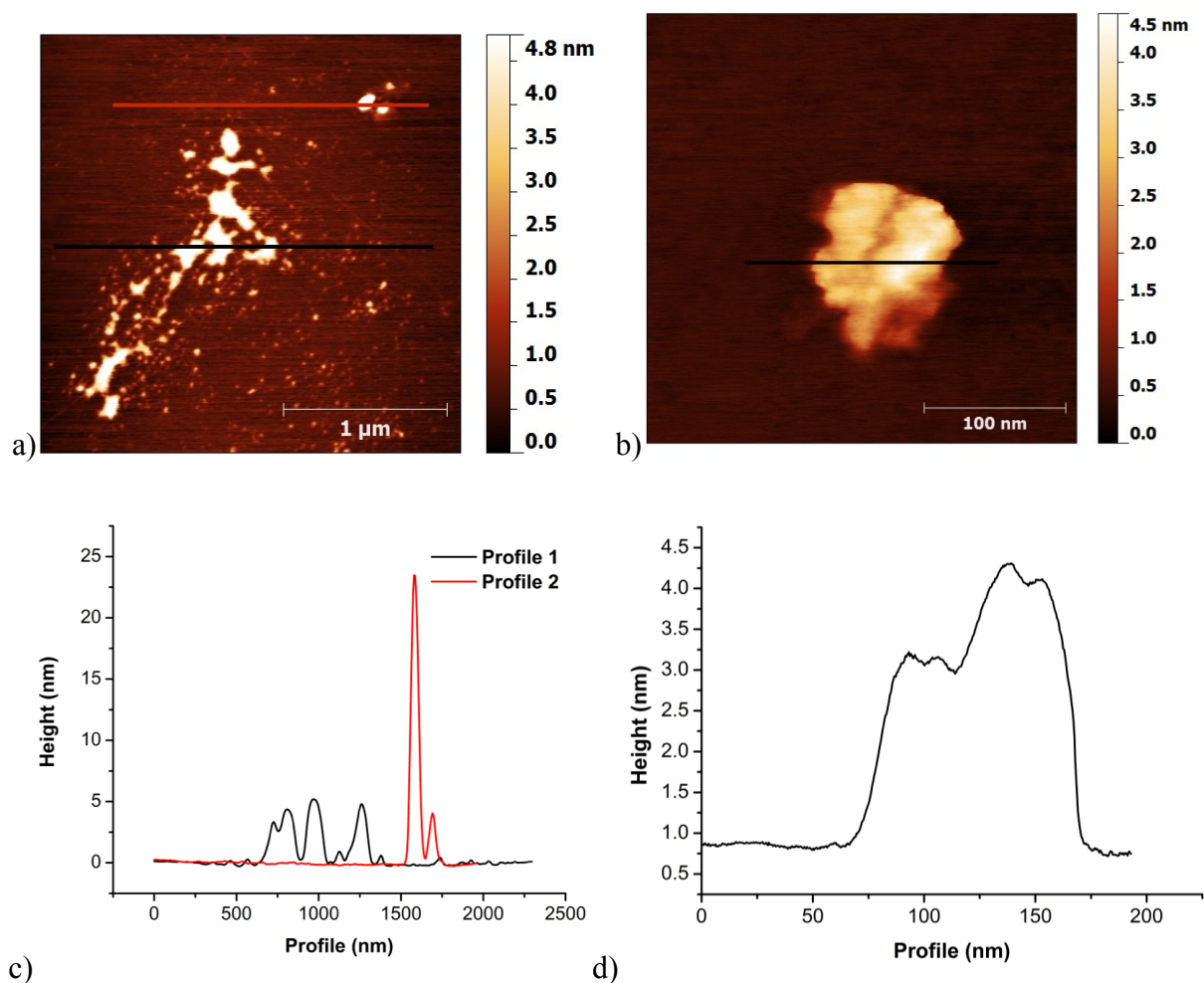
Figure 3.12: AFM topographic images of the LecA-M3 complex of size a) 2 x 2 μm², b) size 0.4 x 0.4 μm², c) profile of the structure shown in a) and d) profile of the structure shown in b).

On MD simulations, differences in potential energy are lower than 30 kcal/mol therefore the probability of having both 2D and 3D arrangements is not negligible, if arrangements between one glycocluster and one or two lectins are considered (Figure 3.13). The stoichiometry of the LecA lectin-M3 glycocluster interaction is $n = 0.52$, leading to the interaction between two galactose residues of the glycocluster with two lectin monomers. Therefore, the spreading of the complex, thanks to dimer arrangements ("V dimer", ΔE = -201 kcal/mol, Figure 3.13aI; "Linear dimer", ΔE = -195 kcal/mol, Figure 3.13aII), could be blocked by "monomer" arrangements where the glycocluster binds two CRDs of the same lectin, situated both at the same side of the tetrameric protein, thus impeding the expansion of the assembly on the *xy*-plane (Figure 3.13aIII). The structures can grow along the vertical direction and two or more lectins can stack together (Figure 3.13b). MD simulations describe well the AFM images. Thus, one can consider that the lectin-glycocluster interaction mostly drives the complex formation even though the lectin-lectin interaction is still present.

a) **2D structures**

I) V dimer

II) Linear dimer

III) Monomer

ΔE = -201 kcal/mol

ΔE = -195 kcal/mol

ΔE = -186 kcal/mol
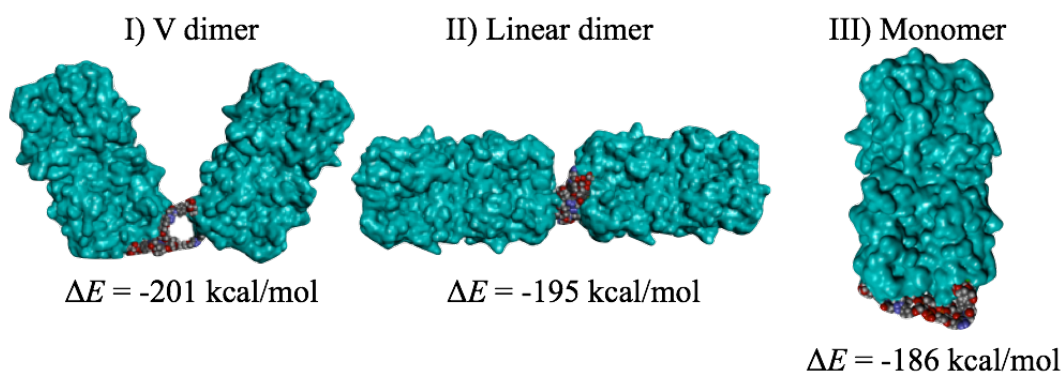
b) **3D structures**

2 LecA + 1 M3

ΔE = -174 kcal/mol

Figure 3.13: MD simulations of a) 2D and b) 3D arrangement of the most energetically favorable interactions between M3 glycocluster(s) and LecA lectin(s) monomers.

3.3.1.4 M4 glycocluster: the influence of lectin-lectin interaction

M4 glycocluster was chosen as a control molecule since it does not bring the galactose moieties, therefore it cannot specifically bind the lectin. AFM images show extended flat monolayers architectures (Figure 3.14). The average height of the LecA lectin-M4 glycocluster 2D arrangement is 1.0 ± 0.2 nm, consistent with values previously found for monolayer structures. Structures present rounded edges and holes where the mica substrate can be seen. The architectures are similar to the ones obtained for the lectin-M1 glycocluster complex, rather than to the ones obtained with M2 and M3 glycoclusters.

a)

b)
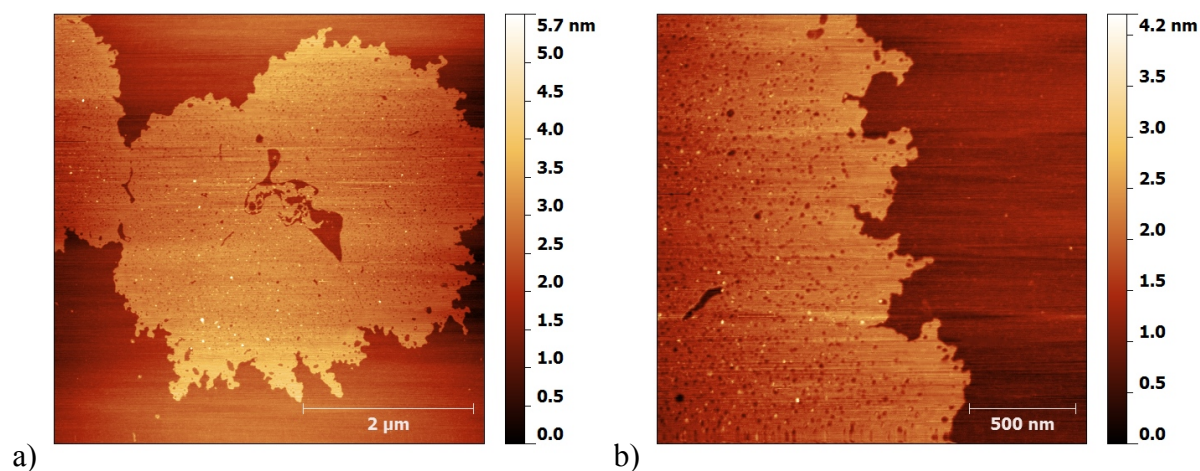
Figure 3.14: AFM topographic images of LecA-M4 complex. Image size: a) 5 X 5 μm^2, b) 2 X 2 μm^2.

3.3.1.5 Comparison between M1, M2 and M3 glycoclusters

The comparison of mannose-centred glycoclusters allows understanding the influence of the branches in the complex formation, thus the affinity for the lectin. The most visible distinction is between the arrangements obtained with M1 glycocluster and the ones obtained in presence of M2 and M3. In fact, increasing the rigidity of the branch (M2 and M3) favours cluster formation and mostly the 3D development of the structures. LecA-M1 interaction induces the formation of extended 2D monolayer assemblies while the interaction between the lectin and both M2 and M3 supports packing and piling architectures. This is due to the fact that the flexibility/rigidity of the branch affects the affinity [21]. M2 and M3 glycoclusters present a quite strong affinity for the lectin due to the presence of an aromatic group as L2 linker, therefore the lectin-lectin interaction is completely driven by the lectin-glycocluster interaction and compact architectures are more energetically favoured, as the potential energy is lowered. In fact, the interaction through "large" faces is not the most energetically favoured arrangement when only lectin-lectin interaction takes place. But, it becomes the most favoured arrangement in presence of a high affine glycocluster, resulting in a decreasing of potential energy and a stabilization of the complex. Therefore, the interaction favours the formation of small confined 3D clusters.

Furthermore, a distinction between the effects of the two linkers (L1 and L2) that form the branches can be made (Figure 3.1). In particular, the same linker L1 (propyl) characterizes M1 and M2 while the linker L2 is different. In the case of M1, the linker L2 is made by a flexible EG_3 group albeit M2 is constituted by a more rigid aromatic-group. This difference determines an increased affinity for M2 glycocluster, and the stiffening of the branch eases the interaction between the CRD of the lectin and the galactose residue. This is also due to the additional interaction with the aromatic compound present in the L2 linker of M2 glycocluster that stabilizes the binding, giving rise to a decreasing of the dissociation constant of two orders of magnitude (K_d = 11000 nM for M1 *vs*. K_d = 194 nM for M2, Table 3.1).

The comparison between M2 and M3 glycoclusters can help understanding the influence of linker L1 in the complex formation. In fact, the two molecules differ from each other by the group that form the first part of the branch: M2 presents a more rigid structure characterized by a propyl group, while M3 is characterized by a flexible EG_2M group (Table 3.1). The presence of a flexible linker in M3 increases the degree of freedom of the molecule and the galactose can easily orient itself to enter on the CRD of the lectin. This improvement is translated in a slightly higher affinity of M3 glycocluster, characterized by a somewhat lower dissociation constant (K_d = 157 nM, Table 3.1).

Therefore, by examining the contribution of the two linkers that compose the branch of a mannose-centred glycocluster, a clear evidence of the influence of the L2 linker is underlined. In fact, the modification of L2 between M1 and M2 shows a huge increase in the affinity while the change in L1 linker (M2 *vs*. M3 glycoclusters) is not as effective as the modification of L2 for increasing the affinity.

3.3.2 Influence of the core on the complex arrangement

To study the influence of the core in the LecA-glycocluster complex formation, three different molecules were used as core to design the glycoclusters (Table 3.1): the porphyrine (P1 glycocluster), the calix[4]arene (C1) and the mannose (M1 M2 and M3). The core influences the directionality of the binding and the separation between branches. M1, P1 and C1 are characterized by the same L2 flexible linker and two different linkers L1 (pro and OM, Table 3.1). However, the previous discussion shows that L1 does not greatly influence the affinity, thus we can assume that the branch contribution in the affinity, for these three molecules, is almost the same. Consequently, the core contribution can be extrapolated. The three cores present highly different geometries that affect the spacing between branches and their spatial disposition. In particular, for C1 and P1 the final structure of the glycocluster has an "X" shape, meaning that the branches are two by two on the same side. In contrast, for the mannose-centred glycocluster (M1), the branches are spread in a semicircle manner leading to a mostly globular shape of the molecule.

3.3.2.1 C1 glycocluster

The "X" shape of C1 glycocluster, together with its stoichiometry of $n = 0.24$, leads to the formation of mostly mono-dimensional LecA lectin-C1 glycocluster architectures (Figure 3.15a and b). On the high-resolution images, the arrangement spreads on the mica surface forming long filaments of width 36.4 ± 8.5 nm and average height of 1.7 ± 0.5 nm (Figure 3.15c) [75]. The dimensions of the filament can be related to the ones of a single lectin [75], therefore the structures should be characterized by single lectins connected together by the glycoclusters (Figure 3.15b). The behaviour can be explained by a chelate binding of C1 glycocluster with four lectin monomers belonging to two different tetramers [75]. The cobblestone structures can be attributed to individual lectins that form the filament. The height is not constant along the filament; sometimes it oscillates between a maximum of 1.7 nm and a minimum of 1.2 nm (Figure 3.15c). According to the architecture of C1 glycocluster (section 1.4.2), lectins seem to be forced to lie on the surface along their "large" or "small" faces, alternatively (Figure 3.15d). Then an alternation of 0.3 nm in the height of the cobblestones should be observed on the cross-section of the filament, but unfortunately is not visible. This is due to the fact that the resolution limit is reached; therefore the shift in height is masked by the roughness of the mica, even though the surface presents one of the lowest roughnesses. Moreover, the presence of bifurcations, consequence of aggregation defects, leads to the formation of a net structure.
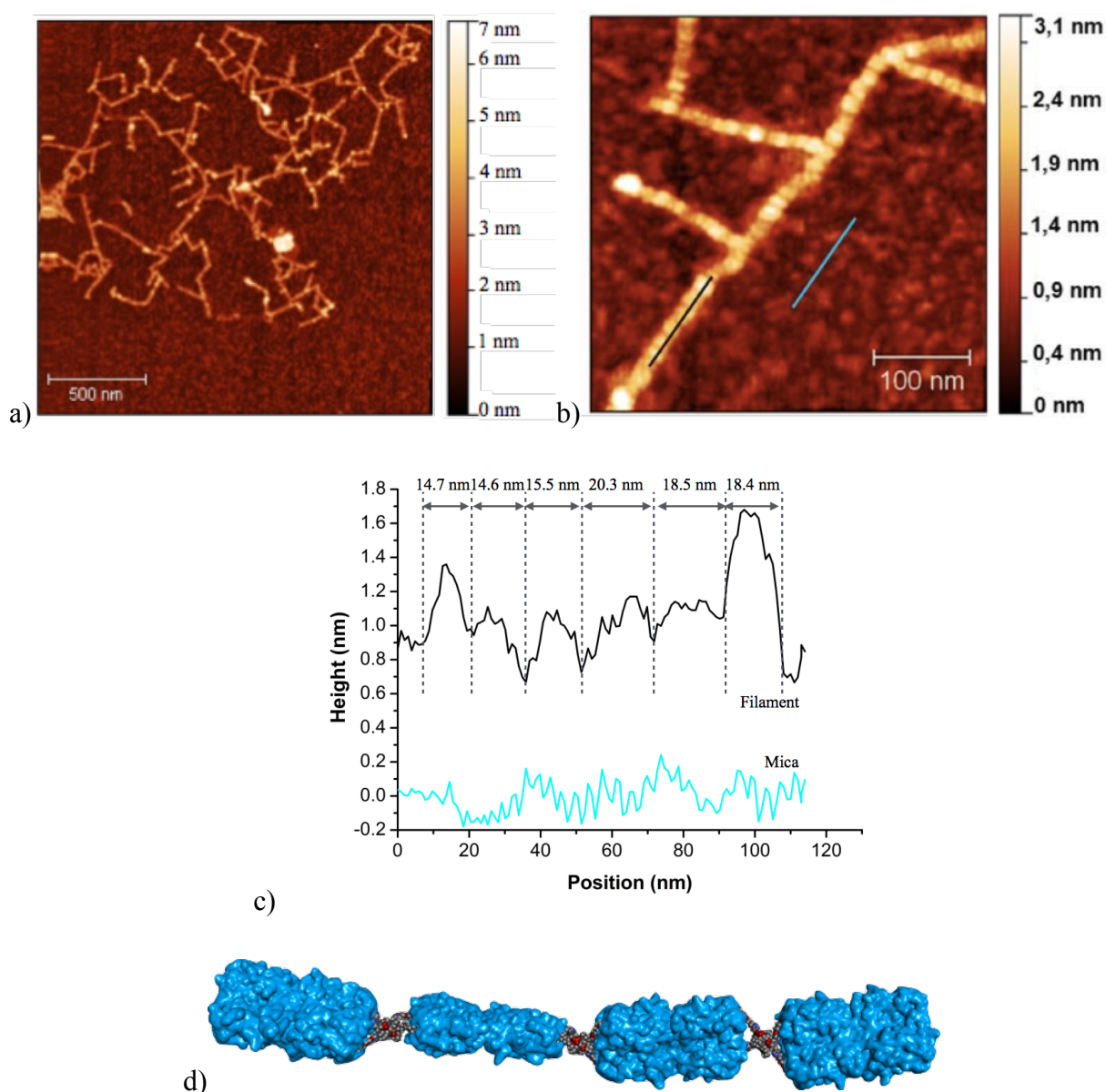
Figure 3.15: AFM topographic images of the LecA-C1 complex of size a) 2 x 2 μm², b) 0.5 x 0.5 μm² and c) profile of the structure shown in b). Adapted form [180]. d) Simulated linear filament where the lectins are separated one from the other by a C1 molecule. The possible alternated disposition of the lectins is shown.

MD simulations support these statements. In fact, most energetically favourable interactions are obtained when 2D linear structures are formed (Figure 3.16a I and II). In particular, "perpendicular dimer" (ΔE = -328 kcal/mol) dispositions, characterized by an alternate arrangement of the lectins, are slightly more favoured than the linear ones ("linear dimer", ΔE = -318 kcal/mol) where lectins can lie flat either on their "large" or "middle" faces. In principle, the formation of a 3D structure ("4 LecA + 1 C1", ΔE = -302 kcal/mol, Figure 3.16b), where the filament is formed by the alternation between a glycocluster and two lectins piled along their "large" faces, cannot be excluded. In fact, the potential energy of the complex is only 26 kcal/mol higher than the one of the "perpendicular dimer" (Figure 3.16aI), but in this case the lectin-lectin interaction between "large faces" is involved in complex formation. However, on AFM image, we rarely found such 3D structures, at

such low concentration of 25 pM. Some of them might be identified as brighter spots on the complex (Figure 3.15a). Finally, bifurcations in the arrangements can be explained by "tetramer" (ΔE = -232 kcal/mol, Figure 3.16aIII) and "trimers" (ΔE = -240 kcal/mol, Figure 3.16aIV) constructions, where a C1 glycocluster interacts with four monomers of four different lectins or with four monomers of three different lectins, respectively.

a) **2D structures**

I) Perpendicular dimer

ΔE = -328 kcal/mol

II) Linear dimer

ΔE = -318 kcal/mol

III) X tetramer

ΔE = -232 kcal/mol

IV) Y trimer

ΔE = -240 kcal/mol

b) **3D structures**

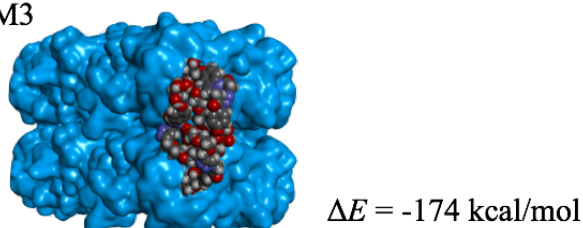4 LecA + 1 C1

LecA

ΔE = -302 kcal/mol
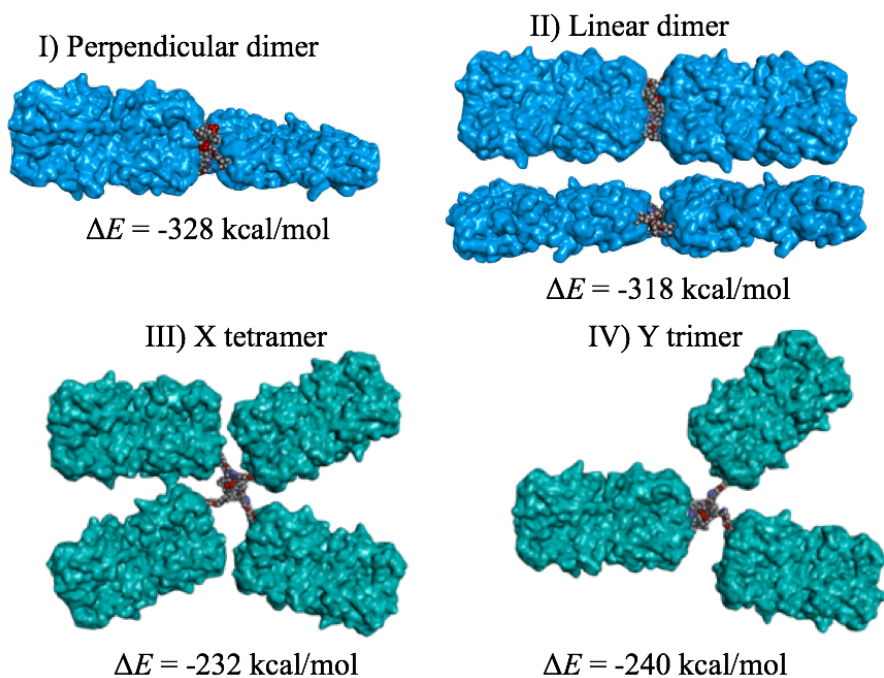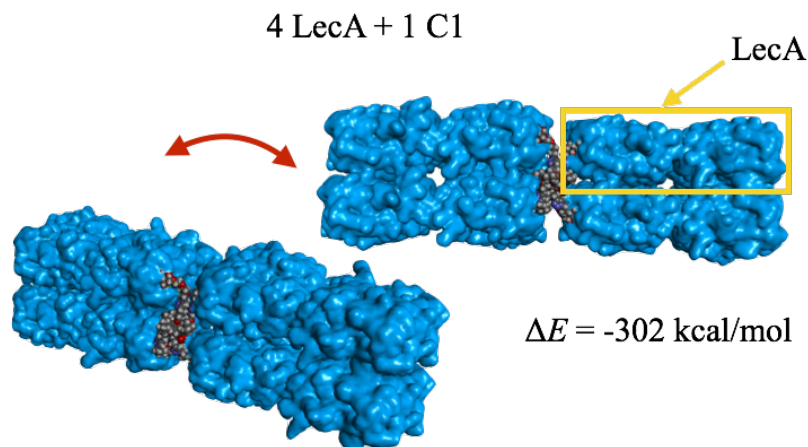
Figure 3.16: MD simulations of a) 2D and b) 3D arrangement of the most energetically favorable interactions between C1 glycocluster(s) and LecA lectin(s) monomers. The yellow square in b) shows one single lectin on the structure.

3.3.2.2 P1 glycocluster

Typical AFM images of LecA lectin-P1 glycocluster complexes (Figure 3.17a and b) display arrangements in a large cross-linked network with winding branches [180]. The height of the structure is evaluated to 1.4 ± 0.2 nm (Figure 3.17c), in accordance with the height values found for the other lectin-glycocluster structures. The molecular architecture is planar on the mica substrate. Individual lectins inside the structure cannot be resolved despite the high-resolution images obtained, displaying some holes in the branches of less than 20 nm and some isolated lectins.
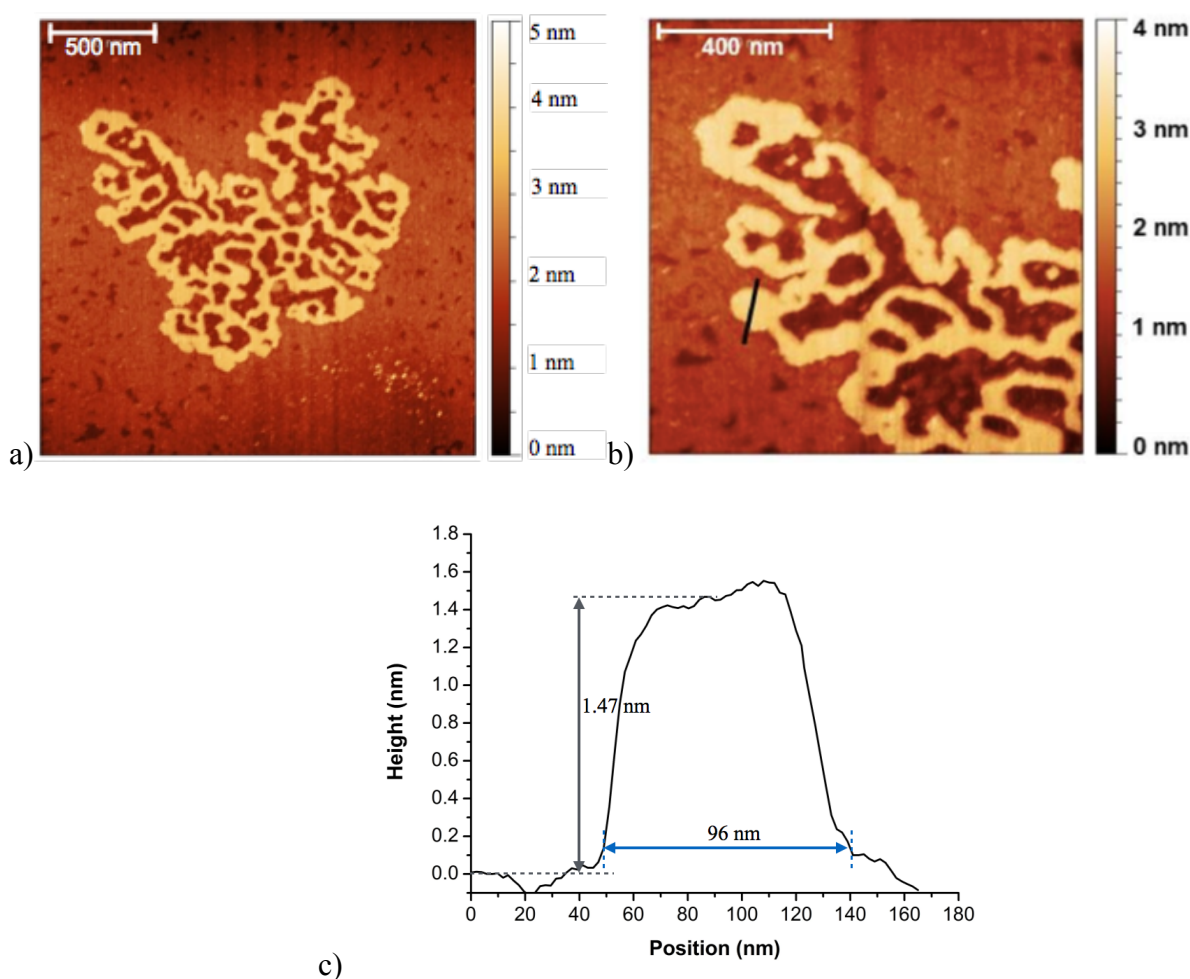
Figure 3.17: AFM topographic images of the LecA-P1 complex of size a) 2 x 2 μm^2, b) 1 x 1 μm^2 and c) profile of the structure shown in b). Adapted from [180].

Considering the stoichiometry of $n = 0.46$ of the complex, the interaction can more likely happen between two galactose residues of the glycocluster and two binding sites of two different lectins while the two remaining galactose residues will stay unbound, as MD simulations show (Figure 3.18). The galactose can link indifferently the four binding sites of the lectin. The length and the flexibility of the spacer arms might offer the opportunity to two galactose residues to simultaneously bind to two CRDs of a single lectin tetramer in a chelate binding (section 1.3.1). As in the case of M2 and M3 glycoclusters (Figure 3.10 and Figure 3.12), chelate binding would have blocked the extension of the arrangement by forming small and compact complexes rather than large molecular structures. MD simulations confirm this hypothesis by displaying as most

energetically favoured structures "linear" arrangements ("Linear and shifted dimer", ΔE = -167 kcal/mol, Figure 3.18a I; "Linear dimer", ΔE = -135 kcal/mol, Figure 3.18aII). Furthermore, the difference in potential energy between the "Linear and shifted dimer" and the "V dimer" (ΔE = -124 kcal/mol, Figure 3.18aII) is only 43 kcal/mol, therefore a mixture of all the three conformations can explain the winding of the structure with the different bifurcations. In fact, only the first two linear structures would have lead to 1D filament arrangements, similar to the ones obtained with C1 glycocluster (Figure 3.15).

Even though MD simulations seem to show that LecA lectin-P1 glycocluster 3D structures have a potential energy close to the ones obtained for 2D structures, the stacking arrangement is not favoured (Figure 3.18b). This potential energy should be discussed in detail since it is not really significant as in the case of the other glycoclusters. In fact, the potential energy of the protein alone ($\Delta E_{protein}$) is smaller than the one of the complex ($\Delta E_{complex}$), even though the resulting potential energy (ΔE) has still a negative sign (Equation (0.51)). This means that the creation of the 3D complex is not favoured as there is no gain in energy for the protein assembling in the complex. The resulting complex will not be energetically stable. Therefore, 2D monolayers structures are more convenient, as shown by AFM images, and lectin-lectin interaction cannot be excluded during complex formation, even though this interaction should be strongly driven by LecA-P1 interaction due to the intermediate affinity of the glycocluster to the lectin (K_d = 330 nM).

a) **2D structures**

I) Linear and shifted dimer   II) Linear dimer   III) V dimer

ΔE = -135 kcal/mol

ΔE = -167 kcal/mol

ΔE = -124 kcal/mol
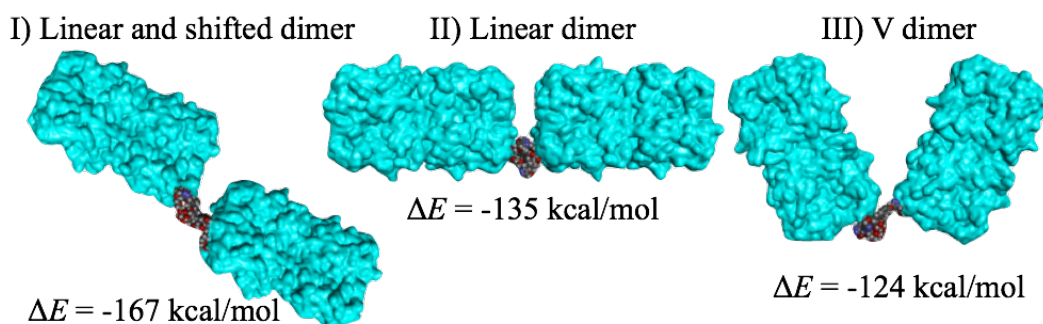
b) **3D structures**

2 LecA + 1 P1

ΔE = -145 kcal/mol
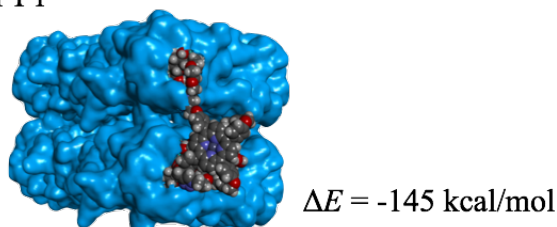
Figure 3.18: MD simulations of a) 2D and b) 3D arrangement of the most energetically favorable interactions between P1 glycocluster(s) and LecA lectin(s) monomers

3.3.2.3 Comparison between C1, P1 and M1 glycoclusters

These results show that having flexible branches imply having a core that imposes a strong orientation to the branches and fixes their distances. Calix[4]-arene (C1) seems to be the most

appropriate candidate to perform such a task. The rigidity of the core leads to the formation of a chelate aggregation between the lectins and the glycoclusters, which originates a mostly mono-dimensional complex (Figure 3.15), defined as type 1 reticulation [69] (section 1.3.1). Porphyrine-centred glycoclusters (P1) give rise to structures characterized by long polymorphic branches with connection points between three branches (Figure 3.17). This leads to a molecular structure that is a mixture of type 1 and type 2 reticulations. Structures are flat on the mica surface and extended, even though the spreading is not effective as in the case of M1 glycocluster. In fact, arrangements obtained with M1 glycocluster are extended monolayer structures (Figure 3.8) mainly given by type 2 reticulations, where the assembly formation is mostly driven by a competition between LecA-M1 interaction and lectin-lectin interaction. Therefore, in this case, the arrangement of the complex is mostly driven by other parameters than the nature of the core, since a more 3D structure would have been expected, as in the case of M2 and M3 glycoclusters and as MD predicts. The low concentration used and the low affinity of the glycocluster strongly influences the complex formation.

It would be interesting to compare the structures obtained for a calix-arene centred-glycocluster with a L2 aromatic linker with M2 and M3 glycoclusters. In literature, a calix[4]-arene with aromatic branches has been studied [188]. It is characterized by a K_d = 90 nM and n = 0.24, therefore 1D linear arrangements would be expected, as in the case of C1 glycocluster. Thus, a huge influence of the core in the directionality of the binding is shown, and for molecules with high affinity it mainly drives the architecture of the complex.

3.4 Summary

In this Chapter, the LecA-glycocluster arrangement for different glycoclusters has been studied by a combination of high-resolution AFM images, MD simulations and ITC measurements. By AFM images, we showed that depending on the glycocluster, very different arrangements could be created. The architecture of the arrangement depends on different factors, such as the geometry and design of the glycocluster (nature of core and branches), its stoichiometry and affinity for the lectin. In particular, the roles of the branches (L1 and L2 linkers) and the core were shown and MD simulations helped to define the more probable organisation, in agreement with the images.

Especially, it was shown that the linker L2 of the branch strongly influences the ease of the galactose to enter in the CRD of the lectin, rather than the linker L1. Rigid L2 linker induces the formation of small and dense structures as in the case of M2 and M3 glycoclusters. This increases the tendency of forming compact and sometimes 3D structures, rather then extended 2D arrangements. Increasing the flexibility of the branch implies increasing the degree of freedom, while the affinity decreases, as for M1 glycocluster. The interaction with the lectin leads to the formation of 2D monolayer extended structures, similar to the ones obtained with M4 control glycocluster, where mostly no specific interaction with the lectin can be found.

Moreover, the role played by the core was studied by comparing the complexes formed in presence of C1, P1 and M1 glycoclusters. The interaction between LecA lectin and C1 glycocluster forms mostly mono-dimensional structures where the filament is characterized by the alternation between one lectin and one glycocluster. Each C1 glycocluster interacts with four recognition domains of two different lectins, in a chelate binding. Therefore, lectin-lectin interaction is completely avoided due to the ability of C1 of occupying all the CRD's and space out the lectins. On the contrary, a porphyrine core (P1) determines the formation of more extended winding 2D structures. The spreading of the structure is intermediate, if compared to the one of the structures obtained with M1 glycocluster. Therefore, AFM images show that the nature of the core influences the spatial arrangement and the orientation of the binding, as well as the distance between the branches. Given the same flexible linker L2, the affinity is increased in presence of a core capable of strongly orient the branches. Thus, small linear structures characterized by high affinity between the lectin and the glycocluster are formed rather than extended ones, as in the case of intermediate (P1) and low (M1) affinity glycoclusters.

In conclusion, the presence of the glycocluster drives the interaction, stabilizes the binding and favours the stacking [179]: depending on the affinity of the synthetized molecule to the lectin, the interplay between lectin-glycocluster and lectin-lectin interactions will determine the final arrangement of the complex.

To further understand the lectin-glycocluster interaction, we decided to select some of the glycoclusters studied by AFM images and estimate their unbinding force via Single Molecule Force Spectroscopy (SMFS) experiments. For this, the three mannose-centred glycocluster were chosen for their low and high affinity, respectively. The AFM tip was chemically modified to bear the lectin while the glycoclusters were immobilized on a solid support. The configuration consents studying the dissociation of the lectin-glycocluster complex by taking into account the multivalency of both the lectin and the glycocluster. The results of this study will be presented in the next Chapter.

Chapter 4.   Single Molecule Force Spectroscopy to study lectin-glycocluster interactions

Pour mieux comprendre l'interaction lectine-glycomime, le mode spectroscopie a été utilisé. Ce Chapitre présente les résultats de mesure de spectroscopie de force par molécule unique (SMFS) sur les trois glycomimes M1, M2 et M3. Pour réaliser ces expériences, la pointe AFM en nitrure de silicium a été fonctionnalisée chimiquement. En utilisant le procédé d'amino-fonctionnalisation développé par le groupe de P. Hinterdorfer, la lectine LecA a été attachée à la sonde et utilisée pour effectuer des expériences SMFS sur des glycomimes greffés sur un support de silice.

L'interaction entre la lectine LecA et différents glycomimes a été étudiée afin de caractériser les différences dans la liaison en fonction de l'affinité des glycomimes pour la lectine à l'échelle nanométrique. La technique « DNA-Directed Immobilization » (DDI) a été utilisée pour immobiliser les glycomimes sur la surface. Cette technique d'immobilisation du glycomime est très robuste et reproductible. De plus, le glycomime étant immobilisé sur la surface par son centre, les quatre bras sont accessibles à la lectine. Toutefois, la densité de glycomime greffé n'est pas très élevée par rapport au nombre d'oligonucléotide greffé (1 glycomime pour 8 oligonucléotides). Cela conduit à une grande probabilité d'interaction non-spécifique, du même ordre de grandeur que l'interaction spécifique étudiée. De plus, très peu de courbes mettent en évidence une interaction, et parmi elles très peu correspondent donc à l'interaction spécifique. Les courbes de force sont, par conséquent, difficiles à exploiter, il faut identifier les composantes spécifique et non spécifique. Aussi, devant le faible nombre de courbes caractéristiques, il nous est apparu difficile de proposer une analyse quantitative et comparative des forces d'interaction en fonction du glycomime.

L'interaction de LecA avec le glycomime de plus grande affinité (M3) a été étudiée à différentes vitesses de traction afin d'extrapoler la valeur de la constante de dissociation cinétique (k_{off}). La valeur obtenue montre une dissociation rapide mais il est nécessaire de tenir compte du fait que ce paramètre est affecté par la nature multivalente de l'interaction. En effet, la lectine et le glycomime sont des molécules multivalentes et la probabilité d'avoir des effets cluster n'est pas négligeable. Par exemple, les courbes obtenues à la vitesse de $v = 100$ nm/s, pour le glycomime de plus grande affinité, montrent plusieurs évènements dus à des interactions spécifiques. Ces événements présentent la plupart du temps la même valeur de force d'interaction. Cela pourrait être expliqué par l'interaction entre un site de reconnaissance de la lectine et un galactose du glycomime. Dans les courbes où il y a plusieurs événements, la distance de séparation entre les évènements est du même ordre de grandeur que la dimension de la lectine, ce qui semble indiquer que deux monomères de la même lectine peuvent interagir avec deux galactoses du même glycomime, conformément à la stœchiométrie de la molécule étudiée. Ceci pourrait être interprété comme une mesure de l'effet cluster au niveau moléculaire.

4.1 Introduction

In Chapter 3, the influence of glycocluster architecture has been studied via AFM high-resolution images. These data, combined with MD simulations and ITC measurements allowed investigating the binding of different glycoclusters with LecA lectin, showing the influence of the design of the molecule on the interaction. In this Chapter, the LecA lectin-glycocluster interaction force has been characterized by means of Single Molecule Force Spectroscopy (SMFS) experiments. Force-distance measurements were acquired to obtain information on the strength of the binding between one lectin and one glycocluster. The mannose-centred glycoclusters M1, M2 and M3 were selected to perform spectroscopy analysis. Due to the different affinities of these glycoclusters, the strength of their binding with the lectin should be different. AFM-SMFS technique seems to be well adapted to study the binding since it enables measuring interaction forces of the order of picoNewton up to nanoNewton, with a sub-nanometric spatial resolution. To do that, the AFM tip must be chemically modified to bare the lectin, while the glycoclusters must be immobilized on the surface. The tip is then repeatedly approached and retracted from the surface to acquire force *vs.* distance curves, where the backward curve can present a characteristic pattern, specific of the lectin-glycocluster interaction. In the following, the results obtained for the LecA lectin-glycocluster interaction force will be presented.

4.2 Material and Methods

4.2.1 Experimental Setup

To quantify the interaction between different glycoclusters and the LecA lectin, AFM-SMFS measurements were performed. Taking advantage of surface chemistry it is possible to immobilize a single lectin (3 at most) [127,143] on top of the AFM tip, while the glycoclusters are grafted on a solid support [76]. The quantification of the unbinding force is done to compare the affinity of different glycoclusters at the molecular level.

The general experimental setup has been already described in section 2.6.1. Figure 4.1 presents a schematic description of the system, with the LecA lectin anchored to the AFM tip using a poly(ethylene)glycol (PEG) linker and the glycoclusters immobilized on a silica support via DNA Directed Immobilization (DDI) technique [189,190].
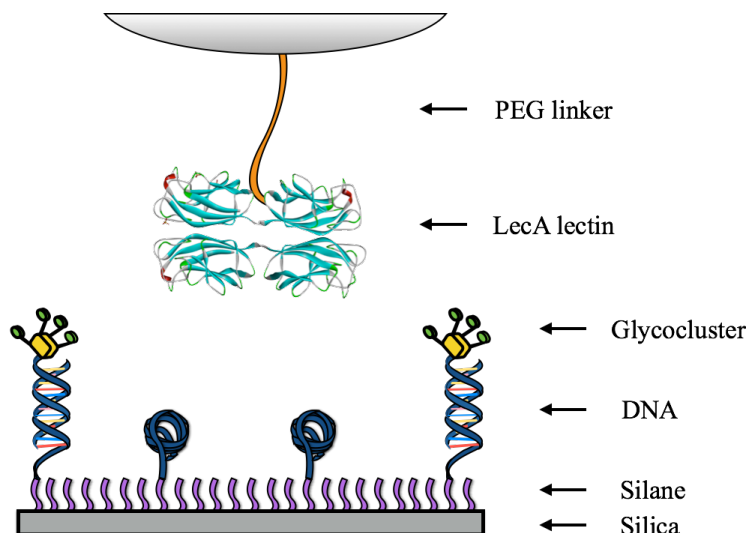
Figure 4.1: Schematic representation of the experimental system. The LecA lectin is linked to the AFM tip via a PEG spacer. The glycoclusters are immobilized on a silanized silica support via DNA molecules.

Four different glycoclusters were subsequently grafted on the substrate to perform SMFS experiments. For one of them (M3), data were recorded at different velocities to extrapolate the off-rate constant, k_{off}, of the interaction (section 1.3.3). In Table 4.1, a summary of the tested molecules is presented.

	Structure	K_d (nM)	n
M1	Man(ProTzEG$_3$Gal)$_4$	11000	0.25
M2	Man(ProTzAcNPhGal)$_4$	194	0.46
M3	Man(EG$_2$MTzAcNPhGal)$_4$	157	0.52
D1	(DMCH-MTzEG$_3$-Man)$_3$	n.a.	n.a.

Table 4.1: Glycoclusters used in SMFS experiments.

M1, M2 and M3 glycoclusters were studied via AFM imaging and the results obtained for their complex formed with LecA lectin have been presented in Chapter 3. They are characterized by a mannose core and different linkers that form the branches. M1 and M2 have the same linker L1, a propyl group (pro), whereas M2 and M3 have the same linker L2 (AcNPh).

The D1 is a new glycocluster that was chosen for negative control. In fact, when performing SMFS experiments one has to discriminate specific and non-specific interactions, thus negative controls must be performed. D1 glycocluster is a linear molecule with three mannose-terminated branches, thus it is not supposed to present affinity for the lectin since it does not bring galactose residues (section 1.4). Therefore, it will be a negative control able to discriminate non-specific interactions. In general, the specific unbinding manifests on the curve mostly at the same distance while non-specific unbinding can appear at various distances [136], therefore this parameter could help in discriminating between the two types of interactions.

4.2.2 Sample preparation

4.2.2.1 Tip Functionalization

To become sensitive to LecA lectin-glycocluster specific interaction, the AFM tip has to be converted into a specific biosensor capable of recognizing and specifically interacting with the molecules grafted on the sample surface. To do that, the AFM tip was functionalized with the lectin. The functionalization method used has been developed by Gruber and co-workers [136,143,145]: the protein is anchored to the AFM tip by a PEG linker. The use of a PEG linker allows reducing the density of immobilized proteins on the tip and give a certain degree of freedom to the protein, which freely orient itself face to the ligand bound to the surface [127,143].

The functionalization method is schematically presented in Figure 4.2 [145].

i) During the first step (Figure 4.2, step 1), the tips were cleaned with chloroform (3 x 5 min). By taking advantage of the spontaneous oxidation of silicon nitride in ambient atmosphere, tips can be chemically modified. In fact, the oxidation leads to the formation of a silanol (Si-OH) thin layer that can bind amino-groups. Tips were incubated with ethanolamine hydrochloride overnight and basically the Si–OH groups becomes $Si-O-(CH_2)_2-NH_2$, carrying the amino-group.

ii) The second step is the grafting of the PEG linker to the amino functionalized tip (Figure 4.2, step 2). The tips were therefore incubated with the acetal-PEG18-NHS linker to enable the reaction between the amino group of the tip and the ester group ($NHS-CO_2-R$) of the linker.

iii) Then, the acetal group must be converted into an aldehyde (R-CHO) (Figure 4.2, step 3), by using citric acid, for the subsequent coupling of the protein. The main advantage of using acetal linkers instead of aldheyde linkers is that acetal groups are inert and cannot form loops between closest NH_2 groups of the tip. Thus, a high functionalization efficiency is obtained [145]. The linking of the protein was done by taking advantage of the amino-groups of the proteins (such as the ones of lysine amino acid) by using sodiumcyanoborohydride ($NaCNBH_3$).

iv) Finally, the tips were incubated with ethanolamine to block the remaining aldehyde groups that did not react with the proteins. Tips were therefore washed with PBS buffer and stored in the same buffer at 4 ºC for at most 1 week.

More detailed information on the functionalization protocol can be found in the references [136,145,191] and in the related protocol [192].
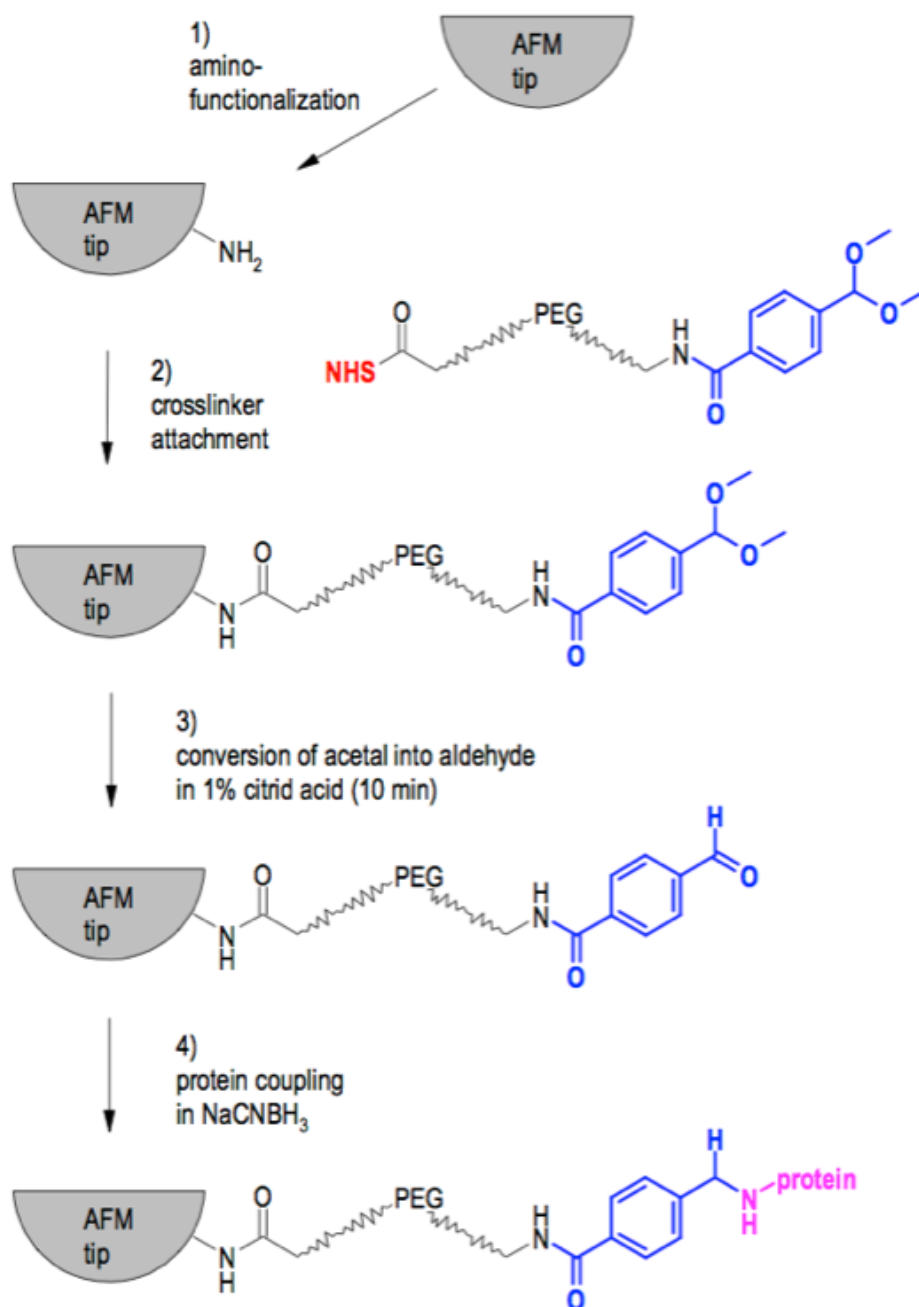
Figure 4.2: Schematic representation of the functionalization protocol. Taken from [192].

4.2.2.2 Surface functionalization

The surface functionalization is made on silicon dioxide (silica) wafers. The grafted molecule is the *tert*-butyl-11-(dimethylamino) silylundecanoate (TDSUM), a monofunctional silane which leads to the creation of a single uniform monolayer that overlaps the silica surface without increasing its roughness [189]. The silanization was made by following a liquid phase protocol developed in our team for several years [190].

Silane:	ssDNA:	Glycocluster:
10^{14} molecules/cm^2	10^{11}-10^{12} molecules/cm^2	1-4 10^{10} molecules/cm^2
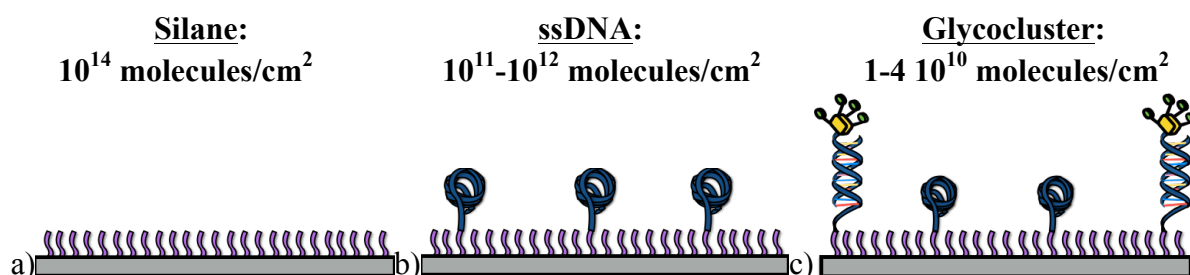
Figure 4.3: Representation of the substrate after a) silanization, b) immobilization of the amino-modified oligonucleotides (ssDNA) and c) the hybridization of the oligonucleotides with the complementary strand bearing the glycocluster.

i) **Silanization** (Figure 4.3a). Basically, the surfaces were cleaned by overnight immersion in a detergent solution 0.5%, rinsed in ultra-pure water and subsequently immersed in a freshly prepared piranha solution (mixture of H_2SO_4/H_2O_2 35% solution, 3:2) to ensure the formation of a silanol layer (Si-OH). The substrates were rinsed with ultra-pure water and readily used for silanization. Cleaned silica surfaces are flat, presenting a roughness of RMS = 0.28 ± 0.02 nm.

Then, the samples were heated at 147 ºC under nitrogen flux for 2 hours. The system was then let cool down. Subsequently, 50 mL of pentane and 60 µL of TDSUM were added in the reaction chamber. The nitrogen flux was established and the system was incubated at 147 ºC overnight. Afterward, the silanized substrates were washed in:
1) Tetrahydrofuran (THF) (1 x 10 min, ultrasound),
2) Dichloromethane (CH_2Cl_2) (1 x 10 min, ultrasound),
3) Sodium dodecyl sulphate (SDS) 0,1% (1 x 10 min, ultrasound),
4) Ultra-pure water (4 x 5 min, ultrasound) and dried with nitrogen.

The silanization process leads to the coverage of the mineral substrate with a homogeneous monolayer, which conserves the RMS value of the substrate (Annex II) and has a surface density of the order of 10^{14} molecules/cm^2 [189].

ii) **Deprotection and activation** steps allow substituting the *tert*-butyl ($C_6H_{12}O_2$) group with an amide group for subsequently covalently bind the amino-modified oligonucleotides (zip 1.1, 18 bps). A schematic representation of the deprotection and activation steps is presented in Figure 4.4, step 2. The deprotection is characterized by the incubation of the silanized samples in formic acid for 7 hours. After, the samples were washed in dichloromethane (1 x 10 min, ultrasound) and in ultra-pure water (1 x 10 min, ultrasound). The activation step is characterized by overnight incubation of the samples in a solution of 10 mL of THF + 120 mg of N-hydroxysuccinimide (NHS) and 160 µL of diisopropylcarbodiimide (DIC).
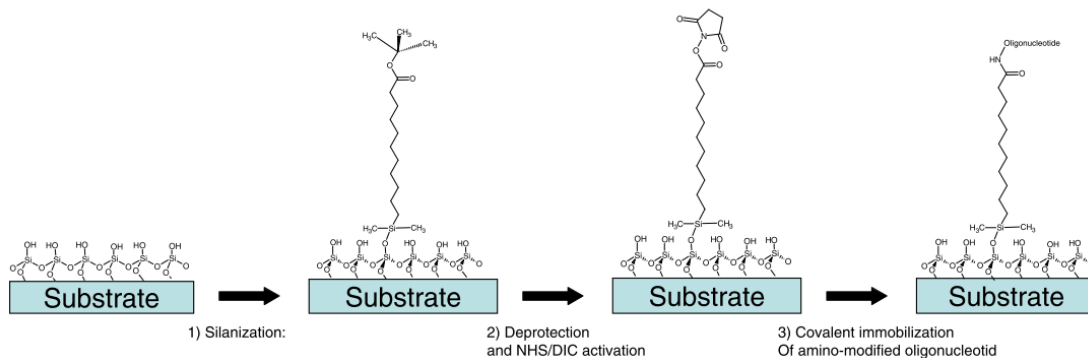
Figure 4.4: Schematic representation of the surface functionalization steps. Image taken from [190].

- **Immobilization of amino-modified oligonucleotides** (Figure 4.3b). The samples were washed in THF (1 x 10 min, ultrasound) and in dichloromethane (1 x 10 min, ultrasound). Then, amino-modified oligonucleotides (ssDNA) [sequence (5'-GTG AGC CCA GAG GCA GGG-$(CH_2)_7$-NH_2)] were covalently bound to the surface by overnight incubation of the samples with 40 μL of ssDNA 25 μM in PBS 10X, in a water-saturated atmosphere. The final surface density of oligonucleotides grafted is about 10^{11}-10^{12} molecules/cm^2 [189].

- **Hybridization of the oligonucleotides via the complementary strands bearing the glycoclusters** (Figure 4.3c). After immobilization, the samples were washed at 70 ºC for 30 min in 5 mL of SDS 0.1%, then 10 min at 70 ºC in 5 mL of ultra-pure water and gently dried with nitrogen. ssDNA probes were subsequently hybridized by DDI technique with complementary oligonucleotide-glycoclusters, leading to a final coverage of 1-4 x 10^{10} molecules/cm^2, as described by [189,193]. The complementary oligonucleotide bears a fluorescent tag (Cy3) at the 5' extremity to prove the success of the hybridization step and the glycocluster at the 3' extremity [76], as shown in Figure 4.5a.

a)   b)
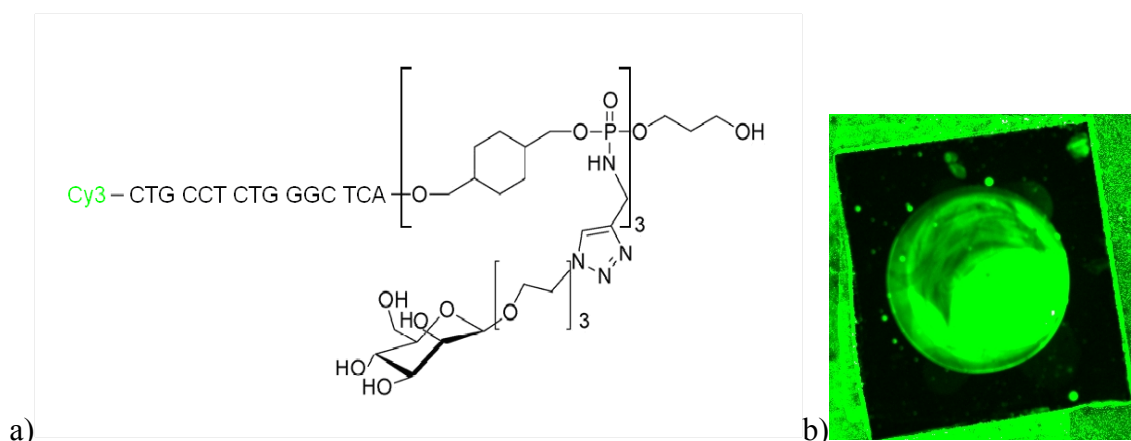
Figure 4.5: a) Complementary DNA sequence bearing the fluorescent tag and the glycocluster D1; b) Fluorescent image of a hybridized sample.

The hybridization step was made by incubating the sample at 37 ºC for 3 hours, in water-saturated atmosphere, with 40 µL of 1 µM solution of glycocluster prepared in SSC 5 X + SDS 0.1%. Samples were then washed in SSC 2X + SDS 0.1% (1 x 1 min at 51 ºC), then in SSC 2X (1 x 5 min at room temperature), rinsed with water and dried with nitrogen. After that, the surface density of immobilized glycoclusters was checked by scanning the samples at 532 nm (excitation of Cy3) with Axon microscanner, GenePrix 4100 A software package (Figure 4.5b).

Due to the functionalization step and the surface chemistry, the surface density of both grafted oligonucleotides and glycoclusters are low. It has been demonstrated that the maximum density of grafted ssDNA is about 10^{11}-10^{12} molecules/cm^2 [189] and for the glycocluster is 1-4 x 10^{10} molecules/cm^2 [193]. This implies that, in an ideal situation, the distance between two glycoclusters is larger than lectin dimensions; therefore it appears unlikely that one single lectin interacts with two different glycoclusters. Furthermore, between two glycocluster molecules there will be several molecules of oligonucleotides.

In fact, if we assume an homogeneous distribution of the grafted molecules on the surface, it is possible to determine the theoretical distance between two glycoclusters [193] and how many oligonucleotides could stand between them. Given the surface density of the grafted glycoclusters, and knowing that generally mannose-centred glycoclusters assume a globular shape with an estimated dimension of 3 nm, one can find the surface occupied by a glycocluster and the available surface for each of them. Upon calculations, the minimum distance between two glycoclusters results to be 32 nm. To calculate the area occupied by a ssDNA, it is necessary to take into account the radius of gyration (R_g) of the polymer, the surface density (Γ) and the constraint of not overlapping of different oligonucleotides (Annex I). In this case, the condition to have a brush ($\Gamma \ll 1/R_g^2$) is not satisfied: the ssDNA are likely arranged in blobs, forming a polymer mushroom and separated one from each other of at least 11 nm. Therefore, the ideal situation will be two hybridized DNA, carrying the glycoclusters, spaced by two ssDNA oligonucleotides separated by a distance of 11 nm, as shown in Figure 4.6.
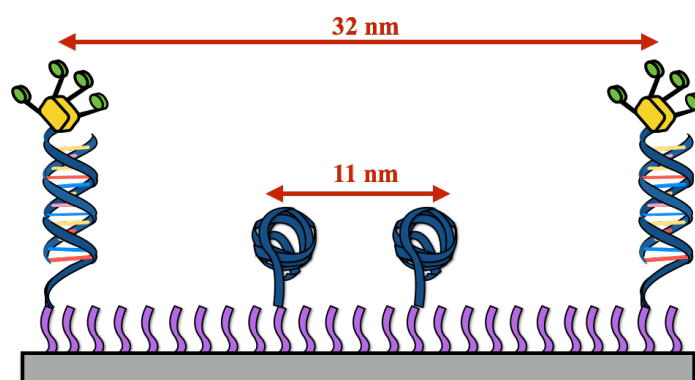
Figure 4.6: Schematic representation of the glycol-functionalized surface.

4.2.3 Atomic Force Microscopy and data analysis

4.2.3.1 Atomic Force Microscopy

Measurements have been performed at the AFM platform of the Institut Lumière Matière (Université Claude Bernard, UMR5306, Villeurbanne CEDEX, France) under the supervision of Dr. Agnès Piednoir. Data were acquired using an Asylum Research MFP-3D™ (Santa Barbara, California, USA), presented in Figure 4.7.
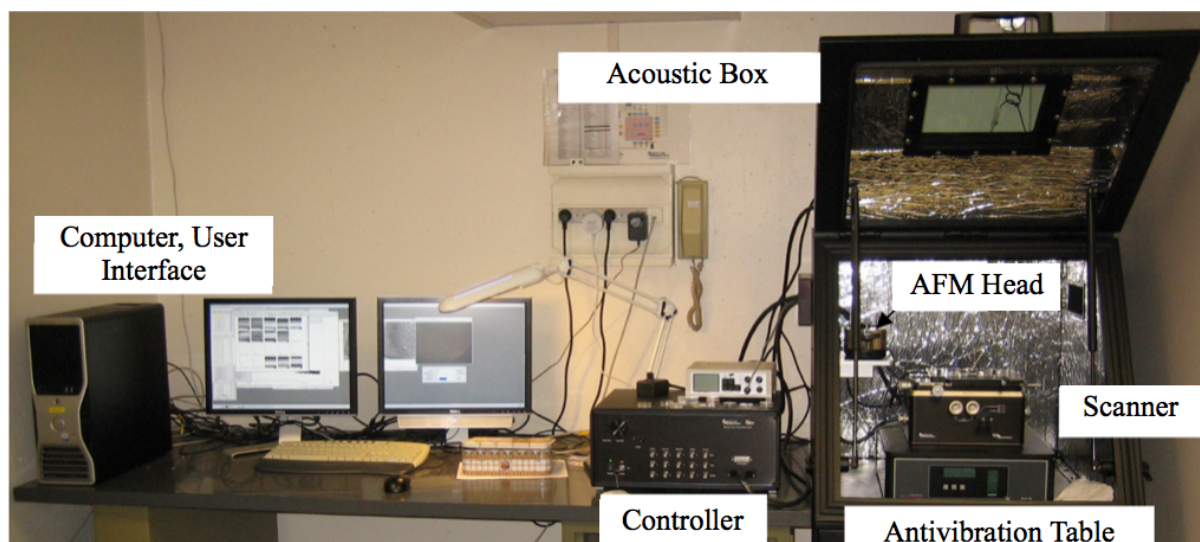
Figure 4.7: Asylum MFP 3D AFM.

The microscope is characterized by the AFM head, which contains the photodiode, the laser, the *z* scanner and the optical system that allows visualizing the cantilever and the sample surface. The sample is positioned on the *xy* scanner, situated on a plate that performs the lateral displacement via micrometric screws. The controller contains all the electronics used to control the microscope and the interface is displayed on the computer.

Measurements were performed in 200 μL of phosphate-buffered saline (PBS) 1X buffer pH 7.4 + 0.83 μg/mL $CaCl_2$. This solution is typically used *in vitro* LecA lectin-glycocluster assays since the presence of calcium ions mediates the binding between the lectin and its ligand (section 1.1.2.2). Silicon-nitride MSCT cantilever from Bruker (Santa Barbara, California, USA) (tip A, nominal k = 70 pN/nm and nominal f_r = 21 kHz) were functionalized as described above. At the end of the experiment, the cantilevers were calibrated via thermal noise method (section 2.2.1.1) to determine the spring constant. Force-curves were acquired at different pulling speeds: 50 nm/s, 100 nm/s and 1000 nm/s, with a dwell time of 0.99 s, a force ramp of 250 nm and a setpoint of 0.03 V (~ 150 pN).

Force curves were analysed by AFM Asylum Software that runs in Igor Pro (WaveMetrics, Inc. Lake Oswego, Oregon, USA) and allows smoothing (all the curves undergo a Box smoothing with a smoothing width of 20) and correcting (represent force *vs.* tip-sample separation, correct the tilt, find the contact point, etc.) the raw curves. Data were then analysed with PUNIAS (Protein

Unfolding and Nano-Indentation Analysis Software) [194] to determine characteristic parameters of the curves (Figure 4.8), such as the **unbinding force** (the maximum force detected) and the **rupture length** (the distance between the contact point and the position of the unbinding event).
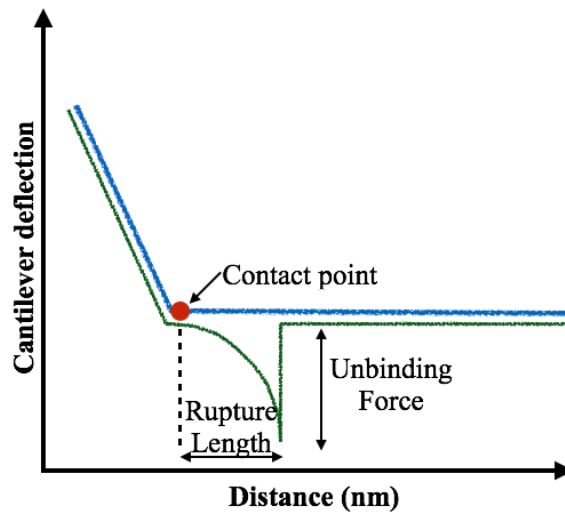
Figure 4.8: Sketch of a force-distance curve presenting the parameters analyzed.

The unbinding is a stochastic event that can be described with a Gaussian distribution. Due to that, at least 1000 curves have to be acquired per experiment to have a good statistics. In literature, different ways of performing data analysis are used since, most of the time, AFM constructors do not provide software to process force curves. Mostly, the analysis is performed with homemade algorithms that consist of screening huge amount of data and distinguishing false events (nonspecific interactions) from the true ones (specific receptor-ligand interactions). For example, the group of Hinterdorfer [132] developed an algorithm that allows visualizing the data distribution via their probability density function, therefore each data is weighted by its reliability and the discrimination of the events is done by applying *t*-Student test (Annex III), where the discontinuities in the curves (possible events) are compared to the noise on the baseline. The group of Dietler [195] developed an algorithm based on the fuzzy logic which allows expressing each event as a function of the degree of ambiguity of being a true event. Another method [196,197] considers the expression of the force as a function of the contour length (Annex I) instead of the tip-sample distance. The knowledge of the contour length of the spacer allows selecting a threshold in order to discriminate specific and non-specific events. In fact, both the ligand and the receptor can be bound via the same linker to the tip and the sample surface, respectively. Therefore, by using a well characterized spacer, of well known contour length, one can take advantage of this parameter to discriminate true unbinding events [196].

In the experiments presented here, curves were selected by setting a threshold at three times the standard deviation of the noise at the baseline to discriminate unbinding events. The rupture length parameter was then used to distinguish specific interactions from non-specific ones. Maxima unbinding force (x_c) and rupture length were obtained from Gaussian fit of data distributions and expressed as ($x_c \pm \sigma$), being σ the standard deviation, and accompanied by the full width at half maximum (FWHM).

4.3 Results and Discussion

4.3.1 Control experiments for screening non-specific interactions.

In all single molecule recognition experiments, i.e. protein-protein or antibody-antigen interactions, avoiding unspecific events is a crucial point since they can obscure the binding under study [198]. Due to the complexity of our system, it is mandatory to find a way to discriminate the real receptor-ligand interaction from the 'sea' of non-specific ones. In general, reducing non-specific interactions can be done by both tip and sample modifications. For example, the use of a flexible linker that connects the ligand to the tip reduces the non-specific interactions of the tip with the surface and at the same time increases the degree of freedom of the ligand [127]. Also, playing with dwell time and loading force (setpoint) will help in the task: adhesion is promoted by the increasing of loading force and the consequent decreasing of the dwell time required for non-specific interactions [198].

In the experiments presented here, the probability of having non-specific interactions is increased by the fact that the biofunctionalized surface presents four different types of molecules, all with their characteristics (i.e. hydrophobic, hydrophilic), and all contributing to the final surface chemistry and charge. Probably, capping the system with BSA (bovine serum albumin) would have helped decreasing the non-specific interactions. Since it is not clear how BSA interacts and covers the surface and since probably it could non-specifically interact with the functionalized tip, other ways for discriminating non-specific interactions were chosen. We decided to quantify the interaction between the lectin functionalized tip and the surface after each step of preparation:

> *i)*   After the grafting of silane molecules on the surface;
> *ii)*   After the immobilization of the oligonucleotides;
> *iii)*   After hybridization of the oligonucleotides, with a complementary strand bearing the D1 glycocluster (negative control).

4.3.1.1 Force spectroscopy on silanized surfaces

To characterize the possible unspecific interaction between the silane and the LecA lectin functionalized tip, force spectroscopy measurements were performed and the result was compared with the one obtained with a bare tip (Figure 4.9). To have a good statistic, 800 curves were taken with two functionalized tips and 200 with the bare one. All the measurements were performed in PBS buffer 1X (pH 7.4) + 0.83 mg/ml $CaCl_2$ and were taken at constant pulling speed of $v = 100$ nm/s, with a dwell time between the forward and the backward curves of 0.99 s.
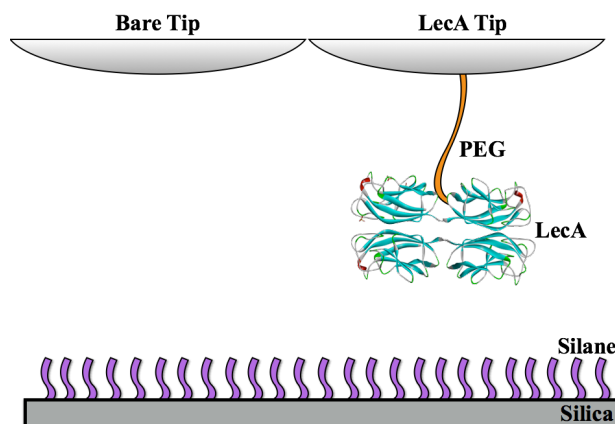
Figure 4.9: Schematic representation of the experimental system. The silane molecules were grafted on the silica support and SMFS experiments were performed with a functionalized tip carrying LecA lectin and a bare tip.

A strong adhesion is present in both cases: 5.6 ± 0.3 nN (FWHM = 0.8 nN) for functionalized tips and 9.8 ± 0.5 nN (FWHM = 1.3 nN) for the bare tip (Figure 4.10a), with a rupture length of $L_R = 66 \pm 3$ nm (FWHM = 8 nm) and $L_R = 126 \pm 7$ nm (FWHM = 18 nm) (Figure 4.10b), respectively. The shape of the curves refers to an attractive interaction which is completely absent when the probe is opposed to the bare silica support: the isoelectric point of silica is about 1.7-3.5 which means that at neutral pH it carries a negative charge; therefore the formation of an electrostatic double layer avoids the interaction between the probe and the silica support. The hydrophobic nature of silane molecules changes the surface charge and modifies the interaction with the probe, which becomes attractive.

In the case of the bare tip, the adhesion is stronger with a higher rupture length ($F_u \sim 9.8$ nN, $L_R \sim 126$ nm), compared to the functionalized tip. Upon functionalization, the probe becomes more hydrophilic mostly because of the amino-functionalization (-NH_2 groups) and the grafting of the PEG. This may lead to a screening of the interaction with the surface and therefore a decreasing of the adhesion.
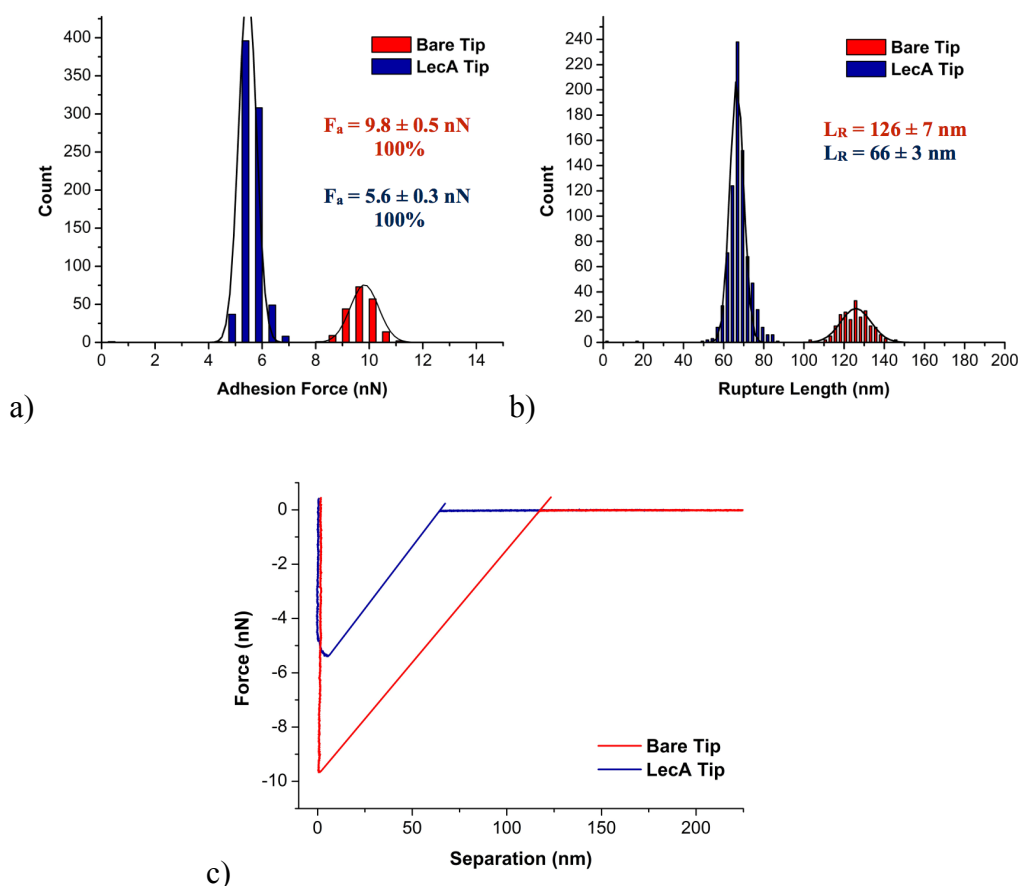
Figure 4.10: Plot of a) the adhesion force and b) the rupture length of the interaction between the silanized surface and the functionalized tip (blue) and the bare tip (red), respectively. Values are expressed as (xc ± σ). c) Typical force-distance curves (backward) recorded.

All the curves (100% of curves) present a characteristic that demonstrates the high adhesion between the tip and the surface with an adhesion force of several nN (Figure 4.10c). However, some of those curves (22% for functionalized tips and 36% for bare tip) present also discrete events after the adhesion peak. These events can be of two types: they can be related to the adhesion at the edge of the chain (stretching events, Figure 4.11a), or the polymer can be stripped by the probe (plateau events, Figure 4.11b) like a Velcro [93]. The shape of the interaction in the force-distance curve allows distinguishing between these two behaviours.
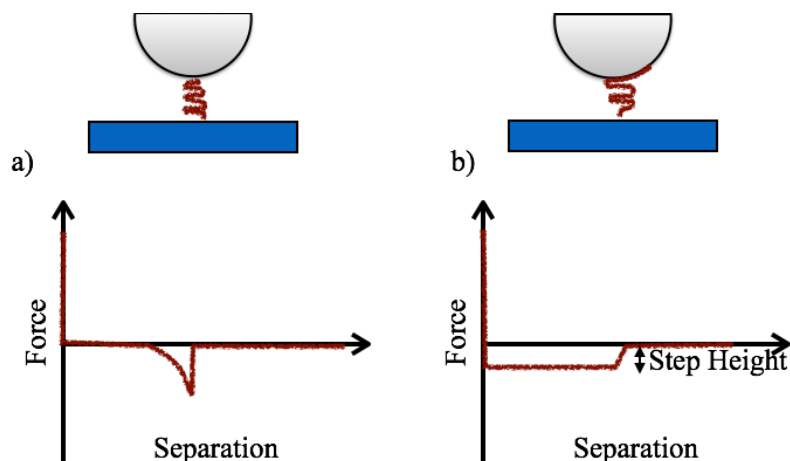
Figure 4.11: Schematic representation of bridging adhesion: a) single polymer extension where only the head of the grafted molecule binds to the AFM tip; b) the grafted molecule is peeled by the tip. Adapted from [93].

In our system, in the case of functionalized tip, 1.75% of curves present stretching events characterized by an unbinding force of 1.06 ± 0.5 nN (Figure 4.12), while for the bare tip these events were not recorded. Thus, stretching events may be related to the presence of the chemical modification and the protein on the tip. In fact, proteins present a varied structure that comprehend a mixture of hydrophobic and hydrophilic regions (charged groups and non-polar ones) [199] that allows the specific recognition and the binding. Since it has been shown that biomolecules are able to modify the local context in order to tune the interaction [200], the specific extension might be due to the specific recognition (polymer extension) between the CH_3 groups of the head of the silane and some hydrophobic parts of the functionalized probe. Hydrophobic interactions are influenced by temperature, pH, ionic concentration in solution and the presence of methanol in aqueous solution since it breaks water molecules closed to non-polar entities and avoids hydrophobic interactions [103]. Also, it has been shown that the strength of hydrophobic interactions can be influenced by the surrounding, in particular it can be modulated by the vicinity of other molecules [199] such as NH_3^+/NH_2 groups. Therefore a way to verify the hydrophobic nature of this interaction would be, for example, changing the ionic strength of the solution.
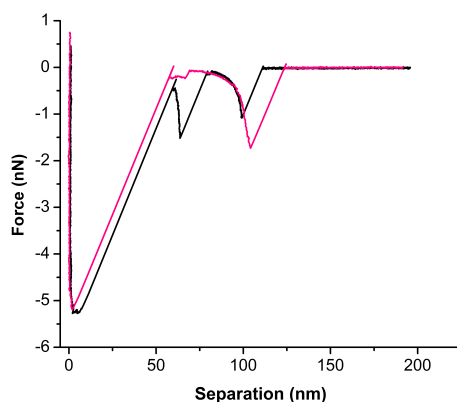
Figure 4.12: Typical force-distance curve (backward) recorded for stretching events.

Whereas, both the bare tip and the functionalized one show a peeling off of the silane (Figure 4.13a), characterized by plateaus of step height of almost 82 pN in both cases ($F_{un.} = 82 \pm 28$ pN, FWHM = 28 pN, 20% of events for functionalized tips LecA; $F_{un.} = 81 \pm 15$ pN, FWHM = 35 nm, 36% of events for the bare tip) (Figure 4.13b). These events correspond to low force interactions characterized by the stripping of the hydrophobic silane molecules with a huge variability in the step length of the plateaus, probably due to the statistical variability of the number of molecules that interact with the probe.
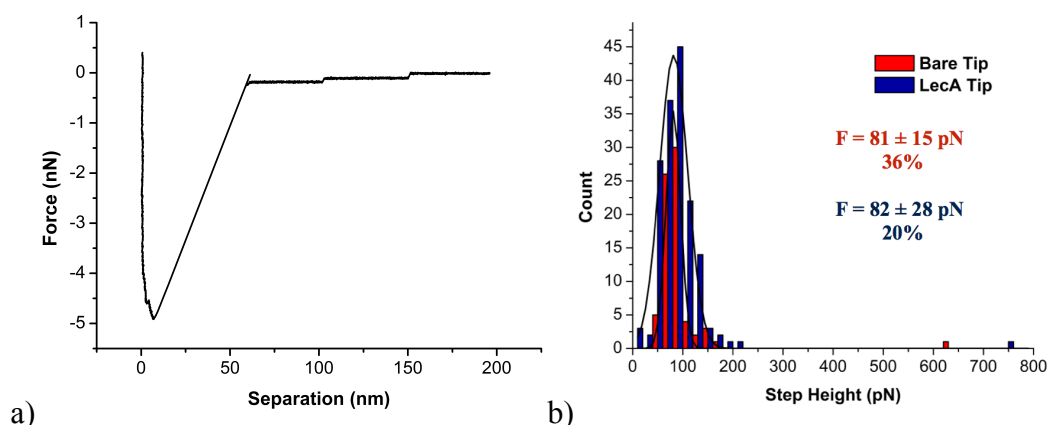
Figure 4.13: a) Typical force-distance curve (backward) recorded plateau events; b) Distribution of the step height (pN) of the plateau events between the silanized surface and the functionalized probe (blue) and the control one (red), respectively. Values are expressed as (xc ± σ).

4.3.1.2 Force spectroscopy on grafted ssDNA surfaces
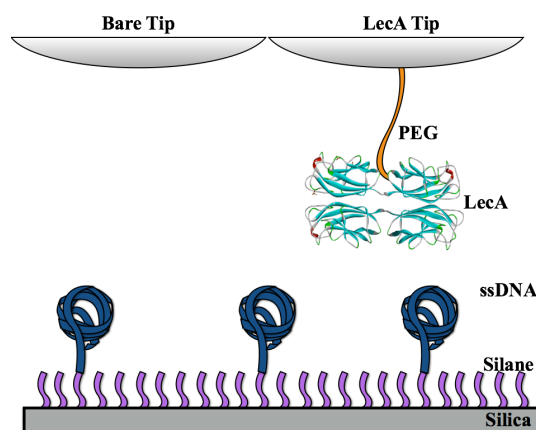
Figure 4.14: Schematic representation of the experimental system. The oligonucleotides are grafted on the silica support and SMFS experiments were performed with a functionalized tip carrying LecA lectin.

The interaction between the functionalized tip and the oligonucleotides grafted on the silanized surface was studied and compared to the one of a bare tip. To have a consistent statistics, 1152 curves were acquired with LecA tip and in the 94.4% of cases no adhesion events were recorded. The interaction with immobilized oligonucleotides was studied in the same conditions as for silanized surfaces: LecA lectin functionalized probes and bare tips were used to characterize the interaction in PBS buffer 1X (pH 7.4) + 0.83 mg/ml $CaCl_2$ and curves were taken at constant

pulling speed of $v = 100$ nm/s, with a dwell time between the forward and the backward curves of 0.99 s (Figure 4.14).

With the functionalized tip, in addition to the classical adhesion curve, a new characteristic appeared on some curves, which was not observed on the silane surface. The former can be related to non-specific interactions since it is characterized by the same slope during the retraction process and may be associated to the normal adhesion (Figure 4.15a) [138]. The latter is characterized by a change in the slope of the retraction curve, which is associated to a change in the effective spring constant and it is supposed to represent a specific interaction [138] (Figure 4.15b). Then, only the second type of events was considered, since they can be attributed to the stretching of the oligonucleotides.
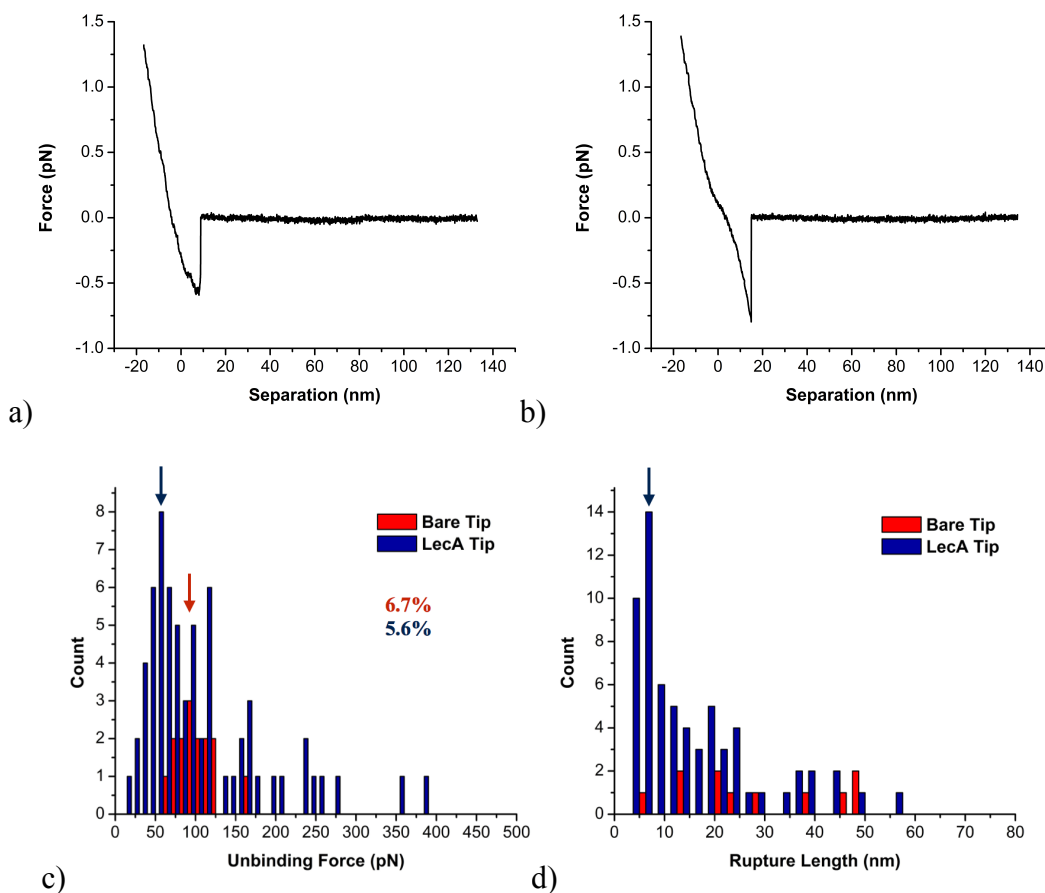
Figure 4.15: Force-distance curves obtained for the interaction between LecA functionalized tip vs. DNA grafted surface where a) the slope does not change during retraction while in b) the slope changes in the retraction curve. Data distribution of c) the unbinding force and d) the rupture length for the stretching of the oligonucleotides grafted on the surface. Arrows show the highest count.

Non-specific interactions were present in the 5.6% of recorded curves, characterized by an unbinding force that seems to have a maximum around $F_u \sim 68$ pN (Figure 4.15a) and a rupture length almost around $L_R \sim 6$ nm (Figure 4.15b). This interaction can be due to the fact that DNA is a polyelectrolyte and can interact with the amine groups but also with the silicon nitride. In fact, a

similar interaction was found with bare tip and also reported in literature [201]. Therefore, it may unlikely be due mainly to the presence of the protein.

In conclusion, it seems that the presence of the grafted oligonucleotides on the surface highly decreases the attraction between the tip and the substrate, leading to a smaller adhesion force. This behaviour should be related to the polyelectrolyte nature of the oligonucleotide that modifies the surface charge, probably increasing the repulsion.

4.3.1.3 Force spectroscopy on D1 glycocluster

To further understand the role of non-specific interactions in the measurements, the glycocluster D1 (Table 4.1) was grafted on the surface. This molecule does not specifically interact with the lectin since it does not bring galactose residues. In this case, the AFM probe can interact with the silane, the grafted ssDNA and the hybridized oligonucleotide that bears the glycocluster.

The experiments were performed at a pulling velocity of $v = 100$ nm/s and a huge contribution of non-specific interactions were detected. In particular 17% of curves recorded present interaction events. The unbinding force presents the highest number of count around $F_{un.} \sim 36$ pN (Figure 4.16a) while the distribution of the rupture length is quite dispersed, presenting a maxima around $L_R \sim 19$ nm (Figure 4.16b).

a)   b)

Figure 4.16: Data distribution of a) unbinding force and b) rupture length for the interaction with D1 glycocluster at pulling speeds v = 100 nm/s.

This negative control experiment shows the complexity of the system under study and especially the presence of a non-specific interaction that is not negligible. In fact, all the molecules immobilized on the surface (silane, ssDNA and hybridized filament) can interact with the functionalized probe with an unbinding force that seems to be mostly of the same order of magnitude of the one expected for the specific LecA lectin-glycocluster interaction, making more difficult the distinction between specific and non-specific events.

4.3.2 LecA lectin-glycocluster specific interaction

4.3.2.1 Comparison of different glycoclusters: M1, M2 and M3

To compare the strength of the interaction between LecA lectin and the three mannose-centred glycoclusters, M1, M2 and M3, force distance curves were acquired at pulling speed $v = 1000$ nm/s. Each set of data was obtained by recording $N = 2000$-2800 total number of curves acquired with four different LecA-modified tips.

Figure 4.17 presents the histograms obtained for the rupture length parameter for M1 (Figure 4.17a), M2 (Figure 4.17b) and M3 (Figure 4.17c). All the recorded events were used to construct these histograms, without differentiating the specific and the non-specific interactions.
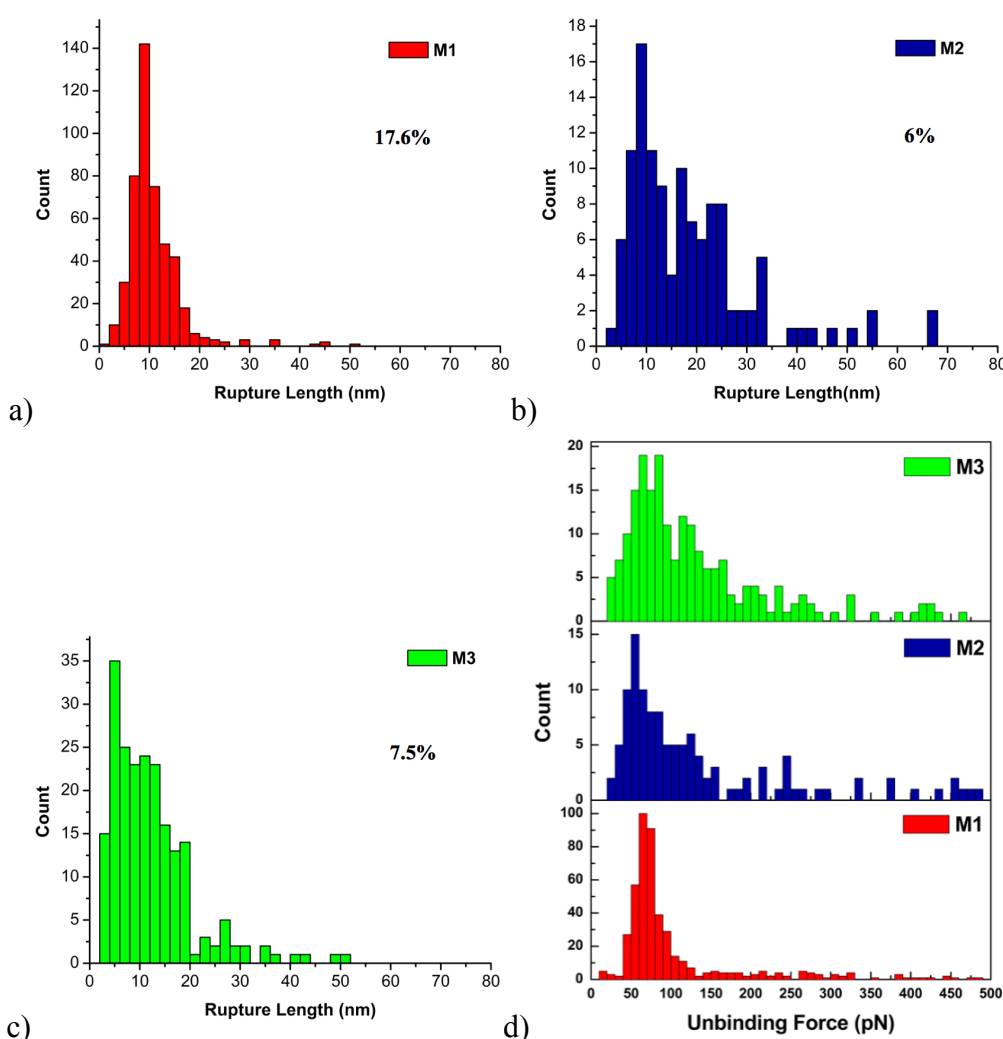
Figure 4.17: Data distribution of the rupture length recorded for the interactions LecA vs. a) M1, b) M2 and c) M3. d) Data distribution of the unbinding force of the interactions LecA vs. M1 (red), M2 (blue) and M3 (green). No distinctions between specific and non-specific events have been made.

The majority of stretching events present a rupture length smaller than $L_R = 20$ nm, less dispersed than in the case of D1 glycocluster. For these events, the highest frequency is obtained for $L_R \sim 6$-

10 nm, which can be associated to an interaction with the oligonucleotides, according to previous results (Figure 4.15b). They all seem to present a maximum unbinding force around ~ 75 pN (Figure 4.17d), meaning that they similarly interact with the lectin even though their present different affinities for LecA. Thus, they are probably mainly associated to non-specific interactions. Consequently, if all these events would be considered, it would be unlikely to determine the true strength of the lectin-glycocluster interaction since it will be lost in the "sea" of non-specific interactions.

As a consequence, to limit the contribution of non-specific interaction in the data analysis, only interaction events presenting ruptures lengths larger than L_R = 26 nm have been considered. This separation length has been chosen from considerations on the length of the molecules involved in the interaction and the previous analysis (silane, ssDNA, D1).

In fact, the probe is characterized by a PEG linker of length L ~ 6.44 nm, considering 0.358 nm the estimated length of a zigzag backbone [168] and the number of backbones that form the molecule. Also, the lectin has the shape of a parallelepiped of dimensions 7 nm x 3 nm x 1.9 nm (section 1.1.2.2). The binding between the lectin and the PEG is formed between the reactive amino function of the lectin and the aldehyde group of the spacer (section 4.2.2.1) [145]. This means that the binding can be formed with the amino acids of the lectin that present a not-sterically-hindered nucleophilic nitrogen. In the case of LecA lectin, the most probable amino acid target of the aldehyde group is the lysine (Lys). Each lectin monomer presents four Lys groups among which, one is closed to the CRD of the lectin while the others are far apart (Figure 4.18a). Due to the disposition of the Lys on the lectin and their higher concentration on the central part of the protein structure, it should be more probable that the binding with the spacer happens with one of those Lys, leading to a most probable horizontal disposition of the lectin with all four CRDs available for the interaction with the glycocluster (Figure 4.18b). Thus, the length of the PEG-lectin system is almost 10 nm.

Considering the molecules grafted on the surface, two situations have to be considered: the non-specific interaction with the grafted oligonucleotides and the specific interaction under study. The length of the two systems is mostly the same, if considering the total stretching of the oligonucleotide (L = 15 nm for ssDNA + silane *vs.* L = 14.1 nm for hybridized DNA bearing the glycocluster + silane). Previous experiments show that the stretching of the ssDNA happens at a probable rupture length of 6 nm and for the majority of recorded events it is smaller than 20 nm. Therefore, taking into account the previous results, the estimated total length of the non-specific interaction should be more likely smaller than 20 nm, while the specific one should be around 25 nm (Figure 4.18b). Also, specific events should appear as last in the curve. For that, we decide to consider specific LecA lectin-glycocluster interactions as all the events characterized by a rupture length L_R > 26 nm.
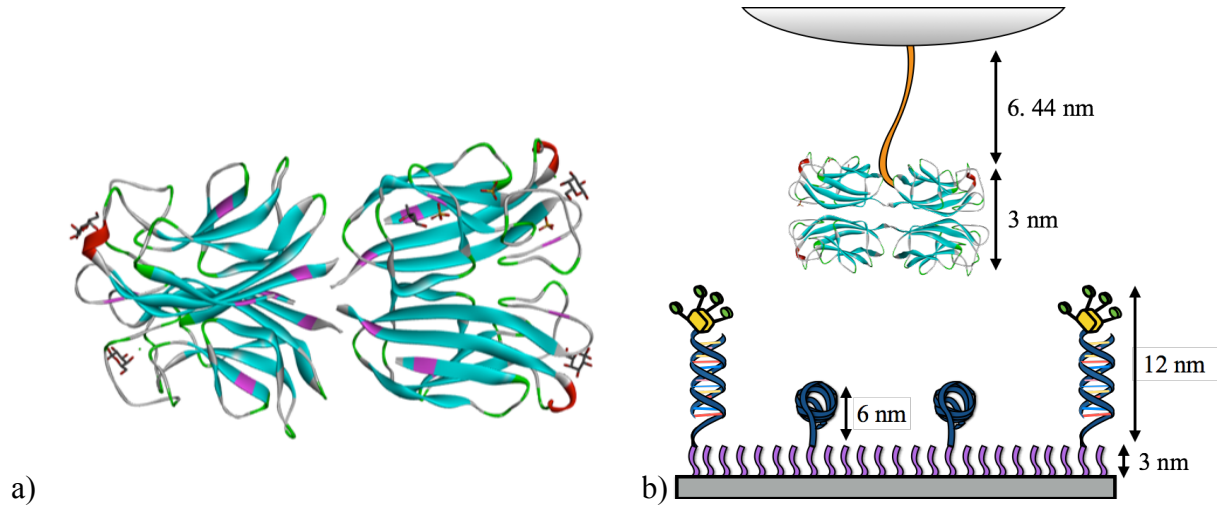
Figure 4.18: a) Cristal structure of the LecA lectin (4LKD), where in pink are shown the Lys amino acids; b) Sketch of the experimental setup where the estimated length of the molecules involved in the interaction are presented.

Fixing $L_R > 26$ nm as threshold implies discard a huge number of events and leading with a small number of recorded events. For the three systems under study, the resulting number of specific events is: $N_{events} = 14$ for M1, $N_{events} = 20$ for M2 and $N_{events} = 15$ for M3. Therefore, the frequency of unbinding events results to be of 0.5%, 1% and 0.5% for the three lectin-glycocluster interactions, respectively.

In general, a minimum sample size of $N_{events} = 6$ is sufficient to obtain a force distribution with a error margin of $E = 10$ pN with 99% of confidence, while reducing the error margin to ± 1 pN requires a sample size of at least $N_{events} = 53$ samples, given the error margin E as

$$E = \frac{z^* \sigma}{\sqrt{N_{events}}} \tag{0.53}$$

where $z^* = 3$ is the score used to have a confidence of 99%, σ is the standard deviation of the Gaussian distribution and N_{events} is the number of recorded unbinding events [202].

It seems that the highest number of unbinding events for M1 glycocluster is obtained for unbinding forces lower than $F_{un.} = 50$ pN (Figure 4.19a), for M2 glycocluster a maxima unbinding force appears to be at $F_{un.} \sim 120$ pN (Figure 4.19b), while for M3 glycocluster it looks to be at $F_{un.} \sim 84$ pN (Figure 4.19c). Therefore, data distributions seems to show an increasing of the unbinding force for M2 and M3 glycoclusters with respect of M1, consistent with the higher affinity of the two glycoclusters for the lectin. Unfortunately, consistent considerations cannot be made since the low statistics influences the reliability of the data. More experiments should be performed to validate these results and relate the affinity of the glycoclusters to the unbinding forces.
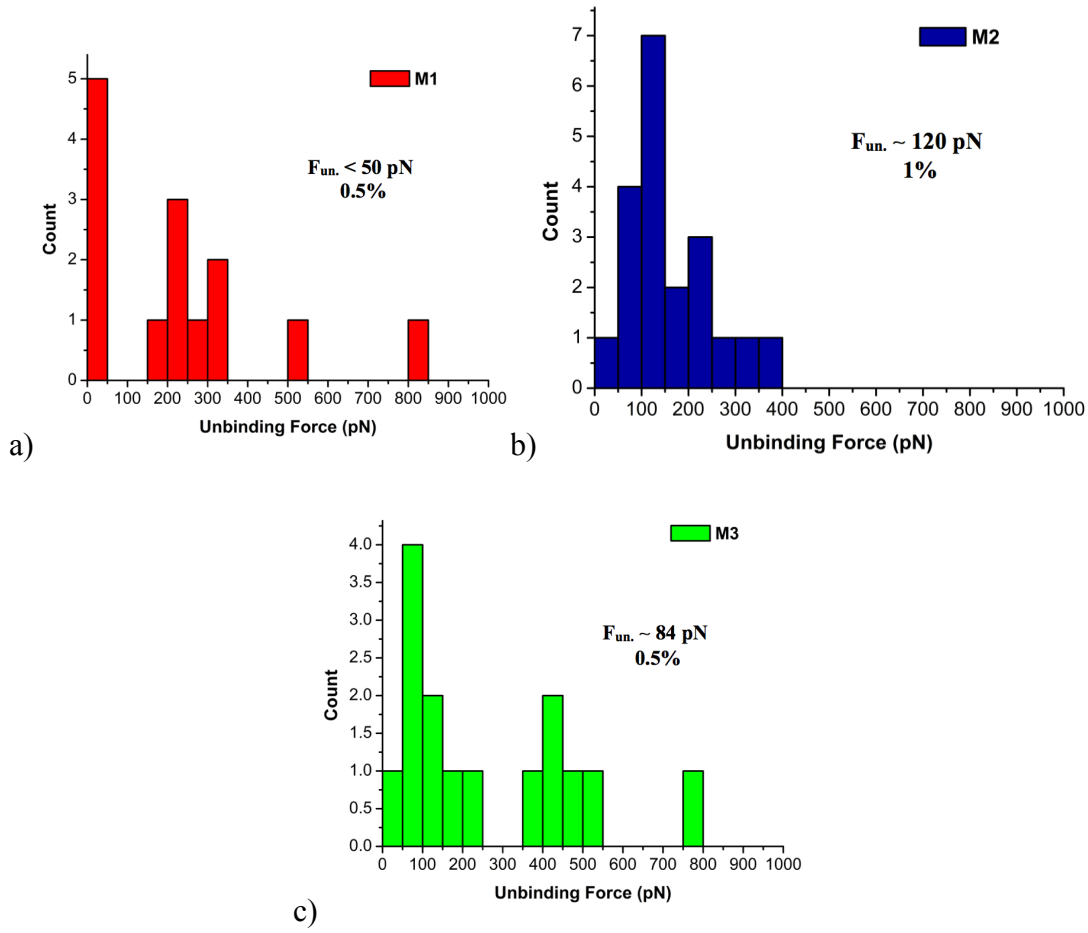
Figure 4.19: Data distribution of the unbinding force recorded for the interactions LecA vs. a) M1 (red), b) M2 (blue) and c) M3 (green).

4.3.2.2 Estimation of k_{off} constant for M3 glycoclusters

We decided to focalize our attention on the study of the interaction between LecA lectin and M3 glycocluster, by estimating the k_{off} constant of the unbinding process. For this, the pulling speed was reduced to $v = 100$ nm/s and $v = 50$ nm/s and the interactions between the LecA lectin AFM probe and the glycocluster was studied.

At pulling speed of $v = 100$ nm/s, 2300-2600 curves were acquired and 7% of events were detected. The value obtained for the unbinding force for LecA lectin-M3 glycocluster interaction is $F_{un.} = 55 \pm 19$ pN (FWHM = 46 pN) with a rupture length of $L_R = 34 \pm 5$ nm (FWHM = 12 nm) (Figure 4.20a and b, respectively). Decreasing the pulling speed allowed having a better statistics ($N_{events} = 161$) and the probability of unbinding events was increased, probably due to the fact that the lectin might have more time to orient itself and interact with the galactose residues of the glycocluster.
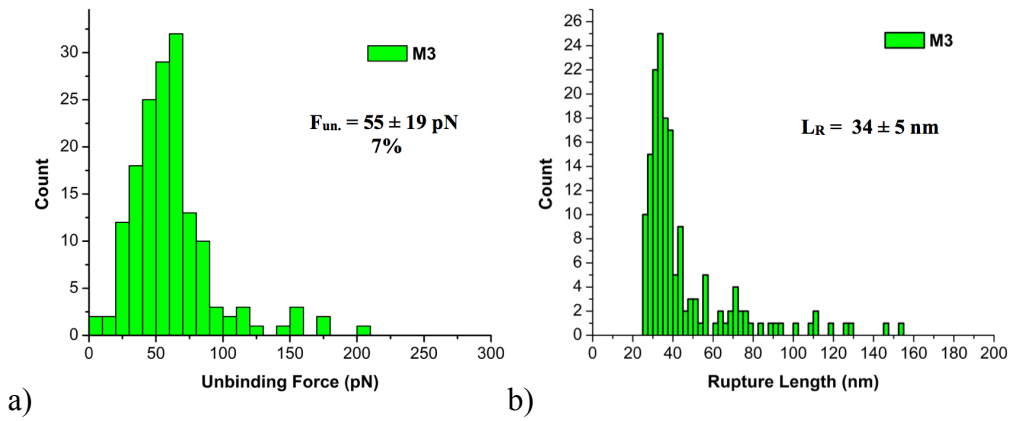
Figure 4.20: Data distribution of a) unbinding force and b) rupture lengths obtained for the interaction between LecA and M3 at v = 100 nm/s. Values are expressed as (xc ± σ).

Data were also acquired at pulling speed of $v = 50$ nm/s. LecA lectin-M3 glycocluster interaction is characterized by a frequency of 3.4% ($N_{events} = 78$) of having unbinding events, with maxima unbinding force at $F_{un.} = 42 \pm 16$ pN (FWHM = 39 pN) (Figure 4.21a) and maxima rupture length at $L_R = 32 \pm 5$ nm (FWHM = 12 nm) (Figure 4.21b). This is in accordance with the dynamic theory of receptor-ligand interaction under an applied force, showing a dependence of the unbinding force to the pulling speed (section 2.6.1.2). The unbinding force increases as the pulling speed increases moving from 42 pN at $v = 50$ nm/s to 55 pN at $v = 100$ nm/s and 84 pN at $v = 1000$ nm/s.
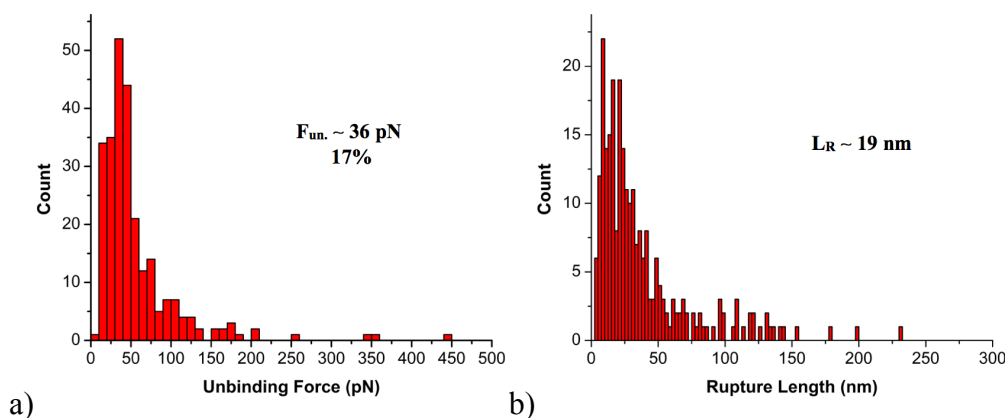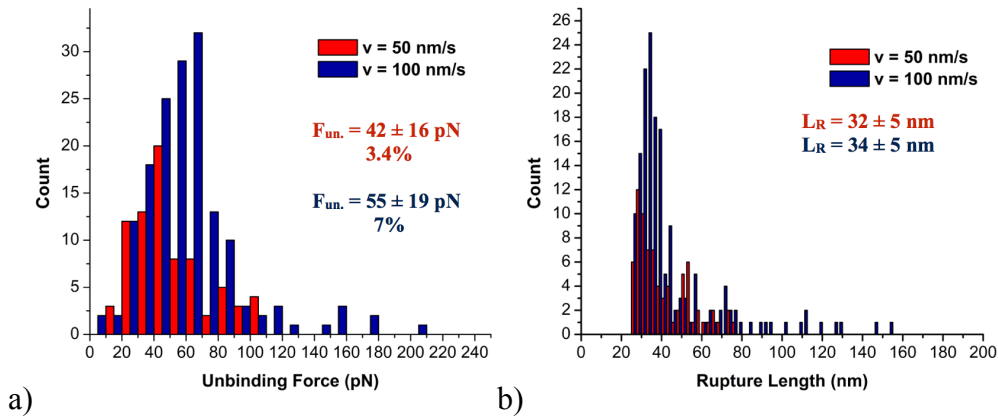

Figure 4.21: Data distribution of a) unbinding force and b) rupture length obtained for M3 glycocluster at pulling speed v = 50 nm/s (red) and v = 100 nm/s (blue).

Even though the value obtained at $v = 1000$ nm/s is affected by the low statistics, its increase seems to follow the tendency of the two other values obtained at lower pulling speeds. Therefore, we decided to extrapolate the off-rate constant (k_{off}) of the interaction (Figure 4.22). The k_{off} constant gives information on the selectivity of the interaction and it is completely related to the VdW interactions, protein conformational changes, hydrogen bonds, etc. that happen specifically at the binding pocket once the receptor interacts with the ligand [203]. It can be directly related to the duration of occupancy (residence time), which stands for the interval of time in which the receptor interaction site is occupied by the ligand. This parameter is an indicator of the efficacy of the

binding *in vivo*. It is given by the relaxation constant $\tau = 1/k_{off}$ and it can be related to the half-life by $t_{1/2} = 0.639/k_{off}$ [203]. In our case, the value found for the k_{off} constant for LecA lectin-M3 glycocluster interaction is $k_{off} = 0.67 \pm 0.39$ s^{-1}, leading to a half-life of $t_{1/2} \sim 950$ ms, which reflects a fast dissociation process. It summarises a general behaviour since all unbinding events were equally considered. Clearly, the value is affected by the bad statistics obtained at high pulling speed. Therefore, further measurement should be performed to obtain a better statistic. In this way, the incertitude may be decreased and the result can be proved.

To our knowledge, the off-rate of LecA-galactose interaction has not been characterized by AFM technique. The majorities of studies were performed by ITC measurement where the dissociation constant is directly obtained. The two constants describe the dissociation process from two different points of view. From the microscopic point of view, the off-rate describes the dynamic of the process while the dissociation constant (K_d) describes the process at the equilibrium, and they are related one to the other via the on-rate constant (section 1.3.3). AFM-SMFS technique is capable of studying the unbinding process but not the formation of the receptor-ligand complex, thus only the off-rate constant can be determined impeding the evaluation of the dissociation constant (K_d) and the comparison with the values obtained with others techniques such as the ITC assays. In any case, this values seems to be in accordance with values obtained for other lectin-glycoconjugates interactions [204].
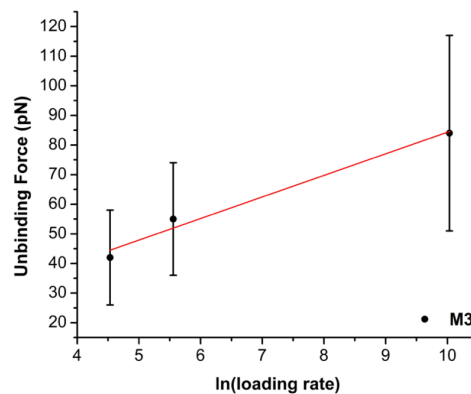
Figure 4.22: Extrapolation of off-rate constant for the interaction LecA lectin vs. M3 glycocluster.

4.3.2.3 The multivalent nature of the LecA lectin-glycocluster interaction

An interesting result that can be related to the multivalent nature of both the lectin and the glycocluster is the fact that the curves present, most of the time, multiple stretching events. To study this effect, the number and separation of stretching events obtained in each curve for data recorded for M3 glycocluster at pulling speed $v = 100$ nm/s was analysed in order to get information on the interaction. In general, curves present at most one stretching event (68% of curves) that can be related to the specific LecA lectin-M3 glycocluster interaction. Multiple events were also been detected: 20.6% of curves present two single stretching events, while 7.5% are characterized by three specific events and only the 2.8% present four stretching events (Figure 4.23a). The unbinding force of these multiple events is almost the same ($F_{un.} \sim 50$ pN, Figure 4.23b), therefore the

interactions seem to be similar. They are probably related to the rupture of the binding between one lectin CRD and a galactose residue of the glycocluster. Also, the separation of consecutive events was studied (Figure 4.23c). Results show a distribution characterized by a maxima at almost $\Delta L_R \sim$ 7 nm.
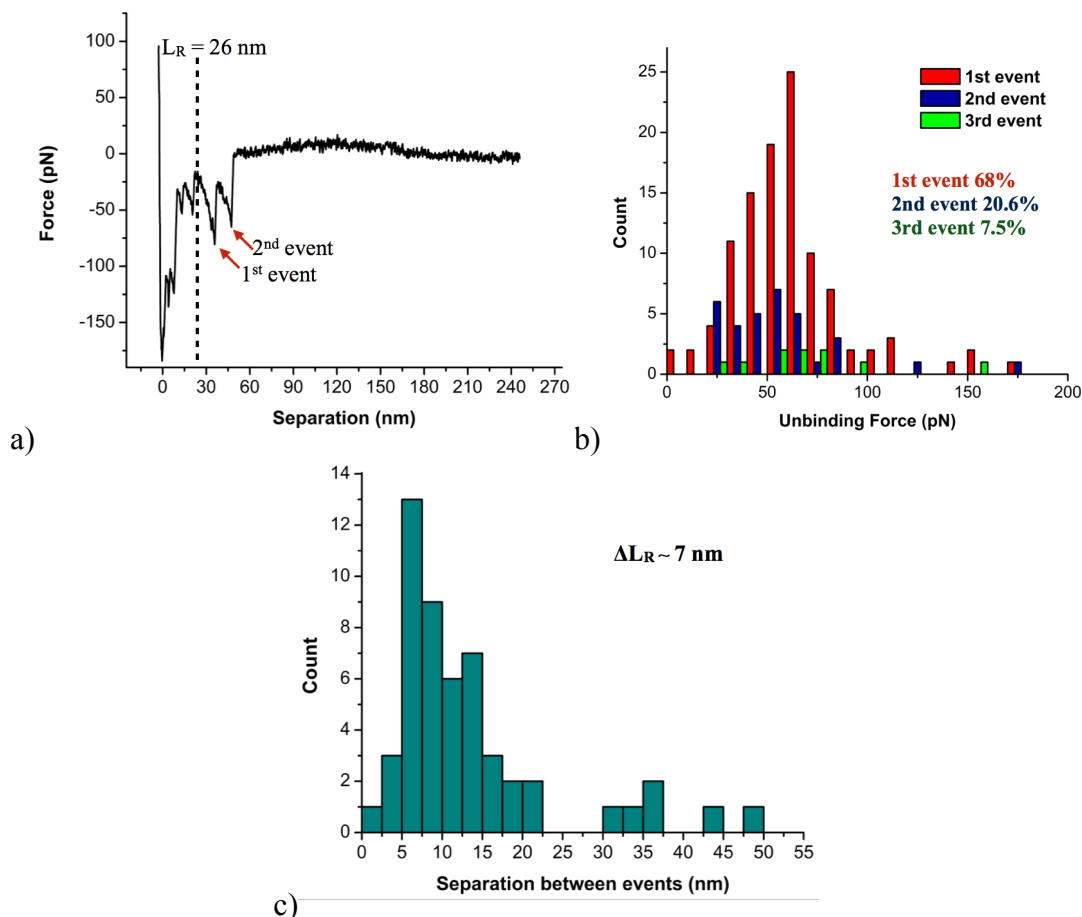
Figure 4.23: a) Typical force-distance curves obtained for the interaction LecA lectin-M3 glycocluster; data distribution of b) unbinding force of the multiple events recorded in the curves, and c) separation between two consecutive events of the same curve.

This can be explained by the fact that the interaction between the lectin and the glycocluster is multivalent. In fact, the lectin presents four CRDs and the glycocluster has four galactose residues. In particular, the interaction can be between one CRD of the lectin and one galactose residue of the glycocluster (Figure 4.24a), or between two or more lectin CRDs and two or more galactose residues of the glycocluster (Figure 4.24b). Also, it can be between two or more CRDs of two lectins and two or more galactose moieties, if two lectins happened to be close to the tip apex (Figure 4.24c). The first type of interaction described will lead to the formation of a single stretching event, while the other two can lead to the formation either of a single peak characterized by a stepwise rupture (rupture of bonds in series, one after the other) or a single peak that has a different shape due to the different number of bonds broken simultaneously (rupture of parallel bonds) [202], or multiple peaks [135]. This multiple bond behaviour is not easy to interpret due to the absence of a reliable way to establish the number of interacting molecules [205]. This is also

due to the fact that the unbinding is a stochastic event and the variation in the bond loading rate can determine the overlap of binding force distributions [205]. Also, parallel ruptures can happen with the same unbinding force of a single rupture if the intrinsic breakage and reformation rates are faster than the pulling rate [99]. Therefore, the unbinding force for breaking an individual bond is not reached by each parallel bond [99].
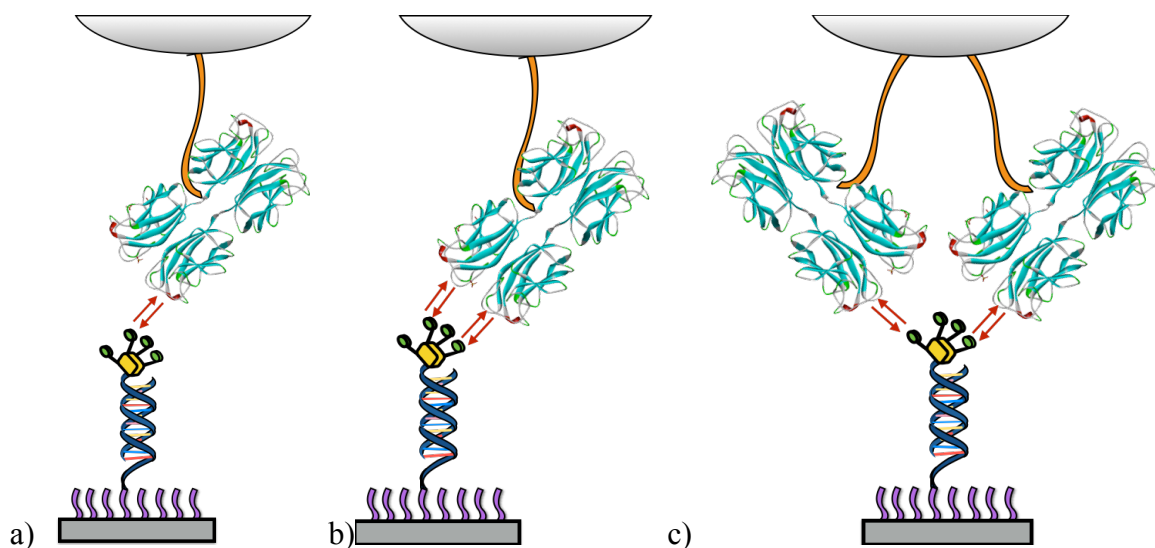
Figure 4.24: Sketch of the possible LecA lectin-glycocluster interactions, where red arrows represent the interaction.

In our case, the four residues of the glycoclusters can in principle interact with a CRD of one or more lectins, but the stoichiometry establishes the number of possible interactions that the glycocluster is able to form. For M3 glycocluster, even if the glycocluster is a tetrameric molecule, its stoichiometry is $n = 0.52$ (Table 4.1), therefore only two galactose residues can interact with the binding pockets of the lectins.

Moreover, due to the immobilization method of the glycocluster on the surface, all the four residues are exposed and, in principle, they can interact with a lectin-binding pocket. Also, it is highly probable that the lectin can interact with only one glycocluster at the time since, in an ideal situation, the distance between two glycoclusters immobilized on the surface is almost four times larger than the dimensions of the lectin ($D_{\text{glycocluster-glycocluster}} = 32$ nm vs. $l_{\text{LecA}} = 7$ nm) (Figure 4.6) [193]. Thus, multiple interactions can more likely happen between one glycocluster and the four CRDs of one (or two at most) tetrameric lectin(s).

Therefore, the high frequency of having one or two stretching events in the recorded curves seems consistent with the stoichiometry of the M3 glycocluster, which assumes a capability of binding up to two lectin monomers (Figure 4.23b). However, a high number of stretching events per curve (more than two) is likely due to the interaction of a second lectin, or most probably to a formation of a further bond, with a CRD of the same lectin, after the rupture of the first one. Also, the distance between consecutive rupture events is quite interesting since ΔL_R (Figure 4.23c) is comparable to the length of the lectin ($l = 7$ nm), therefore the events could be related to the interaction of two CRDs of the same lectin with two galactose residues of the same glycocluster. In principle, an

interaction with the two CRDs of the short side of the lectin should be expected, due to the small dimensions of the glycocluster.

Therefore, despite the complexity of the experimental setup and the drawback of having a huge non-specific interaction, it seems that "cluster effect" has been detected at the single molecule level, showing the capability of the glycocluster in binding the lectin.

4.4 Summary

In this Chapter, the results obtained from SMFS experiments were presented. The experiments were performed with the aim of studying the interaction between LecA lectin and different glycoclusters and investigating differences in the binding as a function of the affinity of the glycoclusters for the lectin, at the nanoscale. The experimental setup was chosen to ensure as much as possible the interaction between one single lectin and one glycocluster, to take advantage of the multivalency and study the cluster effect. For this, a complementary DNA strand, bearing the glycocluster, is used to hybridized the oligonucleotide grafted on the silanized surface, and consequently, immobilize the glycocluster to the support. The glycocluster is bound to the DNA strand by its core, thus the four branches are free to interact with the lectin. However, the immobilization of the glycocluster implies the presence of different molecules on the surface, i.e. the silane and the DNA, leading to a huge probability of non-specific interactions of the same order of magnitude than the specific interaction under study. For instance, for force curves recorded at $v = 100$ nm/s for M3 glycocluster, the frequency of having curves that do not show interaction events is 77%, while 16% of curves present non-specific events and only 7% are characterized by specific binding events. This is due to the fact that the probability of having specific interaction depends on the ratio between the density of the molecules grafted on the surface (ssDNA vs. hybridized DNA): for each glycocluster immobilized on the surface there are likely eight molecules of oligonucleotides, for a homogeneous distribution. Therefore, in our case, the expected frequency of specific interactions is lower than in a usual SMFS experiment, since our setup leads, in principle, to at most 12% of specific interactions, while the expected frequency of true unbinding events is commonly around 20% [11,136].

We tried to compare the unbinding of the lectin and three different glycoclusters (M1, M2 and M3). Data were obtained at a pulling velocity of $v = 1000$ nm/s and unfortunately only few curves presented specific unbinding events. In particular, only 0.5%, 1% and 0.5% of curves show LecA-glycocluster specific interactions for M1, M2 and M3 respectively. This low statistics does not allow making a reliable comparison between the behaviour of the three glycoclusters, thus no consistent considerations can be made.

Then, the LecA lectin-M3 glycocluster interaction was studied at different pulling speed to get inside on the dynamic of the interaction. In particular off-rate constant was extrapolated, showing a fast dissociation of the binding. This parameter is affected by the multivalent nature of the interaction. Both the lectin and the glycocluster are multivalent molecules and the probability of

having cluster effect is not negligible. For example, curves obtained for M3 glycocluster at pulling speed of v = 100 nm/s show multiple stretching events. These events present mostly the same unbinding force and can be mainly related to the interaction between one lectin CRD and one galactose residue of the glycocluster. Multiple events show a separation distance of the same order of the size of the lectin, demonstrating that two monomers of the same lectin can interact with two galactose residues of the same glycocluster, in accordance with the stoichiometry of the M3 molecule.

To further investigate the affinity and specificity of M3 glycocluster, Single Cell Spectroscopy experiments were performed. The anti-adhesive strength of M3 glycocluster was tested by studying the changes in the interaction between a single pulmonary human cell and PA bacteria. For this, a single cell was attached on a tipless cantilever while different strains of PA bacteria were adsorbed on a glass surface. To display the inhibition effect of the glycocluster, the adhesive interaction was measured before and after the addition of the glycocluster on the working solution. The results of this study will be presented in the next Chapter.

Chapter 5. Cell-bacteria Interaction to study the inhibition of LecA lectin via glycoclusters

L'AFM permet aussi dans son mode spectroscopie d'étudier l'adhésion cellulaire. Aussi, le Chapitre 5 est consacré à l'étude de l'interaction cellule-bactérie par des mesures de spectroscopie à cellule unique (SCFS). Plus particulièrement, les propriétés antiadhésives du meilleur glycomime (M3) ont été étudiées. Pour ce faire, une cellule unique a été fixée sur un levier AFM sans pointe tandis que différentes souches de bactéries PA ont été adsorbées sur une surface de verre. L'interaction cellule-bactéries a été mesurée avant et après ajout du glycomime dans la solution de travail. La technique AFM-SCFS permet de mimer l'environnement *in vivo* et ainsi de caractériser l'interaction entre bactéries et cellule épithéliale.

Nous avons extrait des courbes de forces, trois paramètres majeurs : la force maximale de détachement caractérisée par un pic, la position de ce pic par rapport au point de contact et le travail de détachement (aire sous la courbe). L'analyse de ces trois paramètres a permis de démontrer que l'ajout de 130 µM du glycomime conduit à un affaiblissement notable de l'adhésion bactérienne. Ce résultat valide totalement la démarche de notre projet. Nous avons poussé un peu plus l'analyse des courbes en prenant en compte les évènements discrets qui apparaissent en fin de détachement, des petits pics « step » caractéristiques de l'interaction intermoléculaire et des plateaux « tethers » caractéristiques d'un étirement de la membrane. Il a été observé une augmentation du nombre de steps et une diminution du nombre de tethers en présence du glycomime. Il semble possible que la présence du glycomime modifie l'hétérogénéité de la membrane et conduit à une rigidité membranaire. L'effet inhibiteur du glycomime est vérifié par le résultat négatif de l'étude cellule-bactérie mutante. Cette bactérie ne comprend pas de lectines LecA. Ce résultat confirme aussi la présence de la lectine sur la membrane externe des bactéries, en montrant clairement le rôle adhésif joué par LecA.

5.1 Introduction

In the previous Chapter (Chapter 4), LecA lectin-glycoclusters interaction has been studied by AFM-SMFS showing the affinity and multivalency of M3 glycocluster at the molecular level. In this Chapter the focus will be pointed out on the interaction at the single cell level. In particular, Single Cell Force Spectroscopy (SCFS) was applied to study the anti-adhesive capabilities of M3 glycocluster in a system that mimics the *in vivo* situation. For this, SCFS measurements were performed between one host cell immobilized on the AFM cantilever and a bacterial layer adsorbed on a glass surface. At this scale, single-molecule binding and cell-cell interaction can be studied without the need of labelling or purification [130,206].

5.2 Experimental Setup

5.2.1 The setup

These experiments were performed at the Institute of Physiology II in Münster (Germany) in collaboration with Prof. Hermann Schillers.

The experimental setup chosen for performing AFM-SCFS measurement is the one depicted in Figure 5.1. The cell was captured on an AFM tipless cantilever and the bacteria adsorbed on a solid glass support. In this way, the interaction between a single cell and different bacteria was studied. Also, by adding the glycocluster on the working solution, its inhibition effect could be studied.
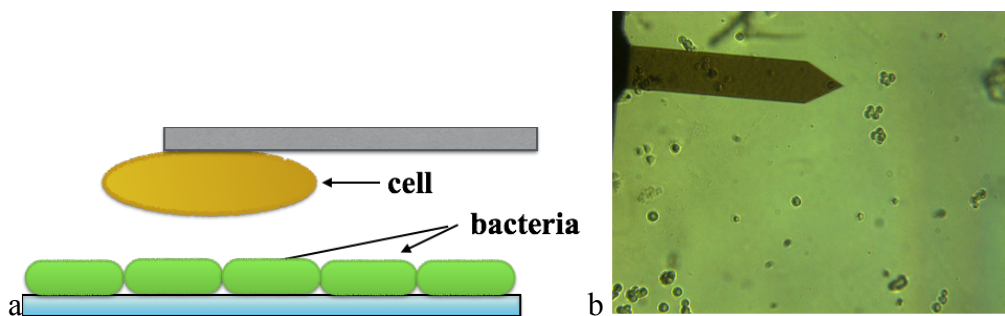
Figure 5.1: a) Schematic representation of the experimental setup, b) optical image of a single cell attached on the tipless cantilever.

Contrary to the majority of SCFS studies, which involve interactions between two eukaryotic cells [152], our experiments focused on cell-bacteria interactions. Also, only recently SCFS measurements were applied to study the anti-adhesive effect of a glycoconjugate against FimH from *Escherichia coli* bacteria [206].

The glycocluster chosen for SCFS measurements is the mannose-centred M3 (Man(EG$_2$MTzAcNPhGal)$_4$, section 1.4.1). This choice was motivated by its high affinity already established by ITC, DNA carbohydrate microarray technique and biofilm inhibition assay [22,71]. Also, the LecA lectin-M3 glycocluster interaction was investigated in Chapter 3 and Chapter 4 by

AFM imaging and SMFS, respectively. In this context, AFM-SCFS represents an interesting assay for qualitative and quantitative evaluations of the anti-adhesive properties against PA infection, bridging the gap between molecular studies and conventional *in vitro* studies.

The model cell line 16HBE14o⁻ (16HBE) was chosen to study the anti-adhesive effect of the glycocluster since it is the natural target of PA bacteria. Also, different bacterial strains of PA were used to characterize the role of LecA lectin in the interaction and the inhibition strength of the glycocluster: PAO1 bacteria, *lecA* and *pilA* mutants were used. PAO1 is a wild-type strain of PA bacteria that is largely employed in literature to study antibiotics against PA and also biofilm formation [6,71]. The two mutants are characterized by the inexpression of one particular gene that codifies the production of a specific protein. In particular, *lecA* mutant does not express LecA lectin, the target molecule of the glycocluster, while *pilA* mutant lacks in the production of PilA, a subunit of the pili type IV (section 1.1.2.1). Therefore, the absence of a particular unit could influence the general behaviour of the bacteria, hence the interaction with the host cell. PAO1 wild-type and *lecA* mutant were incubated with 130 μM of M3 glycocluster to test its anti-adhesive effect. Furthermore, the behaviour of the wild-type bacteria was compared to the ones of *lecA* and *pilA* mutants. A summary of the performed experiments is presented in Table 5.1.

Cell Line	Bacteria strain	Without Glycocluster	With Glycocluster
	PAO1	✔	✔
16HBE	*lecA* mutant	✔	✔
	pilA mutant	✔	✗

Table 5.1: Summary of the SCFS experiment performed.

5.2.2 Sample Preparation

5.2.2.1 Bacteria sample

PA strains, wild-type PAO1 (kindly provided by Pr. Reuben Ramphal, University of Florida Gainsville, FL, USA), *lecA* and *pilA* mutants (Two-Allele Library, PW5313, Pseudomonas Transposon Mutant Collection, UW Genome Sciences, Washington, USA) were grown in LB medium 24 h prior to investigation, since it was shown that *lecA* gene expression is enhanced in stationary phase [207].

A number of 10^9 cells of each culture was washed and suspended on Tris buffer (Tris(hydroxymethyl)aminomethane), HCl 10 mM, CaCl₂ 1 mM, pH 8. For AFM experiments, bacteria were incubated for 1 h for adsorption on a glass dish. Just before incubation, bacterial cells were treated with gentamicin (200 μg/mL final concentration) for safety reasons. The sample was washed twice with HEPES buffer (HEPES (4-(2-hydroxyethyl)-1-piperazine-ethanesulfonic acid) 5mM; NaCl 140mM; KCl 4mM; CaCl₂ 2 mM; MgCl₂ 1 mM; D-glucose 1 mM; pH 7.4) and 3 mL of the same buffer were added in order to perform AFM experiments at room temperature.

The effects of antibiotics belonging to the same family of gentamicin, after 18- 24 h incubation, are shown in literature [6,169]. In order to test the effects of the antibiotic in our experimental setup, we analysed the behaviour of wild-type PAO1 before and after 5 h incubation with gentamicin. The 5 h

lapse was chosen because single-cell experiments were carried in shorter time intervals (1 h incubation of bacteria on the solid substrate plus 1-2 h of AFM single-cell measurements). Before performing AFM experiments, we ran viability tests to check the bacterial integrity upon 5 h incubation with gentamicin. The results show that bacteria conserved their fluorescence even after incubation, which means that bacteria do not undergo lysis, thus cellular integrity was preserved. Also, identical bacterial mobility was detected before and after gentamicin treatment, meaning that the superficial constituents of the bacteria (pili, etc.) were intact. These results were further confirmed by filming bacterial activity before and after 5 h incubation. This second test was performed on PAK bacterial strain and two snapshot of the 5 min video are presented in Figure 5.2.

a) b)
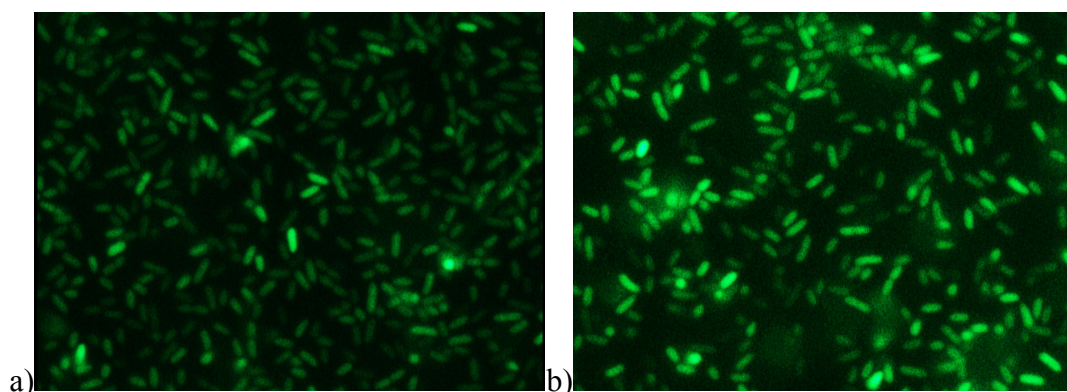
Figure 5.2: Snapshots of electron microscopy films of PAK bacteria performed a) before incubation with Gentamicin and b) after 5 h of incubation.

5.2.2.2 Cell Preparation

16HBE14o⁻ (16HBE) cell line was used to study the inhibition effect of glycocluster and its specificity. 16HBE cells are human bronchial epithelial cells, the natural target of PA bacteria.

The cell line is generated by the transformation of normal bronchial epithelial cells with SV40 large T-antigen [208]. The cells retain differentiated epithelial morphology by forming polarized layers with microvilli and cilia [209,210]. The human respiratory cell line was a gift from Dr. Dieter C. Gruenert (Cardiovascular Research Institute at the University of California, San Francisco, Calif., USA) [208]. Cells were grown in Eagle's Minimal Essential Medium (Invitrogen, Karlsruhe, Germany) and supplemented with 10% Foetal Bovine Serum (PAA Laboratories, Pasching, Austria), 2 mM L-glutamine, 50 U/ml penicillin and 50 µg/ml streptomycin in a 5% CO_2-95% air incubator at 37°C. The cell culture medium was changed three times per week.

Cell cultures were suspended in HEPES buffer before being immobilized on the cantilever and for each experiment a fresh culture dish was used. After removing the supernatant, the dish was washed once with 2 mL EDTA buffer (Ethylenediaminetetraacetic acid). Then, 2 mL of EDTA buffer were added and the dish was incubated at 37 ºC for almost 10-15 min to allow the detachment and separation of the cells. For cell detachment, we used EDTA instead of trypsin, since EDTA perturbs divalent ions of the cell such as calcium and magnesium, while trypsin cleaves proteoglycans that contribute to cell adhesion. Therefore, using trypsin contributes to stickier cells that need a longer time of recovery [211]. Thus, cell detachment is less invasive with EDTA and it was preferred in

our case. Once the cells were detached from the dish, they were suspended and centrifuged at 140 g for 5 min, leading to the formation of a pellet (cells precipitate on the bottom of the flask). Next, the supernatant was removed and the pellet was washed and finally suspended in 1 mL HEPES buffer. The cells were stored on ice until use.

5.2.2.3 Glycocluster

The glycocluster selected for inhibition assay is M3 (section 1.4.1). Briefly, M3 is characterized by a core mannose, which determines the globular form of the final molecule, and four semi-flexible branches. The branches are made by two linkers, L1 and L2, separated by a triazole molecule. In the case of M3 glycocluster, the linker L1 is characterized by a flexible diethyleneglycol group that allows the free movement of the branch, and the orientation of the galactose residue to ease the entry on the CRD of the lectin. The second linker L2 consists of an aromatic group (Ph), situated close to the galactose moiety. It enables increasing the affinity to the lectin due to the formation of a $\pi\pi$ interaction between the Ph motif and the His50 close to the CRD of the lectin. The glycocluster was chosen for its higher affinity for LecA lectin, since it has a dissociation constant of $K_d = 157$ nM [22].

5.2.3 AFM measurements and force curve treatment

5.2.3.1 Data acquisition and analysis

Data were acquired with CellHesion AFM from JPK, with a z-piezo of 100 μm (Figure 5.3). Measurements were performed in HEPES buffer at room temperature. Tipless cantilever (Arrow TL (NanoAndMore, Wezlar, Germany) with a nominal spring constant of $k = 0.03$ N/m were incubated for 30 min with 13 μL of Cell-Tak™ [212] and immediately after mounted on the AFM. The probe was then calibrated by using thermal noise method (section 2.2.1.1) [87]. A single cell was picked up by the sticky cantilever while performing a force-distance curve with a probe-cell contact of 6 s. Once the cell was firmly attached to the cantilever apex, force-distance curve cycles were performed on the bacterial layer (Figure 5.1). The curves were acquired using the following settings: an applied force of 1 nN, a ramp size of 80 μm, a pulling speed of 5 μm/s, a contact time of 1.0 s and a sample rate of 2048 Hz. The contact time was chosen to be enough long to let the cell interact with the bacteria, but not enough long to have a non-reversible interaction. Each curve was taken on a different spot and for each set of conditions an average of 20 curves were acquired per experiment.
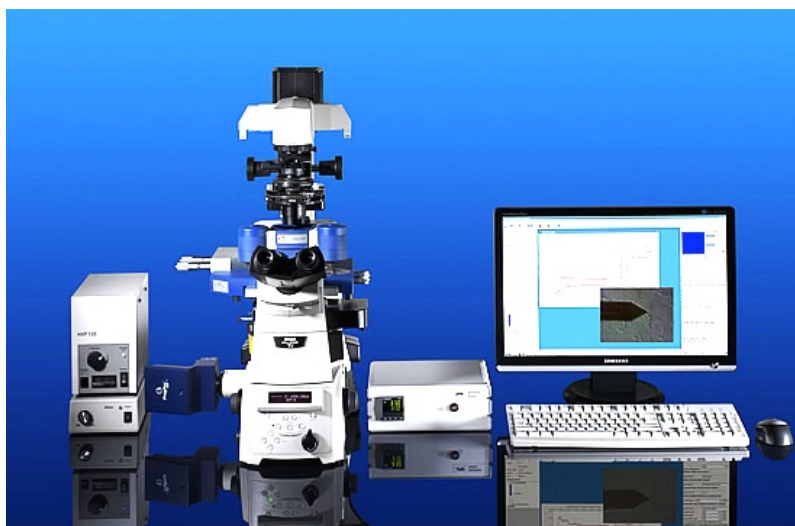
Figure 5.3: CellHesion setup. Image taken from http://usa.jpk.com/zoom-cellhesion-r-200-setup-on-nikon-eclipse-ti.589.us.html.

Force-distance curves were analysed by JPKSPM Data Processing software that allows smoothing (all the curves undergo a Gaussian smoothing with a smoothing width of 10) and correcting (represent force *vs*. tip-sample separation, correct the tilt, find the contact point, etc.) the raw curves. The important parameters (Figure 5.4) such as the **detachment work** (W_D), the **detachment force** (F_D) and the **peak position** (P_P) were extracted from the curves (section 2.6.2.1) [150].

Statistical analysis was performed to appreciate differences between different populations. The necessity of using statistical tests arises from the fact that the state of the cell, the way in which it adheres to the cantilever and other factors can influence the cell-bacteria interaction and therefore increase the variability of results [149]. That's also why experiments were performed in a comparative way: the parameters under study were obtained by comparing the behaviour of the same cell before and after incubation with the glycocluster. After the analysis of individual experiments, data were combined together to obtain median values and to identify a general behaviour of the system. Data did not seem to follow a normal distribution and the history of the interaction did not affect systematically curves taken repeatedly or taken before and after incubation with the glycocluster. Thus, it can be assumed that force curves are independent one from each other. Therefore, nonparametric test for unpaired data were applied to study the distributions differences. In particular, Mann-Whitney *U* tests [213] were performed with a confidence level of 99% by using Prism Software (GraphPad InStat, GraphPad, La Jolla, USA). Mean, standard error of the mean (SEM), expressed as the ratio between the standard deviation and the square root of the size of the population, and *p*-values were obtained. Further, analysis of discrete events (**step** and **tethers** events) was done with PUNIAS (Protein Unfolding and Nano-Indentation Analysis Software, http://punias.free.fr/) [194,214].
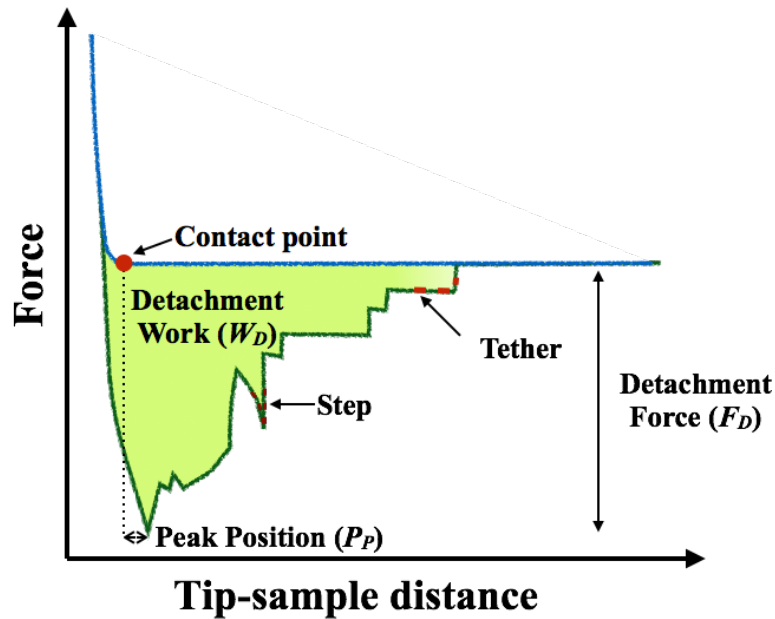
Figure 5.4: Sketch of a force-distance curve presenting the parameters analyzed.

5.2.3.2 Mann-Whitney *U* test

The Mann-Whitney *U* test is used to test the null hypothesis (H_0) between two independent sample populations when the assumptions of parametric and normal distributions are not fulfilled [213]. Therefore, it represents the nonparametric version of the Student-*t* test (Annex III).

Nonparametric tests are a class of statistical analyses that are used when one or more of the requirements of parametric statistics are not satisfied. For example [215]:

i)   Assumptions on the shape of data distribution are not made (distribution-free), i.e. data are not normally distributed;

ii)   The observations are dependent one from the other;

iii)   The sample size is not sufficiently large ($n > 20$-30).

When performing a statistical test, a statement hypothesis is made. The hypothesis represents the condition that the data distribution has to satisfy. In particular, the null hypothesis (H_0) assumes that differences do not exist between the populations under study. This means that the two distributions have to be identical to fulfil the null hypothesis.

To perform the test, the populations have to be ranked. The ranking of data values implies sorting the data in ascending order and attributing to each value in the list a number from 1 to *n*, for comparison. For example, the first value (the smallest one) will receive a rank of 1, the second of 2 and so on. Then, the ranks of the two populations are combined. If the ranks of the two populations are randomly mixed, then the two distributions are not different. While, if their ranks are grouped at the opposites extremities of the ranking, then the two distributions are significantly different [213]. Therefore, the test compares the ranks of the distributions, not mean values. The null hypothesis is satisfied when there is no significant evidence that the rank of one distribution is higher or lower

than the one of the other: the two populations have mixed ranks [213]. To better clarify the concept, an example of the test is given in Annex III.

A level of risk (or level of significance) is defined as the probability that any observed statistical difference will be real and not due to chance [213]. The level of risk is given by the p-value. In general, p-value is settled to $p = 0.05$ which means that the confidence interval of having real statistical differences not related to chance is of 95%. In the experiments presented here, p-value was chosen to be equal to $p = 0.01$ to set the confidence interval to 99%. Thus, the statistical significance has been defined as $p < 0.1$ (*), $p < 0.01$ (**) and $p < 0.001$ (***).

5.3 Results and Discussion

SCFS experiments were performed to study the anti-adhesive properties of M3 glycocluster at the single-cell level. In our experimental setup, the cell was captured on a tipless cantilever and PA bacteria immobilized on a solid support, as shown in Figure 5.1. Series of force-distance curves were acquired at different spots of the bacterial layer. Important parameters, such as detachment work (W_D), detachment force (F_D) and changes in peak position (P_P) were analysed to establish the inhibition effect of M3 glycocluster against PA bacteria (Figure 5.4).

5.3.1 16HBE cell against PAO1 wild-type and *lecA* mutant

Firstly, the adhesive interaction of 16HBE cells against PAO1 wild-type was compared with the interaction between 16HBE cell and *lecA* mutant. 16HBE cells were let separately interact with both PAO1 wild-type and *lecA* mutant. Five different 16HBE cells were tested against PAO1 and four against *lecA* mutant.

The two strains interact differently with 16HBE cells: wild-type PAO1 bacteria present stronger adhesion to the cell than *lecA* mutant. The median values $\pm$ SEM obtained for the two strains are: $W_D = 4.14 \pm 0.55$ fJ and $F_D = 0.67 \pm 0.09$ nN for PAO1 bacteria, while $W_D = 2.32 \pm 0.64$ fJ and $F_D = 0.40 \pm 0.08$ nN for *lecA* mutant, which correspond to a decrease in detachment work of almost 44% and of 40% in detachment force. Also, statistical analysis shows a significant difference between the two distributions, ($p = 0.0003$ for W_D and $p < 0.0001$ for F_D Figure 5.5a and b), meaning that the two bacterial strains behave differently. The peak position was also statistically analysed and no significant differences were obtained between the two populations (Figure 5.5c). Thus, detachment happens mostly at the same distance for both bacterial strains. The results are summarized in Table 5.2.
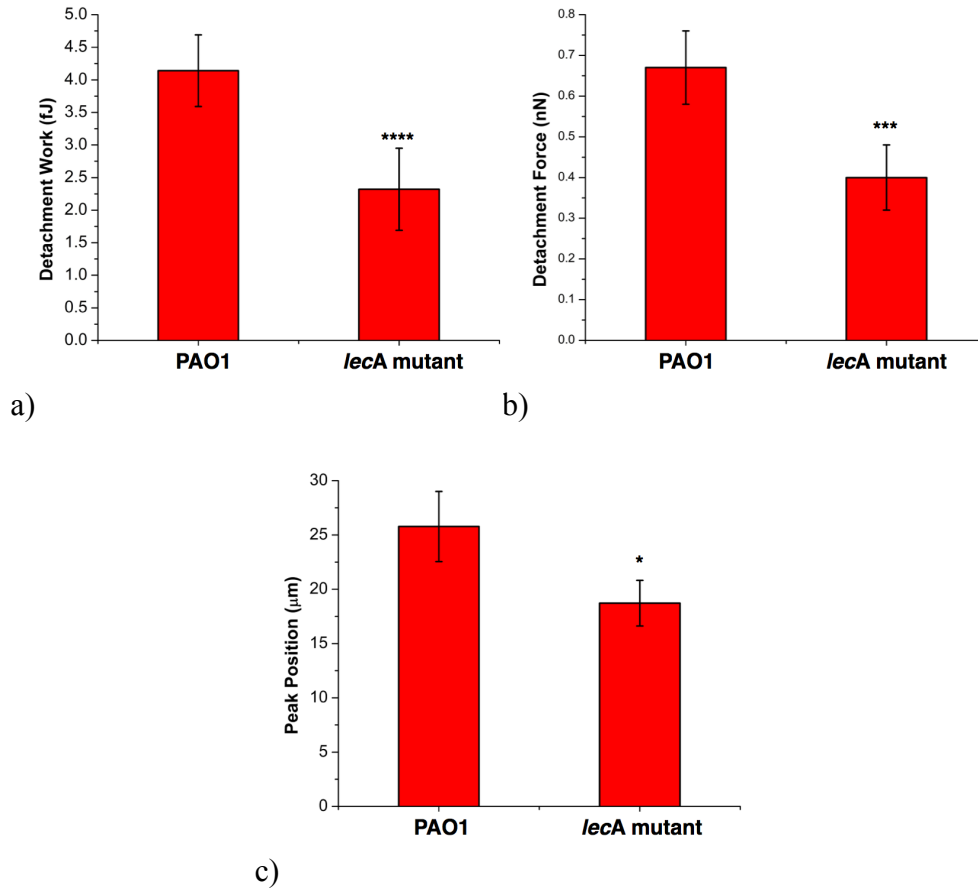
*Figure 5.5: Data distribution of a) detachment work b) detachment force obtained and d) peak position for 16HBE cells against PAO1 wild-type and lecA mutant. Median values and SEM are represented. p-values are * p < 0.1, *** p < 0.001 and **** p < 0.0001.*

	PAO1	*lec*A mutant
Nr. of curves	98	112
W_D **[fJ]**	4.14 ± 0.55	2.32 ± 0.64
F_D **[nN]**	0.67 ± 0.09	0.40 ± 0.08
P_P **[µm]**	26 ± 3	19 ± 2

Table 5.2: Results obtained for the interaction between 16HBE cell against PAO1 wild-type and lecA mutant, respectively. Values are expresses as Median ± SEM.

The two bacterial strains mainly differ for the expression of LecA lectin. The lectin is present for 95% in the bacterial cytoplasm and in small percentage (5%) in the bacterial outer membrane [46,207]. The different adhesive power of the two bacterial strains can be attributed to the presence or absence of the lectin, which could affects the whole bacterial properties. Probably, the non-production of membrane and cytoplasmic LecA lectin influences the expression of some of the other structures present on the membrane, as well as their disposition on the envelope. This could originate a different heterogeneity in the composition of the bacterial membrane. Due to that, the mechanical properties of the wild-type and the mutant would not be necessary the same. Consequently, electrostatic charge and surface roughness might be no longer similar [216]. In fact,

the intracellular variability happens to be as important as cell-to-cell variability [171], in particular for adhesion properties. Only recently, it has been accepted that bacterial heterogeneity plays an important role on the enhancement of the adhesion strength, but very few studies have tried to represent that [216]. In the case of *Pseudomonas* bacteria, it has been already shown the influence of heterogeneity in adhesion properties. In particular, the heterogeneity in polysaccharides (EPS and LPS) on the bacterial surface affects the adhesive power both at the bacterium level and across population [171].

To summarize, our results show the existence of a different behaviour between PAO1 wild-type and *lecA* mutant. This difference can be attributed to the expression or not of the lectin LecA, which plays the role of adhesins. In fact, its expression leads to an increasing of W_D and F_D, meaning that the presence of the lectin LecA contributes to the adhesion of the bacteria to the host cell. On the contrary, the absence of the lectin could determine a different heterogeneity of the bacterial membrane and affect the adhesion properties of the mutant, comparably to what has been shown in literature for EPS and LPS structures [171].

5.3.2 16HBE cell against PAO1 wild-type with and without M3 glycocluster

5.3.2.1 The anti-adhesive effect of M3 glycocluster on PAO1 wild-type

The anti-adhesive effect of M3 glycocluster was tested for five different 16HBE cells against PAO1 bacteria. The cell-probe was repeatedly approached to the sample and a series of force-distance curves was acquired in different spots of the sample. Then, the glycocluster was introduced in the liquid cell and let interact with the bacteria on the surface. Next, another series of force-distance curves was acquired to estimate the changes in cell-bacteria interaction due to the presence of the glycocluster. Mainly, the choice of the concentration was made by taking into account the microbial charge (10^6 CFU per mL) and previous biofilm inhibition assays, which showed the concentration-dependent anti-adhesive effect of the glycocluster [71]. Also, preliminary tests, made at concentration of 60 μM of glycocluster, did not show any change in the adhesion upon the addition of M3. Therefore, a concentration of 130 μM of glycocluster was selected to highlight any possible difference on the adhesive properties due to the presence of the glycocluster.
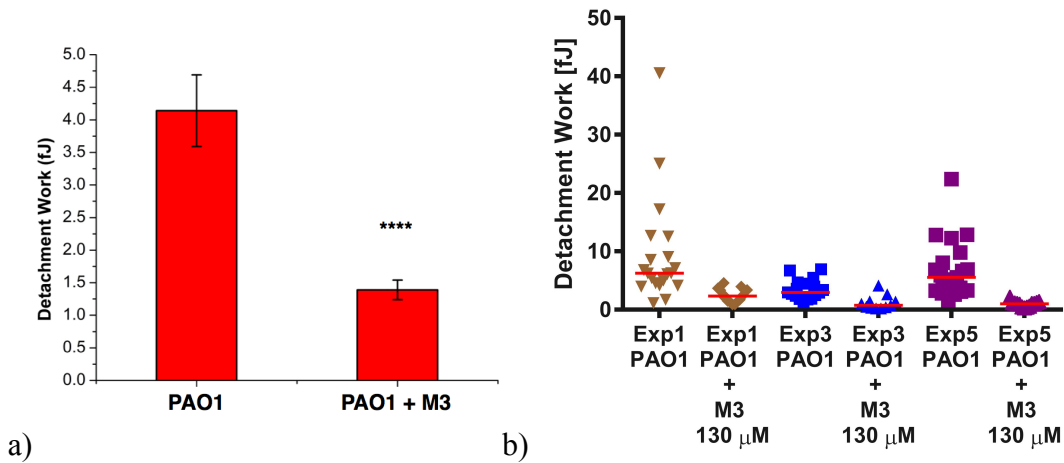
*Figure 5.6: a) Data distribution of W_D obtained for 16HBE vs. PAO1 wild-type with and without M3. Median ± SEM are presented. p-values: **** p < 0.0001. b) Detachment work with and without M3. Data from three different experiments are presented. Median is represented as red bar.*

In Figure 5.6 are presented the results obtained, before and after the addition of M3, for the detachment work (W_D). Basically, the presence of M3 induces a huge decrease of the median value of W_D upon incubation with 130 µM of M3 glycocluster: it changes from 4.14 ± 0.55 fJ (without glycocluster) to 1.39 ± 0.15 fJ (upon addition of 130 µM glycocluster), leading to a decrease of 66% upon the addition of M3. This behaviour is identified for each individual experiment (Figure 5.6b), even though the median values obtained for each experiment differ one from the other due to biological variability.

A similar response is obtained for the detachment force (F_D) even if it is less marked: upon the addition of 130 µM of M3 the median value of the F_D shifts from 0.67 ± 0.09 nN to 0.53 ± 0.06 nN (Figure 5.7a), leading to a decrease of 21%. Also for this parameter, the tendency is identified in each individual experiment (Figure 5.7b), showing a decrease in detachment force upon the addition of 130 µM of M3. Changes were also detected in the peak position (P_P) parameter, before and after addition of M3 glycocluster (Figure 5.7). In particular, the median P_P decreases from 26 ± 3 µm to 11 ± 2 µm at 130 µM of M3. Similarly, the behaviour is well respected in each single experiment, showing the influence of the lectin in the cell-bacteria interaction. All the data presented are summarized in Table 5.3.
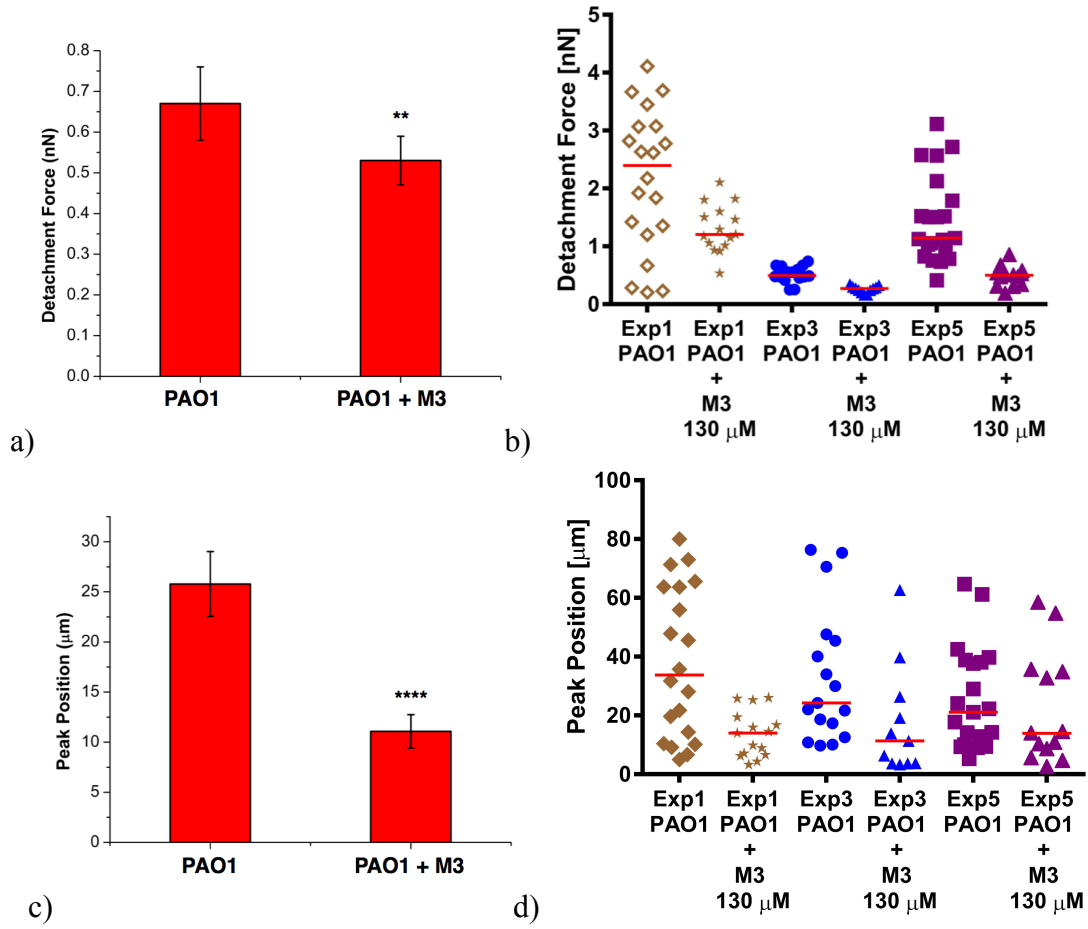
Figure 5.7: a) Data distribution of F_D obtained for 16HBE vs. PAO1 wild-type with and without M3. Median ± SEM are presented. b) Detachment force with and without M3. Data from three different experiments are presented. Median is represented as red bar. c) Data distribution of P_P obtained for 16HBE vs. PAO1 wild-type with and without M3. Median ± SEM are presented. d) Detachment work with and without M3. Data from three different experiments are presented. Median is represented as red bar. p-values are: ** p < 0.01 and **** p < 0.0001.

	PAO1	PAO1 + 130 μM M3
Nr. of curves	98	96
W_D **[fJ]**	4.14 ± 0.55	1.39 ± 0.15
F_D **[nN]**	0.67 ± 0.09	0.53 ± 0.06
P_P **[μm]**	26 ± 3	11 ± 2

Table 5.3: Results obtained for the interaction between 16HBE cell and PAO1 bacteria at different concentration. Values are expresses as Median ± SEM.

As described in section 2.6.2.1, W_D, F_D and P_P parameters can describe the strength of cell-bacteria interaction. Thus, lower values of W_D, F_D and P_P are representative of a reduction of the bacterial adhesion. The reduction of these parameters stands for an easier detachment of the bacteria from the cell upon the addition of the glycocluster. Therefore, these results show that the glycocluster interaction with LecA lectin induces a global reduction of the cell-bacteria binding. It seems that upon incubation, the lectins present on the bacteria are less able to bind the Gb3 epitopes of the host

cell due to the competition with the glycocluster in solution. Due to the high affinity of the glycocluster, the binding between the galactose residues, present on the epithelial cell, are less favoured with respect of the interaction with the glycocluster. In addition, the change in peak position (P_P) is an interesting result since it is associate to the cell-bacteria detachment [130]: for PAO1 wild-type the detachment happens at a distance roughly twice that for PAO1 upon the addition of M3. This means that it is easier to detach the cell from the bacterial layer in presence of the glycocluster. The change of peak position can be explained by different type of interactions, as described in section 2.6.2.1 and in the reference [150]. In our case, the binding between the LecA lectin and the glycocluster probably makes the bacterial membrane more rigid and blocks micro-extension associated bindings where LecA might be located.

5.3.2.2 Analysis of the discrete events

We decided to analyse the discrete events (step and tethers events) that contribute to the detachment. As previously described in section 2.6.2.1, the parameters analysed for step events are: the **step height**, the **frequency**, the **step position** and the **average number of step per curve**. While for tethers events the parameters are the **tethers height**, the **frequency**, the **tethers length** and the **average number of tethers per curve**. By comparing step and tether events in presence and absence of M3 glycocluster, it would be possible to find some characteristic features of the binding that may give some insides on the role of LecA lectin in the interaction [7].

The comparison of the curves, before and after the addition of the glycocluster, shows that the most striking differences are:

> *i)* The decrease of the frequency for tether events;
> *ii)* The increase of step events frequency.

The frequency of tether events moves from 74% in absence of glycocluster to 52% when bacteria are incubated with M3 glycocluster. Also, the probability of having more than one tether event within the same curve varies: without M3 multiple tether events are more likely than in presence of the inhibitor. In particular, the average number of tether per curves decreases from 2.0 ± 0.6 without glycocluster to 1.2 ± 0.3 upon the addition of M3. Since only the last force plateau, the one to the zero level, is representative of the trues height and length of the tethers [149], only these last events were considered to construct the histograms of Figure 5.8a and b. In fact, the formation and rupture of a tether depend on the mechanics of the membrane and most of the time the tether events are not related to the interaction of a single receptor-ligand couple but to the formation of many bonds [149]. Thus, only the last tether is a measure of the true force height. In our case, it seems that the tethers height increases upon the addition of M3 (Figure 5.8a). The range in which the tether height varies is consistent with previously published results [153,206], while the tethers length varies mostly between 8 μm and 14 μm, both in presence and absence of M3 glycocluster (Figure 5.8b).

Contrary to tethers, step events are more frequent upon glycocluster addition (34% without and 52% with M3). The distribution of step height is more dispersed for PAO1 incubated with the glycocluster with respect to the wild-type (Figure 5.8c). In addition, these events appear mostly at

short step position (below 5 μm) (Figure 5.8d). All these differences lead to a clear change in the shape of the curves before and after the incubation with the glycocluster (Figure 5.8e and f).
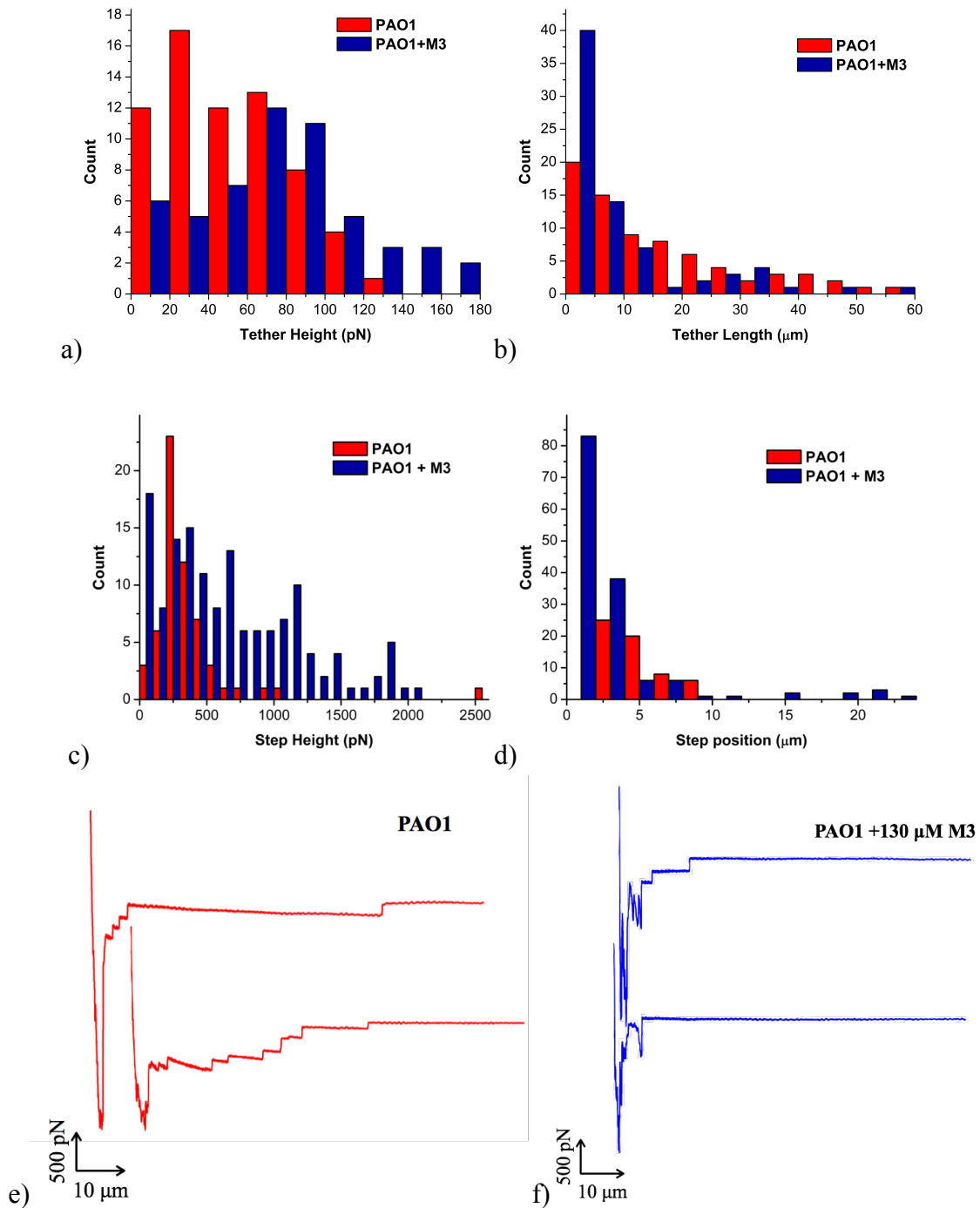
Figure 5.8: Histograms of tether a) height and b) length for 16HBE cells vs. PAO1 with and without M3. Histograms of step events c) height and d) position for 16HBE cells vs. PAO1 with and without M3. Typical force vs. distance curves recorded for e) 16HBE cell vs. PAO1 and f) 16HBE cell vs. PAO1+M3.

Modifications at the receptor level can regulate cell adhesion by [148]:

i)   Changing the number of binding site,
ii)   Controlling the mechanical force of adhesive interaction,
iii)   Regulating the load sharing and cooperativity of adhesive interactions.

In our case, the inhibition of LecA lectin could determine a reduction of the number of binding sites and a consequent modification of membrane heterogeneities. The frequency of tether events decreases as well as the average number of tethers per curve, probably contributing to an easiest tethers fusion [153]. On the contrary, the average number of step events per curve, as well as the step frequency, increases upon the addition of the glycocluster. This might suggest a competition of the two types of events related to a change in the receptor cortex anchoring strength (Figure 5.9) [148]. Probably, the bacterial membrane becomes more rigid upon the LecA lectin-glycocluster binding, facilitating the receptor-ligand interaction while the tether formation becomes unfavourable due to a possible stiffening of the membrane.
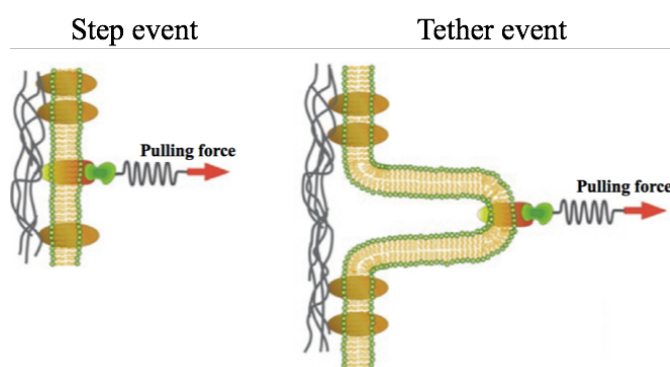
Figure 5.9: Sketch of pulling events. Adapted from [148].

Due to the presence of the glycocluster, the lectin-galactose interaction is weakened. Thus, the adhesive properties of the bacteria and the adhesive efficiency are no longer the same. Consequently, the cell adhesion has to be ensured by other virulence factors. It has been shown that, depending on the infection state of PA bacteria on pulmonary host cells, different virulence factors are expressed increasing the ability of the bacteria to infect cells [217]. Since the bacteria used in these experiments were maintained in phase state before adsorption on the glass support, it is reasonable to think that LecA lectin was highly expressed [207]. For this reason and for the specificity of the glycocluster [71], the obtained decrease of adhesive strengths can be mainly associated with the inhibition of LecA lectin via M3 glycocluster. The decreasing of interaction parameters upon the addition of the glycocluster demonstrates the role played by LecA lectin in the adhesion process: the lectin can be found in the outer membrane of the bacteria and it is an adhesin.

5.3.2.3 16HBE cell against PAO1 wild-type upon incubation with M3 glycocluster and *lecA* mutant

The behaviour of PAO1 wild-type bacteria upon the addition of 130 μM M3 glycocluster was compared to the one of *lecA* mutant. In particular, if the glycocluster specifically targets LecA

lectin, then the adhesion parameters obtained for PAO1 wild-type incubated with M3 should be closer to the ones obtained for *lecA* mutant than to the ones of the wild-type before addition of M3.

Figure 5.10a shows a lower detachment work for the wild-type bacteria incubated with the glycocluster than for the *lecA* mutant. Thus, the LecA lectin-glycocluster binding seems to be more efficient in decreasing the detachment work than the absence of LecA lectin (*lecA* mutant). On the contrary, not so different values were found for the detachment force of the two systems (Figure 5.10b, $p = 0.0186$), proving that somehow the glycocluster influences the cell-bacteria interaction by inhibiting the lectin. Thus, it seems that the F_D parameter can better show the influence of the lectin on the binding, since it refers to more localized features of the binding and it depends on physicochemical properties, surface components [218] and to the shape and deformation of the cell [148]; while W_D is a global parameter that reflects all the stretching events occurring between the cell and the bacterial membrane that lead to the complete disruption of the contact.
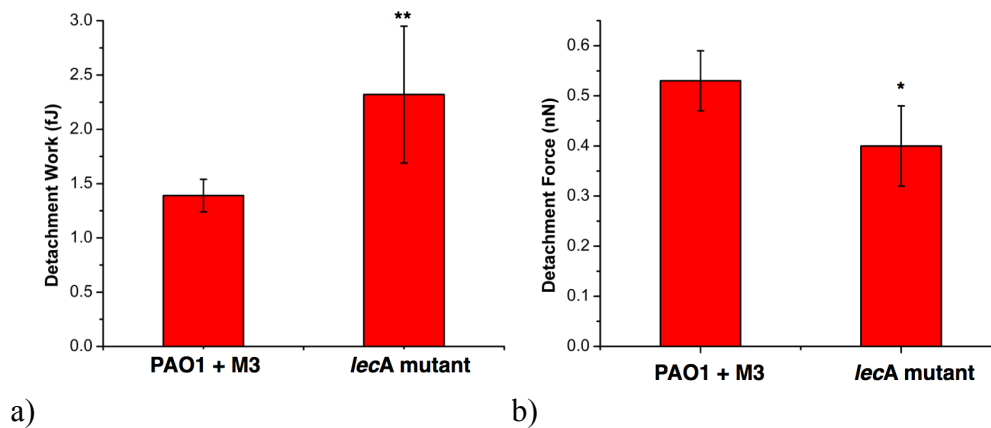
*Figure 5.10: Data distribution of a) detachment work b) detachment force obtained for 16HBE cells against PAO1 upon incubation with M3 and lecA mutant. Median values and SEM are represented. p-values are: * p < 0.1 and ** p < 0.01.*

5.3.3 Comparison with the mutants

5.3.3.1 *lecA* mutant incubated with M3 glycocluster

SCFS experiments were also carried out between 16HBE cells and *lecA* mutant in presence of M3 glycocluster. The *lecA* mutant is devoid of LecA lectin production; therefore no significant inhibition effect is expected after the incubation of the *lec*A mutant with the glycocluster. Thus, comparative experiments were performed. The detachment work, the detachment force and the peak position were compared in order to locate differences in the behaviour of *lecA* mutant before and after the addition of M3 glycocluster. Unfortunately, only two experiments were done and they did not give the same results (Figure 5.11). One of the two assays (Exp.1 in the graphs) shows the expected results: no differences in the detachment work, detachment force and peak position were detected upon the addition of the glycocluster ($p = 0.1481$ for W_D, $p = 0.4401$ for F_D and $p = 0.0216$ for P_P; not significantly different). But, the other experiment (Exp.2 in the graphs) shows a significant decrease of detachment work (89%) and force (42%) after incubation of M3, as well as

for the peak position (55%), and statistical analysis confirms the existence of a significant difference between the two distributions ($p < 0.0001$ for W_D, $p = 0.0005$ for F_D and $p < 0.0001$ for P_P; significantly different).
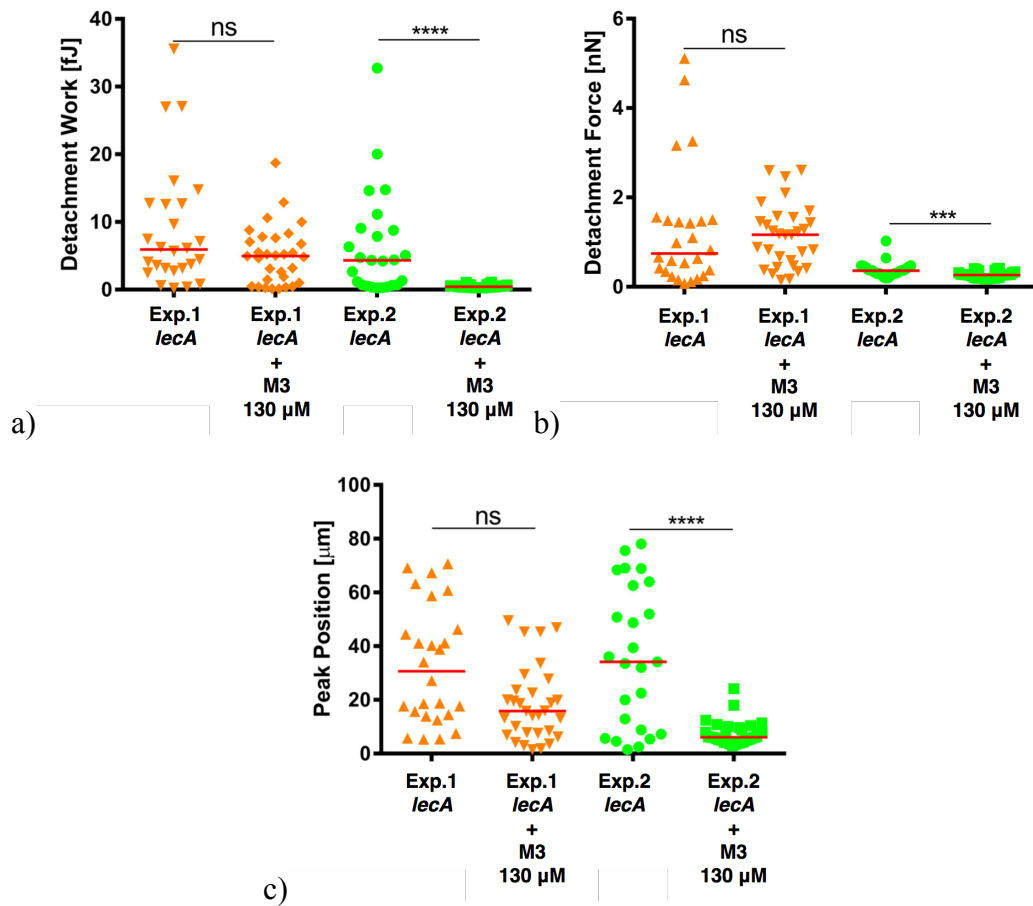
Figure 5.11: a) Detachment work and b) detachment force and c) peak position for 16HBE vs. lecA mutant with and without M3. Data from two different experiments are presented. Median is represented as red bar, p values are: ns not significant difference, *** p < 0.001 and **** p < 0.0001.

Thus, we will draw some considerations on the two experiments separately, to do not exclude the two possible situations from the analysis. Clearly, further experiments would be needed to understand the general behaviour. Probably, such difference is due to cell and bacteria variability. The results obtained for Exp.1 show no significant differences in the behaviour of *lecA* mutant before and after the addition of the glycocluster. This would mean that when the lectin is not expressed, the presence of the glycocluster does not modify the whole adhesive properties of the mutant. On the contrary, the variation of detachment parameters, as in the case of Exp.2, indicates that the glycocluster can probably interact with other carbohydrate-binding proteins of the cell-bacteria system. This would also explain the result obtained for the detachment work from the comparison between the wild-type upon the addition of the glycocluster and the *lecA* mutant (Figure 5.10a). In fact, the lower W_D obtained for PAO1 bacteria in presence of M3 could be due to the fact that M3 not only inhibits the lectin LecA but also other receptors that recognize the galactose residues. Furthermore, this result is in accordance with previous findings obtained for cell adhesion assays where C1 glycocluster has been used as anti-adhesive compound [24]. In the study,

the mutant devoid of LecA lectin showed a residual adhesion suggesting that the glycocluster may interact with other proteins that recognize galactose moieties. Therefore, even though the two results are quite different, both can be explained and justified. Thus, further experiments should be performed to determine which result is the most significant and can explain the general behaviour of the system.

5.3.3.2 *pilA* mutant

To study the behaviour of different stains against the same cell line, the interactions between 16HBE cells *vs*. PAO1, and *pilA* mutant were compared. *pilA* mutants are devoid of the production of the pilin PilA, which is the main constituent of pili type IV. Thus, this mutant should not present pili type IV, but only pili type Cup (section 1.1.2.1). In principle, pili type IV should be involved in long-range interactions [7], therefore its absence should modify the interaction at the whole cell level. Two different 16HBE cells were tested against *pil*A mutant ($N = 60$ curves) and interestingly, not significant differences between the behaviour of the wild-type and the one of the *pilA* mutant were shown by statistical analysis (Figure 5.12).

a)   b)

c)
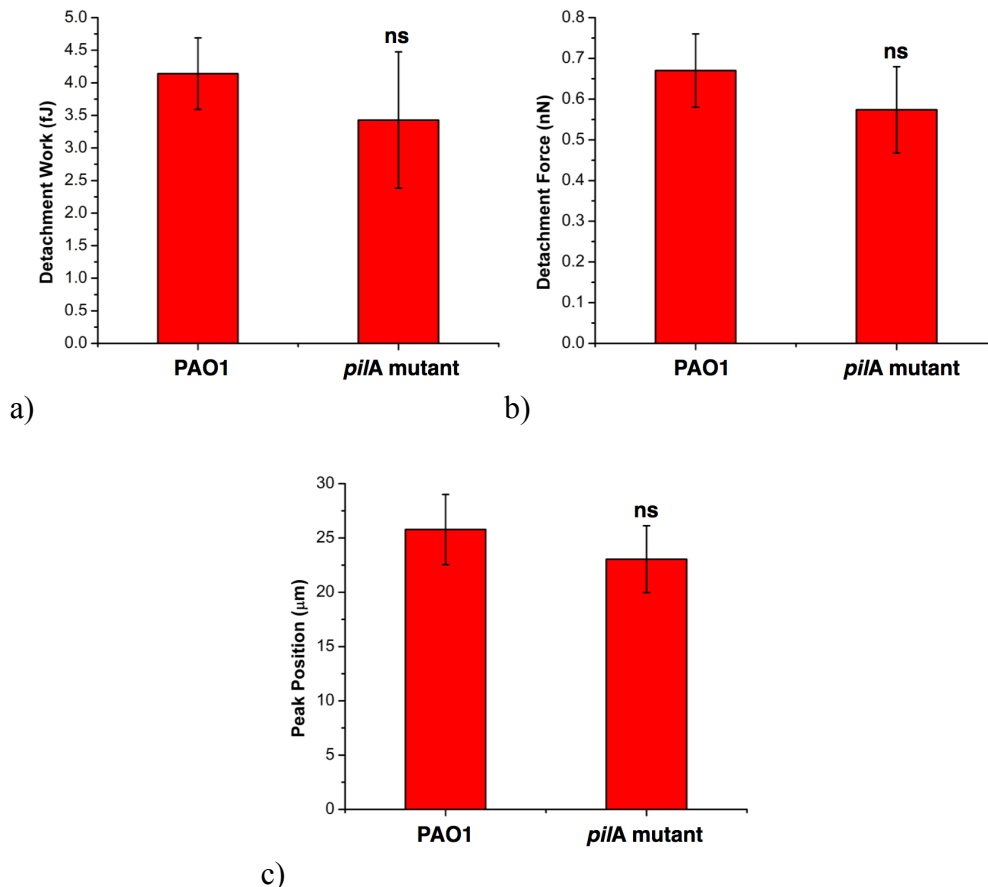
Figure 5.12: Data distribution of a) detachment work, b) detachment force and c) peak position of the interaction between 16HBE cells against PAO1 wild-type and pilA mutant. Median values and SEM are represented. p-values obtained are: ns not significant difference.

The result is quite surprisingly since, as in the case of *lecA* mutant (Figure 5.5), a difference in the adhesion properties is expected. In fact, the absence of the pili may induce a modification of the

aspect of the outer membrane, thus change the heterogeneity and the mechanical properties of the bacteria. Therefore, the *pilA* mutant should, in principle, interact differently compared to PAO1 wild-type due to a different structural envelope. Even though the obtained results was not expected, it is in accordance with what found by Beaussart et al. [7]. Probably a shorter contact time would have helped to discriminate the role played by the pili. In fact, Beaussart et al. have shown via SCFS that pili type IV from PA bacteria can interact with hydrophilic substrates for short contact time of 100 ms [7]. Probably, in our case the long contact time does not allow investigating the interaction of the pili since they probably detach before the cell is pulled away. Thus, changing the settings parameters could help in better understanding the interaction.

5.4 Summary

In this Chapter, the previously observed capabilities of M3 glycoclusters [71] as new therapeutic approach to inhibit bacterial activity by targeting LecA lectin have been demonstrated. In particular, AFM-SCFS technique made possible to mimic the *in vivo* environment and characterize the interaction between PAO1 bacteria and epithelial cells. The modification in global parameters, such as W_D and F_D, proves the ability of the synthesized molecule to block the activity of the lectin, in accordance with previous biofilm assays [71]. In particular, a concentration of 130 μM of glycocluster leads to a marked weakening of bacterial adhesion. This result confirms the role played by the lectin in the adhesion process and also that the synthetized M3 glycocluster is a good competitor face to the natural carbohydrate to reduce the adhesion. Also, characteristic features of the curves are influenced by the inhibition effect of the glycocluster, showing a modification of the general behaviour of the system. Tethers and step events were analysed to relate discrete events to the inhibition of the activity of LecA lectin. Mainly, a decrease of the frequency of having tethers, and at the same time an increase of the tether height, might be related to a modification of the heterogeneity of the bacterial outer membrane due to the presence of the glycocluster. Furthermore, step events were analysed showing an increased probability of having such events upon the addition of the glycocluster. Therefore, the final shape of the curve before and after the addition of the glycocluster significantly changes, leading to a destabilization of the interaction and a whole weakening. These differences lead to suppose a possible competition able to reveal strength changes and suggest a hardening of the membrane [148].

Also the comparison with *lecA* mutant underlined the specificity of the glycocluster, exhibiting a similar behaviour on the detachment force of the wild-type upon the addition of M3 and the mutant. Therefore, these results not only corroborate biofilm formation inhibition assays [71], but also demonstrate the presence of LecA lectin on the outer membrane of the bacteria by clearly showing the adhesive role played by the lectin, among an interaction with the native carbohydrate, in the cell-bacteria system. The lectin has the role of adhesin and it binds selectively the Gb3 epitopes present on the host membrane. The glycocluster is able to compete with these epitopes, leading to a weakening of the adhesive strength of the bacteria. In particular, it targets LecA lectin since proof of principle experiments show similar behaviour between the wild-type incubated with the glycocluster and the *lecA* mutant, demonstrating the anti-adhesive capabilities of the glycocluster.

Finally, the behaviour of the wild-type was compared to the one of *pilA* mutant. Unfortunately, only two experiments were performed with the mutant and probably more assays would help clarifying the obtained results. No significant differences were detected, even though a change is expected. In fact, the absence of the PilA should alter the envelope as in the case of *lecA* mutant, leading to a modification in bacteria mechanical properties. Probably the contact time used was too long to show differences between the two strains. If it is the case, a more instantaneous interaction of the pili could be supposed, showing the different role of this virulence factor in the adhesion process.

Chapter 6.   Conclusions and Outlook

In this Ph.D. thesis, the inhibition effect of synthetized glycoclusters against LecA lectin from *Pseudomonas aeruginosa* (PA) has been studied by means of Atomic Force Microscopy (AFM) technique. This work is encompassed within a project devoted to the synthesis and characterization of possible inhibitors of the LecA activity, with the aim of developing a new therapeutic approach able to interfere during the bacterial colonization of the human lungs. The pathogenicity of PA and the difficultness of eradicating the bacterial infection from lungs epithelium make, most of the time, the bacteria lethal for patients. In fact, the bacterium has developed huge resistances against almost all antibiotic treatments, due to its ability of growing in biofilm structures. Therefore, one major problem is the development of alternative therapies able to avoid bacterial infections. One of them is focused on targeting the virulence factors, such as the lectin LecA, which the bacteria use to infect and colonize the lungs. In fact, inhibiting the activity of the lectin will lead to a destabilization of the infection process.

To this aim, a library of more than 150 glycoclusters have been produced and screened in order to find the best candidate to target LecA lectin. These molecules are mainly characterized by a core and four branches, which bring as carbohydrate residue a galactose, the natural ligand of the lectin. Due to the multivalent presentation of the glycocluster, the affinity to the lectin is increased with respect of the monovalent ligand. Additionally, they can take advantage of the cluster glycoside effect to compete to the natural ligand of the lectin and interfere in the infection process.

Different assays can be used to study the interaction between the lectin and the glycocluster. Most of them are ensemble experiments that lead to the knowledge of an average behaviour of the system, making impossible the study of rare events or systems not at the equilibrium. On the contrary, single molecule methods allow investigating the behaviour of one molecule at the time in conditions that mimic the physiological ones. In particular, Atomic Force Microscopy (AFM) is an excellent tool to study receptor-ligand and cell-bacteria interactions at the single molecule/cell level. In fact, AFM not only allows measuring the interaction forces involved in the receptor-ligand and cell-bacteria systems, but also it is an imaging technique capable of visualizing small biological objects at high-resolution.

During these three years of Ph.D., AFM imaging and spectroscopy were used to understand the influence of the glycocluster design on the arrangement of the lectin-glycocluster complex, to

quantify the unbinding force of the LecA lectin-glycocluster interaction and to test the anti-adhesive effect of the glycocluster on the cell-bacteria system.

In **Chapter 3** the combination of high-resolution AFM images with Molecular Dynamic simulations and Isothermal Titration Calorimetry has highlighted the influence of the core and the branches in increasing the affinity. For this, the arrangements of the lectin with six different glycoclusters were studied. The glycoclusters differed one from the other by the choice of the branch (same core, different branch) or the core (different core, same branch). AFM images show very different arrangements depending on the changed parameter.

In particular, AFM images show the influence of the two linkers L1 and L2 that form the branch. The structure formation is mostly driven by the properties of L2 linker while L1 gives length and flexibility to the glycocluster. The choice of the linker L2 strongly stabilizes the galactoside in the CRD by a $\pi\pi$ interaction with the His50 close to the binding pocket of the lectin. Thus, rigid L2 linker induces the formation of small, compact and dense structures that sometimes can origin 3D organizations rather than extended 2D arrangements, even if the experimental conditions favour the formation of monolayers aggregates. Also, increasing the flexibility of the branch implies increasing the degree of freedom, while the affinity decreases.

Moreover, the choice of the core determines the spatial orientation of the branches and the distance between them. Given the same flexible linker L2, the affinity is increased in presence of a core capable of strongly orient the branches, and small, mostly 1D structures characterized by high affinity between the lectin and the glycocluster are formed rather than extended ones, as in the case of intermediate and low affinity glycoclusters.

These results let us assume that the formation of the arrangements is mostly driven by the competition between lectin-lectin and lectin-glycocluster interactions. The presence of the glycocluster improves the aggregation while the lectin-lectin interaction enhances the spreading of the structure on the *xy*-plane.

Therefore, a smart design of the glycocluster increases the possibilities of enhancing the affinity and making the molecule a good candidate to inhibit LecA lectin. It would be interesting to study competition effects of different glycoclusters by incubating two different glycoconjugates with LecA and analyse the topological arrangements to see whether a preferential architecture is remarked, and if it is preferentially related to one of the two glycoclusters, showing an easiest interaction between two glycoclusters having a similar affinity.

In **Chapter 4,** the LecA lectin-glycocluster interaction has been quantified by means of Single Molecule Force Spectroscopy. The AFM tip was chemically modified to bear the lectin while the glycoclusters were immobilized on a solid substrate by means of DNA-Directed Immobilization technique. The experimental setup was chosen to ensure as much as possible the interaction between one single lectin and one glycocluster. Therefore, the setup leads the study of the cluster glycoside effect with the main disadvantage of a huge probability of having non-specific interactions. In fact, supposing a homogeneous distribution of the molecules on the surface, for each

glycocluster immobilized on the surface there are likely eight molecules of oligonucleotides. Unfortunately, the complexity of the substrate lead sometimes to a lower statistics making impossible any reliable considerations on the interaction.

However, the off-rate constant was extrapolated for the glycocluster that presented the highest affinity, showing a fast dissociation of the binding. This parameter is affected by the multivalent nature of the interaction since multiple stretching events were recorded. These events present mostly the same unbinding force and can be mainly related to the interaction between one lectin CRD and one galactose residue of the glycocluster. Multiple events show a separation distance of the same order of magnitude of the dimensions of the lectin, demonstrating that probably two monomers of the same lectin interact with two galactose residues of the same glycocluster, in accordance with the stoichiometry of $n = 0.52$ obtained for this glycocluster.

Increasing the statistics could further develop this set of experiments, even though this would be time consuming. Probably, modifying the experimental setup would be a good idea to increase rapidly the statistics and compare the behaviour of different glycoclusters at the single-molecule level. One possibility would be increasing the density of the glycoclusters immobilized on the surface. This would include a modification of the chemical functionalization of the surface since the density of immobilized probes used here cannot be further improved. For example, using gold substrates instead of silica ones can avoid the silanization step and increase the hybridization efficiency up to 60-80% [219]. Another option would be inverting the system by means of immobilizing the lectin of the surface and the glycocluster on the tip. LecA lectin can be adsorbed on a chemically modified substrate, as in the case of ConcanavalinA lectin [105], while DDI technique, used to modify the surface, can be applied for tip modification. By playing with concentrations, the density of the glycocluster immobilized on the probe can be easily adjusted. With this experimental setup, single lectin-glycocluster interaction would be less probable (as the lectin will lie on the surface) but affinity can be tested as well as the ability of the glycocluster to bind more than one lectin monomer from different lectins. Also, the LecA-glycocluster interaction should be compared to the LecA-galactose one, to estimate the gain in affinity at the single molecule level. Another strategy would be to use a glycocluster-functionalized tip against a bacteria layer, to map the disposition of the lectin on the bacteria envelope and their selectivity to the glycocluster.

In **Chapter 5**, AFM Single Cell Spectroscopy technique was used to study the anti-adhesive capabilities of the glycocluster with the highest affinity, in a system able to mimic the *in vivo* environment. In particular, the inhibition of the adhesion of PAO1 bacteria to epithelial cells via the glycocluster was characterized. A single epithelial cell was attached to a tipless cantilever while bacteria were adsorbed on a glass surface. Force curves were acquired and analysed to investigate the modification of global parameters characteristic of the cell-bacteria interaction.

The results prove the ability of the synthesized molecule to block the activity of the lectin, in accordance with previous biofilm assays [71]. The final shape of the curve, before and after the addition of the glycocluster, significantly changes, leading to a destabilization of the interaction and a whole weakening. In fact, the presence of the glycocluster may modify the heterogeneity of the

envelope leading to a modification in the mechanical properties of the bacteria. Moreover, the glycocluster may compete with the Gb3 epitopes of the epithelial cell, which may not be able to bind the lectin due to the higher affinity of the glycocluster. Thus, the analysis of the discrete events (tethers and step events) shows a difference in the behaviour of the two events before and after the incubation with the glycocluster. This leads to suppose a possible competition between the two types of events, able to reveal possible changes in the strength of the membrane [148].

Also, the comparison with *lecA* mutant demonstrates the presence of LecA lectin on the outer membrane of the bacteria by clearly showing the adhesive role played by the lectin. Furthermore, the specificity of the glycocluster in targeting LecA lectin was proved by the similar behaviour displayed by the wild-type incubated with the glycocluster and the *lecA* mutant before and after the addition of the synthetized molecule.

Therefore, these experiments corroborate the ability of synthetic molecules to inhibit the activity of PAO1 bacteria and open up to a wide possibility of experiments that would enable further studies on the glycocluster structures as possible therapeutic replacement. For example, due to the variability of the mechanisms that bacteria use to adhere and colonize epithelial cells, combining different targeting molecules for different virulence factors (other lectins, pili, etc.) might be a fascinating way to improve the inhibition effect at the cell-bacteria level.

Annex I. Theory of polymers: fitting the stretching events with WLC and FJC model

A polymer can be defined as a long macromolecule formed by the assembly of small molecules, in general organic molecules, called monomers. The chemical reaction that allows the formation of the polymer, starting from the monomers, is called polymerization. The degree of polymerization is defined as the number of monomers that constitutes the polymer. In liquid solution, the polymers are flexible chains: the chain can rotate and turn. After a certain length, there is no more correlation between the direction of a monomer and the starting one. This length is nothing more than a characteristic decay length specific of the polymer, which also depends on the nature of the solvent. In fact, the behaviour of the polymer in solution is influenced by the nature of the solvent, that can favour or not repulsive forces between polymer monomers. Often, the temperature can influence the nature of the solvent and a distinction between good, bad or ideal (Θ) solvents can be made. A good solvent at temperature $T = T_1$ can be a bad solvent at $T = T_2$. An ideal solvent is called theta solvent and the temperature at which the polymer behaves ideally is called theta temperature, T_Θ [93]. Using the model of Flory, which takes into account the interaction between distant parts of the polymer, one can define the excluded volume v associated to each polymer's monomer [93]. In this model, the decreasing of the excluded volume is related to the decreasing of the solvent quality. Therefore, a good solvent will be characterized by a positive value of v and a temperature T higher than the T_Θ. In these conditions, the polymer will swell and the forces acting between the polymer's monomers are repulsive (expanded chain or coil, Figure I.1a). On the contrary, a bad solvent ($v < 0$ and $T < T_\Theta$) determines attractive forces between the monomers and a shrinking of the polymer (globular chain, Figure I.1c).
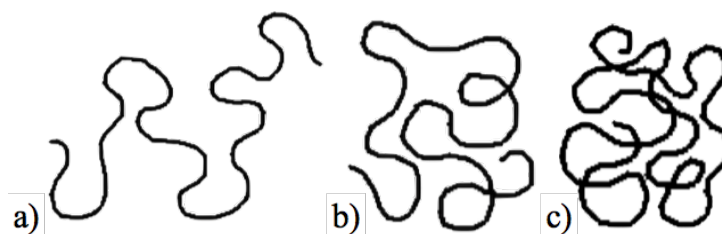
Figure I.1: Schematic representations of the coil-globule transition: a) a coil polymer in a good solvent (v > 0, T > T$_\Theta$), b) an ideal chain or Gaussian in a Θ solvent (v = 0, T = T$_\Theta$), c) a globular chain in a bad solvent (v < 0, T < T$_\Theta$).

For a mathematical point of view, there are two main models that can be used to describe the stretching of a polymer: the Freely Joined Chain (FJC) and the Worm-Like Chain (WLC) models. They are based on the idea that the application of a force allows decreasing the entropy of the chain by increasing the order and thus its elongation.

The two models differ in the description of the polymer: the FJC model describes the polymer as a chain of N segments each of length l_s, the Kuhn length. There is no preferential angle between two neighbour rods and also, in the ideal case, they do not interact. The force calculated with FJC model refers to the entropic contribution and is expressed as:

$$\frac{x}{L_C} = \coth\left(\frac{Fl_s}{k_B T}\right) - \frac{k_B T}{Fl_s} \qquad (I.1)$$

where x is the distance between the two ends of the chain and F the applied force [93]. The force can be explicitly written as a function of the distance only in the high and low limits. In these cases, the equation (I.1) becomes:

$$F = \frac{3x k_B T}{N l_s^2} \quad \text{in the low force limit } (Fl_s << k_B T) \qquad (I.2)$$

$$F = \frac{k_B T L_C}{2 l_s (L_C - x)} \quad \text{in the high force limit } (Fl_s >> k_B T) \qquad (I.3).$$

Besides, the model is not always sufficient to describe the polymer at high forces and high elongations. This is mostly due to the fact that the chain is described as a rigid object. Therefore, this model has been modified introducing the contribution of the elastic stretching, leading to the equation for the WLC model. In the WLC model, the polymer is considered as a continuous flexible isotropic rod, characterized by a contour length L_c that is the length of the fully extended polymer ($L_c = N l_s$) and it is expressed as:

$$\frac{x}{L_C} = \left[\coth\left(\frac{Fl_s}{k_B T}\right) - \frac{k_B T}{Fl_s}\right] - \left(1 + \frac{F}{l_s k_s}\right) \quad (I.4) \text{where} \quad k_s \quad \text{is the segment}$$

elasticity, the spring constant of the links [93].

Most of the time, polymers are employed to steric stabilization of colloid dispersions. For this, polymers are used as a coating on solid substrates via physisorption or grafting (Figure I.2). A polymer group is strongly adsorbed on the surface or it is fixed at one extremity to the substrate and the number of chains per units area Γ is constant, thus molecules cannot move laterally [93].
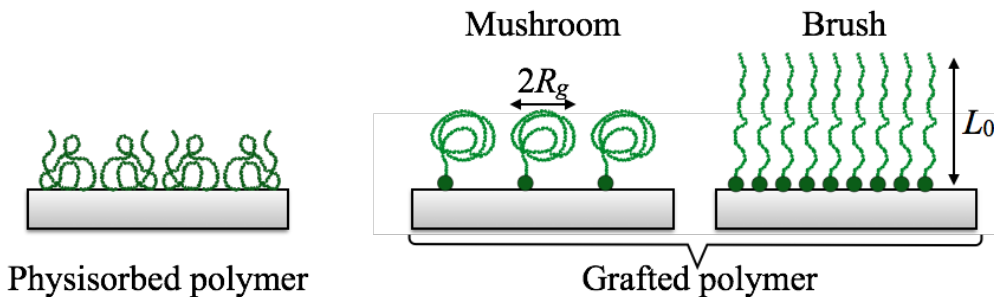
Figure I.2: Schematic representation of physisorbed and grafted polymers. Adapted from [93].

In the case of a grafted polymer, the molecules usually arrange themselves on the surface in two different ways, depending on the surface density and the steric stabilization of the system. A

mushroom organization is achieved if the density of grafted molecules is low and if polymers can organize themselves in non-overlapping folded balls with dimensions dependent on the radius of gyration $R_g = l_s \sqrt{N/6}$. Once the density is increased $\Gamma << 1/R_g^2$, the polymer tends to an unfolded organization called brush. The chains are organized in order to compensate the steric repulsion; therefore they stretch along the z-direction resulting in a thickness of the coverage $L_0 > R_g$ (Figure I.2) [93].

Annex II. Homogeneous coverage of the functionalized surfaces

In Figure II. are presented AFM images of *i*) the silanized surface (Figure II.a), *ii*) the grafted ssDNA on the surface (Figure II.b) and *iii*) the glycocluster immobilized (Figure II.c) on the solid substrate. In all cases the coverage is homogeneous. The roughness (RMS) obtained for the silanized surface does not differ to the one found for the ssDNA-functionalized sample (RMS = 0.28 ± 0.02 nm for the silanized surface and RMS = 0.28 ± 0.05 nm for the ssDNA immobilized on the surface), while contact angle measurements clearly show the different hydrophobicity of the two surfaces. In fact, contact angle of ~ 82º has been obtained for the silane grafted on the substrate while the ssDNA-modified surface shows a value of ~ 52º, both in agreement with what found in literature [190]. Finally, the glycocluster (M2)-modified surface presents an RMS of 0.65 ± 0.02 nm and a contact angle similar to the one obtained in the case of the ssDNA grafted on the surface (~ 52º).

a)   b)

c)
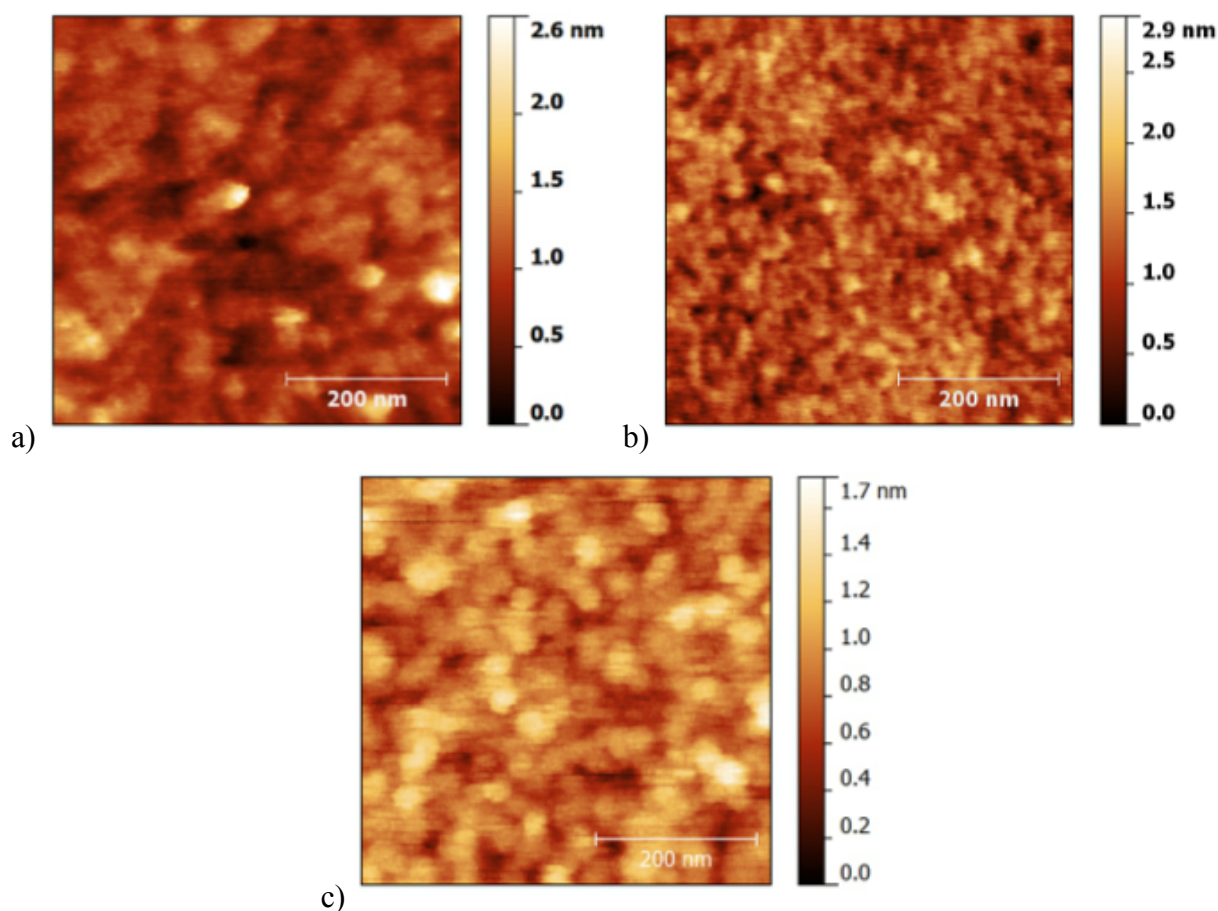
Figure II.1: AFM topographic images of size 0.5 X 0.5 μm^2 of a) silanized silica surface, b) ssDNA grafted on the surface and c) M2 glycocluster molecules immobilized on the sample. Images were acquired in tapping mode.

Annex III. Statistical analysis

In statistical analysis a major distinction is made between parametric and non-parametric tests. Parametric tests are used if the samples satisfy the requirements listed below; otherwise non-parametric tests are used. The requirements are [213]:

i) The data are random;
ii) The observations are independent one from the other;
iii) Consist of values on a interval;
iv) The populations have similar variances (homogeneity of variance assumption);
v) The distributions are adequately large;
vi) They resemble a normal distribution.

The two main tests used for comparing two distributions are the Student-*t* test and the Mann-Whitney *U* test. The former is a parametric test while the latter is a non-parametric test. Other tests can be used, such as the ANOVA statistic or the Kolmogorov-Smirnov two-sample test, but their description is out of the scope of this dissertation.

III.I   Student-*t* test

The Student-*t* test is a parametric test used to compare the means of two independent populations. To use this test, the samples have to satisfy the requirements listed above. The test compares the mean values of the two distributions for testing the null hypothesis (the difference between the means is zero), assuming that their variances are similar.

Given the mean $\overline{X}_{m=1,2}$ and the variance $\hat{\sigma}^2_{m=1,2}$:

$$\overline{X}_m = \frac{\sum_i X_i}{n_m} \tag{III.1};$$

$$\hat{\sigma}^2_m = \frac{\sum_i (X_i - X_m)^2}{n_m - 1} \tag{III.2}$$

and the pooled variance $\hat{\sigma}^2_{Pooled}$, which is a weighted mean of $\hat{\sigma}^2_{m=1,2}$, where the weights are the respective degrees of freedom [215]:

$$\hat{\sigma}^2_{Pooled} = \frac{(n_1 - 1)\hat{\sigma}^2_1 + (n_2 - 1)\hat{\sigma}^2_2}{(n_1 - 1) + (n_2 - 1)} \tag{III.3}$$

the t statistic is given by:

$$t = \frac{\overline{X}_1 - \overline{X}_2}{\sqrt{\hat{\sigma}^2_{Pooled}\left(1/n_1 + 1/n_2\right)}}$$ (III.4).

The value obtained is compared to the tabulated values for the t statistics for the given score ν and the confidence level α. If the obtained value is larger than the tabulated one, then the null hypothesis is not rejected otherwise the two distributions are different.

The test is also robust when variances are not similar, but the sample size is the same. Therefore, accurate p-values can be obtained in this case. The statistics can be also used if the two samples are not normally distributed, if the sample sizes are equal and small ($n_1 = n_2 < 5$), the populations have similar shape, are unimodal and do not have outliers.

III.II   Application of the Mann-Whitney U test

In the following, an example taken from reference [213] is shown to clarify how a Mann-Whitney U test is applied.
The data presented were obtained from a study to teach reading recovery at the 4th grade. Two methods were compared (Method 1 and Method 2). In Method 1, children were taken out of the classroom for 30 min a day, 4 days a week. In Method 2, children were taught in groups of four or five for 45 min a day in the classroom, 4 days a week. After four weeks program, children were tested. The results are presented in the Table III.1.

Method 1	Method 2
48	14
40	18
39	20
50	10
41	12
38	102
53	17

Table III.1: Results of the test.

Since the sample size is small and an outlier exists, the assumption of normality is violated, thus a non-parametric test has to be used to compare the two distributions. A Mann-Whitney U test can be used in this case, since the populations are independent.

The first step is to combine and rank the data of the two samples.

Rank	Score	Sample
1	10	Method 2
2	12	Method 2
3	14	Method 2
4	17	Method 2
5	18	Method 2
6	20	Method 2
7	38	Method 1
8	39	Method 1
9	40	Method 1
10	41	Method 1
11	48	Method 1
12	50	Method 1
13	53	Method 1
14	102	Method 2

Table III.2: Ordered scores.

Then, the sum of the ranks ($\sum R_i$) for each method is computed:

$$\sum R_1 = 7+8+9+10+11+12+13 = 70 \quad \text{for Method 1} \qquad \text{(III.5)},$$

$$\sum R_2 = 1+2+3+4+5+6+14 = 35 \quad \text{for Method 2} \qquad \text{(III.6)}.$$

Next, the U-value is obtained for each sample and the smaller between U_1 and U_2 will be the Mann-Whitney U test statistic.

For Method 1:

$$U_1 = n_1 n_2 + \frac{n_1(n_1+1)}{2} - \sum R_1$$

$$= 7(7) + \frac{7(7+1)}{2} - 70 \qquad \text{(III.7)}$$

$$= 7$$

For Method 2:

$$U_2 = n_1 n_2 + \frac{n_1(n_1+1)}{2} - \sum R_2$$

$$= 7(7) + \frac{7(7+1)}{2} - 35 \qquad \text{(III.8)}$$

$$= 42$$

where n_1 and n_2 are the number of values of each sample.

In this case, the Mann-Whitney U test statistics is given by $U_1 = 7$. Given this statistics, an appropriate table is used to find the critical value for rejecting the null hypothesis. The critical value

is found on the table at the point for $n_1 = 7$ and $n_2 = 7$, for $\alpha = 0.05$ (confidence level 95%). In this case, the critical value is 8.

If the critical value is equal or bigger than the obtained value, we must reject the null hypothesis. Otherwise, if the critical value is less than the obtained value, we must not reject the null hypothesis. Since the critical value exceeds the obtained value, we must reject the null hypothesis, suggesting that a real difference exists between the two methods.

Bibliography

[1] Neuman, K. C. & Nagy, A. Single-molecule force spectroscopy: optical tweezers, magnetic tweezers and atomic force microscopy. *Nat. Methods* **5,** 491–505 (2008).

[2] Deniz, A. A., Mukhopadhyay, S. & Lemke, E. A. Single-molecule biophysics: at the interface of biology, physics and chemistry. *J. R. Soc. Interface* **5,** 15–45 (2008).

[3] Binnig, G. & Quate, C. F. Atomic Force Microscopy. *Phys. Rev. Lett.* **56,** 930–933 (1986).

[4] Ashkin, A., Dziedzic, J. M., Bjorkholm, J. E. & Chu, S. Observation of a single-beam gradient force optical trap for dielectric particles. *Opt. Lett.* **11,** 288 (1986).

[5] Pillet, F., Chopinet, L., Formosa, C. & Dague, É. Atomic Force Microscopy and pharmacology: From microbiology to cancerology. *Biochim. Biophys. Acta - Gen. Subj.* **1840,** 1028–1050 (2014).

[6] Formosa, C., Grare, M., Jauvert, E., Coutable, A., Regnouf-de-Vains, J. B., Mourer, M., Duval, R. E. & Dague, E. Nanoscale analysis of the effects of antibiotics and CX1 on a Pseudomonas aeruginosa multidrug-resistant strain. *Sci. Rep.* **2,** 1–9 (2012).

[7] Beaussart, A., Baker, A. E., Kuchma, S. L., El-kirat-chatel, S., Toole, G. A. O. & Dufrêne, Y. F. Nanoscale Adhesion Forces of Pseudomonas aeruginosa Type IV Pili. *ACS Nano* **8,** 10723–10733 (2014).

[8] Abu-Lail, L. I., Liu, Y., Atabek, A. & Camesano, T. A. Quantifying the adhesion and interaction forces between Pseudomonas aeruginosa and natural organic matter. *Environ. Sci. Technol.* **41,** 8031–8037 (2007).

[9] Ivanov, I. E., Kintz, E. N., Porter, L. A., Goldberg, J. B., Burnham, N. A. & Camesano, T. A. Relating the physical properties of pseudomonas aeruginosa lipopolysaccharides to virulence by atomic force microscopy. *J. Bacteriol.* **193,** 1259–1266 (2011).

[10] Touhami, A., Jericho, M. H., Boyd, J. M. & Beveridge, T. J. Nanoscale characterization and determination of adhesion forces of Pseudomonas aeruginosa pili by using atomic force microscopy. *J. Bacteriol.* **188,** 370–377 (2006).

[11] Tripathi, P., Beaussart, A., Alsteens, D., Dupres, V., Claes, I., von Ossowski, I., de Vos, W. M., Palva, A., Lebeer, S., Vanderleyden, J. & Dufrêne, Y. F. Adhesion and nanomechanics of pili from the probiotic Lactobacillus rhamnosus GG. *ACS Nano* **7,** 3685–97 (2013).

[12] Bjarnsholt, T., Jensen, P. Ø., Jakobsen, T. H., Phipps, R., Nielsen, A. K., Rybtke, M. T., Tolker-Nielsen, T., Givskov, M., Høiby, N. & Ciofu, O. Quorum sensing and virulence of Pseudomonas aeruginosa during lung infection of cystic fibrosis patients. *PLoS One* **5,** 1–10 (2010).

[13] Hentzer, M. & Givskov, M. Pharmacological inhibition of quorum sensing for the treatment of chronic bacterial infections. *J. Clin. Invest.* **112,** 1300–1307 (2003).

[14] Diggle, S. P., Stacey, R. E., Dodd, C., Cámara, M., Williams, P. & Winzer, K. The galactophilic lectin, LecA, contributes to biofilm development in Pseudomonas aeruginosa. *Enviromental Microbiol.* **8,** 1095–1104 (2006).

[15] Imberty, A., Wimmerová, M., Mitchell, E. P. & Gilboa-Garber, N. Structures of the lectins from Pseudomonas aeruginosa: Insights into the molecular basis for host glycan recognition. *Microbes Infect.* **6,** 221–228 (2004).

[16] Chemani, C., Imberty, A., De Bentzmann, S., Pierre, M., Wimmerová, M., Guery, B. P. & Faure, K. Role of LecA and LecB lectins in Pseudomonas aeruginosa-induced lung injury and effect of carbohydrate ligands. *Infect. Immun.* **77,** 2065–2075 (2009).

[17] Blanchard, B., Nurisso, A., Hollville, E., Tétaud, C., Wiels, J., Pokorná, M., Wimmerová, M., Varrot, A. & Imberty, A. Structural Basis of the Preferential Binding for Globo-Series Glycosphingolipids Displayed by Pseudomonas aeruginosa Lectin I. *J. Mol. Biol.* **383,** 837–853 (2008).

[18] Imberty, A., Chabre, Y. M. & Roy, R. Glycomimetics and glycodendrimers as high affinity microbial anti-adhesins. *Chemistry* **14,** 7490–7499 (2008).

[19] Cecioni, S., Imberty, A. & Vidal, S. Glycomimetics versus Multivalent Glycoconjugates for the Design of High Affinity Lectin Ligands. *Chem. Rev.* **115,** 525–561 (2015).

[20] Lundquist, J. J. & Toone, E. J. The cluster glycoside effect. *Chem. Rev.* **102,** 555–578 (2002).

[21] Pertici, F. & Pieters, R. J. Potent divalent inhibitors with rigid glucose click spacers for Chemical Communications Accepted Manuscript. *Chem. Commun. (Camb).* **48,** 4008–4010 (2012).

[22] Casoni, F., Dupin, L., Vergoten, G., Meyer, A., Ligeour, C., Géhin, T., Vidal, O., Souteyrand, E., Vasseur, J.-J., Chevolot, Y. & Morvan, F. The influence of the aromatic aglycon of galactoclusters on the binding of LecA: a case study with O-phenyl, S-phenyl, O-benzyl, S-benzyl, O-biphenyl and O-naphthyl aglycons. *Org. Biomol. Chem.* **12,** 9166–9179 (2014).

[23] Gerland, B., Goudot, A., Ligeour, C., Pourceau, G., Meyer, A., Vidal, S., Gehin, T., Vidal, O., Souteyrand, E., Vasseur, J.-J., Chevolot, Y. & Morvan, F. Structure Binding Relationship of Galactosylated Glycoclusters toward Pseudomonas aeruginosa Lectin LecA Using a DNA-Based Carbohydrate Microarray. *Bioconjugate Chem.* **25,** 379–392 (2014).

[24] Boukareb, M. A. *et al.* Anti-adhesive Properties of Glycoclusters against Pseudomonas aeruginosa Lung Infection. *J. Med. Chem.* **57,** 10275–10289 (2014).

[25] Dupin, L. Validation et criblage de nouvelles molécules anti-infectieuses sur microarray : applications à Pseudomonas aeruginosa. (Ecole Centrale de Lyon, 2016).

[26] Stuart, B., Lin, J. H. & Mogayzel Jr., P. J. Early Eradication of Pseudomonas aeruginosa in Patients with Cystic Fibrosis. *Paediatr. Respir. Rev.* **11,** 177–184 (2010).

[27] Bellis, G., Lemonnier, L. & Sponga, M. *le registre française de la mucoviscidose.* (2012).

[28] Cistic Fibrosis Foundation. Available at: https://www.cff.org/What-is-CF/About-Cystic-Fibrosis/. (Accessed: 6th July 2015)

[29] Genetics Home Reference. Available at: http://ghr.nlm.nih.gov/gene/CFTR. (Accessed: 6th July 2015)

[30] Moreau-Marquis, S., Stanton, B. A. & O'Toole, G. A. Pseudomonas aeruginosa biofilm formation in the cystic fibrosis airway. *Pulm. Pharmacol. Ther.* **21,** 595–599 (2008).

[31] O'Sullivan, B. P. & Freedman, S. D. Cystic fibrosis. *Lancet* **373,** 1891–1904 (2009).

[32] NHS choices. Available at: http://www.nhs.uk/Conditions/cystic-fibrosis/Pages/Causes.aspx. (Accessed: 6th July 2015)

[33] Gibson, R. L., Burns, J. L. & Ramsey, B. W. Pathophysiology and Management of Pulmonary Infections in Cystic Fibrosis. *Am. J. Respir. Crit. Care Med.* **168,** 918–951 (2003).

[34] Qaisar, U., Luo, L., Haley, C. L., Brady, S. F., Carty, N. L., Colmer-Hamood, J. A. & Hamood, A. N. The pvc Operon Regulates the Expression of the Pseudomonas aeruginosa Fimbrial Chaperone/Usher Pathway (Cup) Genes. *PLoS One* **8,** (2013).

[35] Cowles, K. N., Moser, T. S., Siryaporn, A., Nyakudarika, N., Dixon, W., Turner, J. J. & Gitai, Z. The putative Poc complex controls two distinct Pseudomonas aeruginosa polar motility mechanisms. *Mol. Microbiol.* **90,** 923–938 (2013).

[36] Costerton, J. W., Stewart, P. S. & Greenberg, E. P. Bacterial biofilms: a common cause of persistent infections. *Science* **284,** 1318–1322 (1999).

[37] Hoiby, N., Bjarnsholt, T., Givskov, M., Molin, S. & Ciofu, O. Antibiotic resistance of

bacterial biofilms. *Int. J. Antimicrob. Agents* **35,** 322–332 (2010).

[38]   Feldman, M., Bryan, R., Rajan, S., Scheffler, L., Brunnert, S., Tang, H., Prince, A. & Scheffler, L. E. E. Role of Flagella in Pathogenesis of Pseudomonas aeruginosa Pulmonary Infection Role of Flagella in Pathogenesis of Pseudomonas aeruginosa Pulmonary Infection. **66,** 43–51 (1998).

[39]   McNamara, N., Gallup, M., Sucher, A., Maltseva, I., McKemy, D. & Basbaum, C. AsialoGM1 and TLR5 cooperate in flagellin-induced nucleotide signaling to activate Erk1/2. *Am. J. Respir. Cell Mol. Biol.* **34,** 653–660 (2006).

[40]   Scharfman, A., Arora, S. K., Delmotte, P., Van Brussel, E., Mazurier, J., Ramphal, R. & Roussel, P. Recognition of lewis x derivatives present on mucins by flagellar components of Pseudomonas aeruginosa. *Infect. Immun.* **69,** 5243–5248 (2001).

[41]   Mahenthiralingam, E., Campbell, M. E. & Speert, D. P. Nonmotility and phagocytic resistance of Pseudomonas aeruginosa isolates from chronically colonized patients with cystic Nonmotility and Phagocytic Resistance of Pseudomonas aeruginosa Isolates from Chronically Colonized Patients with Cystic Fibrosis. **62,** 596–605 (1994).

[42]   Bradley, D. E. A function of Pseudomonas aeruginosa PAO polar pili: twitching motility. *Can J Microbiol* **26,** 146–154 (1980).

[43]   Skerker, J. M. & Berg, H. C. Direct observation of extension and retraction of type IV pili. *Proc. Natl. Acad. Sci. U. S. A.* **98,** 6901–4 (2001).

[44]   Kocourek, J. & Horejsí, V. Defining a lectin. *Nature* (1981).

[45]   Sharon, N. & Lis, H. *Lectins.* (Kluwer Academic Publishers, 2003).

[46]   Glick, J. & Garber, N. The intracellular localization of Pseudomonas aeruginosa lectins. *J. Gen. Microbiol.* **129,** 3085–3090 (1983).

[47]   Gilboa-Garber, N. Multiple aspects of Pseudomonas aeruginosa lectins. *Nov. Acta Leopoldina NF* **75,** 153–177 (1997).

[48]   Kirkeby, S., Hansen, A. K., D'Apice, A. & Moe, D. The galactophilic lectin (PA-IL, gene LecA) from Pseudomonas aeruginosa. Its binding requirements and the localization of lectin receptors in various mouse tissues. *Microb. Pathog.* **40,** 191–197 (2006).

[49]   Loris, R., Tielker, D., Jaeger, K. E. & Wyns, L. Structural basis of carbohydrate recognition by the lectin LecB from Pseudomonas aeruginosa. *J. Mol. Biol.* **331,** 861–870 (2003).

[50]   Bajolet-Laudinat, O., Girod-De Bentzmann, S., Tournier, J. M., Madoulet, C., Plotkowski, M. ., Chippaux, C. & Puchelle, E. Cytotoxicity of Pseudomonas aeruginosa Internal Lectin PA-I to Respiratory Epithelial Cells in Primary Culture. *Infect. Immun.* **62,** 4481–4487 (1994).

[51]   Eierhoff, T., Bastian, B., Thuenauer, R., Madl, J., Audfray, A., Aigal, S., Juillot, S., Rydell, G. E., Müller, S., de Bentzmann, S., Imberty, A., Fleck, C. & Römer, W. A lipid zipper triggers bacterial invasion. *Proc. Natl. Acad. Sci. U. S. A.* **111,** 6–11 (2014).

[52]   Laughlin, R. S., Musch, M. W., Hollbrook, C. J., Rocha, F. M., Chang, E. B. & Alverdy, J. C. The key role of Pseudomonas aeruginosa PA-I lectin on experimental gut-derived sepsis. *Ann. Surg.* **232,** 133–42 (2000).

[53]   Bernardi, A. *et al.* Multivalent glycoconjugates as anti-pathogenic agents. *Chem. Soc. Rev.* **42,** 4709–27 (2013).

[54]   Cioci, G., Mitchell, E. P., Gautier, C., Wimmerová, M., Sudakevitz, D., Pérez, S., Gilboa-Garber, N. & Imberty, A. Structural basis of calcium and galactose recognition by the lectin PA-IL of Pseudomonas aeruginosa. *FEBS Lett.* **555,** 297–301 (2003).

[55]   RCSB Protein Data Bank. Available at: http://www.rcsb.org/pdb/explore.do?structureId=4LKD. (Accessed: 28th August 2015)

[56]   Ryder, C., Byrd, M. & Wozniak, D. J. Role of polysaccharides in Pseudomonas aeruginosa biofilm development. *Curr. Opin. Microbiol.* **10,** 644–648 (2007).

[57]   Ben Haj Khalifa, A., Moissenet, D., Vu Thien, H. & Khedher, M. Virulence factors in

Pseudomonas aeruginosa: mechanisms and modes of regulation. *Ann. Biol. Clin. (Paris).* **69,** 393–403 (2011).

[58] Pritt, B., O'Brien, L. & Winn, W. Mucoid Pseudomonas in cystic fibrosis. *Am. J. Clin. Pathol.* **128,** 32–34 (2007).

[59] Sutherland, I. W. Biofilm exopolysaccharides: A strong and sticky framework. *Microbiology* **147,** 3–9 (2001).

[60] Lahmann, M. Architectures of Multivalent Glycomimetics for Probing Carbohydrate – Lectin Interactions. *Top Curr Chem* **288,** 17–65 (2009).

[61] Chabre, Y. M. & Roy, R. Multivalent glycoconjugate syntheses and applications using aromatic scaffolds. *Chem. Soc. Rev.* **42,** 4657–708 (2013).

[62] Reynolds, M. & Pérez, S. Thermodynamics and chemical characterization of protein-carbohydrate interactions: The multivalency issue. *Comptes Rendus Chim.* **14,** 74–95 (2011).

[63] Zinger-Yosovich, K. D. & Gilboa-Garber, N. Blocking of Pseudomonas aeruginosa and Ralstonia solanacearum lectins by plant and microbial branched polysaccharides used as food additives. *J. Agric. Food Chem.* **57,** 6908–6913 (2009).

[64] Reynolds, M., Marradi, M., Imberty, A., Penadés, S. & Pérez, S. Multivalent gold glycoclusters: High affinity molecular recognition by bacterial lectin PA-IL. *Chem. - A Eur. J.* **18,** 4264–4273 (2012).

[65] Marotte, K., Préville, C., Sabin, C., Moumé-Pymbock, M., Imberty, A. & Roy, R. Synthesis and binding properties of divalent and trivalent clusters of the Lewis a disaccharide moiety to Pseudomonas aeruginosa lectin PA-IIL. *Org. Biomol. Chem.* **5,** 2953–2961 (2007).

[66] Imberty, A. & Varrot, A. Microbial recognition of human cell surface glycoconjugates. *Curr. Opin. Struct. Biol.* **18,** 567–76 (2008).

[67] Mammen, M., Choi, S.-K. & Whitesides, G. M. Polyvalent Interactions in Biological Systems: Implications for Design and Use of Multivalent Ligands and Inhibitors. *Angew. Chem. Int. Ed. Engl.* **37,** 2754–2794 (1998).

[68] Kiessling, L. L., Gestwicki, J. E. & Strong, L. E. Synthetic multivalent ligands in the exploration of cell-surface interactions. *Curr. Opin. Chem. Biol.* **4,** 696–703 (2000).

[69] Sacchettini, J. C., Baum, L. G. & Brewer, C. F. Multivalent protein-carbohydrate interactions. A new paradigm for supermolecular assembly and signal transduction. *Biochemistry* **40,** 3009–3015 (2001).

[70] Goudot, A. Développement d'une plateforme de criblage pour la recherche de nouvelles molécules anti-infectieuses : applications à Pseudomonas aeruginosa. (Ecole Centrale de Lyon, 2013).

[71] Ligeour, C., Vidal, O., Dupin, L., Casoni, F., Gillon, E., Meyer, A., Vidal, S., Vergoten, G., Lacroix, J.-M., Souteyrand, E., Imberty, A., Vasseur, J.-J., Chevolot, Y. & Morvan, F. Mannose-centered aromatic galactoclusters inhibit the biofilm formation of Pseudomonas aeruginosa. *Org. Biomol. Chem.* **13,** 8433–8444 (2015).

[72] Blanchard, B., Imberty, A. & Varrot, A. Secondary sugar binding site identified for LecA lectin from Pseudomonas aeruginosa. *Proteins Struct. Funct. Bioinforma.* **82,** 1060–1065 (2014).

[73] Cecioni, S., Faure, S., Darbost, U., Bonnamour, I., Parrot-Lopez, H., Roy, O., Taillefumier, C., Wimmerová, M., Praly, J. P., Imberty, A. & Vidal, S. Selectivity among two lectins: Probing the effect of topology, multivalency and flexibility of 'clicked' multivalent glycoclusters. *Chem. - A Eur. J.* **17,** 2146–2159 (2011).

[74] Cecioni, S., Lalor, R., Blanchard, B., Praly, J.-P., Imberty, A., Matthews, S. E. & Vidal, S. Achieving high affinity towards a bacterial lectin through multivalent topological isomers of calix[4]arene glycoconjugates. *Chemistry* **15,** 13232–13240 (2009).

[75] Sicard, D., Cecioni, S., Iazykov, M., Chevolot, Y., Matthews, S. E., Praly, J.-P., Souteyrand, E., Imberty, A., Vidal, S. & Phaner-Goutorbe, M. AFM investigation of Pseudomonas

aeruginosa lectin LecA (PA-IL) filaments induced by multivalent glycoclusters. *Chem. Commun. (Camb).* **47,** 9483–9485 (2011).

[76] Goudot, A., Pourceau, G., Meyer, A., Gehin, T., Vidal, S., Vasseur, J.-J., Morvan, F., Souteyrand, E. & Chevolot, Y. Quantitative analysis (K(d) and IC(50)) of glycoconjugates interactions with a bacterial lectin on a carbohydrate microarray with DNA Direct Immobilization (DDI). *Biosens. Bioelectron.* **40,** 153–60 (2013).

[77] Eaton, P. & West, P. *Atomic Force Microscopy. Oxford University Press* (2010).

[78] Baro, A. M. & Ronald G., R. *Atomic Force Microscopy in Liquids*. (Wiley-VCH, 2012).

[79] Viani, M. B., Schäffer, T. E., Chand, A., Rief, M., Gaub, H. E. & Hansma, P. K. Small cantilevers for force spectroscopy of single molecules. *J. Appl. Phys.* **86,** 2258 (1999).

[80] Leitner, M., Fantner, G. E., Fantner, E. J., Ivanova, K., Ivanov, T., Rangelow, I., Ebner, A., Rangl, M., Tang, J. & Hinterdorfer, P. Increased imaging speed and force sensitivity for bio-applications with small cantilevers using a conventional AFM setup. *Micron* **43,** 1399–407 (2012).

[81] Butt, H. J., Cappella, B. & Kappl, M. Force measurements with the atomic force microscope: Technique, interpretation and applications. *Surf. Sci. Rep.* **59,** 1–152 (2005).

[82] Lévy, R. & Maaloum, M. Measuring the spring constant of atomic force microscope cantilevers : thermal R L ′. *Nanotechnology* **13,** 33–37 (2002).

[83] Sader, J. E., Chon, J. W. M. & Mulvaney, P. Calibration of rectangular atomic force microscope cantilevers. *Rev. Sci. Instrum.* **70,** 3967 (1999).

[84] Sader, J. E., Sanelli, J. a, Adamson, B. D., Monty, J. P., Wei, X., Crawford, S. a, Friend, J. R., Marusic, I., Mulvaney, P. & Bieske, E. J. Spring constant calibration of atomic force microscope cantilevers of arbitrary shape. *Rev. Sci. Instrum.* **83,** 103705 (2012).

[85] Cleveland, J. P., Manne, S., Bocek, D. & Hansma, P. K. A nondestructive method for determining the spring constant of cantilevers for scanning force microscopy. *Rev. Sci. Instrum.* **64,** 403 (1993).

[86] Torii, A., Sasaki, M., Hane, K. & Okuma, S. A method for determining the spring constant of cantilevers for atomic force microscopy. *Meas. Sci. Technol.* **7,** 179–184 (1999).

[87] Butt, H.-J. & Jaschke, M. Calculation of thermal noise in atomic force microscopy. *Nanotechnology* **6,** 1–7 (1995).

[88] Sader, J. E. & White, L. Theoretical analysis of the static deflection of plates for atomic force microscope applications. *J. Appl. Phys.* **74,** 1 (1993).

[89] Gibson, C. T., Watson, G. S. & Myhra, S. Determination of the spring constants of probes for force microscopy/spectroscopy. *Nanotechnology* **7,** 259–262 (1996).

[90] Hutter, J. L. & Bechhoefer, J. Calibration of atomic-force microscope tips. *Rev. Sci. Instrum.* **64,** 1868 (1993).

[91] Stark, R. W., Drobek, T. & Heckl, W. M. Thermomechanical noise of a free v-shaped cantilever for atomic-force microscopy. *Ultramicroscopy* **86,** 207–215 (2001).

[92] Cappella, B. & Dietler, G. Force-distance curves by atomic force microscopy. *Surf. Sci. Rep.* **34,** 1–104 (1999).

[93] Butt, H.-J. & Kappl, M. *Surface and Interfacial Forces*. (Wiley-VCH, 2010).

[94] Colchero, J., Storch, A., Luna, M., Gómez-Herrero, J. & Baró, A. M. Observation of Liquid Neck Formation with Scanning Force Microscopy Techniques. *Langmuir* **14,** 2230–2234 (1998).

[95] Jones, R., Pollock, H. M., Cleaver, J. A. & Hodges, C. S. Adhesion Forces between Glass and Silicon Surfaces in Air Studied by AFM: Effects of Relative Humidity, Particle Size,Roughness, and Surface Treatment. *Langmuir* **18,** 8045–8055 (2002).

[96] García, R. & San Paulo, A. Attractive and repulsive tip-sample interaction regimes in tapping-mode atomic force microscopy. *Phys. Rev. B* **60,** 4961–4967 (1999).

[97] Yang, G., Vesenka, J. P. & Bustamante, C. Effects of tip-sample forces and humidity on the

imaging of DNA with a scanning force microscope. *Scanning* **18,** 344–350 (1996).

[98] García, R. & Pérez, R. Dynamic atomic force microscopy methods. *Surf. Sci. Rep.* **47,** 197–301 (2002).

[99] Leckband, D. & Israelachvili, J. *Intermolecular forces in biology. Quarterly reviews of biophysics* **34,** (2001).

[100] Butt, H.-J. J. Measuring electrostatic, van der Waals, and hydration forces in electrolyte solutions with an atomic force microscope. *Biophys. J.* **60,** 1438–1444 (1991).

[101] Müller, D. J. & Engel, a. The height of biomolecules measured with the atomic force microscope depends on electrostatic interactions. *Biophys. J.* **73,** 1633–1644 (1997).

[102] Medalsy, I. D. & Müller, D. J. Nanomechanical properties of proteins and membranes depend on loading rate and electrostatic interactions. *ACS Nano* **7,** 2642–50 (2013).

[103] Ma, C. D., Wang, C., Acevedo-Vélez, C., Gellman, S. H. & Abbott, N. L. Modulation of hydrophobic interactions by proximally immobilized ions. *Nature* **517,** 347–350 (2015).

[104] Rief, M., Oesterhelt, F., Heymann, B. & Gaub, H. Single Molecule Force Spectroscopy on Polysaccharides by Atomic Force Microscopy. *Science* **275,** 1295–7 (1997).

[105] Touhami, A., Hoffmann, B., Vasella, A., Denis, F. A. & Dufrêne, Y. F. Probing Specific Lectin-Carbohydrate Interactions Using Atomic Force Microscopy Imaging and Force Measurements†. *Langmuir* **19,** 1745–1751 (2003).

[106] Carrasco, C., Castellanos, M., Pablo, P. J. De & Mateu, M. G. Manipulation of the mechanical properties of a virus by protein engineering. *Proc Natl Acad Sci U S A* **105,** 4150–4155 (2008).

[107] Ando, T., Uchihashi, T. & Kodera, N. High-speed AFM and applications to biomolecular systems. *Annu. Rev. Biophys.* **42,** 393–414 (2013).

[108] Fuchs, H. *Nanotechnology Volume 6: Nanoprobes*. (Wiley-VCH, 2009).

[109] Martin, Y., Williams, C. C. & Wickramasinghe, H. K. Atomic force microscope-force mapping and profiling on a sub 100-A scale. *J. Appl. Phys.* **61,** 4723–4729 (1987).

[110] Garcia, R. *Amplitude Modulation Atomic Force Microscopy*. (Wiley-VCH, 2010).

[111] Moreno-Herrero, F., Colchero, J., Gomez-Herrero, J. & Baro, A. M. Atomic force microscopy contact, tapping, and jumping modes for imaging biological samples in liquids. *Phys. Rev. E - Stat. Nonlinear, Soft Matter Phys.* **69,** 1–9 (2004).

[112] Santos, S., Barcons, V., Christenson, H. K., Font, J. & Thomson, N. H. The intrinsic resolution limit in the atomic force microscope: implications for heights of nano-scale features. *PLoS One* **6,** 1–7 (2011).

[113] Hansma, P. K., Cleveland, J. P., Radmacher, M., Walters, D. A., Hillner, P. E., Bezanilla, M., Fritz, M., Vie, D., Hansma, H. G., Prater, C. B., Massie, J., Fukunaga, L., Gurley, J. & Elings, V. Tapping mode atomic force microscopy in liquids. *Appl. Phys. Lett.* **64,** 1738–1740 (1994).

[114] Moreno-Herrero, F., de Pablo, P. J., Colchero, J., Gómez-Herrero, J. & Baró, A. M. The role of shear forces in scanning force microscopy: a comparison between the jumping mode and tapping mode. *Surf. Sci.* **453,** 152–158 (2000).

[115] Albrecht, T. R., Grtitter, P., Horne, D. & Rugar, D. Frequency modulation detection using highd-Q cantilevers for enhanced force microscope sensitivity. *J. Appl. Phys.* **69,** 668–673 (1991).

[116] Gross, L., Mohn, F., Moll, N., Liljeroth, P. & Meyer, G. The chemical structure of a molecule resolved by atomic force microscopy. *Science (80-.).* **325,** 1110–4 (2009).

[117] Higgins, M. J., Riener, C. K., Uchihashi, T., Sader, J. E., McKendry, R. & Jarvis, S. P. Frequency modulation atomic force microscopy: a dynamic measurement technique for biological systems. *Nanotechnology* **16,** S85–S89 (2005).

[118] Ido, S., Kimura, K., Oyabu, N., Kobayashi, K., Tsukada, M., Matsushige, K. & Yamada, H. Beyond the helix pitch: Direct visualization of native DNA in aqueous solution. *ACS Nano* **7,**

1817–1822 (2013).

[119] Ando, T., Kodera, N., Naito, Y., Kinoshita, T., Furuta, K. & Toyoshima, Y. Y. A High-speed Atomic Force Microscope for Studying Biological Macromolecules in Action. *ChemPhysChem* **4,** 1196–1202 (2001).

[120] Moreno-Herrero, F., Colchero, J. & Baro, A. M. DNA height in scanning force microscopy. *Ultramicroscopy* **96,** 167–174 (2003).

[121] Martínez, L., Tello, M., Díaz, M., Román, E., Garcia, R. & Huttel, Y. Aspect-ratio and lateral-resolution enhancement in force microscopy by attaching nanoclusters generated by an ion cluster source at the end of a silicon tip. *Rev. Sci. Instrum.* **82,** 23710 (2011).

[122] Villarrubia, J. S. Algorithms for scanned probe microscope image simulation, surface reconstruction, and tip estimation. *J. Res. Natl. Inst. Stand. Technol.* **102,** 425 (1997).

[123] Butt, H. J., Jaschke, M. & Ducker, W. Measuring surface forces in aqueous electrolyte solution with the atomic force microscope. *Bioelectrochemistry Bioenerg.* **38,** 191–201 (1995).

[124] Fuentes-Perez, M. E., Dillingham, M. S. & Moreno-Herrero, F. AFM volumetric methods for the characterization of proteins and nucleic acids. *Methods* **60,** 113–121 (2013).

[125] Müller, D. J. & Dufrêne, Y. F. Atomic force microscopy: A nanoscopic window on the cell surface. *Trends Cell Biol.* **21,** 461–469 (2011).

[126] Hinterdorfer, P., Baumgartner, W., Gruber, H. J., Schilcher, K. & Schindler, H. Detection and localization of individual antibody-antigen recognition events by atomic force microscopy. *Proc. Natl. Acad. Sci. U. S. A.* **93,** 3477–81 (1996).

[127] Hinterdorfer, P. & Dufrêne, Y. Detection and localization of single molecular recognition events using atomic force microscopy. *Nat. Methods* **3,** (2006).

[128] Garcia-Manyes, S., Dougan, L., Badilla, C. L., Brujic, J. & Fernández, J. M. Direct observation of an ensemble of stable collapsed states in the mechanical folding of ubiquitin. *Proc. Natl. Acad. Sci. U. S. A.* **106,** 10534–9 (2009).

[129] Ludwig, M., Rief, M., Schmidt, L., Li, H., Oesterhelt, F., Gautel, M. & Gaub, H. E. AFM, a tool for single-molecule experiments. *Appl. Phys. A Mater. Sci. Process.* **68,** 173–176 (1999).

[130] Helenius, J., Heisenberg, C.-P., Gaub, H. E. & Muller, D. J. Single-cell force spectroscopy. *J. Cell Sci.* **121,** 1785–1791 (2008).

[131] Zlatanova, J., Lindsay, S. M. & Leuba, S. H. Single molecule force spectroscopy in biology using the atomic force microscope. *Prog. Biophys. Mol. Biol.* **74,** 37–61 (2000).

[132] Baumgartner, W., Hinterdorfer, P. & Schindler, H. Data analysis of interaction forces measured with the atomic force microscope. *Ultramicroscopy* **82,** 85–95 (2000).

[133] Zoldák, G. & Rief, M. Force as a single molecule probe of multidimensional protein energy landscapes. *Curr. Opin. Struct. Biol.* **23,** 48–57 (2013).

[134] Zhuang, X. & Rief, M. Single-molecule folding. *Curr. Opin. Struct. Biol.* **13,** 88–97 (2003).

[135] Francius, G., Alsteens, D., Dupres, V., Lebeer, S., De Keersmaecker, S., Vanderleyden, J., Gruber, H. J. & Dufrêne, Y. F. Stretching polysaccharides on live cells using single molecule force spectroscopy. *Nat. Protoc.* **4,** 939–46 (2009).

[136] Riener, C. K., Stroh, C. M., Ebner, A., Klampfl, C., Gall, A. a., Romanin, C., Lyubchenko, Y. L., Hinterdorfer, P. & Gruber, H. J. Simple test system for single molecule recognition force microscopy. *Anal. Chim. Acta* **479,** 59–75 (2003).

[137] Carrasco, C., Gilhooly, N. S., Dillingham, M. S. & Moreno-Herrero, F. On the mechanism of recombination hotspot scanning during double-stranded DNA break resection. *Proc. Natl. Acad. Sci. U. S. A.* **110,** E2562-71 (2013).

[138] Lee, C. K., Wang, Y. M., Huang, L. S. & Lin, S. Atomic force microscopy: Determination of unbinding force, off rate and energy barrier for protein-ligand interaction. *Micron* **38,** 446–461 (2007).

[139] Kramers, H. A. Brownian motion in a field of force and the diffusion model of chemical

reactions. *Phys.* **7,** 284–304 (1940).

[140] Merkel, R., Nassoy, P., Leung, a, Ritchie, K. & Evans, E. Energy landscapes of receptor-ligand bonds explored with dynamic force spectroscopy. *Nature* **397,** 50–3 (1999).

[141] Allison, D. P., Hinterdorfer, P. & Han, W. Biomolecular force measurements and the atomic force microscope. *Curr. Opin. Biotechnol.* **13,** 47–51 (2002).

[142] Jauvert, E., Dague, E., Séverac, M., Ressier, L., Caminade, A.-M., Majoral, J.-P. & Trévisiol, E. Probing single molecule interactions by AFM using bio-functionalized dendritips. *Sensors Actuators B Chem.* **168,** 436–441 (2012).

[143] Ebner, A., Hinterdorfer, P. & Gruber, H. J. Comparison of different aminofunctionalization strategies for attachment of single antibodies to AFM cantilevers. *Ultramicroscopy* **107,** 922–7 (2007).

[144] Kamruzzahan, A. S. M., Ebner, A., Wildling, L., Kienberger, F., Riener, C. K., Hahn, C. D., Pollheimer, P. D., Winklehner, P., Hölzl, M., Lackner, B., Schörkl, D. M., Hinterdorfer, P. & Gruber, H. J. Antibody linking to atomic force microscope tips via disulfide bond formation. *Bioconjug. Chem.* **17,** 1473–81 (2006).

[145] Wildling, L., Unterauer, B., Zhu, R., Rupprecht, A., Haselgrübler, T., Rankl, C., Ebner, A., Vater, D., Pollheimer, P., Pohl, E. E., Hinterdorfer, P. & Gruber, H. J. Linking of sensor molecules with amino groups to amino-functionalized AFM tips. *Bioconjug. Chem.* **22,** 1239–48 (2011).

[146] Evans, E. & Ritchie, K. Strength of a Weak Bond Connecting Flexible Polymer Chains. *Biophys. J.* **76,** 2439–2447 (1999).

[147] Dufrêne, Y. F. Atomic Force Microscopy in Microbiology : New Structural and Functional Insights into the Microbial Cell Surface. *mbio.asm.org* **5,** 1–14 (2014).

[148] Muller, D. J., Helenius, J., Alsteens, D. & Dufrene, Y. F. Force probing surfaces of living cells to molecular resolution. *Nat Chem Biol* **5,** 383–390 (2009).

[149] Friedrichs, J., Legate, K. R., Schubert, R., Bharadwaj, M., Werner, C., Müller, D. J. & Benoit, M. A practical guide to quantify cell adhesion using single-cell force spectroscopy. *Methods* **60,** 169–178 (2013).

[150] Sariisik, E., Docheva, D., Padula, D., Popov, C., Opfer, J., Schieker, M., Clausen-Schaumann, H. & Benoit, M. Probing the Interaction Forces of Prostate Cancer Cells with Collagen I and Bone Marrow Derived Stem Cells on the Single Cell Level. *PLoS One* **8,** e57706 (2013).

[151] Tulla, M., Helenius, J., Jokinen, J., Taubenberger, A., Müller, D. J. & Heino, J. TPA primes α2β1 integrins for cell adhesion. *FEBS Lett.* **582,** 3520–3524 (2008).

[152] Benoit, M., Gabriel, D., Gerisch, G. & Gaub, H. E. Discrete interactions in cell adhesion measured by single-molecule force spectroscopy. *Nat. Cell Biol.* **2,** 313–317 (2000).

[153] Sun, M., Graham, J. S., Hegedüs, B., Marga, F., Zhang, Y., Forgacs, G. & Grandbois, M. Multiple membrane tethers probed by atomic force microscopy. *Biophys. J.* **89,** 4320–9 (2005).

[154] Le, D. T. L., Guérardel, Y., Loubire, P., Mercier-Bonin, M. & Dague, E. Measuring kinetic dissociation/association constants between Lactococcus lactis bacteria and mucins using living cell probes. *Biophys. J.* **101,** 2843–2853 (2011).

[155] Ovchinnikova, E. S., Krom, B. P., van der Mei, H. C. & Busscher, H. J. Force microscopic and thermodynamic analysis of the adhesion between Pseudomonas aeruginosa and Candida albicans. *Soft Matter* **8,** 6454 (2012).

[156] Beaussart, A., El-Kirat-Chatel, S., Herman, P., Alsteens, D., Mahillon, J., Hols, P. & Dufrêne, Y. F. Single-cell force spectroscopy of probiotic bacteria. *Biophys. J.* **104,** 1886–92 (2013).

[157] Vadillo-Rodríguez, V., Busscher, H. J., Norde, W., de Vries, J., Dijkstra, R. J. B., Stokroos, I. & van der Mei, H. C. Comparison of Atomic Force Microscopy Interaction Forces between

Bacteria and Silicon Nitride Substrata for Three Commonly Used Immobilization Methods. **70,** 5441–5446 (2004).

[158] Butt, H.-J., Cappella, B. & Kappl, M. Force measurements with the atomic force microscope: Technique, interpretation and applications. *Surf. Sci. Rep.* **59,** 1–152 (2005).

[159] Kappl, M. & Butt, H. J. The colloidal probe technique and its application to adhesion force measurements. *Part. Part. Syst. Charact.* **19,** 129–143 (2002).

[160] Ducker, W. a., Senden, T. J. & Pashley, R. M. Direct measurement of colloidal forces using an atomic force microscope. *Nature* **353,** 239–241 (1991).

[161] Beaussart, A. & El-Kirat-Chatel, S. Quantifying the forces guiding microbial cell adhesion using single-cell force spectroscopy. *Nat. Protoc.* **9,** 1049–55 (2014).

[162] El Kirat, K., Burton, I., Dupres, V. & Dufrene, Y. F. Sample preparation procedures for biological atomic force microscopy. *J. Microsc.* **218,** 199–207 (2005).

[163] Maslova, M. V., Gerasimova, L. G. & Forsling, W. Surface Properties of Cleaved Mica. *Colloid J.* **66,** 322–328 (2004).

[164] Ebner, A., Kienberger, F., Kada, G., Stroh, C. M., Geretschläger, M., Kamruzzahan, a S. M., Wildling, L., Johnson, W. T., Ashcroft, B., Nelson, J., Lindsay, S. M., Gruber, H. J. & Hinterdorfer, P. Localization of single avidin-biotin interactions using simultaneous topography and molecular recognition imaging. *Chemphyschem* **6,** 897–900 (2005).

[165] Hansma, H. G. & Laney, D. E. DNA binding to mica correlates with cationic radius: assay by atomic force microscopy. *Biophys. J.* **70,** 1933–9 (1996).

[166] Henger, M., Wagner, P. & Semenza, G. Ultralarge atomically flat template-stripped Au surfaces for scanning probe microscopy. *Surf. Sci.* **291,** 39–46 (1993).

[167] Louise Meyer, R., Zhou, X., Tang, L., Arpanaei, A., Kingshott, P. & Besenbacher, F. Immobilisation of living bacteria for AFM imaging under physiological conditions. *Ultramicroscopy* **110,** 1349–1357 (2010).

[168] Osterhelt, F., Rief, M. & Gaub, H. E. Single molecule force spectroscopy by AFM indicates helical structure of poly(ethylene glycol) in water. *New J. Phys.* **1,** 6.1-6.11 (1999).

[169] Formosa, C., Grare, M., Duval, R. E. & Dague, E. Nanoscale effects of antibiotics on P. aeruginosa. *Nanomedicine Nanotechnology, Biol. Med.* **8,** 12–16 (2012).

[170] Atabek, A. & Camesano, T. A. Atomic force microscopy study of the effect of lipopolysaccharides and extracellular polymers on adhesion of Pseudomonas aeruginosa. *J. Bacteriol.* **189,** 8503–8509 (2007).

[171] Camesano, T. A. & Abu-Lail, N. I. Heterogeneity in bacterial surface polysaccharides, probed on a single-molecule basis. *Biomacromolecules* **3,** 661–667 (2002).

[172] Kannan, A., Karumanchi, S. L., Krishna, V., Thiruvengadam, K., Ramalingam, S. & Gautam, P. Nanoscale investigation on Pseudomonas aeruginosa biofilm formed on porous silicon using atomic force microscopy. *Scanning* **36,** 1–3 (2014).

[173] Francius, G., Lebeer, S., Alsteens, D., Wildling, L., Gruber, H. J., Hols, P., De Keersmaecker, S., Vanderleyden, J. & Dufre, Y. F. Detection, Localization and Conformational Analysis of Single Polysaccharide Molecules on Live Bacteria. *ACS Nano* **2,** 1921–1929 (2008).

[174] Waner, M. J., Gilchrist, M., Schindler, M. & Dantus, M. Imaging the Molecular Dimensions and Oligomerization of Proteins at Liquid / Solid Interfaces. *J. Phys. Chem. B* **5647,** 1649–1657 (1998).

[175] Pyne, A., Thompson, R., Leung, C., Roy, D. & Hoogenboom, B. W. Single-molecule reconstruction of oligonucleotide secondary structure by atomic force microscopy. *Small* **10,** 3257–3261 (2014).

[176] Santos, N. C. & Castanho, M. a R. B. An overview of the biophysical applications of atomic force microscopy. *Biophys. Chem.* **107,** 133–149 (2004).

[177] Gour, N. & Verma, S. Synthesis and AFM studies of lectin-carbohydrate self-assemblies.

Tetrahedron **64,** 7331–7337 (2008).

[178] Kadam, R. U., Garg, D., Schwartz, J., Visini, R., Sattler, M., Stocker, A., Darbre, T. & Reymond, J. L. CH-π 't-shape' interaction with histidine explains binding of aromatic galactosides to Pseudomonas aeruginosa lectin LecA. *ACS Chem. Biol.* **8,** 1925–1930 (2013).

[179] Sicard, D., Chevolot, Y., Souteyrand, E., Imberty, A., Vidal, S. & Phaner-Goutorbe, M. Molecular arrangement between multivalent glycocluster and Pseudomonas aeruginosa LecA (PA-IL) by atomic force microscopy: influence of the glycocluster concentration. *J. Mol. Recognit.* **26,** 694–699 (2013).

[180] Sicard, D. Caractérisation par microscopie à force atomique des arrangements protéine/sucre impliquant la lectine PA-IL de la bactérie pseudomonas aeruginosa. (Ecole Centrale de Lyon, 2012).

[181] Phaner-Goutorbe, M., Iazykov, M., Villey, R., Sicard, D. & Robach, Y. Energy dissipation effects on imaging of soft materials by dynamic atomic force microscopy: a DNA-chip study. *Mater. Sci. Eng. C. Mater. Biol. Appl.* **33,** 2311–2316 (2013).

[182] Dam, T. K. & Brewer, C. F. Thermodynamic Studies of Lectin−Carbohydrate Interactions by Isothermal tritration Calorimetry. *Chem. Rev.* **102,** 387–429 (2002).

[183] Martinez, J. C., Murciano-Calles, J., Cobos, E. S., Iglesias-Bexiga, M., Luque, I. & Ruiz-Sanz, J. in *Applications of Calorimetry in a Wide Context - Differential Scanning Calorimetry, Isothermal Titration Calorimetry and Microcalorimetry* 73–104 (2013).

[184] Freyer, M. W. & Lewis, E. A. in *Methods in Cell Biology* **84,** 79–113 (2008).

[185] Metropolis, N. & Ulam, S. The Monte Carlo Method. *J. Am. Stat. Assoc.* **44,** 335–341 (1949).

[186] Derreumaux, P. & Vergoten, G. A new spectroscopic molecular mechanics force field. Parameters for proteins. *J. Chem. Phys.* **102,** 8586–8605 (1995).

[187] Lagant, P., Nolde, D., Stote, R., Vergoten, G. & Karplus, M. Increasing Normal Modes Analysis Accuracy: The SPASIBA Spectroscopic Force Field Introduced into the CHARMM Program. *J. Phys. Chem. A* **108,** 4019–4029 (2004).

[188] Cecioni, S., Praly, J. P., Matthews, S. E., Wimmerová, M., Imberty, A. & Vidal, S. Rational design and synthesis of optimized glycoclusters for multivalent lectin-carbohydrate interactions: Influence of the linker arm. *Chem. - A Eur. J.* **18,** 6250–6263 (2012).

[189] Dugas, V., Depret, G., Chevalier, Y., Nesme, X. & Souteyrand, É. Immobilization of single-stranded DNA fragments to solid surfaces and their repeatable specific hybridization: covalent binding or adsorption? *Sensors Actuators B Chem.* **101,** 112–121 (2004).

[190] Phaner-Goutorbe, M., Dugas, V., Chevolot, Y. & Souteyrand, E. Silanization of silica and glass slides for DNA microarrays by impregnation and gas phase protocols: A comparative study. *Mater. Sci. Eng. C* **31,** 384–390 (2011).

[191] Ebner, A., Wildling, L., Kamruzzahan, a S. M., Rankl, C., Wruss, J., Hahn, C. D., Hölzl, M., Zhu, R., Kienberger, F., Blaas, D., Hinterdorfer, P. & Gruber, H. J. A new, simple method for linking of antibodies to atomic force microscopy tips. *Bioconjug. Chem.* **18,** 1176–84 (2007).

[192] Gruber, H. J. Probes Functionalization. Available at: http://www.jku.at/biophysics/content.

[193] Dupin, L., Zuttion, F., Géhin, T., Meyer, A., Phaner-Goutorbe, M., Vasseur, J.-J., Souteyrand, E., Morvan, F. & Chevolot, Y. Effects of the Surface Densities of Glycoclusters on the Determination of Their IC $_{50}$ and K_d Value Determination by Using a Microarray. *ChemBioChem* **16,** 2329–2336 (2015).

[194] Carl, P. & Schillers, H. Elasticity measurement of living cells with atomic force microscopy: data acquisition and processing. *Pflugers Arch.* **457,** 551–559 (2008).

[195] Kasas, S., Riederer, B. M., Catsicas, S., Cappella, B. & Dietler, G. Fuzzy logic algorithm to extract specific interaction forces from atomic force microscopy data. *Rev. Sci. Instrum* **71,** 2082–2086 (2000).

[196] Dutta, S., Armitage, B. A. & Lyubchenko, Y. L. Probing of miniPEGγ-PNA-DNA Hybrid Duplex Stability with AFM Force Spectroscopy. *Biochemistry* **55,** 1523–1528 (2016).

[197] Ott, W., Jobst, M. A., Schoeler, C., Gaub, H. E. & Nash, M. A. Single-molecule force spectroscopy on polyproteins and receptor-ligand complexes: The current toolbox. *J. Struct. Biol.* (2016).

[198] Celik, E. & Moy, V. T. Nonspecific interactions in AFM force spectroscopy measurements. *J. Mol. Recognit.* **25,** 53–6 (2012).

[199] Garde, S. Hydrophobic interactions in context. *Nature* **517,** 277–279 (2015).

[200] Patel, A. J., Varilly, P., Jamadagni, S. N., Hagan, M. F., Chandler, D. & Garde, S. Sitting at the edge: How biomolecules use hydrophobicity to tune their interactions and function. *J. Phys. Chem. B* **116,** 2498–2503 (2012).

[201] Bustamante, C., Smith, S. B., Liphardt, J. & Smith, D. Single-molecule studies of DNA mechanics. *Curr. Opin. Struct. Biol.* **10,** 279–85 (2000).

[202] Noy, A. & Friddle, R. W. Practical single molecule force spectroscopy: how to determine fundamental thermodynamic parameters of intermolecular bonds with an atomic force microscope. *Methods* **60,** 142–50 (2013).

[203] Copeland, R. A., Pompliano, D. L. & Meek, T. D. Drug–target residence time and its implications for lead optimization. *Nat. Rev. Drug Discov.* **5,** 730–739 (2006).

[204] Dettmann, W., Grandbois, M., André, S., Benoit, M., Wehle, A. K., Kaltner, H., Gabius, H.-J. & Gaub, H. E. Differences in Zero-Force and Force-Driven Kinetics of Ligand Dissociation from OI-Galactoside-Specific Proteins (Plant and Animal Lectins, Immunoglobulin G) Monitored by Plasmon Resonance and Dynamic Single Molecule Force Microscopy. *Arch. Biochem. Biophys.* **383,** 157–170 (2000).

[205] Sulchek, T., Friddle, R. W. & Noy, A. Strength of multiple parallel biological bonds. *Biophys. J.* **90,** 4686–4691 (2006).

[206] Beaussart, A., Abellán-Flos, M., El-Kirat-Chatel, S., Vincent, S. P. & Dufrêne, Y. F. Force Nanoscopy as a Versatile Platform for Quantifying the Activity of Antiadhesion Compounds Targeting Bacterial Pathogens. *Nano Lett.* **16,** 1299–1307 (2016).

[207] Winzer, K., Falconer, C., Garber, N. C., Diggle, S. P., Camara, M. & Williams, P. The Pseudomonas aeruginosa lectins PA-IL and PA-IIL are controlled by quorum sensing and by RpoS. *J. Bacteriol.* **182,** 6401–6411 (2000).

[208] Cozens, A. L., Yezzi, M. J., Kunzelmann, K., Ohrui, T., Chin, L., Eng, K., Finkbeiner, W. E., Widdicombe, J. H. & Gruenert, D. C. CFfR Expression and Chloride Secretion in Polarized Immortal Human Bronchial Epithelial Cells. *Am J Respir Cell Mol. Bio.* **10,** 38–47 (1994).

[209] Ehrhardt, C., Kneuer, C., Fiegel, J., Hanes, J., Schaefer, U., Kim, K. J. & Lehr, C. M. Influence of apical fluid volume on the development of functional intercellular junctions in the human epithelial cell line 16HBE14o-: Implications for the use of this cell line as an in vitro model for bronchial drug absorption studies. *Cell Tissue Res.* **308,** 391–400 (2002).

[210] Wan, H., Winton, H. L., Soeller, C., Stewart, G. a., Thompson, P. J., Gruenert, D. C., Cannell, M. B., Garrod, D. R. & Robinson, C. Tight junction properties of the immortalized human bronchial epithelial cell lines Calu-3 and 16HBE14o-. *Eur. Respir. J.* **15,** 1058–68 (2000).

[211] Schubert, R., Strohmeyer, N., Bharadwaj, M., Ramanathan, S. P., Krieg, M., Friedrichs, J., Franz, C. M. & Muller, D. J. Assay for characterizing the recovery of vertebrate cells for adhesion measurements by single-cell force spectroscopy. *FEBS Lett.* **588,** 3639–3648 (2014).

[212] Ng, G., Sharma, K., Ward, S. M., Desrosiers, M. D., Stephens, L. A., Schoel, W. M., Li, T., Lowell, C. A., Ling, C. C., Amrein, M. W. & Shi, Y. Receptor-Independent, Direct Membrane Binding Leads to Cell-Surface Lipid Sorting and Syk Kinase Activation in Dendritic Cells. *Immunity* **29,** 807–818 (2008).

[213] Corder, G. W. & Foreman, D. I. *Nonparametric Statistics. A Step-by-Step Approach*. *Journal of Chemical Information and Modeling* **53,** (John Wiley & Sons, Inc., Hoboken, New Jersy, 2014).

[214] Carl, P., Kwok, C. H., Manderson, G., Speicher, D. W. & Discher, D. E. Forced unfolding modulated by disulfide bonds in the Ig domains of a cell adhesion molecule. *Proc Natl Acad Sci U S A* **98,** 1565–1570 (2001).

[215] Kirk, R. E. *STATISTICS An Introduction*. (Thomson Wadsworth, 2008).

[216] Ostvar, S. & Wood, B. D. A multiscale model describing bacterial adhesion and detachment. *Langmuir* **32,** 5213–5222 (2016).

[217] Kube, D., Sontich, U., Fletcher, D. & Davis, P. B. Proinflammatory cytokine responses to P. aeruginosa infection in human airway epithelial cell lines. *Am.J.Physiol Lung Cell Mol.Physiol.* **280,** 0 (2001).

[218] Razatos, A., Ong, Y. L., Sharma, M. M. & Georgiou, G. Molecular determinants of bacterial adhesion monitored by atomic force microscopy. *Proc.Natl.Acad.Sci.U.S.A* **95,** 11059–11064 (1998).

[219] Herne, T. M. & Tarlov, M. J. Characterization of DNA probes immobilized on gold surfaces. *J. Am. Chem. Soc.* **119,** 8916–8920 (1997).

Francesca ZUTTION
54 rue Ney
69006 Lyon France
francescazuttion@gmail.com
Italienne

DOMAIN DE COMPETENCES

Expertise	Spectroscopie et Imagerie AFM
	Fonctionnalisation des surfaces et des pointes AFM
	Préparation des échantillons biologiques pour études AFM
	Pinces optique et magnétique
Communication scientifique	Rédaction de rapports ANR et de publications
	Communication orale dans des conférences internationales
Management	Encadrement de stagiaires en Master 1er année
Langue	Anglais : Courant
	Français : Courant
	Espagnol : Courant
	Italien : langue maternelle
	Allemand : Basique
Bureautique	Pack Office, Origin, Gwyddion, Igor, PUNIAS, Prism, LabView, COMSOL Multiphysics

EXPERIENCE DANS LA RECHERCHE

2013 – 2016 (3 ans)	**Doctorat – Institut des Nanotechnologies de Lyon, Ecully, France**
	Responsable : Pr. Magali Phaner-Goutorbe(*magali.phaner@ec-lyon.fr*)
	Caractérisation de l'effet inhibiteur des glycomime dans l'adhésion bactérienne de P. aeruginosa par imagerie et spectroscopie (single-molecule et single-cell force spectroscopy) AFM
2015 (2 semaines)	**Stage de recherche – Institute of Physiology II Université de Münster, Münster, Allemagne**
	Responsable : Dr. Hermann Schillers (schille@uni-muenster.de)
	Étude de l'interaction cellule-bactérie par spectroscopie AFM (single-cell force spectroscopy)
2013 (6 mois)	**Contrat de recherche – Centre National de Biotechnologie, CSIC, Madrid, Espagne**
	Responsable : Dr. Fernando Moreno-Herrero (*fernando.moreno@cnb.csic.es*)
	Étude de moteurs moléculaires (AddAB hélicase-nucléase) par pince optique
2012 – 2013 (1 an)	**Stage de recherche – Centre National de Biotechnologie, CSIC, Madrid, Espagne**
	Responsable : Dr. Fernando Moreno-Herrero (*fernando.moreno@cnb.csic.es*)
	Dessin d'une cellule liquide pour l'étude de moteurs moléculaires par pince magnétique à différent températures
2010 (5 mois)	**Stage de recherche – Lab. NanoInnovation (ELETTRA-Sincrotrone), Trieste, Italie**
	Responsable : Dr. Loredana Casalis (*loredana.casalis@elettra.trieste.it*)
	Étude du complexe glucose oxydase-peroxydase de raifort (Gox-HRP) par AFM
2008 – 2009 (1 an)	**Stage de recherche – Lab. NanoInnovation (ELETTRA-Sincrotrone), Trieste, Italie**
	Responsable : Dr. Loredana Casalis (*loredana.casalis@elettra.trieste.it*)
	Étude de nanostructures d'ADN obtenu par nanografting en fonction du pH par AFM
2009 (1 mois)	**Stage de recherche – Massachusetts Institute of Technology (MIT), Boston, États-Unis**
	Responsable : Pr. Francesco Stellacci
	Caractérisation de nanostructures d'ADN par AFM de haute résolution en milieu liquide

EXPERIENCE D'ENSEGNEMEINT

2014 – 2016	Travaux Pratiques (TP) 64h par an: Nanotechnologies (techniques de champ proche) (3eme année et Master 1er année), Surface Spécifique (par BET) et Chromatographie (1er et 2eme années)

FORMATIONS

2013 – 2016	**Doctorat** – Spécialité en Biophysique – soutenance le 24/10/2016 École Centrale de Lyon, Ecully, France
2010 – 2013	**Master** en Microstructure et Structure de la Matière spécialité : Physique de la Matière Condensée Università degli Studi di Trieste, Trieste, Italie Erasmus (2011 - 2012) : Université Autonome de Madrid (UAM), Madrid, Espagne
2006 – 2009	**Diplôme** en Physique Università degli Studi di Trieste, Trieste, Italie

PUBLICATIONS

F. Palazon, P. Rojo Romeo, C. Chevalier, T. Ghin, A. Belarouci, A. Cornillon, **F. Zuttion**, M. Phaner-Goutorbe, E. Souteyrand, Y. Chevolot, J.P. Cloarec "*Nanoparticles selectively immobilized onto large arrays of gold micro and nanostructures through surface chemical functionalizations*", Journal of Colloid Interface Science, 447, 152-158 (2014)

F. Palazon, D. Leonard, T. Le Mogne, **F. Zuttion**, C. Chevalier, G. Grenet, M. Phaner-Goutorbe, E. Souteyrand, Y. Chevolot, J.P. Cloarec, "*Orthogonal chemical functionalizations of patterned gold on silica surfaces*", Beilstein Journal of Nanotechnology, 6, 2272–2277 (2015)

L. Dupin, **F. Zuttion**, T. Gehin, A. Meyer, M. Phaner-Goutorbe, J.J. Vasseur, E. Souteyrand, F. Morvan, Y. Chevolot, "*Effects of the Surface Densities of Glycoclusters on the Determination of Their IC50 and Kd Value Determination by Using a Microarray*", ChemBioChem, 16, 2329-2336 (2015)

B. Gollnick, C. Carrasco, **F. Zuttion**, N. S. Gilhooly, M. S. Dillingham, F. Moreno-Herrero, "*Probing DNA Helicase Kinetics with Temperature-Controlled Magnetic Tweezers*", Small, 11, 1273-1284 (2015). Cover article

COMMUNICATIONS ORALES

F. Zuttion, D. Sicard, C. Ligeour, Y. Chevolot, G. Vergoten, A. Imberty, F. Morvan, S. Vidal, J.J. Vasseur, E. Souteyrand, M. Phaner-Goutorbe, "*Inhibition of host-pathogen interactions in cystic fibrosis The role of lectin-glycoconjugates interaction*", AFM BioMed, 13-17/12/2014, San Diego, Etats-Unis

F. Zuttion, D. Sicard, C. Ligeour, Y. Chevolot, G. Vergoten, F. Morvan, S. Vidal, J.J. Vasseur, E. Souteyrand, M. Phaner-Goutorbe, "*Inhibition of host-pathogen interaction in cystic fibrosis: a new therapeutic approach*", 18ème Journèe Scientifique du Groupe Lyonnais des Glyco-Sciences, 25/02/2015, Lyon, France

F. Zuttion, C. Ligeour, Y. Chevolot, G. Vergoten, F. Morvan, S. Vidal, J.J. Vasseur, E. Souteyrand, M. Phaner-Goutorbe, "*Mesure de l'interaction PA-IL/glycomime à la nano-échelle*", Workshop NanoNano, 15-16/06/2015, Lyon, France

POSTERS

F. Zuttion, D. Sicard, Y. Chevolot, F. Morvan, A. Imberty, G. Vergoten, S. Vidal, J. Vasseur, E. Souteyrand, M. Phaner-Goutorbe, "*The cystic fibrosis pathogen Pseudomonas aeruginosa: an atomic force microscopy study for the bacterium inhibition via multivalent glycocluster*", XVI. Annual Linz Winter Workshop, 31/01-03/02/2014, Linz, Autriche

F. Zuttion, D. Sicard, C. Ligeour, Y. Chevolot, G. Vergoten, A. Imberty, F. Morvan, S. Vidal, J. J. Vasseur, E. Souteyrand, M. Phaner-Goutorbe, "*Inhibition of host-pathogen interactions in cystic fibrosis. The role of lectin-glycoconjugates interaction*", AFMBioMed, 13-17/12/2014, San Diego, États-Unis

AUTORISATION DE SOUTENANCE

Vu les dispositions de l'arrêté du 7 août 2006,

Vu la demande du Directeur de Thèse

Madame M. PHANER-GOUTORBE

et les rapports de

M. M. MOLINARI
Professeur - Laboratoire en nanosciences LRM EA 4682 - pôle Farman - Bâtiment INSERM
21 rue Clément Ader - 51685 Reims cedex 2

et de

Mme T. COHEN-BOUHACINA
Professeur - Laboratoire Ondes et Matière d'Aquitaine UMR 5798 - Université de Bordeaux
351 cours de la libération - 33405 Talence cedex

Madame ZUTTION Francesca

est autorisée à soutenir une thèse pour l'obtention du grade de **DOCTEUR**

Ecole doctorale MATERIAUX

Fait à Ecully, le 19 octobre 2016

P/Le directeur de l'E.C.L.
La directrice des Etudes

M-A. GALLAND

Abstract. *Pseudomonas aeruginosa* (PA) is a human opportunistic pathogen responsible for 20% -30% of nosocomial infections in French hospitals. For healthy people, it presents no real danger, but for people with cystic fibrosis disease and immune-compromised patients, it is the leading cause of mortality and lung infections. PA has developed antibiotic multi-resistant strains and new and more effective therapeutic approaches are needed. It binds to the surface of the host cells by an interaction between proteins (lectins) present on the membrane and sugars of the host-cell membrane. The lectin-sugar interaction plays an important role in adherence of the bacteria and in the manufacture of a pathogenic biofilm.

A new therapeutic approach is to create synthetic molecules (glycoclusters) of greater affinity than the natural sugars present on the cells. To this aim, more than 150 glycoclusters have been synthetized and screened to find the best candidate to inhibit the bacteria infection process. Some of them have been selected and studied by Atomic Force Microscopy (AFM). In particular, this thesis is devoted to study the lectin-glycocluster and cell-bacteria interactions by AFM. The combination of AFM imaging with molecular dynamic simulations let understanding the role of the geometry of the glycoclusters on the complex formation, while AFM spectroscopy accesses the lectin-glycocluster interaction forces at the molecular and cellular levels. The reduction of bacterial adhesion has been observed upon the addition of the glycocluster. This confirms the anti-adhesive properties of the glycocluster and validates the procedure. The ultimate goal is the identification of the best glycoclusters in order to develop new drugs.

Résumé. La bactérie *Pseudomonas aeruginosa* (PA) est un pathogène responsable de 20%-30% des infections nosocomiales en milieu hospitalier. Pour les individus sains, elle ne présente pas de réel danger, mais pour les personnes atteintes par la mucoviscidose et les patients immunodéprimés, elle est la cause principale de mortalité et des infections pulmonaires. PA a développé des souches multi-résistantes aux antibiotiques et des nouvelles approches thérapeutiques plus efficaces sont donc nécessaires. Elle se fixe à la surface des cellules-hôtes par une interaction entre des protéines (lectines) présentes sur sa membrane et des sucres présents sur la membrane cellulaire. L'interaction lectine-sucre joue un rôle important dans l'adhésion de la bactérie puis dans la fabrication d'un biofilm pathogène.

Une nouvelle approche thérapeutique consiste à créer des molécules synthétiques (glycomimes) de plus grande affinité que les sucres présents sur les cellules. Pour cela, plus de 150 glycomimes ont été synthétisés et examinés afin de trouver le meilleur candidat pour empêche le processus d'infection de bactéries. Certains d'entre eux ont été choisis et étudiés par la Microscopie à Force Atomique (AFM). Cette thèse est consacrée à l'étude des interactions lectine-glycomime et aussi cellule-bactérie par AFM. L'imagerie combinée avec la modélisation permet de comprendre le rôle du glycomime sur la géométrie des complexes créés et la spectroscopie permet de mesurer les forces d'interaction présentes lors de l'adhésion, au niveau moléculaire et cellulaire. Une réduction de l'adhésion bactérienne a été observée après l'introduction du glycomime, confirmant son rôle d'inhibiteur et la validité de toute la démarche. L'objectif ultime est l'identification des meilleurs glycomimes à introduire afin de développer de nouveaux médicaments.